Distribution Agreement

In presenting this thesis or dissertation as a partial fulfillment of the requirements for an advanced degree from Emory University, I hereby grant to Emory University and its agents the non-exclusive license to archive, make accessible, and display my thesis or dissertation in whole or in part in all forms of media, now or hereafter known, including display on the world wide web. I understand that I may select some access restrictions as part of the online submission of this thesis or dissertation. I retain all ownership rights to the copyright of the thesis or dissertation. I also retain the right to use in future works (such as articles or books) all or part of this thesis or dissertation.

Signature:

_____ _____

Ming Hin Lee Date

Pathogenic Mechanisms of Charcot-Marie-Tooth disease caused by mutations in SIMPLE

By

Ming Hin Lee
Doctor of Philosophy

Graduate Division of Biological and Biomedical Science
Neuroscience Graduate Program

_____	_____
Lian Li, Ph.D. Advisor	Lih-Shen Chin, Ph.D. Advisor
_____	_____
Victor Faundez, M.D., Ph.D. Committee Member	Yue Feng, Ph.D. Committee Member
_____	_____
Jonathan Glass, M.D. Committee Member	Yoland Smith, Ph.D. Committee Member

_____

Thomas Wichmann, M.D.
Committee Member

Accepted:

_____

Lisa A. Tedesco, Ph.D.
Dean of the Graduate School

_____

Date

Pathogenic Mechanisms of Charcot-Marie-Tooth disease caused by mutations in SIMPLE

By

Ming Hin Lee
B.S., Texas A&M University, 2004

Advisors: Lih-Shen Chin, Ph.D.
Lian Li, Ph.D.

An Abstract of
A dissertation submitted to the Faculty of the Graduate School of Emory University in partial fulfillment of the requirements for the degree of Doctor of Philosophy

Graduate Division of Biomedical and Biological Sciences
Neuroscience Graduate Program

2014

Abstract

Mutations in SIMPLE cause autosomal dominant, Charcot-Marie-Tooth disease (CMT) type 1C. The cellular function of SIMPLE is unknown and the pathogenic mechanism of SIMPLE mutations remains elusive. Results described in this dissertation show that SIMPLE is highly expressed in the peripheral nerves and Schwann cells. Our analysis has identified a transmembrane domain (TMD) embedded within the cysteine-rich (C-rich) region for anchoring SIMPLE to the membrane. We found that SIMPLE associates with endosomal sorting complex required for transport (ESCRT) components STAM1, Hrs, and TSG101 on early endosomes and functions with the ESCRT machinery in the control of endosome-to-lysosome trafficking. Our analyses reveal that SIMPLE is required for efficient recruitment of these ESCRT components to endosomal membranes and for regulating endosomal trafficking and signaling attenuation of ErbB receptors.

Results described in this dissertation show that CMT1C-linked pathogenic mutations are clustered within or around the TMD of SIMPLE, and these mutations cause mislocalization of SIMPLE from the early endosome membrane to the cytosol. The CMT1C-associated SIMPLE mutant proteins are unstable and prone to aggregation, and they are selectively degraded by both the proteasome and aggresome-autophagy pathways. We find that the ability of SIMPLE to regulate ErbB trafficking and signaling is impaired by these SIMPLE mutations, resulting in the prolonged activation of ERK1/2 signaling. We also examined the effects of a CMT1C-linked mutation *in vivo* by generating transgenic mice expressing a CMT1C-linked human SIMPLE mutant protein. Mice expressing mutant SIMPLE develop a progressive motor and sensory neuropathy

that recapitulates some of the key clinical features of CMT1C disease, including behavioral impairments, nerve conduction defects, and myelin pathology. Together, our findings support that SIMPLE mutation disrupts myelin homeostasis and causes progressive peripheral neuropathy via a combination of loss-of-function, toxic gain-of-function and dominant-negative mechanisms. Furthermore, our results suggest that dysregulation of endocytic trafficking and receptor signaling could contribute to the pathogenesis of demyelinating CMT1C neuropathy.

Pathogenic Mechanisms of Charcot-Marie-Tooth disease caused by mutations in SIMPLE

By

Ming Hin Lee
B.S., Texas A&M University, 2004

Advisors: Lih-Shen Chin, Ph.D.
Lian Li, Ph.D.

A dissertation submitted to the Faculty of the Graduate School of Emory University in partial fulfillment of the requirements for the degree of Doctor of Philosophy

Graduate Division of Biomedical and Biological Sciences
Neuroscience Graduate Program

2014

Acknowledgments

I owe an enormous gratitude to my advisors, Dr. Lian Li and Dr. Lih-Shen Chin, for their guidance and support over one of the most challenging and exciting phase of my life. Their mentorship helped instilled courage in my heart and encouraged me to continue challenging myself throughout the rest of my career as a physician-scientist. I am also grateful for all past and present members of the laboratory, especially graduate students James Olzmann, James Lee, Elizabeth Webber, Lisa Giles, Jue Chen, Jeanne McKeon, Cheryl Ho, Dana Fallaize, Cris Lee, and Brandi Whatley, as well as postdoctoral fellows Haishan Yin, Di Sha, Maksim Chudaev, Patrick Reynolds, Jennifer Hurst-Kennedy, and Hong Tang for their wonderful spirit and patience as well as for exchanging important skills and techniques and for helping my intellectual growth as a scientist. I would like to extend my thanks to research technicians Yi-Fei Pu, Jongbin Lee, and undergraduate researchers Dan Tangpisuthipongsa and Anum Ali Mohammed, who have helped the progress of my research. I want to acknowledge collaborator and committee member Dr. Jonathan Glass and his laboratory specialist Seneshaw Asress for their technical support on the transgenic mouse project, and committee members, Dr. Victor Faundez, Dr. Yoland Smith, Dr. Yue Feng, and Dr. Thomas Wichmann for their encouragement and insights throughout my graduate training. In addition, I want to thank the Emory Neuroscience Graduate Program, the Emory Department of Pharmacology, the Emory Medical Scientist Training Program, and the entire scientific community at Emory for providing a great place for scientific discovery and education.

I am most grateful for having a family that is both loving and supportive. I would like to thank my parents for providing me the best that parents could give and supported my decisions to let me be the person I am today. I would also like to thank my sisters Angela and Joyce as well as my brother-in-laws Lawrence and Edwin, whom have provided enormous support beyond what a younger brother can ask for. Moreover, I thank Dr. Jack R. Nation and Dr. Howard Gershenfeld for triggering and supporting my interest in science prior to my time as a student at Emory that has blossomed over the years. Finally, I thank my wife, Hailey, for her love and being the better half in our continuing journey together. Her support and company has provided a great sense of optimism, harmony, and progress in our lives.

Table of Contents

List of Figures

Chapter 1. Introduction and background

Chapter 2. Mutations associated with Charcot-Marie-Tooth disease cause SIMPLE protein mislocalization and degradation by proteasome and aggresome-autophagy pathways

Chapter 3. Charcot-Marie-Tooth disease-associated protein SIMPLE functions with the ESCRT machinery to regulate endosomal trafficking

List of Tables

Chapter 1. Introduction and background

Chapter 1

Introduction and Background

1.1. Opening remarks

Charcot-Marie-Tooth disease (CMT), also referred to as hereditary motor and sensory neuropathy (HMSN), was first described by Jean-Martin Charcot and his student Pierre Marie and by Howard Henry Tooth in 1886. Patients suffering from CMT present with weakness, sensory loss, and muscle wasting, all of which drastically decrease the standard of living for these patients. Currently, very few treatment options are available for this disease. Despite the identification of mutations in many different genes that cause CMT, the molecular and cellular pathogenic mechanisms of these mutations remain very poorly understood. Therefore, a better understanding of the pathways involved in CMT pathogenesis would be invaluable for developing therapeutic targets for patients suffering from CMT. Results described in this dissertation provide new insights to the pathogenesis of a subtype of demyelinating CMT, CMT type 1C (CMT1C), and suggest that multiple subtypes of CMT are caused by dysfunctions in the same cellular pathways. These findings have also furthered our understanding of the basic biological processes behind the clearance of misfolded proteins, transport and signaling of membrane-bound receptors, and myelination of neuronal axons by Schwann cells in the peripheral nervous system.

1.2. Clinical features of Charcot-Marie-Tooth disease

CMT is the most common inherited peripheral neuropathy with an estimated prevalence of 1 in 2,500 and occurs in all examined ethnic groups worldwide (Patzko and Shy, 2011). Studies have identified mutations in more than 30 different genes that are responsible for

causing CMT, with the severity, onset, and inheritance pattern being variable depending on the mutation acquired by the patient (Jani-Acsadi et al., 2008; Pareyson and Marchesi, 2009; Patzko and Shy, 2011; Reilly and Shy, 2009). Patients with CMT show motor defects and sensory loss that begin at the most distal parts of the body including the feet and calves that could progress proximally to the arms and hands (Pareyson and Marchesi, 2009; Patzko and Shy, 2011). Symptoms of CMT include decreased muscle tone and muscle wasting, foot drop and foot deformity, atrophy of calf muscles, as well as weakness, numbness, and pain of the legs and feet (Pareyson and Marchesi, 2009; Patzko and Shy, 2011). These symptoms drastically decrease the quality of life, with the most severe forms causing an inability to walk by the first decade of life (Jani-Acsadi et al., 2008; Pareyson and Marchesi, 2009; Patzko and Shy, 2011).

1.3. Demyelinating types of Charcot-Marie-Tooth disease

CMT is subdivided into two forms: demyelinating CMT is the major form (~80%) where the primary defect is an inability of Schwann cells to properly myelinate peripheral axons (Table 1), and axonal degenerating CMT is the minor form (~20%) where the primary defect is axonal degeneration without marked demyelination (Table 2) (Pareyson and Marchesi, 2009; Patzko and Shy, 2011). The demyelinating form of CMT is identified by a nerve conduction velocity (NCV) test where a NCV of less than 38 m/s in the arms signifies peripheral demyelination, and diagnoses of demyelinating CMT are made by further genetic testing (Pareyson and Marchesi, 2009; Patzko and Shy, 2011). Although not required for diagnosis, nerve biopsies show demyelination and “onion bulb”

formation describing the reduplication of Schwann cell basement membrane caused by repeated demyelination and remyelination (Patzko and Shy, 2011). Demyelination and subsequent degeneration of axons then manifest as dysfunctions in peripheral nerves that are responsible for causing the motor and sensory phenotypes (Pareyson and Marchesi, 2009; Patzko and Shy, 2011). Although how mutations in genes with seemingly different functions lead to demyelinating CMT remain largely unknown, recent studies have begun to identify potential converging cellular and molecular mechanisms in the pathogenesis of demyelinating CMT. In the sections below, I will first provide an extensive overview of the potential causative mechanisms for each subtype of demyelinating CMT (Sections 1.3.1-1.3.12), followed by a discussion of the possible mechanisms that may be common to several subtypes of demyelinating CMT (Section 1.4).

1.3.1. Peripheral Myelin Protein 22, PMP22 (CMT1A)

CMT1A, which represents 70% to 80% of all demyelinating CMT cases (Bird, 1993), is considered as the prototypic clinical presentation of demyelinating CMT. Patients suffering from CMT1A revealed progressive demyelination and the pathological structures known as “onion bulbs” that represent abnormally hypertrophic Schwann cells wrapping around demyelinated axonal processes (Sander et al., 1998). CMT1A is an autosomal dominant form of demyelinating neuropathy that is mapped to chromosome 17p11.2 (Vance et al., 1991) at the *PMP22* gene which encodes peripheral myelin protein 22 (PMP22). The most common cause of CMT1A (>90%) is a 1.4 Mb duplication of chromosome 17p11.2 encompassing the *PMP22* gene (Ionasescu et al., 1993; Wise et al.,

1993), but it is also caused by point mutations in the *PMP22* gene (Gabreels-Festen et al., 1995). Mice and rats overexpressing the *PMP22* gene or expressing point mutant forms of *PMP22* demonstrate demyelination and slowed peripheral nerve conduction velocities (NCVs) that are characteristic of CMT1A (Magyar et al., 1996; Niemann et al., 1999; Robaglia-Schlupp et al., 2002; Robertson et al., 2002), which supports that *PMP22* genetic duplication and point mutations cause the CMT1A phenotype. Interestingly, deletion of this identical 1.4 Mb region causes a related neuropathy known as hereditary neuropathy with liability to pressure palsies (HNPP) (Chance et al., 1993), which suggests that the maintenance of *PMP22* expression within homeostatic levels is important for the normal function of Schwann cells.

The encoded protein, PMP22, is a 220-amino-acid protein that dimerizes with another myelin protein in Schwann cells known as myelin protein zero (MPZ) (D'Urso et al., 1999; Hasse et al., 2004). The PMP22/MPZ dimer, together with major constituent proteins such as myelin basic protein and lipids such as cerebrosides and sphingomyelin, form the basic structure of the myelin sheath in the peripheral nervous system (Evans and Finean, 1965; Uyemura et al., 1995). PMP22 has also been implicated as a signaling protein involved in regulating cell death (Brancolini et al., 2000), but this function has not been well established. PMP22 is a type III tetra-spanning hydrophobic membrane protein that contains one intracellular and two extracellular loops with a glycosylation site located at the first extracellular loop (D'Urso et al., 1999; Kitamura et al., 2000). It is synthesized at the ER and is transported via the Golgi to the cell surface for the assembly of myelin sheath. The majority of newly synthesized PMP22, however, is degraded via the endoplasmic reticulum (ER)-associated degradation (ERAD) pathway with only a

minority is transported to the cell surface (Pareek et al., 1997), which suggest that a large portion of newly synthesized PMP22 are misfolded and require refolding or degradation by the ER machinery.

Accumulating evidence suggests that CMT1A is caused by genetic duplication and over-synthesis of the protein or by missense mutations of the protein, both of which produces large amounts of misfolded PMP22 proteins (Fortun et al., 2006; Myers et al., 2008; Sakakura et al., 2011). Many of the PMP22 missense mutant proteins are not targeted to the plasma membrane but instead accumulate at the endoplasmic reticulum (ER), Golgi apparatus, or the ER-Golgi intermediate compartment (IC) (Colby et al., 2000; D'Urso et al., 1998; Naef and Suter, 1999; Tobler et al., 1999). These misfolded PMP22 proteins accumulated at the ER can potentially disrupt Schwann cell functions by two possible mechanisms. First, they could induce ER stress response that is similar to misfolded Δ508 CFTR mutant (Knorre et al., 2002) or overwhelm the protein folding ability of ER chaperones such as calnexin (Dickson et al., 2002). Second, misfolded PMP22 can retain the ability to bind the wild-type, properly folded PMP22 (Tobler et al., 1999) or its binding partner MPZ to inhibit their transport from the ER/Golgi compartments for myelin synthesis.

In addition to its accumulation at the ER, misfolded PMP22 caused by over-expression or point mutations can also escape from the membrane to accumulate in the cytosol to inhibit proteasome activity (Fortun et al., 2005), up-regulate the endosome-to-lysosome pathway (Notterpek et al., 1997), and to accumulate at cytosolic structures known as aggresomes (Ryan et al., 2002; Tobler et al., 1999). Aggresomes, which contain misfolded proteins, are formed as a result of cells attempting to protect

themselves against these toxic proteins via sequestration (Olzmann et al., 2008), which further supports the view that CMT1A is caused by the toxicity of accumulated misfolded PMP22 proteins that inhibits Schwann cell function in myelinating peripheral axons.

Although this protein-misfolding hypothesis is attractive in explaining the pathogenesis of CMT1A, some evidence suggests that CMT1A can also be caused by mechanisms other than the toxic build-up of misfolded PMP22. For example, several point mutations that cause CMT1A have been found to be autosomal-recessively inherited that may lead to a loss-of-function instead of a toxic gain-of-function in the PMP22 protein (Liu et al., 2004). These rare forms of PMP22 mutations do not cause PMP22 to accumulate at the ER, and some are being sorted to the cell surface (Liu et al., 2004). It is possible that loss-of-function in PMP22 caused by protein misfolding may also partially contribute to autosomal dominant forms of CMT1A as well.

1.3.2. Myelin Protein Zero, MPZ/P0 (CMT1B)

Genetic studies have identified various single point mutations at the coding sequence of the *MPZ* gene at chromosome 1q22-q23 to cause an autosomal dominant demyelinating neuropathy called CMT1B (Hayasaka et al., 1993), which accounts for about 6% to 10% of all demyelinating CMT cases (Bird, 1993). These mutations result in amino acid substitutions of the encoded protein known as myelin protein zero (MPZ). Patients with MPZ mutations present with two distinct clinical and pathological phenotypes of either a severe neuropathy with neonatal onset of motor weakness and sensory loss or a much milder neuropathy with a late onset of motor and/or sensory symptoms in the fourth

decade (Gabreels-Festen et al., 1996; Shy et al., 2004). A subgroup of patients with MPZ mutations do not show reduction in nerve conduction velocity and are sometimes classified as “axonal degeneration” type of CMT (Shy et al., 2004), but it is unknown whether the primary defect is axonal degeneration or dysmyelination in these patients. Histological examination of nerves from CMT1B patients showed the classic pathological findings of demyelinated fibers with onion bulbs (Gabreels-Festen et al., 1996). In addition, nerve fibers from CMT1B patients and mouse models of CMT1B also showed numerous focally folded myelin that were either outfolded or are infolded into axonal space (Fabrizi et al., 2000; Iida et al., 2012; Runker et al., 2004), although the cause for this focal folding of myelin is unknown.

MPZ is a 219-amino-acid single-spanning transmembrane protein that contains an N-terminal immunoglobulin-like extracellular domain. It forms a heterodimer with PMP22 (D'Urso et al., 1999; Hasse et al., 2004) and is one of the major constituent of compact myelin in the peripheral nervous system (Uyemura et al., 1995). Like members of the immunoglobulin superfamily of proteins, the immunoglobulin-like extracellular domain of MPZ can form homotypic interactions, and expression of exogenous MPZ causes cells to adhere to each other *in vitro* (Xu et al., 2001). Loss of MPZ in mice causes myelin to lose its compaction, suggesting that MPZ may have a role in myelin compaction by binding to itself at the adjacent myelin lamellae to act as an adhesive within the myelin sheath (Wrabetz et al., 2006).

A recent report has suggested that late onset CMT1B is caused by partial loss-of-function mutations in MPZ, where the resultant MPZ mutant proteins are properly transported to the plasma membrane but lack the ability to mediate intercellular adhesion

(Grandis et al., 2008). By contrast, early onset CMT1B is caused by mutations via a combination of dominant-negative and toxic gain-of-function mechanisms, where mutant proteins are retained within the cytoplasm, inhibit wild-type MPZ function, and activate unfolded protein response (Grandis et al., 2008; Wrabetz et al., 2006). Moreover, a recent study showed that early onset CMT1B in a Taiwanese family is caused by increased *MPZ* gene dosage which may cause an increased production and accumulation of misfolded MPZ protein (Maeda et al., 2012). Taken together, toxic build-up of unfolded/misfolded PMP22 and/or MPZ may be a common mechanism in causing demyelinating neuropathy.

1.3.3. Small Integral Membrane Protein of Lysosome/Late Endosome, SIMPLE (CMT1C)

Missense mutations in exon 3 of *SIMPLE* located at chromosome 16p13.1-p12.3 cause autosomal dominant demyelinating CMT termed CMT1C (Campbell et al., 2004; Gerding et al., 2009; Latour et al., 2006; Saifi et al., 2005; Street et al., 2003; Street et al., 2002), which represents about 1% to 2% of all demyelinating CMT cases (Bird, 1993). Nerve biopsy from a CMT1C patient demonstrated onion bulb formation which is highly characteristic of demyelinating CMT (Street et al., 2003). Electrophysiological studies in CMT1C patients typically show decreased in NCVs, but a small percentage of patients have “temporal dispersion” of their nerve conduction signals, which describes the spread of the signal from a single peak to several smaller peaks temporally that is not typically found in CMT1A (Campbell et al., 2004; Street et al., 2003). In addition, one report has reported a CMT1C patient with normal NCVs but a decreased action potential amplitude

(Saifi et al., 2005), which suggests axonal degeneration instead of demyelination of the peripheral nerves. Nevertheless, the majority of reports have described CMT1C as a demyelinating disorder that resembles CMT1A (Campbell et al., 2004; Gerding et al., 2009; Latour et al., 2006; Saifi et al., 2005; Street et al., 2003; Street et al., 2002).

All CMT1C-associated mutations identified to date are located at the evolutionarily conserved cysteine-rich (C-rich) domain of the encoded protein known as small integral membrane protein of lysosome/late endosome (SIMPLE) or lipopolysaccharide-induced tumor necrosis factor-alpha factor (LITAF) (Campbell et al., 2004; Gerding et al., 2009; Latour et al., 2006; Saifi et al., 2005; Street et al., 2003; Street et al., 2002). SIMPLE has been implicated as a positive regulator of cytokine signaling that controls the expression of tumor necrosis factor-alpha (TNFα) (Bolcato-Bellemin et al., 2004; Moriwaki et al., 2001), and up-regulation of SIMPLE has been linked to inflammatory bowel diseases (Huang and Bennett, 2007). In addition, studies have also suggested SIMPLE as a tumor suppressor in B cell lymphomas and prostate cancer (Mestre-Escorihuela et al., 2007; Zhou et al., 2011), but its precise cellular function remains elusive. SIMPLE contains a PSAP tetrapeptide motif that is predicted to bind the ubiquitin E2 variant (UEV) domain of TSG101, a subunit of the endosomal sorting complex required for transport (ESCRT) machinery (Figure 1). Ample evidence indicates that the ESCRT machinery, composed of ESCRT-0, -I, -II, and -III complexes, plays a central role in the endosomal sorting of internalized cell surface receptors to the lysosomal pathway (Raiborg and Stenmark, 2009). However, the functional significance of the SIMPLE-TSG101 interaction has not been examined and whether SIMPLE has a role in the regulation of endosomal sorting and trafficking remains unexplored. In

addition to TSG101, SIMPLE contains two PPSY motifs that interact with the WW domains of NEDD4 (Shirk et al., 2005) (Figure 1). NEDD4 has emerged as an essential regulator of endocytic sorting and degradation of cell-surface cargos including the epidermal growth factor receptor (EGFR), epithelial sodium channel, β2 adrenergic receptor, and others (Lin et al., 2010; Nabhan et al., 2010; Staub et al., 2000). However, whether the SIMPLE-NEDD4 interaction has a regulatory role in endocytic trafficking remains unclear.

Previous northern blot analyses showed a ubiquitous expression pattern of SIMPLE mRNA across multiple mouse tissues (Moriwaki et al., 2001; Street et al., 2003), therefore it is puzzling as to how mutations in SIMPLE can cause a demyelinating neuropathy phenotype that specifically affects the peripheral nervous system. The subcellular distribution of SIMPLE is unknown, although a subpopulation was suggested to associate with the late endosome and/or lysosome (Moriwaki et al., 2001). The cysteine-rich (C-rich) domain of SIMPLE (Figure 1) has been proposed to be a putative RING finger domain that may have E3 ubiquitin-protein ligase activity (Moriwaki et al., 2001; Saifi et al., 2005), but the function of this domain remains to be defined. In addition, the pathogenic effects of CMT1C-linked SIMPLE mutations, all of which are clustered within the C-rich domain (Figure 1), have not yet been examined to date.

The following chapters will focus on determining the function of SIMPLE protein as well as the pathogenic role of SIMPLE mutations in causing CMT1C. By elucidating the pathogenic mechanisms of CMT1C, I hope to identify new mechanisms and pathways causing demyelinating peripheral neuropathies. I have provided a more detailed outline of my goals and hypotheses in Section 1.10.

1.3.4. Early Growth Response 2, EGR2/Krox20 (CMT1D and CMT4E)

Several autosomal dominant or autosomal recessive point mutations in the *EGR2/Krox20* gene on chromosome 10q21.1-q22.1 cause subtypes of demyelinating CMT known as CMT1D (autosomal dominant form) and CMT4E (autosomal recessive form) (Boerkoel et al., 2001; Pareyson et al., 2000; Timmerman et al., 1999; Warner et al., 1998; Yoshihara et al., 2001), together representing about less than 2% of all demyelinating CMT cases (Bird, 1993). The encoded protein, early growth response 2 (EGR2), is a master transcription factor that signals the synthesis of myelin proteins and myelin lipid-producing enzymes that is activated by contact with axons (Le et al., 2005; Murphy et al., 1996; Nagarajan et al., 2001; Topilko et al., 1997; Topilko et al., 1994). EGR2 missense mutations associated with CMT1D and CMT4E specifically interfere with the expression of genes required for myelination which includes MPZ (LeBlanc et al., 2007).

The clinical features of CMT1D and CMT4E vary depending on which mutation is acquired by the patient. Some mutations cause severe forms of CMT with childhood onset (Boerkoel et al., 2001; Timmerman et al., 1999) and/or with cranial nerve involvement (Pareyson et al., 2000), while other mutations result in milder forms of CMT (Warner et al., 1998). These variable phenotypes may reflect a partial versus a complete loss-of-function of EGR2 mutant proteins with different binding affinities to myelin gene promoters (Musso et al., 2001; Warner et al., 1999) or other factors that regulate myelin gene expression in Schwann cells. Alternatively, some EGR2 mutants found in CMT1D

exert dominant-negative inhibition on wild-type EGR2 to inhibit the expression of myelin genes (Nagarajan et al., 2001).

1.3.5. Connexin32, Cx32/GJB1 (CMT1X)

A variety of missense or nonsense mutations, deletions, insertions, frameshifts, and 5' untranslated region (UTR) mutations of the *GJB1* gene at chromosome Xq13.1 cause an X-linked inherited CMT known as CMT1X, which are responsible for about 10% of all demyelinating CMT cases (Kleopa et al., 2006; Murphy et al., 2011). Although CMT1X is an X-linked disease that primarily affects males, it can occasionally cause a milder form of the disease in female carriers that have a later onset compared to the male counterparts, which is likely attributed to X-inactivation (Kleopa et al., 2006; Siskind et al., 2011). Patients suffering from CMT1X demonstrate the same weakness, sensory loss, and muscle wasting that are present in CMT1A and CMT1B, although muscle atrophy, paresthesia and sensory loss are more prominent in CMT1X patients (Kleopa et al., 2006). These patients may have some central nervous system involvement but do not generally manifest as symptoms that are clinically significant. Mice with the *GJB1* gene deleted also demonstrate sensory and motor peripheral neuropathy similar to that of CMT1X patients (Nelles et al., 1996; Scherer et al., 1998), and their neuropathy phenotype is abolished by the expression of rat *GJB1* transgene in myelinating Schwann cells (Scherer et al., 2005).

GJB1 encodes connexin32, a gap junction protein highly expressed in myelinating Schwann cells. While connexin32 is expressed in multiple tissues, peripheral neuropathy

is usually the main clinical phenotype of connexin32 mutations (Kleopa et al., 2006). Cellular studies showed that some connexin32 mutants are retained at the ER and/or Golgi (Yum et al., 2002). This suggests that the mutant connexin32 may be misfolded to cause toxicity in a similar fashion as misfolded PMP22 by inducing ER stress or exerting dominant-negative inhibition by inhibiting the transport of other gap junction proteins to the cell surface. Other connexin32 mutants are properly transported to the cell surface as gap junction-like plaques but have altered biophysical properties including forming gap junctions with a shift in voltage gating (Abrams et al., 2002; Yum et al., 2002). Finally, a recent study has implicated loss-of-function of connexin32 in causing myelination defects in mice (Sargiannidou et al., 2009), which indicate an important yet-to-be identified role of connexin32 in the myelination of peripheral axons by Schwann cells.

1.3.6. Ganglioside-induced Differentiation Associated-Protein 1, GDAP1 (CMT4A)

Mutations in *GDAP1* at chromosome 8q13-q21 cause autosomal recessive demyelinating CMT known as CMT4A (Baxter et al., 2002; Ben Othmane et al., 1993). In addition to CMT4A, *GDAP1* also harbors mutations causing an intermediate demyelinating/axonal type of CMT, with some of these mutations inherited in an autosomal-dominant manner (Cassereau et al., 2011). CMT4A generally presents as an aggressive neuropathy with an early onset during infancy or childhood and can cause severe disabilities prior to the second decade of life in some patients (Cassereau et al., 2011). Vocal cord paresis and diaphragmatic paralysis are often seen in patients suffering from CMT4A (Cassereau et al., 2011). Pathological findings of demyelinating CMT4A include myelin infolding and

outfolding, hypomyelination, demyelinated fibers, and onion bulb formation, with signs of axonal degeneration also observed (Chung et al., 2011; Sivera et al., 2010).

The encoded protein, ganglioside-induced differentiation-associated-protein 1 (GDAP1), is expressed both in the cytoplasm of myelinating Schwann cells and in axonal fibers (Niemann et al., 2005). It belongs to a subfamily of glutathione-S-transferases (GSTs) and contains two GST domains with one at the N-terminal and one at the C-terminal region (Cassereau et al., 2011). GDAP1 also contains a single transmembrane domain at the C-terminal and is attached to the outer mitochondrial membrane (Cassereau et al., 2011). Recent reports suggest that GDAP1 increases intracellular glutathione and mitochondrial membrane potential (Noack et al., 2012), and that mutations disrupting its mitochondrial targeting and/or its GST activity have been linked to CMT4A pathogenesis (Kabzinska et al., 2011; Noack et al., 2012). In addition, GDAP1 depletion inhibits mitochondrial fission (Niemann et al., 2005), which suggests that dysregulated mitochondrial dynamics may also be a pathogenic mechanism causing CMT4A.

1.3.7. Myotubularin-related proteins 2 and 13, MTMR2 and MTMR13 (CMT4B1 and CMT4B2)

CMT4B is a severe form of autosomal recessive demyelinating CMT with patients typically presenting symptoms as early as during childhood and become wheelchair-bound in the third decade (Quattrone et al., 1996). CMT4B has been mapped to two genetic loci, chromosome 11q22 and 11p15, and subsequent genetic studies have identified mutations in the genes *mtmr2* and *mtmr13* to cause CMT4B1 and CMT4B2,

respectively (Azzedine et al., 2003; Bolino et al., 2000a; Conforti et al., 2004; Hirano et al., 2004; Senderek et al., 2003b). Histological studies of nerve biopsies from human CMT4B patients showed demyelination and focally folded myelin (Quattrone et al., 1996), which has been described as the pathological hallmark of CMT4B. Whole-body and Schwann cell-specific *Mtmr2* and *mtmr13* knockout mice have subsequently been generated as mouse models of CMT4B1 and CMT4B2, respectively, which closely resembles the pathology seen in CMT4B patients (Bolino et al., 2004; Bolis et al., 2005; Robinson et al., 2008; Tersar et al., 2007). These studies indicate that a loss-of-function in *mtmr2* and *mtmr13* could contribute to CMT4B pathogenesis.

The encoded proteins, myotubularin-related proteins 2 and 13 (MTMR2 and MTMR13), belong to the family of myotubularin-related proteins that consists of 14 members that have conserved orthologues across all eukaryotes (Robinson and Dixon, 2006). MTMR2 contains active phosphatase activity that converts phosphoinositol-3,5-bisphosphate (PI3,5P2) to phosphoinsoitol-5-phosphate (PI5P) and phosphoinositol-3-phosphate (PI3P) to phosphoinositide (PI), whereas MTMR13 is inactive but forms a molecular complex with MTMR2 and facilitates its phosphatase activity (Robinson and Dixon, 2005). MTMR2 depletion in cells causes the accumulation of PI3P in endosomes and blocks the endosome-to-lysosome trafficking of cargoes (Cao et al., 2008), which suggests that disruption of phosphoinositide metabolism and endocytic trafficking could be involved in the pathogenesis of demyelinating CMT4B.

1.3.8. SH3 domain and Tetratricopeptide repeats-Containing protein 2, SH3TC2 (CMT4C)

CMT4C is an early onset, severe form of autosomal recessive demyelinating CMT, characterized by scoliosis, delayed age of walking, motor and sensory weakness, and muscle wasting (Senderek et al., 2003a). Nerve biopsies from CMT4C patients demonstrate severe demyelination and the presence of onion bulbs characteristic of demyelinating CMT (Gabreels-Festen et al., 1992; Houlden et al., 2009b; Kessali et al., 1997; Senderek et al., 2003a). Genetic studies have mapped CMT4C to chromosome 5q31-q33 (Guilbot et al., 1999; LeGuern et al., 1996), and further genetic studies have identified mutations in a protein called SH3 domain and tetratricopeptide repeats-containing protein 2 (SH3TC2) to cause CMT4C (Senderek et al., 2003a). A SH3TC2-null mouse was generated that recapitulated the neurological phenotypes of CMT4C as well as the pathological features seen in human patients including hypomyelination and widened node of Ranvier (Arnaud et al., 2009), which suggests that CMT4C-associated mutations cause a loss-of-function in SH3TC2. Cellular studies have found that CMT4C-associated mutations cause SH3TC2 to dissociate from its binding partner Rab11 and to mislocalize from recycling endosomes (Lupo et al., 2009; Roberts et al., 2010). This mislocalization causes a loss-of-function of SH3TC2 in promoting the recycling of cargoes (Roberts et al., 2010; Stendel et al., 2010), which suggests that dysfunction in the recycling endosome pathway could contribute to demyelinating CMT pathogenesis.

1.3.9. N-myc Downstream Regulated 1, NDRG1 (CMT4D)

Autosomal recessive mutations in the *NDRG1* gene located at chromosome 8q24.3 cause a demyelinating motor and sensory neuropathy known as CMT4D (Kalaydjieva et al., 2000). Two CMT4D-linked mutations in *NDRG1* have been identified to date: a truncation mutation responsible for the majority of CMT4D, and a rare mutation that affects splicing and results in the skipping of exon 9 of the *NDRG1* gene (Hunter et al., 2003; Kalaydjieva et al., 2000). Schwann cell dysfunction in CMT4D patients is evident by extensive demyelination and onion bulb formation as well as the presence of pleomorphic inclusions in Schwann cells cytoplasm and Schmidt-Lanterman incisures (Baethmann et al., 1998; Butinar et al., 1999; Kalaydjieva et al., 1998; King et al., 1999). However, axonal involvement in nerves of CMT4D patients is also seen by early and severe axonal loss and the presence of intra-axonal inclusions (Baethmann et al., 1998; King et al., 1999), suggesting that axonal degeneration could be a part of the primary defects in CMT4D.

The encoded protein, N-myc Downstream Regulated 1 (NDRG1), is a ubiquitously expressed protein of unknown function. Sequence analyses of NDRG1 have identified putative binding sites to phosphopantetheine and to inositol 1,4,5-triphosphate (Kokame et al., 1996), and recent studies have suggested a role of NDRG1 in cell trafficking including the recycling of E-cadherin (Kachhap et al., 2007). Although the function of NDRG1 remains controversial, its importance in Schwann cell function is supported by the fact that *NDRG1* knockout mice showed extensive demyelination (King et al., 2011; Okuda et al., 2004). This suggests that demyelination in CMT4D is likely caused by a loss-of-function mechanism.

1.3.10. Periaxin, PRX (CMT4F)

Autosomal recessive truncation mutations of the *PRX* gene located at chromosome 19q13.1-13.3 causes a early-onset but slowly progressive demyelinating neuropathy known as CMT4F (Guilbot et al., 2001; Kabzinska et al., 2006; Marchesi et al., 2010). Sural nerve biopsy from CMT4F patients showed onion bulb formation and abnormal myelin folding (Guilbot et al., 2001), and loss of the *PRX* gene in mice also showed peripheral demyelinating neuropathy and pathological features that were similar to those in CMT4F patients (Gillespie et al., 2000). The encoded protein, periaxin, is expressed at abaxonal membrane in myelinating Schwann cells adjacent to axons (Gillespie et al., 1994; Scherer et al., 1995) where it interacts with the dystroglycan complex through DRP2 to link the Schwann cell cytoskeleton to the basal lamina (Marchesi et al., 2010). Periaxin is required for the formation of abaxonal domain of Schwann cells, or Cajal bands, that are necessary for the elongation of Schwann cells during myelination (Court et al., 2004; Marchesi et al., 2010). The loss of periaxin function in *PRX*-null mice demonstrates a loss of compartmentalization of myelinating Schwann cells and decreased internodal length (Court et al., 2004), suggesting a similar mechanism may be involved in causing demyelinating CMT4F.

1.3.11. FYVE, RhoGEF, and PH-domain containing protein 4, FRABIN (CMT4H)

An autosomal recessive form of demyelinating CMT known as CMT4H was mapped to chromosome 12p11.21-q13.11 (De Sandre-Giovannoli et al., 2005). Subsequent genetic

studies have identified mutations in the *FGD4* gene encoding the Rho GDP/GTP exchange factor named FGD1-related F-actin binding protein (FRABIN) to cause CMT4H (Delague et al., 2007; Fabrizi et al., 2009; Houlden et al., 2009a). These mutations cause a truncation of FRABIN which results in the loss of the two pleckstrin homology (PH) domains and the cysteine-rich FYVE domain (Delague et al., 2007). It was reported that over-expression of the wild-type FRABIN protein in schwannoma cells and other cell types causes the formation of filopodia-like microspikes, but expression of the mutant, truncated forms of FRABIN in these cells induce fewer microspikes and causes the induced microspikes to be abnormally curled (Delague et al., 2007). These studies suggest that mutations may cause a loss-of-function and a toxic gain-of-function in FRABIN. Interestingly, a number of PH domains have been implicated to specifically bind different types of phosphoinositides (Dowler et al., 2000), and the FYVE domain has been shown to bind to PI3P at the early endosomes in proteins such as Hrs and EEA1 (Kutateladze et al., 1999). It is possible that FRABIN participates in the recognition of phosphoinositides, suggesting that phosphoinositide homeostasis and recognition by cellular proteins could be important in the prevention of demyelinating neuropathies.

1.3.12. Polyphosphoinositide phosphatase, FIG4 (CMT4J)

Missense and truncation mutations in the human *FIG4* gene located on chromosome 6q21 were identified to cause the autosomal recessive form of demyelinating CMT known as CMT4J (Chow et al., 2007; Nicholson et al., 2011). An animal model of CMT4J was identified in mice with spontaneous mutation in the *FIG4* gene that causes abnormal

splicing and low expression level of the *FIG4* transcript (Chow et al., 2007), which results in severe tremor and abnormal gait in these mice. *FIG4* encodes a phosphoinositide phosphatase that cleaves PI3,5P2 to PI3P, and the loss of FIG4 activity has been shown to cause the abnormal accumulation of PI3,5P2 (Chow et al., 2007). Studies performed in cell culture showed that both point mutations and truncations cause a loss-of-function in FIG4 phosphatase activity (Chow et al., 2007). Together with findings from animal studies, these results strongly suggest a loss-of-function in the *FIG4* gene to cause imbalance in phosphoinositide homeostasis which leads to a severe form of demyelinating neuropathy.

1.4. Are different forms of demyelinating CMT caused by common mechanisms?

While the above section illustrates the diversity of causative mutations in demyelinating CMT, some common pathogenic mechanisms shared by several subtypes of this disease are starting to emerge from these studies. The identification of common mechanisms and pathways could help develop novel therapeutic targets for correcting multiple subtypes of demyelinating peripheral neuropathies that share similar etiologies. Some of the common themes of demyelinating CMT pathogenesis are described below.

1.4.1. Accumulation of toxic misfolded proteins and aggregates

Protein misfolding not only can cause loss-of-function of the respective protein but can promote protein aggregation (Olzmann et al., 2008). These resultant misfolded proteins

and aggregates can form aberrant interactions with other cellular proteins to inhibit a wide variety of cellular functions (Olzmann et al., 2008). Recent reports indicate that CMT-linked mutations in proteins such as PMP22 (Fortun et al., 2006; Fortun et al., 2005; Myers et al., 2008) and MPZ (Mandich et al., 2009; Shames et al., 2003) cause protein misfolding and aggregation which suggests that the accumulation of these toxic species in Schwann cells could cause demyelinating neuropathy. Therefore, it is critical to examine whether CMT-linked mutations in other proteins expressed in Schwann cells such as SIMPLE could also promote their protein misfolding and aggregation, and whether up-regulation of protein quality control systems could ameliorate the toxicity caused by these misfolded proteins. A more detailed discussion of misfolded protein toxicity and protein quality control pathways can be found in Section 1.7.

1.4.2. Dysfunction in receptor trafficking and/or intracellular signaling

Since many of the demyelinating CMT-linked mutations are found in proteins regulating receptor trafficking and signaling such as MTMR2/MTMR13 (Berger et al., 2011; Cao et al., 2008) and SH3TC2 (Arnaud et al., 2009), it is possible that dysregulated endosomal trafficking and signaling of receptors is a shared mechanism leading to several subtypes of demyelinating CMT. In addition, CMT-linked mutations in lipid phosphatases such as FIG4 can also indirectly disrupt signaling events downstream of receptor activation (Bird et al., 1997; Quattrone et al., 1996). Together, these findings highlight the importance of identifying other demyelinating CMT-linked mutations that disrupt receptor sorting and signaling which could provide another common mechanism for causing demyelinating

CMT. Given that SIMPLE binds TSG101 (Shirk et al., 2005), a crucial component of the ESCRT machinery regulating endosome-to-lysosome sorting and turnover of receptors, it becomes crucial to investigate the possible effects of CMT-linked mutations in SIMPLE on receptor trafficking and signaling and whether these potential effects are responsible for the pathogenicity of SIMPLE mutations in causing peripheral neuropathy. A more detailed introduction of the cellular mechanisms controlling endocytic trafficking is outlined in Section 1.8.

1.4.3. Disruption of myelin structures and axon-Schwann cell interactions

Studies described above showed that a loss of proper synthesis and/or transport of myelin components, either due to mutations in myelin proteins or dysregulated pro-myelination signaling pathway such as the NRG1-ErbB3 pathway, can have detrimental effects on the structure of myelin and cause various types of demyelinating CMT (Nave and Salzer, 2006; Ogata et al., 2004; Quintes et al., 2010; Syed et al., 2010). Hence, it is important to examine whether CMT1C-linked mutations in SIMPLE could influence myelin structure by directly affecting myelin protein transport or by influencing NRG1-ErbB3 signaling to modulate myelin structure. Given that demyelination is also linked to secondary defects in axonal function and axonal degeneration, it is also crucial to determine whether the effects of SIMPLE mutations on myelin could in turn affect axon function and structure. A brief review of the known mechanisms regulating axon-Schwann cell communications can be found in Section 1.9.

1.5. Non-demyelinating types of Charcot-Marie-Tooth disease

A minority (~20%) of CMT cases that do not show reduction in conduction velocity (NCV > 38 m/s) are associated with primary axonal degeneration without significant demyelination and are classified as axonal degeneration type of CMT (Table 2). This axon degenerating type of CMT can be caused by mutations in axon-specific proteins such as neurofilament light chain (associated with axonal CMT2E) which prevents axon neurofilaments from assembling properly (Shy and Patzko, 2011). However, axonal type of CMT can also be caused by mutations in proteins expressed in multiple tissues outside of axons. Interestingly, mutations in proteins regulating the endocytic sorting pathway can cause demyelinating and/or axonal forms of CMT. As mentioned above, mutations in regulators of endocytic trafficking such as MTMR2 (Bolino et al., 2000a; Senderek et al., 2003b) and SH3TC2 (Gabreels-Festen et al., 1992; Kessali et al., 1997; Senderek et al., 2003a) cause demyelinating CMT. While SH3TC2 is only found in Schwann cells at the peripheral nerves (Stendel et al., 2010), MTMR2 is expressed in both Schwann cells and axons (Bolino et al., 2004), and it is unknown as to why mutations in MTMR2 cause demyelinating instead of axonal CMT. In contrast, mutations in Rab7, a late endosomal protein regulating endosome-to-lysosome trafficking (Vanlandingham and Ceresa, 2009) that is ubiquitously expressed in multiple tissues and cell types (Verhoeven et al., 2003), cause axonal CMT2B without signs of primary demyelination (Shy and Patzko, 2011). Meanwhile, mutations in dynamin 2, a protein found in multiple tissues that regulates membrane sorting and vesicle fusion and fission (Niemann et al., 2006), cause an intermediate axonal/demyelinating neuropathy known as DI-CMTB (Claeys et al., 2009). Although it is unknown as to why mutations in some genes expressed in both Schwann

cells and neurons cause a predominantly demyelinating or axonal disorder while others cause an intermediate phenotype, the fact that multiple genes implicated in endosomal trafficking are involved in CMT pathogenesis indicates an important role for endosomal trafficking in peripheral nerve function both in terms of myelination and axon maintenance.

Axonal CMT is also caused by dysfunctions in other cellular mechanisms and pathways. One such mechanism is dysregulation of mitochondrial dynamics, where mutations in mitofusin 2, a protein involved in mitochondrial fusion and tethering of mitochondria to the endoplasmic reticulum (Chen and Chan, 2005; Chen et al., 2005; Pizzo and Pozzan, 2007), causes axonal CMT2A (Shy and Patzko, 2011; Zuchner et al., 2004). These reports, together with studies showing that mutations in the GDAP1 protein regulating mitochondrial fission causing an intermediate form of CMT (Cassereau et al., 2011), implicate mitochondrial dysfunction as a common mechanism in axonal CMT pathogenesis. In addition, mutations in the *TRPV4* gene encoding the transient receptor potential cation channel, subfamily V, member 4 (TRPV4) increase the basal and maximum calcium channel activities and cause an autosomal dominant form of axonal CMT2C characterized by diaphragmatic weakness and vocal cord paresis (Deng et al., 2010; Shy and Patzko, 2011). Mice lacking *TRPV4* only present with a mild phenotype (Liedtke, 2005), which supports that CMT2C-linked mutations are toxic gain-of-function mutations affecting calcium homeostasis. Recent studies have also identified mutations in glycyl-tRNA synthetase (Antonellis et al., 2003; Shy and Patzko, 2011), tyrosyl-tRNA synthetase, lysyl-tRNA synthetase, and alanyl-tRNA synthetase (Jordanova et al., 2006; McLaughlin et al., 2012; McLaughlin et al., 2010) to cause axonal CMT neuropathy.

These studies suggest that axon function is dependent on aminoacyl-tRNA synthetases. Meanwhile, mutations in two heat shock proteins known as HSP27 and HSP22 cause axonal CMT2F and CMT2L, respectively, characterized by a predominantly motor phenotype (Evgrafov et al., 2004; Irobi et al., 2004). These mutations are mostly located within the α-crystallin domain which is responsible for the function of a variety of heat shock proteins; however, the role of these mutations in causing axonal CMT remains unknown and is currently under investigation (Shy and Patzko, 2011).

1.6. Treatment for Charcot-Marie-Tooth disease

No effective therapy currently exists for CMT, and current treatment includes pain medications and physical therapy that only targets symptoms of the disease. A therapeutic strategy currently under investigation involves the reduction of PMP22 synthesis by drugs such as ascorbic acid to prevent the accumulation of misfolded proteins in human patients (Pareyson and Marchesi, 2009; Patzko and Shy, 2011). Some drugs that have shown promise in cellular and animal studies include curcumin, a sarcoplasmic/ER calcium ATPase (SERCA) inhibitor, which decreases the amount of misfolded myelin proteins accumulated at ER to reduce the cytotoxicity of these misfolded proteins (Pareyson and Marchesi, 2009; Patzko and Shy, 2011). However, the development of potential therapeutics for CMT remains at a novice stage, and a better understanding of the pathogenesis of CMT may overcome the current limitations in designing additional therapies for these patients. As discussed in Sections 1.3 and 1.4, recent studies are starting to identify some of the common pathogenic mechanisms shared

by several subtypes of demyelinating CMT neuropathies, including 1) the accumulation of toxic misfolded proteins and their aggregates, 2) the dysfunction of receptor trafficking and/or signaling, and 3) the disruption of myelin structures and axon-Schwann cell communications. The identification of these common mechanisms could help develop novel therapeutic targets for treating several subtypes of demyelinating peripheral neuropathies that share similar etiologies. More thorough discussions of each mechanism are provided in Sections 1.7, 1.8, and 1.9.

1.7. Protein misfolding and protein quality control systems

1.7.1. Toxicity mediated by misfolded proteins and aggregates

Newly synthesized proteins by the cell are folded during its translation it exits the large subunit of ribosomes or post-translationally upon their targeting to the respective organelle (Hartl and Hayer-Hartl, 2009). Primary amino acid sequences provides the key molecular forces including hydrophilic interactions, collapse of hydrophobic sequences, and burial of electrostatic interactions, where proteins are spontaneously folded to their lowest free energy state typically corresponding to their native conformations (Dobson, 2003; Hartl and Hayer-Hartl, 2009; Olzmann et al., 2008). However, some proteins are kinetically trapped at incorrectly folded conformations, which can be caused by factors such as high levels of protein expression, missense mutations, and post-synthetic damage such as oxidative modifications (Dobson, 2003; Olzmann et al., 2008). Misfolded proteins not only are non-functional but are often prone to aggregation in the cytosol, and these misfolded proteins and their aggregates can form aberrant interactions with cellular

proteins to inhibit a wide range of cellular functions including proteasomal degradation (Olzmann et al., 2008). The accumulation of misfolded proteins and aggregates has been extensively implicated in the pathogenesis of a number of age-related neurodegenerative diseases including Parkinson disease, Alzheimer disease, and amyotrophic lateral sclerosis (Ross and Poirier, 2004). These findings underscore the importance of protein quality control systems to combat against the toxic build-up of misfolded proteins in cells.

1.7.2. Ubiquitin signaling

Ubiquitination is a post-translational modification that regulates many cellular pathways. It involves the conjugation of a 76-amino-acid-protein known as ubiquitin onto lysine residues of substrate proteins through several enzymatic steps (Figure 2) (Weissman, 2001). The E1 ubiquitin activating enzyme, through a cysteine residue, forms a thiol-ester bond with an ubiquitin monomer. E1 then recruits an E2 ubiquitin conjugating enzyme, where the ubiquitin is transferred to a cysteine residue of the E2. Finally, an E3 ubiquitin-protein ligase recruits the substrate protein and the E2 and catalyses the final step of substrate ubiquitination by transferring the ubiquitin to a lysine residue of the substrate protein. Substrates can be monoubiquitinated by a single ubiquitin or multi-monoubiquitinated if multiple sites of the substrate are monoubiquitinated (Komander, 2009; Weissman, 2001). In addition, the seven lysine residues of ubiquitin can conjugate additional ubiquitin moieties to form linkage-specific polyubiquitin chains that allow substrates to be polyubiquitinated (Komander, 2009). Substrate-conjugated ubiquitin can

be detached by deubiquitinating enzymes (DUBs) which allow ubiquitin to serve as a reversible signal (Reyes-Turcu et al., 2009; Weissman, 2001).

Proteins containing ubiquitin-binding domains (UBDs) are ubiquitin receptors that recognize distinct types of ubiquitination and transduce these signals accordingly (Figure 2) (Li and Ye, 2008). Monoubiquitination has a non-proteasome role in signaling gene transcription, DNA repair, and endocytosis of cargoes (Sigismund et al., 2004). Lysine 48 (K48)-linked polyubiquitination is the canonical signal for proteolysis by the proteasome (Pickart, 1997). Although the signaling roles of other polyubiquitin linkages are less clear, recent data indicates that all linkages except Lysine 63 (K63) signal substrates for proteasome degradation (Xu et al., 2009), while K63-linked polyubiquitination have diverse signaling roles in processes such as DNA repair, inclusion body formation, endosome-to-lysosome trafficking, and autophagy (Lauwers et al., 2009; Olzmann et al., 2007; Spence et al., 1995; Tan et al., 2008).

1.7.3. Ubiquitin-proteasome system

Misfolded proteins may be refolded by molecular chaperones (Bukau et al., 2006); but when refolding is not possible, the ubiquitin-proteasome system serves as a major proteolytic pathway that degrades misfolded proteins (Goldberg, 2003). In this system, misfolded proteins are recognized by E3 ligases and are covalently attached to a polyubiquitin chain (Ciechanover, 2006). These polyubiquitinated proteins are then recognized by UBDs at the 19S proteasome cap complex which causes degradation of substrates into small peptides by proteolytic enzymes within the barrel-shaped 20S

proteasome core (Ciechanover, 2006). The polyubiquitin chain is detached from the substrate protein prior to entering the 20S proteasome core and is recycled by deubiquitinating enzymes as free ubiquitin (Ciechanover, 2006). The importance of the ubiquitin-proteasome system in degrading toxic misfolded proteins has been implicated in many neurodegenerative diseases (Ciechanover, 2003).

1.7.4. ER-associated degradation (ERAD)

Unfolded or misfolded proteins at the ER may be targeted for degradation via a process known as ER-associated degradation (ERAD) (DeLaBarre et al., 2006). In this pathway, unfolded or misfolded proteins are recognized by chaperones and associated factors such as heat shock protein 70-family members, calnexin and calreticulin, and protein disulphide isomerases (Vembar and Brodsky, 2008). These misfolded proteins are then retrotranslocated to the cytoplasm by a mechanism that is dependent on energy derived from ATP hydrolysis by the AAA-ATPase p97/VCP (DeLaBarre et al., 2006; Vembar and Brodsky, 2008). Once retrotranslocated, they are ubiquitinated by E3 ligases and are targeted to the proteasome for degradation (DeLaBarre et al., 2006; Vembar and Brodsky, 2008). ERAD dysfunction and accumulation of misfolded proteins at the ER can trigger unfolded protein response, which has been linked to a variety of diseases including neurological disorders (Olzmann et al., 2008).

1.7.5 Aggresome-autophagy pathway

The ubiquitin-proteasome system only degrades monomeric misfolded proteins but not protein aggregates. When misfolded proteins and their aggregates accumulate, proteasome function may be inhibited which causes further build up of these toxic species in cells (Olzmann et al., 2008). One important cellular mechanism for handling these misfolded proteins and aggregates is to target them via microtubule-dependent retrograde transport to a perinuclear organelle known as the aggresome (Garcia-Mata et al., 2002; Kopito, 2000). Once arriving at the aggresome, toxic protein aggregates are sequestered away from the cytosol in a cage consists of the intermediate filament vimentin to protect the cell from further damage (Garcia-Mata et al., 2002; Olzmann et al., 2008). Accumulating evidence support that the targeting of disease-linked misfolded proteins such as mutant huntingtin to aggresomes is cytoprotective (Arrasate et al., 2004; Gutekunst et al., 1999; Tompkins and Hill, 1997), thus supporting aggresome targeting as a crucial mechanism for the cell to combat against misfolded protein toxicity.

Recent studies suggest that aggresomes also act as a stage to facilitate the degradation of its contents by autophagy (Olzmann et al., 2007; Taylor et al., 2003). Autophagic degradation involves the formation of a double-membrane vesicular organelle known as autophagosome that engulfs a portion of cytoplasm containing damaged proteins and organelles (Mizushima, 2007). Upon autophagosome fusion with lysosomes, the internal cytoplasm-derived material is degraded by lysosomal hydrolases (Mizushima, 2007). Although initially thought as a non-selective degradation system, current views indicate that autophagic degradation is a highly selective process, with adaptor proteins such as NBR1 and p62 that recruit ubiquitinated protein aggregates and/or aggresome-like inclusions to autophagosomes for degradation by autophagy

(Johansen and Lamark, 2011). The role of autophagy in selectively degrading misfolded proteins and aggregates within aggresomes is supported by the fact that aggresomes are surrounded by the autophagosome marker LC3 and tightly juxtapose lysosomes (Fortun et al., 2003; Olzmann and Chin, 2008). This aggresome-autophagy pathway may be particularly important in degrading misfolded proteins and aggregates in the peripheral nervous system, as the impairment of aggresome targeting by drugs such as vincristine, cisplatin and docetaxel and inhibition of autophagosome-lysosome fusion by chloroquine can all induce peripheral neuropathies (Weimer and Podwall, 2006; Weimer and Sachdev, 2009).

1.8. Regulation of endocytic trafficking

Endocytic trafficking is crucial to the function and survival of all eukaryotic cells (Figure 3). Cell surface receptors and other membrane-bound proteins are endocytosed either constitutively or induced by post-translational modifications such as phosphorylation and ubiquitination and are then targeted to the early endosome. Once arriving at the early endosome, the endocytosed membrane proteins are either deubiquitinated by DUBs and recycled to the cell surface or remained ubiquitinated and sorted to intralumenal vesicles of multivesicular bodies (MVBs) for delivery to the lysosome for degradation (Katzmann et al., 2002). The sorting of these ubiquitinated cargoes to the intralumenal vesicles of MVBs require their recognition by the ESCRT machinery composed of ESCRT-0, -I, -II, and –III protein complexes (Figure 4) (Roxrud et al., 2010). Biophysical and cellular studies have provided evidence that supports K63-linked polyubiquitination as the

specific signal recognized by the UBDs of ESCRTs (Lauwers et al., 2009; Ren and Hurley, 2010). Reports have also described the subdivision of labor of ESCRTs. Specifically, subunits of ESCRT-0 (Hrs, STAM), ESCRT-I (TSG101, MVB-12), and ESCRT-II (EAP45) contain UBDs and bind ubiquitinated cargoes cooperatively to localize them in place at the endosome membrane, whereas ESCRT-III alters the curvature of the membrane and mediates the abscission process to form internal vesicles of MVBs (Figure 4) (Raiborg and Stenmark, 2009; Roxrud et al., 2010). Subunits of ESCRTs containing UBDs are found to be ubiquitinated in cells (Figure 4), which could be a regulatory mechanism for cargo recognition and sorting (Amit et al., 2004; Hoeller et al., 2007; Katz et al., 2002; Kim et al., 2007; McDonald and Martin-Serrano, 2008; Miller et al., 2004; Tsunematsu et al., 2010). The release of ESCRTs from the endosome membrane has also been attributed to the VPS4 complex, where ESCRTs are recycled for additional cargo sorting events (Raiborg and Stenmark, 2009; Roxrud et al., 2010). Depletion of ESCRT subunits inhibits the formation of multivesicular bodies, causes endosomal enlargement, and blocks endosome-to-lysosome transport of cargo proteins (Babst et al., 2000; Bache et al., 2004; Doyotte et al., 2005; Kanazawa et al., 2003; Razi and Futter, 2006), indicating that ESCRTs are essential for maintaining proper morphology and sorting function of endosomes. Dysfunctions in ESCRTs have been implicated in numerous diseases including tumorigenesis and neurodegeneration (Stuffers et al., 2009), indicating the importance of this process in normal physiology and pathology. However, molecular mechanisms that control the temporal and spatial aspects of ESCRT function, such as the recruitment of these complexes to the early endosome

membrane, are poorly understood, and the roles of ESCRT dysfunction in human diseases remain to be further explored.

1.9. Cellular mechanisms regulating axon-Schwann cell communication

Schwann cells and axons work as a cohesive unit, and theirs functions are interdependent on each other. Disrupted Schwann cell functions in demyelinating diseases such as CMT often cause a secondary degeneration of axons, and axon damage and degeneration can in turn cause myelin degeneration. Therefore, in the context of demyelinating neuropathies such as CMT1C, it is crucial to determine whether the primary defect occurs at Schwann cells or as a secondary effect of disrupted axonal functions. If problems in Schwann cells are truly causative for the observed demyelination, it would also be important to examine how the secondary effects of Schwann cell defects contribute to axonal problems such as decreased conduction of action potentials, disruption of axonal transport of intracellular organelles, and axonal degeneration, all of which are components of demyelinating CMT (Pareyson and Marchesi, 2009; Patzko and Shy, 2011). Although researchers have known the importance of axon-Schwann cell communication in regulating the peripheral nervous system, very little is known about the mechanisms as to how this communication occurs and how its dysregulation could be responsible for peripheral neuropathies. In this section, I have provided a review of the currently known mechanisms in this process. In addition, how CMT-linked mutations in a protein called SIMPLE could affect this process will be examined and discussed in Chapters 3, 4 and 5.

1.9.1. NRG1-ErbB receptor signaling pathway determines myelin sheath thickness

Axons actively provide signals for recruiting Schwann cells for myelination (Aguayo et al., 1976; Weinberg and Spencer, 1976) and help match myelin sheath thickness to axon caliber (Nave and Trapp, 2008; Quintes et al., 2010). NRG1 type III, a signaling protein synthesized by the axon which contains an epidermal-growth-factor-like signal domain that activates ErbB receptors on Schwann cells, has been identified as the essential axonal signal controlling myelin sheath thickness (Nave and Trapp, 2008; Quintes et al., 2010). Upon NRG1 binding, ErbB2 and ErbB3 receptors in Schwann cells form heterodimers, undergo receptor cross-phosphorylation, and cause the activation of downstream signaling pathways including the ERK1/2 and Akt pathways (Birchmeier, 2009; Nave and Salzer, 2006; Quintes et al., 2010). This NRG1-dependent activation of the ERK1/2 and Akt signaling pathways is essential for the proper formation of myelin to ensheath peripheral axons in animal models and *in vitro* Schwann cell-neuronal co-cultures (Nave and Salzer, 2006; Ogata et al., 2004; Quintes et al., 2010; Syed et al., 2010), and dysregulation of these pathways has been linked to a number of demyelinating diseases including demyelinating CMT. The loss of MTMR2 and MTMR13 associated with demyelinating CMT4B1 and CMT4B2, respectively, cause abnormal prolonged Akt signaling in *MTMR2* and *MTMR13* knockout mice (Berger et al., 2011). Moreover, the sustained activation of ErbB2 receptor and the downstream ERK1/2 pathway by leprosy-causing *Mycobacterium leprae* causes demyelination in mice and *in vitro* (Tapinos et al., 2006). Therefore, properly regulated Schwann cell receptor signaling mediated by axonal NRG1 is essential for the maintenance of myelination in the peripheral nervous system.

1.9.2. The effects of myelinating Schwann cells on axon caliber

In the peripheral nerves, unmyelinated axonal segments, such as the non-myelinated stem process of large-sized dorsal root ganglion neuronal axons and the nodes of Ranvier, have reduced axonal diameter in comparison to adjacent myelinated segments (Martini, 2001). The non-myelinated segments demonstrate decreased neurofilament phosphorylation, and the neurofilaments are more densely packed and are also fewer in absolute number when compared to myelinated axon segments (Hsieh et al., 1994). These observations led to the hypothesis that myelination by Schwann cells modify axonal properties and functions. A series of studies by Brady and colleagues (de Waegh and Brady, 1990; de Waegh et al., 1992; Witt and Brady, 2000) tested this hypothesis using allografts from PMP22 mutant Trembler (Tr) mice as bridges to connect proximal and distal stumps of transected nerves in wild-type mice. Wild-type axons are then myelinated by PMP22 mutant Schwann cells as they regenerate through the graft. These studies found that the initially healthy wild-type axons, when surrounded by mutant PMP22 Schwann cells with focal demyelination, demonstrate higher neurofilament densities, low phosphorylation level of neurofilaments, and a marked reduction in axonal caliber. In addition, the distal, host-derived part of the nerves myelinated by wild-type Schwann cells demonstrated normal axonal caliber and other axonal properties. These results were further supported by studies in demyelinating CMT caused by mutations in Schwann cell-specific proteins such as PMP22, MPZ, and Cx32, where dysfunction in myelin proteins not only demonstrate myelination defects but also reductions of axonal caliber (Martini, 2001). Taken together, these reports strongly demonstrated a role for myelination by Schwann cells in regulating axonal caliber.

Factors in Schwann cells regulating axonal caliber remain largely unknown. One potential axon-regulating Schwann cell factor is myelin-associated glycoprotein (MAG) localized to the Schwann cell-axon interface of myelinated nerve fibers (Martini, 2001). MAG-deficient mice, while developing normal myelin architecture during the first month of life, show demyelination and axonal degeneration as the animals age (Carenini et al., 1997; Fruttiger et al., 1995; Yin et al., 1998). These mice demonstrate paranodal infolded and outfolded myelin sheath associated with decreased axonal calibers (Yin et al., 1998). Similar abnormalities were also seen at the paranodes and Schmidt-Lanterman incisures in mice deficient of PMP22, P0, MTMR2, or MTMR13 (Bolino et al., 2004; Bolis et al., 2005; Martini, 2001; Robinson et al., 2008; Tersar et al., 2007), suggesting that myelin at these regions are particularly susceptible to molecular changes that lead to the observed pathology in myelination and axon caliber. Additional studies will be needed to identify other Schwann cell factors that regulate axonal caliber and function.

Hypotheses and goals of this dissertation

In this dissertation, I have undertaken the study of a relatively rare form of autosomal dominant demyelinating CMT (1% to 2% of all demyelinating CMT cases) caused by mutations in SIMPLE in hope of gaining a better overall understanding of the convergent pathogenic mechanisms in demyelinating peripheral neuropathies. Through studying this disease, I also hope to provide novel insights to the basic biological processes governing normal cellular and molecular functions within and outside of the peripheral nervous system. **My overall hypothesis:** SIMPLE is an early-endosomal protein that regulates

ESCRT-mediated endosome-to-lysosome trafficking, and mutations disrupt this process by causing the misfolding of SIMPLE protein which ultimately affect Schwann cell functions and lead to demyelinating CMT1C neuropathy. Specific hypotheses of this dissertation are listed below:

1) I hypothesize that CMT1C-linked mutations cause protein misfolding and aggregation of SIMPLE. Recent reports suggest that PMP22 and MPZ misfolding and aggregation are contributing factors to demyelinating neuropathy, which suggest that mutations in other CMT-linked proteins such as SIMPLE may also induce misfolding and aggregation to cause demyelinating neuropathy. In Chapter 2, we characterized the localization of the SIMPLE protein and performed a comprehensive examination of the effects of CMT1C-linked mutations on SIMPLE protein stability, localization, aggregation, and degradation. My findings reveal that SIMPLE is an early endosome membrane protein and indicate that CMT1C-linked mutations not only disrupt the association of SIMPLE to the early endosomal membrane, but also promote SIMPLE protein aggregation and degradation by protein quality control pathways such as the proteasome and the aggresome-autophagy pathways that protect cells against build-up of misfolded proteins and aggregates. The implications of our findings in the pathogenesis and treatment of demyelinating CMT are discussed in Chapters 2 and 5.

2) I hypothesize that SIMPLE is a regulator of ESCRT-mediated endosome-to-lysosome trafficking, and that CMT1C-linked mutations disrupt this process. Since SIMPLE is an endosomal protein (Chapter 2) that interacts with the ESCRT-I subunit TSG101 (Shirk et

al., 2005), SIMPLE could be a novel regulator of the endosome-to-lysosome trafficking pathway. This hypothesis was tested in Chapter 3 where we found that SIMPLE interacts and colocalizes not only with TSG101 but also with ESCRT proteins STAM1 and Hrs on the early endosome. I also examined the role of SIMPLE in regulating ESCRT functions and found that SIMPLE is crucial for recruiting ESCRTs to the membrane and for the endosome-to-lysosome trafficking and degradation of ErbB receptors. I then examined CMT1C-linked SIMPLE mutant proteins and found that they are loss-of-function mutants acting in a dominant-negative manner to inhibit wild-type SIMPLE function in degrading ErbB3 receptor in Schwann cells. This inhibition of ErbB3 receptor degradation results in prolonged activation of the downstream ERK1/2 signaling pathway upon NRG1 binding. Interestingly, a prolonged activation of the ERK1/2 pathway has recently been implicated in causing demyelination (Nave and Salzer, 2006; Ogata et al., 2004; Quintes et al., 2010; Syed et al., 2010). Together, these results suggest that the dysregulation of ErbB receptor degradation and signaling caused by SIMPLE mutations contributes to demyelinating neuropathies. These results and their implications in the pathogenesis and treatment of CMT are further discussed in Chapters 3 and 5.

3) I hypothesize that CMT1C-linked SIMPLE mutations disrupt Schwann cell functions in myelinating axons and lead to demyelinating neuropathy. Chapters 2 and 3 show that SIMPLE is enriched in peripheral nerves and Schwann cells and that SIMPLE mutations cause CMT1C via toxic gain-of-function and/or dominant-negative mechanisms in cells. In Chapter 4, we further explored SIMPLE localization in the peripheral nervous system and found that it is specifically expressed in the Schwann cell cytoplasm but not in axons,

suggesting that the peripheral neuropathy caused by SIMPLE mutations can be attributed to primary Schwann cell dysfunction rather than primary defects in the axons. Given that CMT1C is an autosomal-dominant disease, we examined the effects of a CMT1C-linked mutation *in vivo* by generating transgenic mice expressing a pathogenic CMT1C-linked SIMPLE mutant protein. Mice expressing mutant SIMPLE develop a progressive motor and sensory neuropathy that recapitulates some of the key clinical features of CMT1C, including behavioral impairments, nerve conduction defects, and myelin pathology. We also found that the myelin pathology of these mice is associated with secondary reduction in axonal caliber, disrupted axonal transport, and signs of axonal degeneration. These findings suggest that CMT1C-linked SIMPLE mutation causes demyelinating neuropathy associated with secondary axonal defects and provide evidence that primary dysfunctions in Schwann cell can induce secondary axonal defects and degeneration. Discussions of these results and their implications in the pathogenesis and treatment of CMT are found in Chapters 4 and 5.

Taken together, the findings described in this dissertation indicate that SIMPLE is an early endosomal protein enriched in the Schwann cell cytoplasm that functions with the ESCRT machinery to regulate the endosome-to-lysosome trafficking and signaling of ErbB receptors. CMT1C-linked SIMPLE mutations disrupt the membrane association of SIMPLE, promote its aggregation and turnover by protein quality control pathways, and inhibit SIMPLE function in regulating the sorting of ErbB receptors and down-regulation of its downstream signaling. Moreover, CMT1C-linked SIMPLE mutation causes a late-onset dysmyelinating neuropathy with secondary axonal dysfunction and degeneration.

These findings provided new understanding to the pathogenic mechanisms of CMT1C-linked SIMPLE mutations in causing peripheral neuropathy and have yielded significant insights into the cellular mechanisms involved in the control of endosomal trafficking and receptor signaling as well as mechanisms mediating the communications between axons and Schwann cells in the peripheral nervous system.

Demyelinating CMT (~80%)			
Disease Type	**Gene/Locus**	**Inheritence**	**Encoded protein function**
CMT1A	*PMP22*	AD (some AR)	Peripheral myelin protein
HNPP	*PMP22*	AD	Peripheral myelin protein
CMT1B	*MPZ*	AD (some AR)	Peripheral myelin protein
CMT1C	*SIMPLE*	AD	Unknown
CMT1D	*EGR2*	AD	Transcription factor regulating myelin protein expression
CMT1X	*GJB1/CX32*	X-linked dominant	Gap junction
CMT4A	*GDAP1*	AR	Unknown, but implicated in mitochondrial function and fission
CMT4B1	*MTMR2*	AR	Phosphoinositide phosphatase
CMT4B2	*MTMR13*	AR	Phosphoinositide phosphatase
CMT4C	*SH3TC2*	AR	Regulation of the recycling pathway
CMT4D	*NDRG1*	AR	Unknown, putative binding sites for phosphoinositides
CMT4E	*EGR2*	AR	Transcription factor regulating myelin protein expression
CMT4F	*Periaxin*	AR	Unknown, binds to dystroglycan complex at the abaxonal domain
CMT4H	*FGD4/FRABIN*	AR	Unknown, binds to phosphoinositides
CMT4J	*FIG4*	AR	Phosphoinositide phosphatase

Table 1. Identified genes and proteins associated with demyelinating CMT. AD, autosomal dominant; AR, autosomal recessive.

Axonal CMT (~20%)			
Disease Type	**Gene/Locus**	**Inheritence**	**Encoded protein function**
CMT2A	*MFN2*	AD	Mitochondrial fusion
CMT2B	*RAB7*	AD	Endosomal sorting
CMT2C	*TRPV4*	AD	Transient receptor potential cation channel
CMT2D	*GARS*	AD	Glycyl-tRNA synthetase
CMT2E	*NEFL*	AD	Neurofilament light chain
CMT2F	*HSP27*	AD	Unknown, Heat shock protein
CMT2G	12q12-q13.3	AD	Unknown
CMT2L	*HSP22*	AD	Unknown, Heat shock protein
HMNSP	3q13.1	AD	Unknown
AR CMT2A	*LMNA*	AR	Nuclear structure and function
AR CMT2B	19q13.1-13.3	AR	Unknown
DI-CMTA	10q24.1-25.1	AD	Unknown
DI-CMTB	*DNM2*	AD	Vesicular transport and function
DI-CMTC	*YARS*	AD	Tyrosyl-tRNA synthetase
Unnamed	*KARS*	AD	Lysyl-tRNA synthetase
Unnamed	*AARS*	AD	Alanyl-tRNA synthetase

Table 2. Identified genes and proteins associated with axonal CMT. AD, autosomal dominant; AR, autosomal recessive.

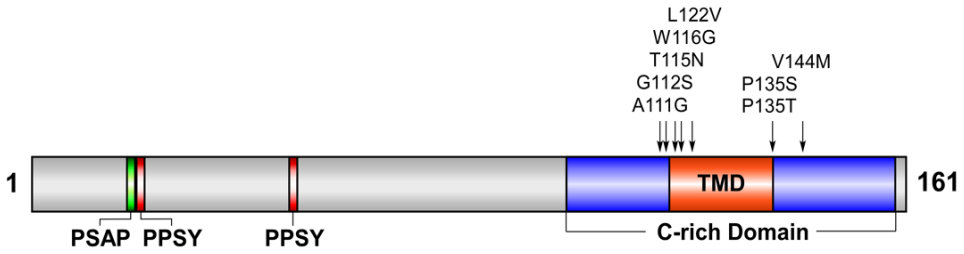

Figure 1. Domain structure of SIMPLE. The locations of the cysteine-rich (C-rich) domain, putative transmembrane domain (TMD), PSAP motif interacting with the ubiquitin E2 variant (UEV) domain of TSG101, PPSY motifs interacting with the WW domains of NEDD4, and the disease-linked mutations are indicated.

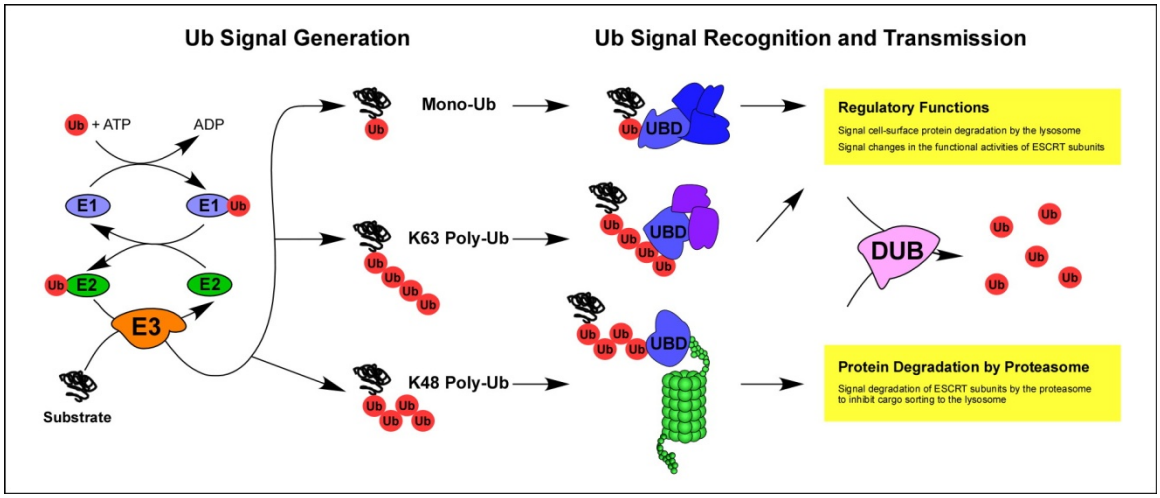

Figure 2. Ubiquitin-mediated signal transduction: signal generation, recognition, and transmission. Ubiquitin (Ub) signals are generated by the sequential actions of ubiquitin-activating enzyme (E1, light blue), ubiquitin-conjugating enzymes (E2, green), and ubiquitin-protein ligases (E3, orange), where the E3 ligases determine specificity of the substrates to be ubiquitinated. Substrates can either be conjugated with monomeric ubiquitins (monoubiquitination, or mono-Ub) or with ubiquitin chains (polyubiquitination, or poly-Ub). Ubiquitin chains can be formed via one of several lysine residues of ubiquitin, with lysine-48-linked polyubiquitin (K48 poly-Ub) and lysine-63-linked polyubiquitin (K63 poly-Ub) chains being the best characterized. These different types of ubiquitination are preferentially recognized by different ubiquitin receptors via ubiquitin-binding domains (UBDs, blue), which transmit ubiquitin signals to different functional consequences. Specifically, monoubiquitination and K63-linked polyubiquitination signal changes in the functional activities, trafficking, and protein-protein interactions of substrates, whereas K48-linked polyubiquitination targets substrates to the 26S proteasome for degradation. Ubiquitin signaling is a reversible process that is also regulated by numerous deubiquitinating enzymes (DUBs, pink),

which serve to hydrolyze ubiquitin from substrates to subvert ubiquitin signaling. In addition, some DUBs are also responsible for removing ubiquitin from substrates prior to their destruction by the proteasome and the lysosome, thus maintaining the free ubiquitin pool to allow subsequent signaling events to occur.

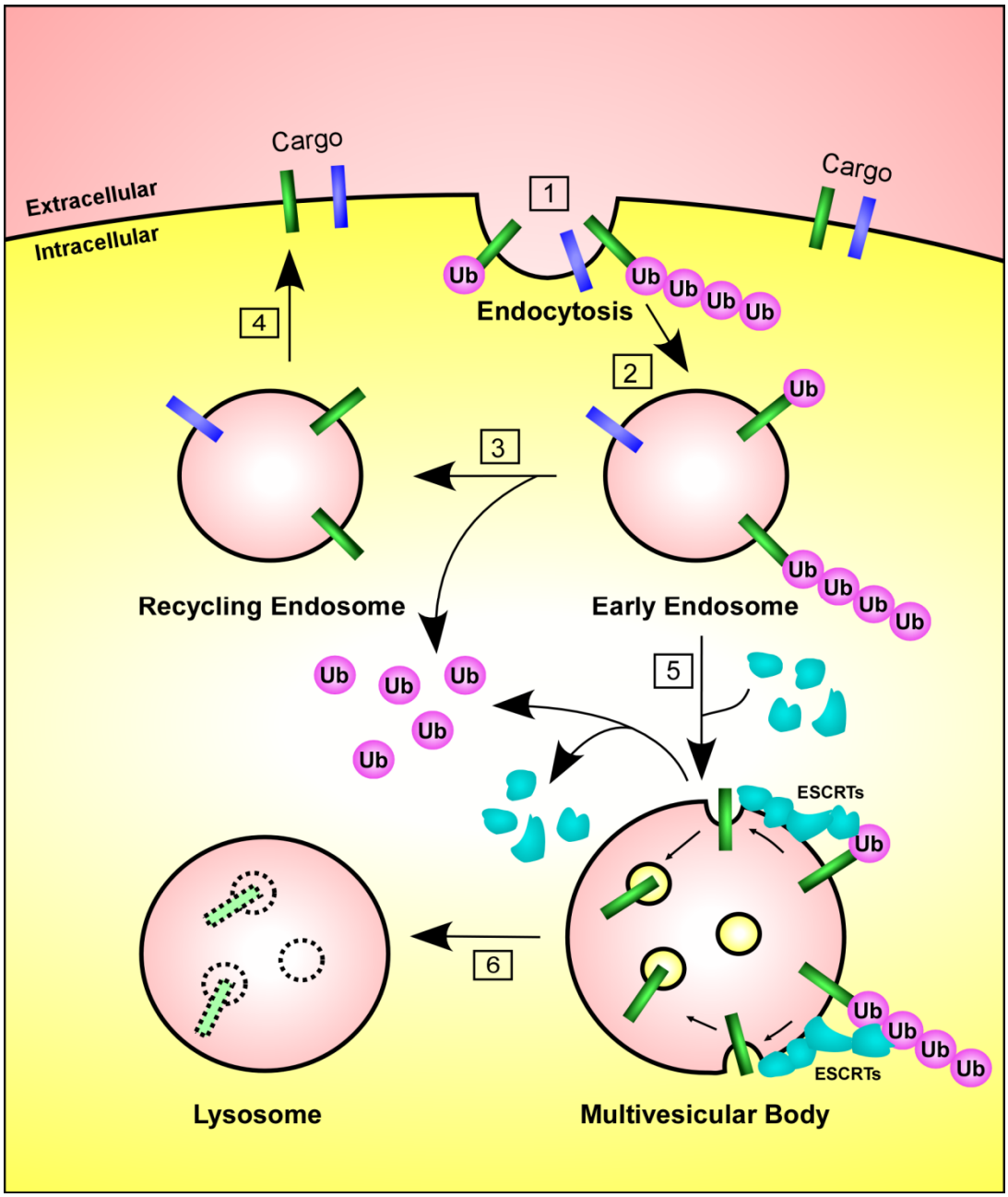

Figure 3. Endocytic trafficking of cargo proteins. Endocytosis of a variety of membrane proteins from the cell surface involves ubiquitin-dependent (green cargo) and -independent (yellow cargo) mechanisms (Step 1). These endocytosed cargoes are subsequently sorted to the early endosome (Step 2). At the early endosome, some cargoes are deubiquitinated and are targeted to the recycling endosomes (Step 3), where

they escape lysosomal degradation and eventually resurface on the cell surface (Step 4). Other cargoes, however, remain ubiquitinated and are recognized by several protein complexes known as Endosomal Sorting Complexes Required for Transport (ESCRTs, blue). Through the actions of ESCRTs and associated proteins, cargoes are deubiquitinated and translocated into internal vesicles of the multivesicular body (MVB) (Step 5), where they undergo proteolysis upon fusion of the MVB with the lysosome (Step 6).

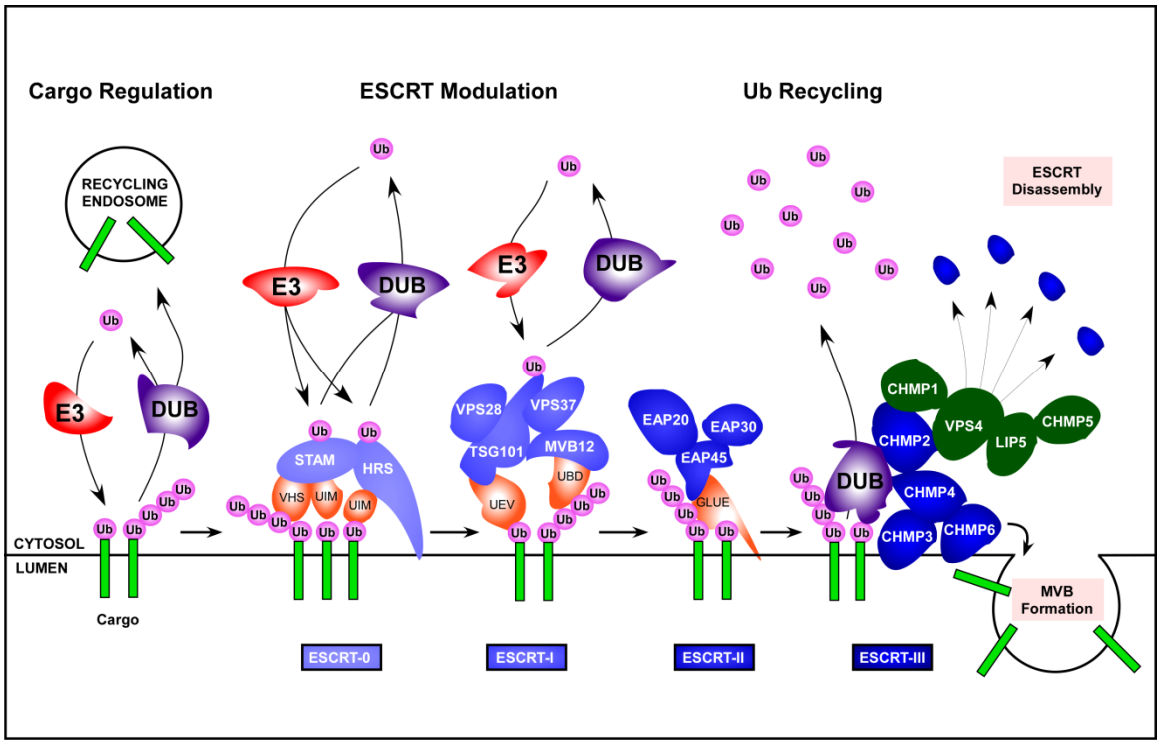

Figure 4. Diverse roles of ubiquitin in regulating multivesicular body (MVB) sorting of cargo proteins. Monoubiquitinated and K63-linked polyubiquitinated cargo proteins (light green) at the early endosome are translocated to the internal vesicles of the MVB by the coordinated actions of ESCRTs (blue). Three ESCRTs, ESCRT-0, ESCRT-I, and ESCRT-II, contain ubiquitin-binding domains (UBDs) such as Vps27-Hse1-STAM (VHS) domains, ubiquitin-interacting motifs (UIMs), and GRAM-like ubiquitin-binding in Eap45 (GLUE) domain that recognize and sort ubiquitinated cargoes toward the site of MVB formation. ESCRT-III does not contain any known UBD, but is implicated in the membrane remodeling and vesicular scission during the formation of MVBs. VPS4 and other accessory proteins (green) then mediate ESCRT disassembly, allowing further rounds of MVB sorting to occur. Ubiquitin signaling tightly modulates ESCRT-mediated cargo sorting to the MVBs through several mechanisms. E3 ligases (orange) and deubiquitination enzymes (DUBs, pink) reversibly modulate the ubiquitination statuses of

cargo proteins at the early endosome, allowing some ubiquitinated cargoes to be deubiquitinated and transported to the recycling endosome, ultimately escaping lysosomal destruction. In addition to the direct modulation of cargo proteins, E3 ligases and DUBs also regulate the ubiquitination statuses of several ESCRT subunits in a reversible manner, which signal different consequences for these ESCRT subunits. Specifically, monoubiquitination and K63-linked polyubiquitination directly modulate the functional activity of these ESCRT subunits, whereas K48-linked polyubiquitination targets these ESCRT subunits for proteasomal degradation and indirectly results in the down-regulation of ESCRT function. DUBs play an additional role in recycling ubiquitin from cargo proteins prior to their sorting to the internal vesicles. Together, ubiquitin signaling intricately modulates ESCRT-mediated sorting of cargoes to the intralumenal vesicles of multivesicular body (MVB) for their degradation by the lysosome. Ub, ubiquitin.

Chapter 2

Mutations associated with Charcot-Marie-Tooth disease cause SIMPLE protein mislocalization and degradation by the proteasome and aggresome-autophagy pathways

---

Part of the work described in this Chapter has been published:

Lee, S.M., Olzmann, J.A., Chin, L.-S., and Li, L. (2011) Mutations associated with Charcot-Marie-Tooth disease cause SIMPLE protein mislocalization and degradation by the proteasome and aggresome-autophagy pathways. *J. Cell Sci.* **124** (19), 3319-31.

Abstract

Mutations in *SIMPLE* cause an autosomal dominant, demyelinating form of peripheral neuropathy termed Charcot-Marie-Tooth disease type 1C (CMT1C), but the pathogenic mechanisms of these mutations remain unknown. Here, we report that SIMPLE is an early endosomal membrane protein which is highly expressed in the peripheral nerves and Schwann cells. Our analysis has identified a transmembrane domain (TMD) embedded within the cysteine-rich (C-rich) region for anchoring SIMPLE to the membrane and suggests that SIMPLE is a post-translationally inserted, C-tail-anchored membrane protein. We find that CMT1C-linked pathogenic mutations are clustered within or around the TMD of SIMPLE and that these mutations cause mislocalization of SIMPLE from the early endosome membrane to the cytosol. The CMT1C-associated SIMPLE mutant proteins are unstable and prone to aggregation, and they are selectively degraded by both the proteasome and aggresome-autophagy pathways. Our findings suggest that *SIMPLE* mutations cause CMT1C peripheral neuropathy via a combination of loss-of-function and toxic gain-of-function mechanisms and highlight the importance of both the proteasome and autophagy pathways in the clearance of CMT1C-associated SIMPLE mutant proteins.

Introduction

Charcot-Marie-Tooth disease (CMT) is the most prevalent inherited peripheral neuropathy, characterized by progressive motor weakness, sensory loss, and muscle wasting (Patzko and Shy, 2011). CMT is divided into two types, the demyelinating type

which includes the majority of CMT cases (80%), and the axonal degeneration type which is less common (20%). The primary defect of demyelinating CMT is the inability for Schwann cells to properly myelinate peripheral axons which manifests as slowed conduction velocities at the peripheral nerves and secondary degeneration of axons (Patzko and Shy, 2011). Examination of the peripheral nerves from patients and rodent models implicate abnormal targeting and accumulation of myelin proteins as potential contributing factors in causing demyelinating CMT (Fortun et al., 2003; Miyanomae et al., 1996; Naef and Suter, 1999; Notterpek et al., 1999; Tobler et al., 1999). However, the pathogenic mechanisms underlying demyelinating CMT remain largely unknown.

Genetic studies have identified eight missense mutations in small integral membrane protein of lysosome/late endosome (SIMPLE) that cause autosomal dominant, demyelinating CMT type 1C (CMT1C) (Campbell et al., 2004; Gerding et al., 2009; Latour et al., 2006; Saifi et al., 2005; Street et al., 2003). SIMPLE, also known as Lipopolysaccharide-Induced TNF-α Factor (LITAF), is a 161-amino-acid protein that has been implicated in cytokine signaling (Bolcato-Bellemin et al., 2004; Moriwaki et al., 2001) and tumor suppression (Mestre-Escorihuela et al., 2007; Wang et al., 2009), but its precise cellular function remains elusive. Northern blot analyses showed a ubiquitous expression pattern of SIMPLE mRNA in multiple tissues (Moriwaki et al., 2001; Street et al., 2003), therefore it is puzzling as to how mutations in SIMPLE can cause a demyelinating neuropathy phenotype that specifically affects the peripheral nervous system. The subcellular distribution of endogenous SIMPLE is unknown, although a subpopulation was suggested to associate with the late endosome and lysosome (Moriwaki et al., 2001). Sequence analysis revealed a cysteine-rich (C-rich) domain at

the C-terminus of SIMPLE (Moriwaki et al., 2001). Although this C-rich domain was proposed to be a putative RING finger domain that may have E3 ubiquitin-protein ligase activity (Moriwaki et al., 2001; Saifi et al., 2005), the function of this domain remains to be defined. Interestingly, CMT1C-associated SIMPLE mutations are all clustered within the C-rich domain. The pathogenic effects of the disease-linked SIMPLE mutations have not yet been examined.

In this study, we undertook the characterization of the tissue distribution, subcellular localization, and membrane association of endogenous SIMPLE protein and investigated the effects of CMT1C-associated mutations on SIMPLE protein stability, localization, aggregation, and degradation. Our results reveal that SIMPLE is an early endosome membrane protein enriched in the peripheral nerves and Schwann cells and indicate that CMT1C-associated mutations not only disrupt the endosome membrane association of SIMPLE, but also promote SIMPLE protein aggregation and degradation via both the proteasome and aggresome-autophagy pathways. Our findings provide new insights into the pathogenic mechanisms of CMT1C-associated SIMPLE mutations and have important implications for understanding and treating peripheral neuropathy.

Materials and methods

Plasmids and antibodies

Conventional molecular biological techniques were used to generate expression vectors encoding N-terminal GST-, Myc-, or GFP-tagged human SIMPLE WT (GenBank™ accession number NM_004862), W116G and P135T mutants, and SIMPLEΔP (residues

96-161) and SIMPLEΔC (residues 1-95) deletion mutants. The SIMPLE-targeting shRNA construct (NM_004862.1-397s1c1, Sigma-Aldrich) and the non-targeting shRNA control construct (SHC001, Sigma-Aldrich) were obtained commercially. A rabbit polyclonal anti-SIMPLE antibody was generated against a synthetic peptide corresponding to amino acid residues 50-64 of SIMPLE and affinity-purified as described previously (Chin et al., 2000). Other antibodies used in this study include anti-β-Actin (C4, Sigma-Aldrich), anti-S-100 (S2644, Sigma), anti-DJ-1 (P7F), anti-LAMP2 (Iowa Developmental Studies Hybridoma Bank), anti-SNAP-25 (SMI81, Sternberger Monoclonals), anti-Thy-1 (AbD Serotec), anti-GFP (B2, Santa Cruz), anti-EEA1 (BD Transduction), anti-KDEL (Stressgen), anti-GM130 (BD Biosciences), anti-Rab5 (Sigma-Aldrich), anti-Myc (9E10); anti-Hsc70/Hsp70 (Stressgen), anti-ubiquitin (FL76, Santa Cruz), anti-vimentin (Sigma-Aldrich), and anti-LC3 (Sigma-Aldrich). All secondary antibodies were purchased from Jackson ImmunoResearch Laboratories, Inc.

Cell cultures and transfections

Primary Schwann cells were isolated from 3-month-old mice and cultured using established protocols (Haastert et al., 2007; Pannunzio et al., 2005). Primary cortical neuronal culture was prepared from postnatal 0.5 day (P0.5) mice as described previously (Chen et al., 2010). All transfections were performed using Lipofectamine 2000 (Invitrogen) according to manufacturer's instructions. Stably transfected HEK 293 cells were selected using 1000 μg/ml G418 (Sigma-Aldrich) as described (Hubbers et al., 2007).

GST-tagged protein purification

Expression of GST-tagged SIMPLE and GST proteins were induced in ArcticExpress competent cells (Agilent Technologies) and purified as described previously (Li et al., 2001).

Immunofluorescence confocal microscopy and quantification of endosomal localization

Cells were fixed in 4% paraformaldehyde and processed for immunofluorescence confocal microscopy as described previously (Olzmann et al., 2007). Endosomal localization of WT or mutant SIMPLE was quantified as the percentage of SIMPLE immunostaining that was colocalized with Rab5 immunostaining. Colocalization of SIMPLE and Rab5 was quantified as described (Giles et al., 2008; Webber et al., 2008) on unprocessed images of cells double-labeled for Myc-tagged WT or mutant SIMPLE and Rab5. Single cells were selected by manually tracing the cell outlines. The background was subtracted and the percentage of WT or mutant SIMPLE pixels overlapping with the Rab5 pixels was determined as described previously (Giles et al., 2008; Webber et al., 2008). For each experiment, 30-40 cells per group were randomly selected for analysis, and experiments were repeated at least three times.

Subcellular fractionations and membrane association analysis

Subcellular fractionations of HeLa, HEK 293, or SH-SY5Y cells into membrane and cytosol fractions were performed as described (Giles et al., 2009). For membrane

association analysis, membrane fractions were subjected to extraction with 1% TX-100, 4 M Urea, 1.5 M NaCl, or 0.1 M Na_2CO_3 (pH 11.5) for 1 h. Extracts were then subjected to centrifugation at 100,000 *g* to isolate the soluble and insoluble fractions as described previously (Li et al., 2001). For the inhibition of palmitoylation, SH-SY5Y cells were incubated for 24 h at 37°C with of 2-bromohexadeconic acid (100 μM, Sigma-Aldrich) or vehicle (0.1% DMSO) as described (Chaudhury et al., 2009). The level of WT or mutant SIMPLE in each fraction relative to the total level in the post-nuclear supernatant was quantified by measuring the intensity of the SIMPLE band from the immunoblot image using the Scion image software as described previously (Giles et al., 2008). For density gradient fractionation analysis, post-nuclear supernatants were placed on a 10-30% linear Optiprep (Sigma-Aldrich) gradient and centrifuged for 20 h at 125,000 *g* in a SW 41 rotor (Beckman Coulter) as described previously (Chin et al., 2001; Li et al., 2002). Following centrifugation, the gradient was harvested into 250 μl fractions using an Auto Densi-Flow gradient harvester (Labconco).

[^{35}S]Methionine pulse-chase analysis

Pulse-chase experiments were performed in stably transfected HEK 293 cells expressing Myc-tagged WT or mutant SIMPLE as described previously (Giles et al., 2008; Olzmann et al., 2004). The protein levels of WT or mutant SIMPLE were quantified by measuring the intensity of the SIMPLE band from the image of the autoradiography films using the Scion image software.

Chemical cross-linking analysis

HEK 293 cells were incubated for 2 h on ice with the cross-linker DSP (2 mM, Pierce) or with vehicle (1X PBS) followed by 20 mM Tris-HCl to quench the cross-linking reaction as described previously (Cline and Mori, 2001). Cells were then lysed with 1% SDS, and an equal amount of total proteins from each lysate were subjected to immunoblot analyses.

Detergent insolubility assays

Stably transfected HEK 293 cells were lysed and centrifuged at 100,000 *g* for 30 min to separate the TX-100-soluble and -insoluble fractions as described previously (Olzmann et al., 2007). Aliquots representing an equal percentage of each fraction were subjected to immunoblot analyses.

Analysis of aggresome formation

Stably transfected HEK 293 cells expressing Myc-tagged WT or mutant SIMPLE were incubated in the presence and absence of 2 μM MG132 for 24 h and processed for immunofluorescence confocal microscopic analysis of aggresome formation as described (Olzmann et al., 2007). An aggresome was defined as a single, perinuclear inclusion containing Myc-tagged WT or mutant SIMPLE proteins. For each experiment, 40-80 cells per group were randomly selected and scored for the presence of an aggresome in a blinded manner.

Treatment of cells with proteasome, lysosome, and autophagy inhibitors and activators

Stably transfected HEK 293 cells expressing WT or mutant SIMPLE were incubated for 24 h at 37°C with protease inhibitor MG132 (20 μM, Sigma-Aldrich), lysosome inhibitor NH_4Cl (50 mM, Sigma-Aldrich), lysosome inhibitor chloroquine (100 μM, Sigma-Aldrich), autophagy inhibitor 3-MA (10 mM, Sigma-Aldrich), autophagy activator rapamycin (100 nM, Sigma-Aldrich) or vehicle (0.1% DMSO) as described previously (Giles et al., 2008). Cells were then lysed with 1% SDS, and an equal amount of total proteins from each lysate were subjected to immunoblot analyses. The protein levels of WT or mutant SIMPLE were quantified as described (Giles et al., 2008) and then normalized to the corresponding β-Actin levels.

Statistical analysis

All experiments were repeated at least three times. Data were subjected to statistical analyses by ANOVA and appropriate post hoc tests using SigmaPlot software (Systat Software, Inc.). A *P*-value of less than 0.05 was considered statistically significant.

Results

SIMPLE protein is highly expressed in peripheral nerves and Schwann cells

In order to study the endogenous SIMPLE protein, we generated and characterized a rabbit polyclonal anti-SIMPLE antibody (supplementary material Fig. S1). Immunoblot analysis showed that our anti-SIMPLE antibody specifically recognized endogenous

SIMPLE protein in HeLa and HEK 293 cells at the expected size of 18 kDa (supplementary material Fig. S1A) as well as a recombinant SIMPLE protein (supplementary material Fig. S1B). The specificity of our anti-SIMPLE antibody was confirmed by selective loss of the SIMPLE-immunoreactive band upon depletion of endogenous SIMPLE protein in HeLa cells with a SIMPLE-specific short hairpin RNA (shRNA) (supplementary material Fig. S1C). Moreover, we showed that the anti-SIMPLE antibody is able to recognize both recombinant and endogenous SIMPLE proteins by immunostaining (supplementary material Fig. S1D,E) and further confirmed the specificity of our anti-SIMPLE antibody by using the SIMPLE shRNAs in the immunostaining experiments (supplementary material Fig. S1E).

We then used the anti-SIMPLE antibody to examine the expression of SIMPLE protein in multiple mouse tissues and in sciatic nerves by immunoblot analysis. The result showed that the 18-kDa SIMPLE protein is widely expressed in many tissues, although at different abundance (Fig. 1A). We observed a second SIMPLE protein band at ~19 kDa in liver and kidney (Fig. 1A). Although its identity remains to be determined, this upper band might represent a phosphorylated form of SIMPLE protein since there are several predicted phosphorylation sites in the SIMPLE sequence (Moriwaki et al., 2001). In liver and intestine, there was an additional SIMPLE protein band at ~17 kDa (Fig. 1A), which might represent a SIMPLE degradation product because its relative intensity as compared with the 18-kDa band varied from preparation to preparation. We found that SIMPLE protein was highly enriched in the sciatic nerves when compared to the brain and muscle (Fig. 1A). Furthermore, our immunoblot analysis showed that the SIMPLE protein expression in Schwann cells was substantially higher than its expression in

primary cortical neurons (Fig. 1B). Immunostaining analysis revealed that SIMPLE was highly expressed in a punctate pattern throughout the cytoplasm of primary Schwann cells that are positive for the Schwann cell-specific marker S-100 (Scarpini et al., 1986) (Fig. 1C). In contrast, SIMPLE expression was much lower in S-100-negative primary fibroblasts (data not shown). Together, our results indicate that SIMPLE protein is highly expressed in peripheral nerves and Schwann cells.

SIMPLE is a C-tail-anchored integral membrane protein

SIMPLE contains an evolutionarily conserved C-rich domain near its C-terminus, which was proposed to be a putative RING finger domain with E3 ligase activity (Moriwaki et al., 2001; Saifi et al., 2005). However, unlike the typical RING finger domain which usually consists of either six cysteines and two histidines (C3H2C3) or seven cysteines and one histidine (C3HC4), the C-rich domain of SIMPLE possesses ten cysteines with no histidine (Fig. 2A,B). Eight of the ten cysteine residues in the SIMPLE C-rich domain align well with those of the zinc finger domains that have no E3 ligase activity (Fig. 2A). Moreover, our sequence analyses using multiple prediction programs (Hirokawa et al., 1998; Rost et al., 2004; Tusnady and Simon, 2001) revealed a potential transmembrane domain (TMD) embedded within the SIMPLE C-rich domain (Fig. 2B), which distinguishes it from known RING finger, FYVE and other zinc finger domains. Together, these results argue against the possibility of the SIMPLE C-rich domain being a RING finger domain with E3 ligase activity.

To determine whether endogenous SIMPLE is associated with the membrane, post-nuclear supernatant of HeLa cells was separated into cytosol and membrane fractions and subjected to immunoblot analysis. SIMPLE was found exclusively in the membrane fraction, as confirmed by co-fractionation with the integral membrane protein marker LAMP2, but not with the cytosolic protein STAM1 (Fig. 2C). In contrast, the palmitoylated protein SNAP-25 was partitioned into both cytosol and membrane fractions (Fig. 2F), consistent with previous reports (Li et al., 2001; Vogel and Roche, 1999).

To investigate the nature of SIMPLE association with membrane, the membrane fraction was extracted with 1.5 M NaCl, 0.1 M Na_2CO_3 (pH 11.5), 4 M urea, and 1% Triton X-100 (TX-100). We found that SIMPLE was resistant to extraction by high salt, high pH, and urea, but was readily extracted when membranes were solubilized by the non-ionic detergent TX-100 (Fig. 2D). The SIMPLE extraction profile is similar to that of integral membrane proteins such as LAMP2 (Fig. 2D), suggesting that SIMPLE is not peripherally associated with the membrane. We also compared the extraction profile of SIMPLE with that of lipid-anchored proteins such as SNAP-25 (Fig. 2E) and the glycophosphatidylinositol (GPI)-anchored protein Thy-1 (supplementary material Fig. S2A). We found that, like SIMPLE, SNAP-25 and Thy-1 were resistant to extraction by high salt, high pH, and urea as reported previously (Li et al., 2001; Lu et al., 1994; Seaton et al., 2000). However, unlike SIMPLE, Thy-1 and a pool of SNAP-25 were resistant to extraction by TX-100 (Fig. 2E; supplementary material Fig. S2A) because of their localization to lipid rafts (Chamberlain et al., 2001; Turner and Shotton, 1989).

Sequence analyses revealed that SIMPLE does not contain the consensus sequence for N-myristoylation (MGXXXS/T), prenylation (CAAX) or GPI-anchor

attachment (Eisenhaber et al., 1999; Sorek et al., 2009). Consistent with these predictions, we found that addition of a Myc tag to the N-terminus of SIMPLE, a manipulation which is known to disrupt the N-myristoylation of proteins (Santonico et al., 2010), had no effect on the membrane association of SIMPLE (Fig. 4A), arguing against the involvement of N-myristoylation in anchoring SIMPLE to the membrane. Similarly, addition of a Myc tag to the C-terminus of SIMPLE, a manipulation which interferes with prenylation of proteins (Yamashita et al., 2009), had no effect on the membrane association of SIMPLE (supplementary material Fig. S2B), thus excluding the involvement of prenylation in the membrane attachment of SIMPLE. The detection of the C-terminal Myc-tagged SIMPLE in the membrane fraction by anti-Myc antibody (supplementary material Fig. S2B) indicated that SIMPLE did not undergo C-terminal cleavage which is associated with GPI-anchor attachment (White et al., 2000), thereby arguing against the involvement of GPI-anchor attachment in the membrane association of SIMPLE. Finally, although sequence analysis identified four cysteine residues of SIMPLE (residues 95, 96, 131, and 132) as potential palmitoylated sites, analysis with the palmitoylation inhibitor 2-bromohexadeconic acid (2-BA) revealed that, unlike palmitoylated protein SNAP-25 which translocated to the cytosol after 2-BA treatment, SIMPLE remained exclusively in the membrane fraction (Fig. 2F), indicating that SIMPLE associates with the membrane via a palmitoylation-independent mechanism. Together, these results support that SIMPLE is an integral membrane protein rather than a lipid-anchored protein.

Since sequence analyses predicted a TMD within the C-rich domain of SIMPLE (Fig. 2B), we performed deletion analysis to determine whether this C-rich domain is

required for membrane association of SIMPLE. We generated two SIMPLE deletion mutants: SIMPLEΔP, which lacks the proline-rich region, and SIMPLEΔC, which lacks the C-rich domain (Fig. 2G). Membrane fractionation analysis revealed that, similar to endogenous SIMPLE, GFP-tagged full-length SIMPLE and SIMPLEΔP mutant were present exclusively in the membrane fraction (Fig 2G). The membrane association of SIMPLE was disrupted by deletion of the C-rich domain, as GFP-tagged SIMPLEΔC mutant was found exclusively in the cytosol fraction similar to GFP and the cytosolic protein DJ-1 (Fig. 2G). These results indicate that the C-rich domain of SIMPLE contains a membrane-anchoring region. Sequence analysis revealed that SIMPLE does not contain any ER-targeting signal sequence (Bendtsen et al., 2004). Moreover, the predicted TMD is localized near the C-terminus of SIMPLE (Fig. 2B). These characteristics suggest that SIMPLE is likely to undergo post-translational insertion as a C-tail-anchored membrane protein (Borgese et al., 2007; Borgese and Fasana, 2011).

Endogenous SIMPLE is localized to early endosome but not late endosome and lysosome

The subcellular localization of endogenous SIMPLE is poorly characterized. Although a previous study reported the presence of SIMPLE in the late endosome and lysosome, the SIMPLE immunostaining at the late endosome and lysosome may be non-specific since it used an anti-SIMPLE antibody that also recognized a non-specific band at the size of ~100 kDa on the immunoblot (Moriwaki et al., 2001). Furthermore, this previous study only examined the colocalization of SIMPLE with the late endosome/lysosome markers but not colocalization with markers for other organelles. To clarify the subcellular

localization of endogenous SIMPLE, we took advantage of our highly specific anti-SIMPLE antibody and performed double-labeling immunofluorescence confocal microscopic analysis to compare the intracellular distribution of endogenous SIMPLE with various organelle markers in HeLa cells. We found that endogenous SIMPLE exhibited substantial colocalization with the early endosome antigen 1 (EEA1) (Fig. 3) and Rab5 (supplementary material Fig. S3A), both of which are widely used markers for the early endosome (Kirk et al., 2006; Li et al., 2002). In contrast, there was very little colocalization of endogenous SIMPLE with the late endosome/lysosome marker LAMP2, the endoplasmic reticulum (ER) marker KDEL, or the Golgi marker GM130 (Fig. 3). The early endosomal localization of SIMPLE was further confirmed by the observation (supplementary material Fig. S3A) that a large population of SIMPLE was accumulated at the enlarged early endosomes induced by Rab5 Q79L, a constitutively active mutant of Rab5 (Ceresa et al., 2001). Together, these results indicate that SIMPLE is predominantly localized to early endosome but not the late endosome, lysosome, ER, or Golgi.

CMT1C-associated mutations cause mislocalization of SIMPLE from the early endosomal membrane to the cytosol

Our findings that all eight CMT1C-associated mutations identified so far are clustered within or around the TMD of SIMPLE (Fig. 2B) prompted us to investigate the effects of CMT1C-associated mutations on the membrane association and subcellular localization of SIMPLE. We focused on two representative CMT1C-associated SIMPLE mutations: W116G, which locates in the middle of a cluster of five mutations (A111G, G112S,

T115N, W116G, and L122V) flanking the N-terminus of the TMD, and P135T, which is one of the two mutations (P135S and P135T) at the C-terminus of the TMD (Fig. 2B). Subcellular fractionation analysis revealed that, unlike endogenous SIMPLE and Myc-tagged SIMPLE WT which were exclusively present in the membrane fraction, substantial amounts of SIMPLE W116G and P135T mutants were found in the cytosol fraction (Fig. 4A,B). Accordingly, the amounts of SIMPLE W116G and P135T mutants in the membrane fraction were significantly less than that of SIMPLE WT (Fig. 4A,C). We found that the membrane-associated SIMPLE W116G and P135T mutants, but not SIMPLE WT, were partially extracted by 0.1 M Na_2CO_3 (supplementary material Fig. S4A) and 4 M urea (data not shown), indicating that a subpopulation of SIMPLE W116G and P135T mutant proteins are peripherally associated with the membrane. Together, these data indicate that CMT1C-associated mutations cause a partial dislocation of SIMPLE from the membrane to the cytosol.

A potential mechanism for dislocating SIMPLE W116G and P135T mutant proteins from the membrane to the cytosol is via the AAA-ATPase p97/VCP-dependent dislocation to the cytosol for ER-associated degradation (ERAD) (DeLaBarre et al., 2006). To address this possibility, we used p97/VCP H317A, a dominant-negative mutant which strongly inhibits p97/VCP-dependent dislocation and degradation of ERAD substrates (DeLaBarre et al., 2006). We found that, although co-expression of p97/VCP H317A increased the steady-state level of the ERAD substrate NHK, it did not affect the steady-state levels of SIMPLE W116G and P135T mutant proteins (supplementary material Fig. S4B,C). These results argue against the possibility that SIMPLE mutant proteins are ERAD substrates and suggest that p97/VCP-dependent

dislocation is not involved in the detachment of SIMPLE mutant proteins from the membrane.

Immunofluorescence confocal microscopic analysis revealed that SIMPLE W116G and P135T mutants showed significant reductions in the localization to Rab5-positive early endosomes compared to that of SIMPLE WT (Fig. 4D,E), consistent with the subcellular fractionation results showing less SIMPLE W116G and P135T mutants in the membrane fraction than that of SIMPLE WT (Fig. 4A,C). We also performed immunostaining experiments to address the possibility that SIMPLE mutants may be mislocalized to other membrane compartments. The results showed that, unlike other mutant membrane proteins such as CFTR (cystic fibrosis transmembrane conductance regulator) ΔF508 mutant (Lukacs et al., 1994), SIMPLE W116G and P135T mutant proteins were not retained at the ER (supplementary material Fig. S4D), nor were they mislocalized to LAMP2-positive late endosome and lysosome (supplementary material Fig. S4E).

We then performed density gradient fractionation experiments to further assess the effects of CMT1C-associated mutations on the subcellular localization of SIMPLE (Fig. 4F-I). As reported previously (Chin et al., 2001; Li et al., 2002), peripherally associated endosomal membrane proteins Rab5 and EEA1 fractionated into a membrane-bound pool (fractions 21-23) and a soluble pool (fractions 1-9) on the Optiprep gradient (Fig. 4F-H). We found that SIMPLE WT co-fractionate exclusively with the early endosomal membrane-associated Rab5 and EEA1 (fractions 21-23) (Fig. 4F,I). In contrast, SIMPLE W116G and P135T mutant proteins co-fractionate with both the early endosomal membrane-associated pool (fractions 21-23) and soluble pool (fractions 1-9)

(Fig. 4G-I). Our analysis revealed no co-fractionation of SIMPLE WT and mutant proteins with LAMP2-positive membranous compartments (Fig. 4F-H). These results are consistent with the subcellular fractionation (Fig. 4A-C) and immunocytochemistry data (Fig. 4D,E; supplementary material Fig. S4E) and provide additional support for the CMT1C mutation-induced mislocalization of SIMPLE from the early endosome membrane to the cytosol.

CMT1C-associated mutations cause SIMPLE protein to be unstable

To determine whether CMT1C-associated mutations affect SIMPLE protein stability, we first assessed the steady-state levels of Myc-tagged SIMPLE WT and mutant proteins in HeLa cells. We found that the steady-state levels of SIMPLE W116G and P135T mutants were significantly lower compared to that of SIMPLE WT (Fig. 5A,B), suggesting that the SIMPLE mutant proteins were less stable than the WT protein. By using the co-transfected GFP as a reporter for transfection efficiency, we confirmed that the reductions in the steady-state protein levels of SIMPLE mutant proteins were not caused by the variability in the transfection efficiency (Fig. 5A,C). Moreover, our data indicated that the observed differences in the SIMPLE WT and mutant protein levels (Fig. 5A-C) were not due to the inability of the anti-SIMPLE antibody to detect aggregated forms of SIMPLE proteins, as this antibody was able to recognize cross-linked, oligomeric/aggregated species of SIMPLE proteins (data not shown).

Next, we performed pulse-chase experiments to examine the turnover of SIMPLE WT and mutant proteins in cells. The results revealed that SIMPLE W116G and P135T

mutants were degraded significantly more than that of SIMPLE WT at 1, 2, and 4 h (Fig. 5D,E). We found the half-life of SIMPLE WT to be ~2 h, whereas the half-life was reduced to ~1.3 h for SIMPLE W116G mutant and ~0.9 h for SIMPLE P135T mutant (Fig. 5E). Together, these results indicate that CMT1C-associated mutations destabilize SIMPLE protein in cells.

CMT1C-associated SIMPLE mutant proteins are prone to aggregation

Our finding of CMT1C mutation-induced mislocalization of SIMPLE protein from the membrane to the cytosol (Fig. 4) raised the possibility that detachment of SIMPLE mutants from the membrane may liberate hydrophobic sequences and thus promote SIMPLE protein misfolding and aggregation. To examine this possibility, we performed detergent insolubility assays (Johnston et al., 2002; Ross and Poirier, 2005) to assess the effects of CMT1C mutations on SIMPLE protein aggregation. The results showed that, under the normal cell culture condition, SIMPLE WT and mutant proteins were predominantly found in the detergent-soluble fraction (Fig. 6A). However, under the condition of proteasome inhibition, the amount of SIMPLE W116G and P135T mutants in the detergent-insoluble fraction was significantly greater than that of SIMPLE WT (Fig. 6A,B), indicating that CMT1C-associated mutations promote the accumulation of SIMPLE in detergent-insoluble aggregates.

Misfolded proteins can form detergent-insoluble, large aggregates or detergent-soluble, small aggregates composed of misfolded protein oligomers (Kubota, 2009; Olzmann et al., 2008; Ross and Poirier, 2005). The apparent lack of detectable amounts

of detergent-insoluble, SIMPLE mutant protein aggregates under the normal condition (Fig. 6A) prompted us to investigate whether SIMPLE mutant proteins aggregate into detergent-soluble, oligomeric species. To capture SIMPLE oligomeric species, we performed chemical cross-linking experiments with the cross-linker dithiobis[succinimidylpropionate] (DSP). We found that treatment of SIMPLE WT-expressing cells with DSP resulted in the appearance of two SIMPLE-immunoreactive bands at ~95 kDa and ~160 kDa, both of which may represent the cross-linked protein complexes formed between SIMPLE and its yet-to-be-identified interacting partners (Fig. 6C). The levels of these two SIMPLE protein complexes were differentially affected by the W116G and P135T mutations (Fig. 6C), suggesting that CMT1C-associated mutations alter SIMPLE protein-protein interactions. In addition, cross-linking analysis revealed that both W116G and P135T mutations caused a shift from the SIMPLE monomer to the higher-molecular-weight SIMPLE-immunoreactive protein smears, which likely represent mutant SIMPLE oligomeric species (Fig. 6C). Together, these results indicate that CMT1C-associated SIMPLE mutant proteins are more prone to aggregation compared to SIMPLE WT protein.

CMT1C-associated mutations promote the formation of SIMPLE-positive aggresomes

Next, we performed immunofluorescence confocal microscopic analysis to examine the nature of SIMPLE mutant protein aggregation in cells. We found that, under the normal cell culture condition, SIMPLE W116G and P135T mutant proteins did not form microscopically visible aggregates in cells (Fig. 7A,B), consistent with the detergent

insolubility data (Fig. 6A,B). Although the SIMPLE mutant oligomers formed under the normal condition (Fig. 6C) were microscopically undetectable, treatment of HEK 293 cells (Fig. 7A,B) and primary Schwann cells (supplementary material Fig. S5D) with proteasome inhibitor MG132 caused SIMPLE W116G and P135T mutant proteins to accumulate in microscopically visible, perinuclear inclusion bodies that spatially and morphologically resemble aggresomes (Kopito, 2000; Olzmann et al., 2008; Olzmann et al., 2007). Further analyses confirmed that the mutant SIMPLE-positive inclusion bodies are *bona fide* aggresomes, as they were enriched with ubiquitin and Hsp70 and encaged by vimentin (supplementary material Fig. S5A,B) and their formation was blocked by microtubule depolymerizing drug nocodazole (supplementary material Fig. S6A,B). Quantitative analysis revealed that the percentage of cells containing SIMPLE W116G or SIMPLE P135T mutant-positive aggresomes under the condition of proteasome inhibition was significantly greater than that of SIMPLE WT (Fig. 7B), indicating that CMT1C-associated mutations promote the formation of SIMPLE-positive aggresomes.

Increasing evidence suggests that aggresome formation serves as a mechanism for concentrating misfolded and aggregated proteins for subsequent clearance by autophagy (Cagliani et al., 2003; Chin et al., 2010; Taylor et al., 2003). Autophagy is a bulk degradation process that involves the formation of a double-membrane structure called an autophagosome to engulf its cytoplasmic substrates and the subsequent fusion of the autophagosome with the lysosome for the degradation of the substrates by lysosomal hydrolases (Mehrpour et al., 2010). Our immunofluorescence confocal microscopic analysis revealed that mutant SIMPLE-positive aggresomes were tightly encircled by the autophagosome marker LC3 (Fig. 7C, supplementary material Fig. S5C). Moreover,

mutant SIMPLE-positive aggresomes were often found to be surrounded by the late endosome/lysosome marker LAMP2 (Fig. 7C, supplementary material Fig. S5C). These results suggest that SIMPLE mutant-containing aggresomes are substrates of autophagy.

CMT1C-associated SIMPLE mutant proteins are degraded by both the proteasome and autophagy pathways

To determine the degradation pathway responsible for the clearance of WT and mutant SIMPLE proteins, we assessed the effects of proteasome, lysosome, and autophagy inhibition on the steady-state levels of Myc-tagged WT and mutant SIMPLE proteins in stably transfected HEK 293 cells. We found that SIMPLE WT protein level was significantly increased by treatment with lysosome inhibitors chloroquine (CQ) or ammonium chloride (NH_4Cl), but it was not affected by treatment with proteasome inhibitor MG132, autophagy inhibitor 3-methyladenine (3-MA) (Fig. 8A,D), or autophagy activator rapamycin (supplementary material Fig. S7A). In addition, immunostaining analysis showed that, although endogenous SIMPLE could not be detected in LAMP2-positive late endosome/lysosome under the normal condition, a significant amount of SIMPLE protein was found in the late endosome/lysosome under the condition of lysosome inhibition, indicating that SIMPLE is transiently present in the lysosome prior to its degradation (supplementary material Fig. S3B). Together, these results suggest that SIMPLE WT protein, like many integral membrane proteins, mainly relies on the endosome-to-lysosome sorting pathway for its degradation (Babst, 2004; Luzio et al., 2009). In contrast, we found that the protein levels of SIMPLE W116G and

P135T mutants were significantly increased upon proteasome inhibition by MG132, autophagy inhibition by 3-MA, or lysosome inhibition by CQ or NH_4Cl (Fig. 8B,C,E,F). Conversely, the SIMPLE mutant protein levels were significantly reduced by treatment with autophagy activator rapamycin (supplementary material Fig. S7B,C). These data support the involvement of both the proteasome and autophagy pathways in selective clearance of CMT1C-associated SIMPLE mutant proteins.

Discussion

The identification of mutations in SIMPLE as the cause of demyelinating CMT1C underscores the importance of understanding the cellular function of this novel protein and the pathogenic mechanisms of its mutations. To elucidate the role of SIMPLE in normal physiology and in CMT pathogenesis, we generated a highly specific anti-SIMPLE antibody and characterized the expression and subcellular localization of endogenous SIMPLE protein by Western blot analysis and immunocytochemistry. Our results showed that SIMPLE protein is highly expressed in peripheral nerves and Schwann cells, suggesting that SIMPLE may participate in Schwann cell function and/or peripheral nerve function. Our finding that SIMPLE protein levels are considerably lower in the brain and muscle compared to peripheral nerves helps explain why the primary defect caused by SIMPLE mutations is peripheral neuropathy but not central nervous system dysfunction or muscular atrophy.

Our immunolocalization analyses with the highly specific anti-SIMPLE antibody revealed that, under the normal physiological condition, endogenous SIMPLE is

predominantly localized to the early endosome but not the late endosome, lysosome, ER, or Golgi. This result differs from the reported presence of SIMPLE at the late endosome and lysosome in a previous study which used an anti-SIMPLE antibody that also recognized a non-specific protein at ~100 kDa (Moriwaki et al., 2001). Our data clearly indicated that SIMPLE is not a resident protein of the lysosome/late endosome as its name implies (Moriwaki et al., 2001). Instead, SIMPLE is a substrate protein for degradation by the lysosome, as we can only detect the presence of SIMPLE in the lysosome/late endosome under the condition of lysosome inhibition. Our finding that SIMPLE is an early endosomal membrane protein is consistent with the reported interaction of SIMPLE with the Endosomal Sorting Complex Required for Transport (ESCRT) subunit TSG101 (Shirk et al., 2005) and suggests that SIMPLE may participate in regulating protein sorting at the early endosome.

Our results strongly argue against the hypothesis that SIMPLE C-rich domain is a RING finger domain with E3 ligase activity (Moriwaki et al., 2001; Saifi et al., 2005). We identified a TMD embedded within the SIMPLE C-rich domain and showed that SIMPLE is a membrane protein which requires the C-rich domain for its membrane association. Our results indicate that SIMPLE is an integral membrane protein rather than a lipid-anchored protein. The lack of an ER-targeting signal sequence and the location of the TMD close to the C-terminus of SIMPLE suggest that SIMPLE is likely to undergo post-translational insertion as a C-tail-anchored membrane protein (Borgese et al., 2007; Borgese and Fasana, 2011).

Our study is the first to examine the pathogenic effects of CMT1C-associated SIMPLE mutations. We found that CMT1C-associated SIMPLE W116G and P135T

mutations cause dislocation of SIMPLE protein from the membrane to the cytosol. Interestingly, only a fraction of SIMPLE W116G and P135T mutant proteins is mislocalized to the cytosol and a substantial amount of the mutant proteins remain attached to the membrane. Although our extraction analysis revealed that a subpopulation of the membrane-associated SIMPLE mutant proteins are peripherally attached to the membrane rather than being inserted as integral membrane proteins, the peripheral membrane association could not fully account for the observed partial dislocation of SIMPLE mutant proteins from the membrane to the cytosol. Moreover, we found that, unlike other mutant membrane proteins such as CFTR ΔF508 mutant (Lukacs et al., 1994), SIMPLE W116G and P135T mutant proteins were not retained at the ER or subjected to p97/VCP-dependent dislocation to the cytosol and ERAD. These results are consistent with the prediction that SIMPLE is a post-translationally inserted, C-tail-anchored membrane protein rather than a co-translationally inserted transmembrane protein (Borgese et al., 2007; Borgese and Fasana, 2011).

While the molecular mechanisms underlying the post-translational insertion of C-tail-anchored membrane proteins remain poorly understood, it is clear that the C-terminal TMD constitutes the only membrane-targeting sequence (Borgese et al., 2007; Borgese and Fasana, 2011). Our findings that SIMPLE W116G and P135T mutant proteins are partially dissociated from the membrane is consistent with previous studies showing that mutations of Trp or Pro residue at the periphery of TMDs could cause a partial rather than a complete defect in membrane insertion (Hessa et al., 2005a; Hessa et al., 2005b). Our results, together with the fact that all CMT1C-associated mutations identified so far are clustered within or around the TMD of SIMPLE, suggest that impairment in the

membrane insertion of SIMPLE protein could be a fundamental pathogenic event in CMT1C peripheral neuropathy.

CMT1C mutation-induced dislocation of SIMPLE protein from the membrane to the cytosol could cause peripheral neuropathy via at least two different mechanisms which are not mutually exclusive. First, mutation-induced mislocalization away from the early endosomal membrane would remove SIMPLE protein from its site of action, thereby contributing to CMT pathogenesis via a loss-of-function mechanism (Kim et al., 2002; Lupo et al., 2009; Roberts et al., 2010). Although the cellular function of SIMPLE is unknown, it has been proposed that SIMPLE may participate in protein sorting at the early endosome (Shirk et al., 2005). Loss of endosomal function of SIMPLE triggered by CMT1C mutations might cause deregulated trafficking of myelin proteins and/or other membrane proteins, resulting in Schwann cell dysfunctions and demyelination. Second, mutation-induced detachment of SIMPLE protein from the membrane would expose its hydrophobic sequences and promote SIMPLE protein misfolding and aggregation, thereby contributing to CMT pathogenesis via a toxic gain-of-function mechanism. Protein misfolding and aggregation caused by genetic mutations or other factors has been shown to underlie the pathogenesis of many neurological diseases, including Parkinson disease and Alzheimer disease (Selkoe, 2004). Our findings that CMT1C mutations cause SIMPLE protein misfolding and aggregation, together with previous reports linking misfolded peripheral myelin protein 22 (PMP22) and myelin protein zero (MPZ) to other subtypes of demyelinating CMT (Mandich et al., 2009; Myers et al., 2008; Shames et al., 2003), suggest protein misfolding as a common cause of demyelinating peripheral neuropathies.

Understanding how cells handle and dispose of CMT-linked misfolded proteins are important because it may provide insights into strategies for combating the disease. Our study showed that CMT1C-associated SIMPLE mutant proteins, but not SIMPLE WT protein, are unstable and degraded by the proteasome. These results suggest that targeting the proteasome pathway might have therapeutic value in treating demyelinating CMT. However, the proteasome is capable of eliminating only soluble, monomeric form of misfolded proteins, but is ineffective in degrading oligomeric and aggregated forms of misfolded proteins (Olzmann et al., 2008; Pickart and Cohen, 2004). Moreover, the proteasome function can even be directly inhibited by misfolded protein oligomers and aggregates (Kubota, 2009). Thus, targeting the proteasome alone might not be sufficient for halting CMT pathogenesis. Recently, impairment in proteasome function was found in a neuropathic mouse model expressing a CMT1A-linked PMP22 mutant protein (Fortun et al., 2005). In addition, the proteasome inhibitor bortezomib prescribed as a chemotherapeutic agent has been shown to cause dysfunction of the myelin sheath (Filosto et al., 2007) and peripheral neuropathy in human patients (Filosto et al., 2007; Hamilton et al., 2005). Together, these findings support a link between proteasome dysfunction and the pathogenesis of CMT demyelinating neuropathy.

The aggresome-autophagy pathway has emerged as a key cellular defense system against toxic buildup of misfolded proteins, particularly under the conditions of proteasome impairment (Fortun et al., 2003; Janen et al., 2010; Olzmann et al., 2008; Olzmann et al., 2007). Our finding of the selective targeting of misfolded SIMPLE mutant proteins to aggresomes upon proteasome inhibition supports the possibility that aggresome formation is a cytoprotective response serving to sequester potentially toxic

misfolded proteins (Kopito, 2000; Olzmann et al., 2008). Consistent with recent reports suggesting the aggresomes as a staging area for the disposal of misfolded proteins by autophagy (Olzmann et al., 2007; Taylor et al., 2003), we found that SIMPLE mutant-containing aggresomes stained with the autophagosome marker LC3 and were tightly encircled by lysosomes. Moreover, the steady-state levels of SIMPLE mutants were significantly reduced by the autophagy activator rapamycin and were increased by the autophagy inhibitor 3-MA, or lysosome inhibitors CQ or NH_4Cl. Together, our data support the involvement of the aggresome-autophagy pathway in the degradation of SIMPLE mutant proteins. Interestingly, aggresomes were also found in Schwann cells expressing misfolded PMP22 mutant proteins (Fortun et al., 2006; Ryan et al., 2002) and pharmacological activation of autophagy by rapamycin was shown to improve myelination in PMP22 mutant mice (Rangaraju et al., 2010). Thus, augmentation of the aggresome-autophagy pathway might be a viable therapeutic strategy for treating a number of demyelinating neuropathies.

Acknowledgements

We thank Ron Kopito (Stanford University) for providing the NHK, p97/VCP WT and mutant constructs. This work was supported by grants from National Institutes of Health (NS063501 [SML], NS050650, AG034126 [LSC], ES015813, GM082828 [LL]). The confocal imaging analysis was performed in Emory Neuroscience Core Facility supported in part by National Institutes of Health (NS055077).

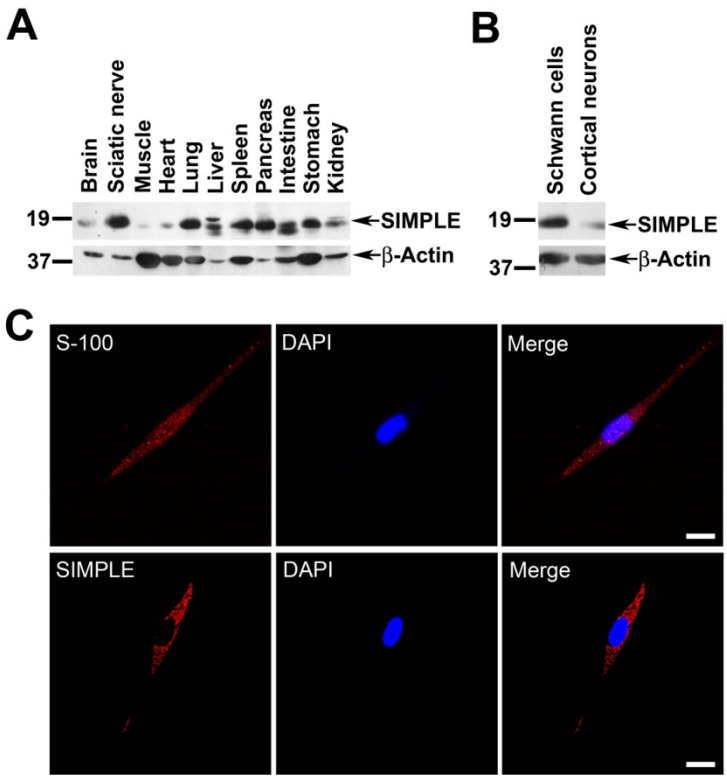

Fig. 1. SIMPLE is widely expressed in multiple tissues and is highly expressed in the peripheral nerves and Schwann cells. (A, B) Equal amounts of total proteins (100 μg protein/lane) from the indicated mouse tissues (A) or primary Schwann cells and cortical neurons (B) were subjected to immunoblot analysis with anti-SIMPLE and anti-β-actin antibodies. **(C)** Primary Schwann cells were immunostained with antibodies against S-100 or SIMPLE. Nuclei were visualized by DAPI stain. Scale bar = 10 μm.

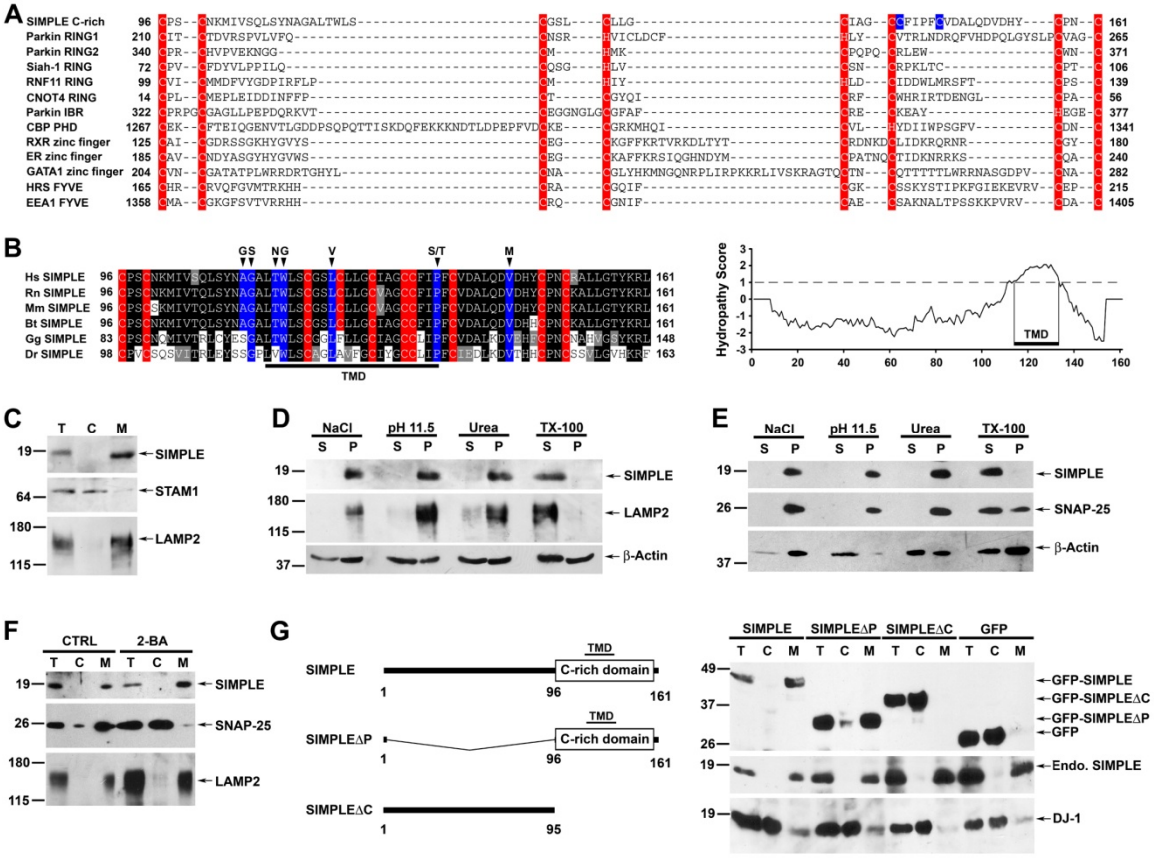

Fig. 2. SIMPLE is a transmembrane protein that requires its cysteine-rich (C-rich) domain for membrane association. **(A)** Sequence alignment of the SIMPLE C-rich domain with known RING finger domains and other C-rich domains. Residues implicated in zinc-binding are highlighted in red, and two unaligned SIMPLE cysteine residues are colored in blue. **(B)** SIMPLE is predicted to be a single-spanning integral membrane protein. Cysteine residues are highlighted in red and residues mutated in CMT1C are highlighted in blue. Hydropathy plot (TMpred) indicates the presence of transmembrane domain (TMD) within the SIMPLE C-rich domain. **(C)** Post-nuclear supernatant (T) from HeLa cells was separated into cytosol (C) and membrane (M) fractions. Aliquots representing an equal percentage of each fraction were subjected to immunoblot analysis with antibodies against SIMPLE, STAM1, and LAMP2. **(D,E)**

Membrane fractions from HeLa cells (D) or SH-SY5Y cells (E) were subjected to extraction by 1.5 M NaCl, 0.1 M Na_2CO_3 (pH 11.5), 4 M urea, or 1% Triton X-100 (TX-100) and were then separated into supernatant (S) and pellet (P) fractions. Aliquots representing an equal percentage of each fraction were analyzed by immunoblotting with antibodies against SIMPLE, LAMP2 (D), SNAP-25 (E), and β-actin. **(F)** The membrane association of SIMPLE is palmitoylation-independent. Post-nuclear supernatants of SH-SY5Y cells treated with 100 μM 2-bromohexadeconic acid (2-BA) or the vehicle control (CTRL) were separated into cytosol (C) and membrane (M) fractions. Aliquots representing an equal percentage of each fraction were subjected to immunoblot analysis with antibodies against SIMPLE, SNAP-25, and LAMP2. **(G)** Domain structures of SIMPLE and its deletion mutants were indicated (left). Post-nuclear supernatants (T) of HeLa cells expressing GFP-tagged SIMPLE, SIMPLEΔP, SIMPLEΔC, or GFP were separated into cytosol (C) and membrane (M) fractions (right). Aliquots representing an equal percentage of each fraction were analyzed by immunoblotting with antibodies against GFP, SIMPLE, and DJ-1.

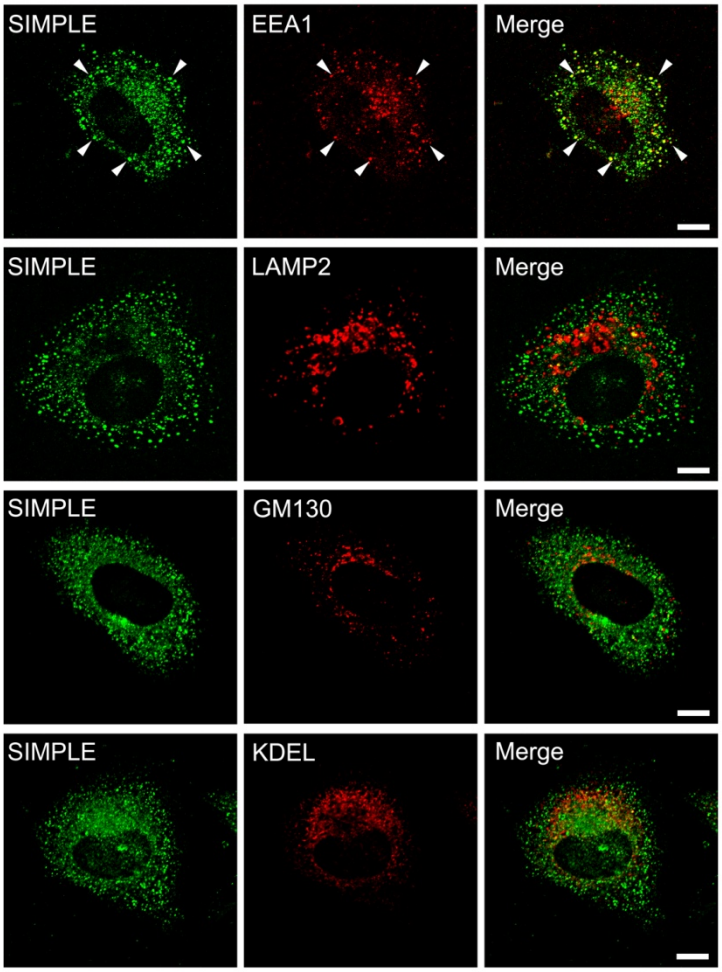

Fig. 3. Endogenous SIMPLE is localized to the early endosome but not to other organelles. HeLa cells were double-immunostained with antibodies against endogenous SIMPLE (green) and EEA1, LAMP2, GM130, or KDEL (red). Colocalizations are indicated by the yellow color in the merge panel, and examples of colocalization are indicated by arrowheads. Scale bar = 10 μm.

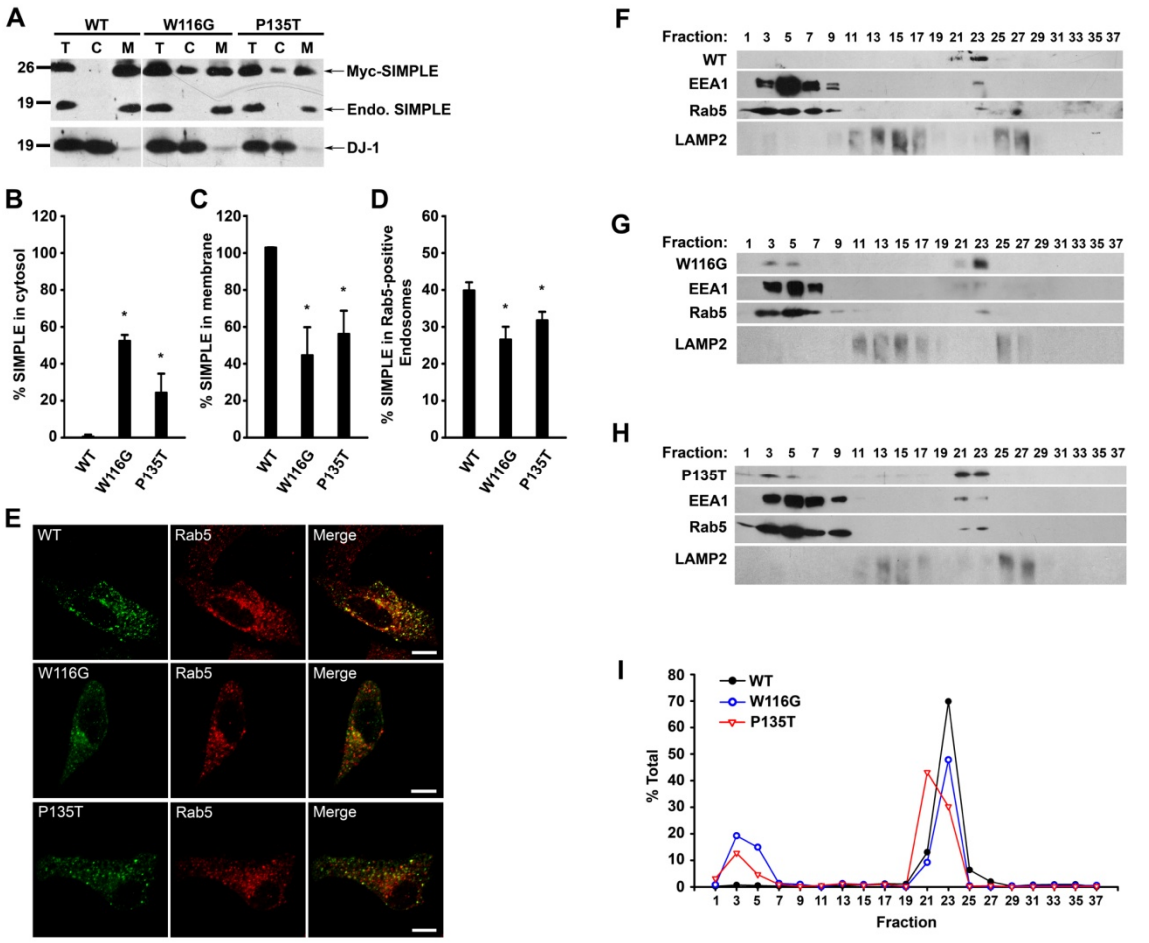

Fig. 4. CMT1C-associated SIMPLE mutants are mislocalized from the early endosomal membrane to the cytosol. **(A)** Post-nuclear supernatants (T) from HeLa cells expressing Myc-tagged WT, W116G, or P135T SIMPLE proteins were separated into cytosol (C) and membrane (M) fractions. Aliquots representing an equal percentage of each fraction were analyzed by immunoblotting with anti-DJ-1 antibody and anti-SIMPLE antibody, which recognized both Myc-tagged and endogenous (endo.) SIMPLE proteins. **(B,C)** The percentages of SIMPLE WT or mutant proteins in the cytosol (B) and membrane (C) fraction relative to the total amount in the corresponding post-nuclear supernatant (T) were quantified and shown as mean ± SEM from three independent experiments. Asterisk (*) indicates significant difference ($P < 0.05$) compared with that

of SIMPLE WT. **(D)** The percentages of SIMPLE WT or mutant proteins localized to Rab5-positive early endosomes in transfected HeLa cells were quantified as described in Materials and Methods. Data represent mean ± SEM from three independent experiments. Asterisk (*) indicates significant difference ($P < 0.05$) compared with that of SIMPLE WT. **(E)** Representative images of (D). HeLa cells expressing Myc-tagged SIMPLE WT or mutant proteins were immunostained with antibodies against the Myc tag (green) and the early endosome marker Rab5 (red). Colocalizations are indicated by the yellow color in the merged panels. Scale bar = 10 μm. **(F-H)** Post-nuclear supernatants from stably transfected HEK 293 cells expressing Myc-tagged WT (F), W116G (G), and P135T (H) SIMPLE were fractionated on a 10-30% linear Optiprep gradient into 38 fractions, with fraction 1 corresponding to the top of the gradient. Equal volumes of each fraction were subjected to SDS-PAGE followed by immunoblot analysis. The lower band in the EEA1 immunoblots represents a EEA1 protein degradation product. **(I)** The level of SIMPLE WT or mutant proteins in each fraction was quantified and shown as a percentage of the total level of the protein. Data are representative of at least three independent experiments.

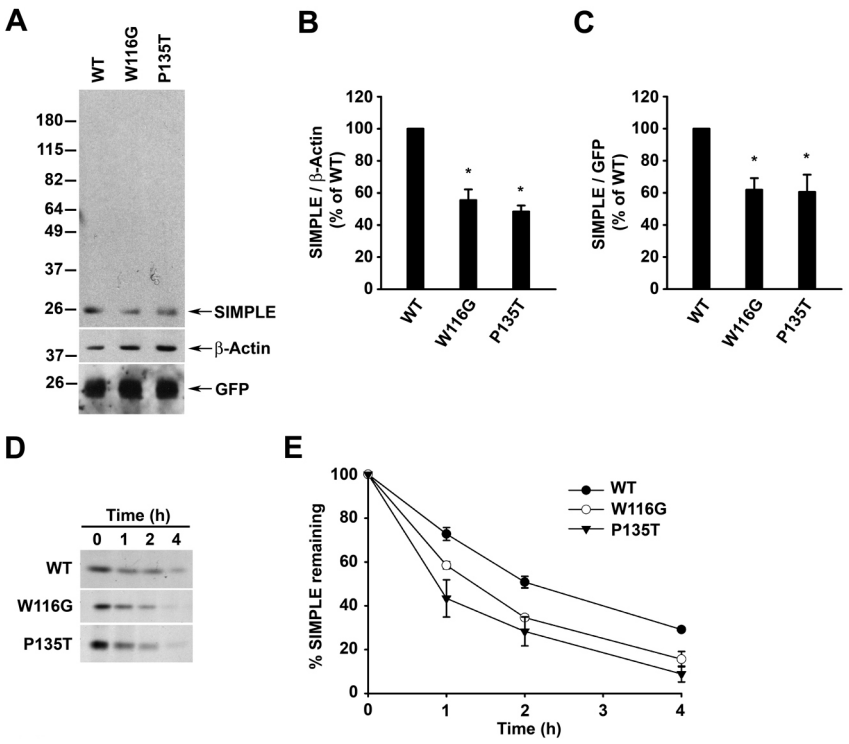

Fig. 5. CMT1C-associated mutations reduce the stability of SIMPLE protein in cells. **(A)** HeLa cells co-transfected with pEGFP vector and an equal amount of cDNAs encoding Myc-tagged WT, W116G, or P135T were analyzed by immunoblotting with antibodies against the Myc tag, β-actin, and GFP. **(B,C)** Quantification of protein levels from (A). After normalization to β-actin (B) or GFP (C), SIMPLE W116G and P135T protein levels relative to that of SIMPLE WT are shown as mean ± SEM from three independent experiments. Asterisk (*) indicates significant difference ($P < 0.05$) compared to that of SIMPLE WT**.** **(D)** The degradation of Myc-tagged SIMPLE WT, W116G, or P135T proteins expressed in HEK 293 cells were analyzed by [^{35}S]Met/Cys pulse-chase assays. ^{35}S-labeled SIMPLE WT or mutant proteins were immunoprecipitated from lysates with anti-Myc antibodies and detected by autoradiography. **(E)** The protein levels of WT and mutant SIMPLE from (D) were

quantified and plotted relative to the corresponding protein levels at 0 h. Data represent mean ± SEM from three independent experiments.

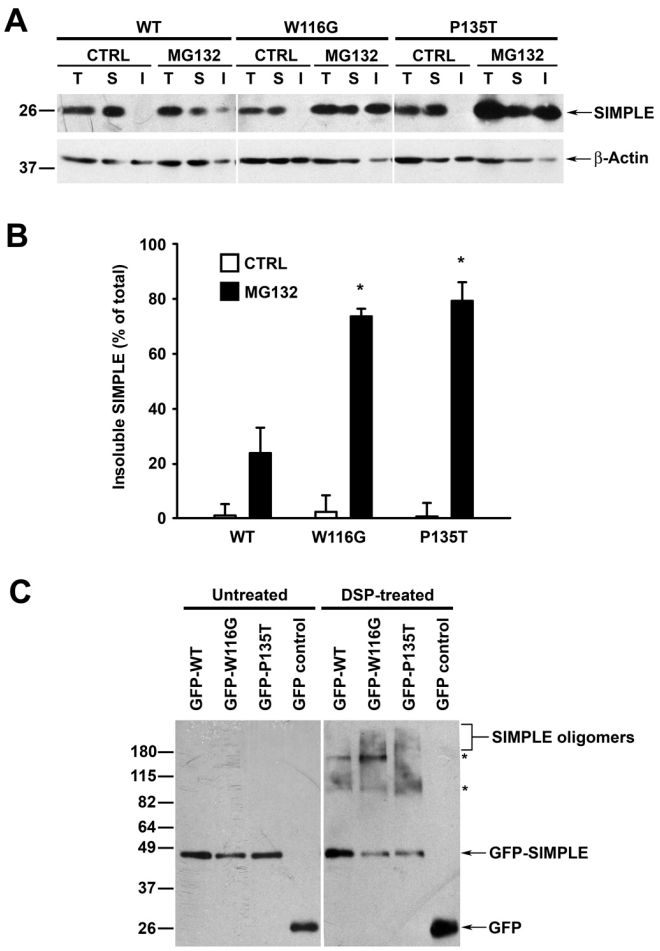

Fig. 6. CMT1C-associated mutations promote aggregation of SIMPLE. (A) Stably transfected HEK 293 cells expressing Myc-tagged WT, W116G, or P135T SIMPLE were treated for 24 h with either 2 μM MG132 or vehicle control (CTRL). Cell lysates (T) were separated into TX-100-soluble (S) and -insoluble (I) fractions. Aliquots representing an equal percentage of each fraction were analyzed by immunoblotting with antibodies against SIMPLE and β-actin. **(B)** The relative level of WT or mutant SIMPLE proteins in the insoluble fraction was quantified and expressed as a percentage of the total SIMPLE protein level in the corresponding cell lysate. Data represent mean ± SEM from three independent experiments. Asterisk (*) indicates significant difference ($P < 0.05$)

compared to that of SIMPLE WT under the same treatment. **(C)** HEK 293 cells expressing GFP or GFP-tagged WT or mutant SIMPLE were treated for 2 h with 2 μM dithiobis[succinimidylpropionate] (DSP) or vehicle control (CTRL) and analyzed by immunoblotting with an anti-GFP antibody. Asterisk (*) indicates cross-linked protein complexes formed between SIMPLE and its interacting proteins.

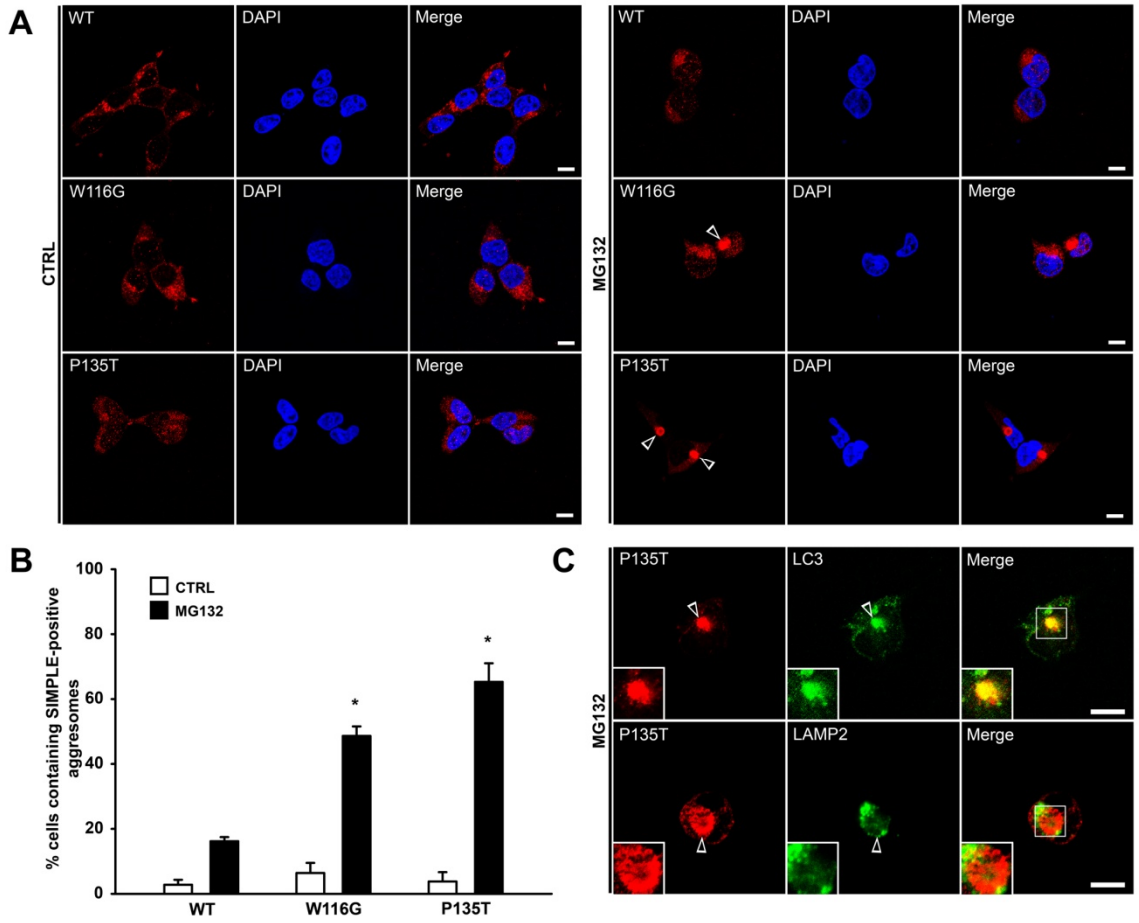

Fig, 7. CMT1C-associated SIMPLE mutants are accumulated in aggresomes. (A) Stably transfected HEK 293 cells expressing Myc-tagged WT, W116G, or P135T SIMPLE were treated for 24 h with 2 μM MG132 or vehicle as control (CTRL) and then immunostained with anti-Myc antibody (red). Nuclei were visualized by DAPI stain. Aggresomes are indicated by open arrowheads. Scale bar = 10 μm. **(B)** The percentages of cells containing SIMPLE-positive aggresomes were quantified and shown as mean ± SEM from three independent experiments. Asterisk (*) indicates significant difference ($P < 0.05$) compared to that of SIMPLE WT under the same treatment. **(C)** HEK 293 cells expressing Myc-tagged P135T SIMPLE were treated with 2 μM MG132 for 24 h

and then double-immunostained with antibodies against the Myc tag (red) and LC3 or LAMP2 (green). Aggresomes are indicated by open arrowheads. Scale bar = 10 μm.

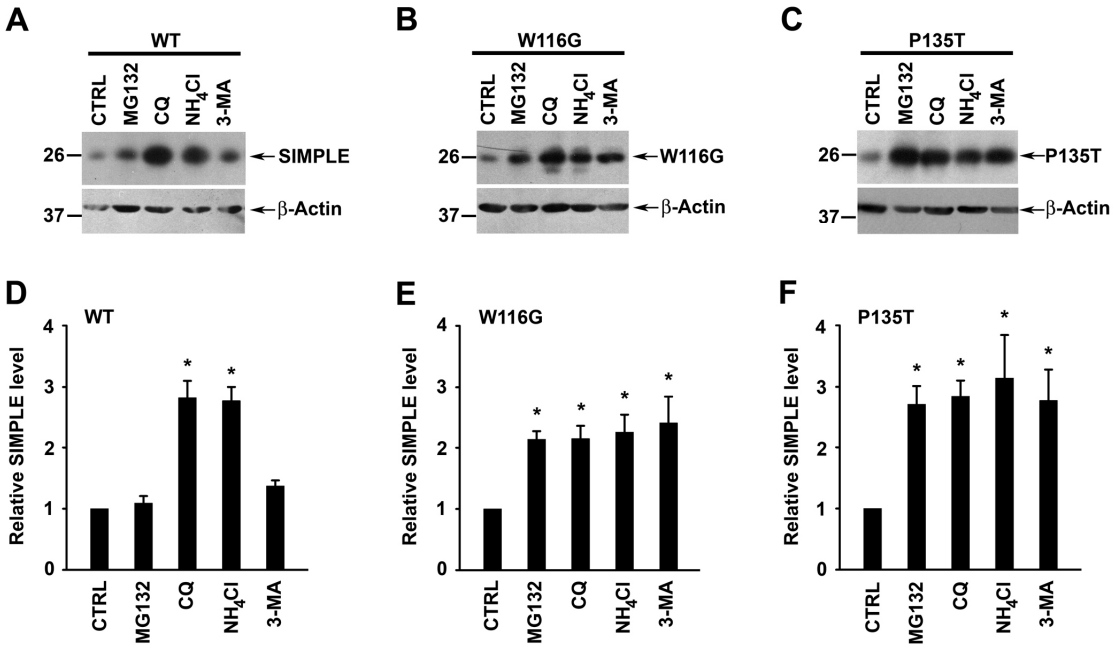

Fig. 8. Clearance of CMT1C-associated mutant SIMPLE proteins by both the proteasome and autophagy pathways. (A,B,C) Steady-state protein levels of WT (A), W116G (B), or P135T (C) SIMPLE in HEK 293 cells treated with 20 μM MG132, 100 μM chloroquine (CQ), 50 μM NH_4Cl, 10 mM 3-methyladenine (3-MA), or vehicle (CTRL) were analyzed by immunoblotting with antibodies against the Myc tag and β-actin. **(D,E,F)** The relative level of WT (D), W116G (E), or P135T (F) SIMPLE protein in the proteolysis inhibitor-treated cell lysates was normalized to the β-actin level and expressed as the fold relative to the normalized SIMPLE protein level in the corresponding vehicle-treated control lysate. Data represent mean ± SEM from at least three independent experiments. Asterisk (*) indicates significant difference ($P < 0.05$) compared with that of the vehicle-treated control.

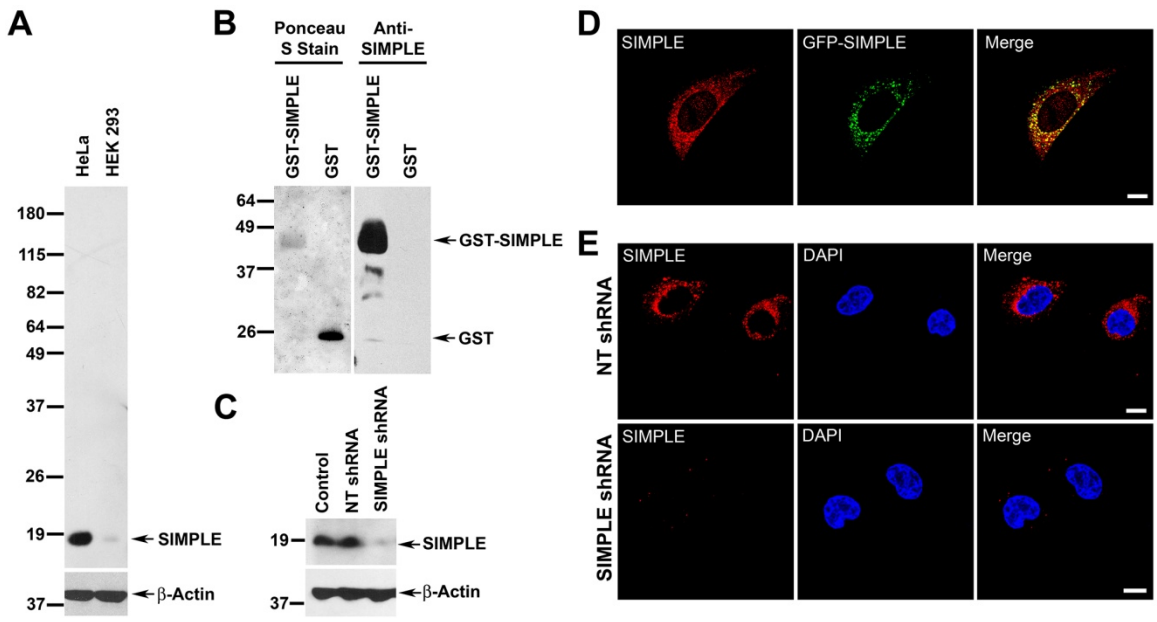

Fig. S1. Generation and characterization of a highly specific anti-SIMPLE antibody for detecting SIMPLE protein. **(A)** Equal amounts of total proteins (100 μg proteins/lane) from the indicated cell lines were subjected to immunoblot analysis with antibodies against SIMPLE and β-actin. **(B)** GST-tagged SIMPLE or GST proteins were analyzed by Ponceau S staining (left) and immunoblotting using anti-SIMPLE antibody (right). **(C)** Equal amounts of total proteins from untransfected HeLa cells (control) and HeLa cells transfected with non-targeting (NT) shRNA or SIMPLE shRNA were subjected to immunoblot analysis using antibodies against SIMPLE and β-actin. **(D)** Transfected HeLa cells expressing GFP-tagged SIMPLE protein (green) were immunostained with antibody against SIMPLE (red). Scale bar = 10 μm. **(E)** Endogenous SIMPLE protein in HeLa cells transfected with NT shRNA (top) or SIMPLE shRNA (bottom) were immunostained with anti-SIMPLE antibody (red). Nuclei were visualized by DAPI stain. Scale bar = 10 μm.

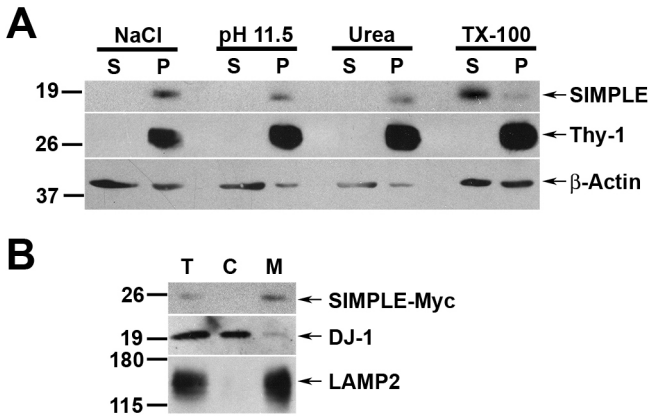

Fig. S2. **Comparison of the extraction profiles of membrane-associated SIMPLE and Thy-1. (A)** Membrane fractions from mouse brain were subjected to extraction by 1.5 M NaCl, 0.1 M Na_2CO_3 (pH 11.5), 4 M urea, or 1% Triton X-100 (TX-100) and were separated into supernatant (S) and pellet (P) fractions. Aliquots representing an equal percentage of each fraction were analyzed by immunoblotting with antibodies against SIMPLE, the GPI-anchored protein Thy-1, and β-actin. **(B)** Post-nuclear supernatant (T) from transfected HEK-293 cells expressing C-terminal Myc-tagged SIMPLE protein was separated into cytosol (C) and membrane (M) fractions. Aliquots representing an equal percentage of each fraction were subjected to immunoblot analysis.

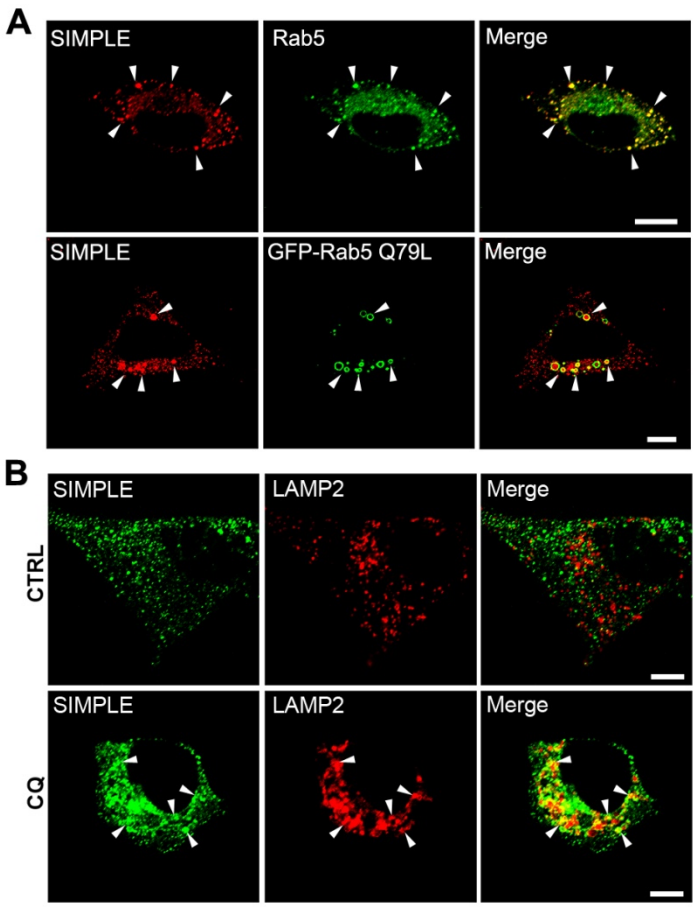

Fig. S3. Effects of Rab5-Q79L mutant expression and chloroquine treatment on subcellular localization of endogenous SIMPLE. **(A)** HeLa cells (top) were immunostained with antibodies against Rab5 (green) and endogenous SIMPLE (red). Transfected HeLa cells (bottom) expressing the GFP-Rab5-Q79L mutant (green) were immunostained with the anti-SIMPLE antibody (red). Colocalizations are indicated by the yellow color in the merge panel, and examples of colocalization are indicated by arrowheads. Scale bar = 10 μm. **(B)** HeLa cells were treated with 50 μM chloroquine (CQ) or vehicle control (CTRL) for 24 h and then double-immunostained with antibodies against endogenous SIMPLE (green) and LAMP2 (red). Colocalizations are indicated by the yellow color in the merge panel, and examples of colocalization are indicated by arrowheads. Scale bar = 10 μm.

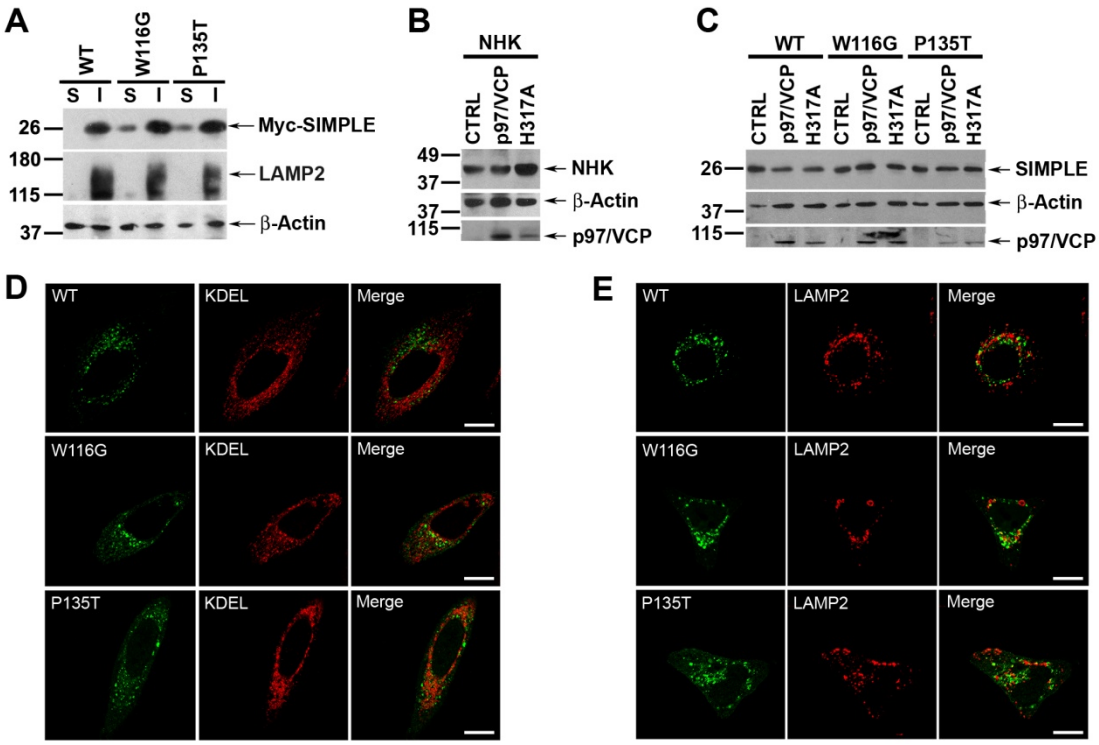

Fig. S4. SIMPLE mutant proteins are not localized to the ER or subjected to p97/VCP-dependent ERAD. (A) Membrane fractions from HeLa cells expressing Myc-tagged WT, W116G, or P135T SIMPLE proteins were subjected to extraction by 0.1 M Na_2CO_3 (pH 11.5) and were then separated into supernatant (S) and pellet (P) fractions. Aliquots representing an equal percentage of each fraction were subjected to immunoblot analysis with antibodies against Myc tag, LAMP2, and β-actin. **(B,C)** Steady-state protein levels of the HA-tagged α1-antitrypsin null mutant (NHK) (B), Myc-tagged WT, W116G, or P135T SIMPLE (C) from HEK 293 cells expressing Myc-tagged p97/VCP WT, H317A mutant, or the Myc vector control (CTRL) were subjected to immunoblot analysis using antibodies against HA tag, Myc tag, and β-actin. **(D,E)** HeLa cells expressing GFP-tagged WT or mutant SIMPLE proteins (green) were immunostained with anti-KDEL (D, red) or anti-LAMP2 (E. red) antibodies. Colocalizations are

indicated by the yellow color in the merge panel, and examples of colocalization are indicated by arrowheads. Scale bar = 10 μm.

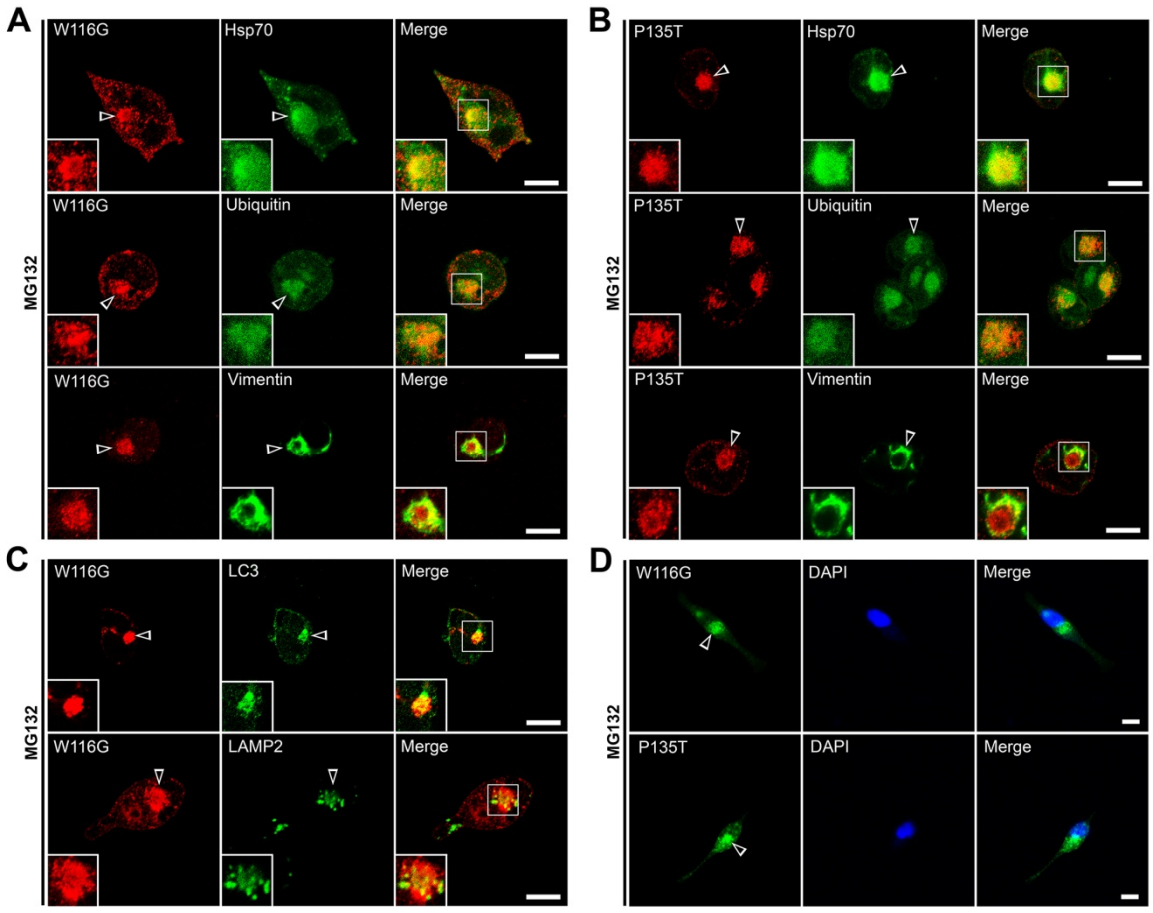

Fig. S5. Mutant SIMPLE-positive aggresomes are sites of autophagy. (A,B) HEK 293 cells expressing Myc-tagged W116G (A) or P135T (B) mutant SIMPLE were treated with 2 μM MG132 for 24 h and then double-immunostained with antibodies against the Myc tag (red) and Hsp70, ubiquitin, or vimentin (green). Aggresomes are indicated by open arrowheads. Scale bar = 10 μm. **(C)** HEK 293 cells expressing Myc-tagged W116G SIMPLE were treated with 2 μM MG132 for 24 h and then double-immunostained with antibodies against the Myc tag (red) and autophagosome marker LC3 or late endosome/lysosome marker LAMP2 (green). Aggresomes are indicated by open arrowheads. Scale bar = 10 μm. **(D)** Formation of mutant SIMPLE-positive aggresomes in Schwann cells. Primary Schwann cells expressing GFP-tagged W116G or

P135T SIMPLE (green) were treated with 5 μM MG132 for 24 h. Nuclei were visualized by DAPI stain. The mutant SIMPLE-positive perinuclear aggresomes are indicated by open arrowheads. Scale bar = 10 μm.

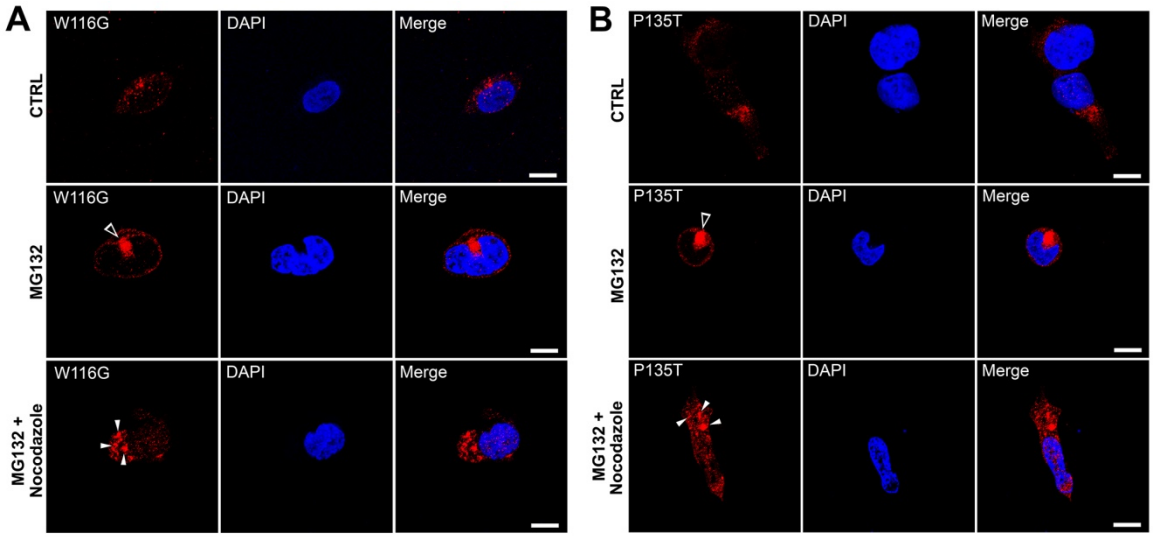

Fig. S6. Formation of mutant SIMPLE-positive aggresomes is microtubule-dependent. (A,B) HEK 293 cells expressing Myc-tagged W116G (A) and P135T (B) SIMPLE were treated with 2 μM MG132, 2 μM MG132 plus 2 μg/ml nocodazole, or vehicle as control (CTRL) for 24 h and were immunostained with anti-Myc antibody (red). Nuclei were visualized with DAPI stain. MG132 treatment alone resulted in the formation of mutant SIMPLE-positive perinuclear aggresomes (open arrowheads). In contrast, MG132 plus nocodazole treatment results in the presence of mutant SIMPLE-positive micro-aggregates (closed arrowheads) instead of aggresomes. Scale bar = 10 μm.

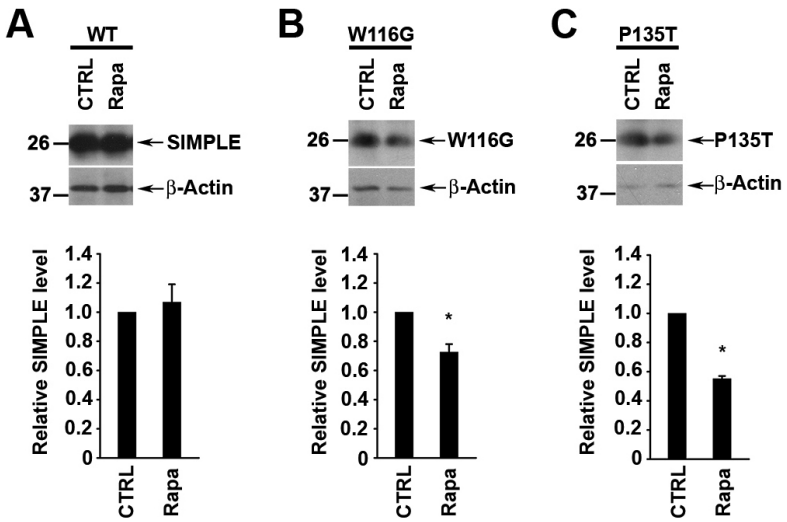

Fig. S7. Rapamycin promotes degradation of SIMPLE mutant proteins but not SIMPLE WT protein. Steady-state protein levels of Myc-tagged WT **(A)**, W116G **(B)**, or P135T **(C)** SIMPLE from stably transfected HEK 293 cells treated with 100 nM rapamycin or vehicle (CTRL) were subjected to immunoblot analysis with antibodies against the Myc tag and β-actin. The levels of WT and mutant SIMPLE proteins in the rapamycin-treated cell lysates were normalized to the β-actin level and expressed as the fold relative to the normalized WT or mutant SIMPLE protein level in the corresponding vehicle-treated control lysate. Data represent mean ± SEM from at least three independent experiments. Asterisk (*) indicates that significant difference ($P < 0.05$) compared with that of the vehicle-treated control.

Chapter 3

Charcot-Marie-Tooth disease-associated protein SIMPLE functions with the ESCRT machinery to regulate endosomal trafficking

---

Part of the work described in this Chapter has been submitted to the *Journal of Cell Biology* and is currently under revision:

Lee, S.M., Chin, L.-S., and Li, L. (2012) Charcot-Marie-Tooth disease-associated protein SIMPLE functions with the ESCRT machinery to regulate endosomal trafficking. Under revision.

Abstract

Mutations in SIMPLE cause autosomal dominant, Charcot-Marie-Tooth disease (CMT) type 1C. The cellular function of SIMPLE is unknown and the pathogenic mechanism of SIMPLE mutations remains elusive. Here we report that SIMPLE interacts and colocalizes with endosomal sorting complex required for transport (ESCRT) components STAM1, Hrs, and TSG101 on early endosomes and functions with the ESCRT machinery in the control of endosome-to-lysosome trafficking. Our analyses reveal that SIMPLE is required for efficient recruitment of ESCRT components to endosomal membranes and for regulating endosomal trafficking and signaling attenuation of ErbB receptors. We find that the ability of SIMPLE to regulate ErbB trafficking and signaling is impaired by CMT-linked SIMPLE mutations via a loss-of-function and dominant-negative mechanism, resulting in prolonged activation of ERK1/2 signaling. Our findings indicate a function of SIMPLE as a regulator of endosomal trafficking and provide evidence linking dysregulated endosomal trafficking to CMT pathogenesis.

Introduction

Charcot-Marie-Tooth disease (CMT), also known as hereditary motor and sensory neuropathy, is the most common inherited neurological disorder affecting the peripheral nervous system (PNS) (Martyn and Hughes, 1997; Parman, 2007). The molecular mechanisms underlying CMT pathogenesis remain unclear and currently there is no effective treatment to stop the progression of this debilitating disease. Small integral membrane protein of lysosome/late endosome (SIMPLE), also known as

lipopolysaccharide-induced TNF-α factor (LITAF), is a ubiquitously expressed, 161-amino-acid protein of unknown function (Moriwaki et al., 2001; Street et al., 2003). Our recent study reveals that endogenous SIMPLE is an early endosomal membrane protein (Lee et al., 2011) rather than a lysosomal/late endosomal protein as previously suggested (Moriwaki et al., 2001). To date, eight distinct point mutations in SIMPLE have been identified as the genetic defects for causing dominantly inherited CMT type 1C (CMT1C) (Campbell et al., 2004; Gerding et al., 2009; Latour et al., 2006; Saifi et al., 2005; Street et al., 2003). Thus, elucidation of the cellular function of SIMPLE and the functional consequences of SIMPLE mutations is essential for a mechanistic understanding of CMT pathogenesis.

Endocytic trafficking is crucial to the function and survival of all eukaryotic cells. Cell surface receptors are endocytosed upon ligand-binding and then targeted to the early endosome. Once arriving at the early endosome, the endocytosed receptors are either recycled to the cell surface or sorted to intralumenal vesicles of multivesicular bodies (MVBs) for delivery to the lysosome for degradation (Katzmann et al., 2002). Ligand-induced lysosomal degradation of cell surface receptors is a major mechanism that attenuates signaling of activated receptors (Katzmann et al., 2002; Waterman and Yarden, 2001). Ample evidence indicates that the endosomal sorting complex required for transport (ESCRT) machinery, composed of ESCRT-0, -I, -II, and -III complexes, plays a central role in the endosomal sorting of internalized cell surface receptors to the lysosomal pathway (Henne et al., 2011; Roxrud et al., 2010). However, the molecular mechanisms that regulate ESCRT function and confer temporal and spatial control to the endosome-to-lysosome trafficking process remain poorly understood.

SIMPLE contains a PSAP tetrapeptide motif that is predicated to bind the ubiquitin E2 variant (UEV) domain of TSG101, a subunit of the ESCRT-I complex (Pornillos et al., 2002). Although SIMPLE has been shown to interact with TSG101 (Shirk et al., 2005), the functional significance of the SIMPLE-TSG101 interaction has not yet been examined and whether SIMPLE has a role in regulation of endosomal sorting and trafficking remains unexplored. SIMPLE also contains a cysteine-rich (C-rich) domain which is hypothesized to be a putative RING finger domain with E3 ubiquitin-protein ligase activity (Moriwaki et al., 2001; Saifi et al., 2005), but whether or not SIMPLE has an E3 ligase function remains to be determined.

In this study, we investigated the biochemical function and cellular role of SIMPLE and assessed the functional consequences of CMT1C-linked SIMPLE mutations. Our results reveal that SIMPLE interacts and colocalizes with ESCRT proteins STAM1, Hrs, and TSG101 on early endosomes and acts as a functional partner of the ESCRT machinery in the control of endosome-to-lysosome trafficking. We find that SIMPLE protein has no E3 ligase activity and is unable to ubiquitinate STAM1 or TSG101. Our analyses show that SIMPLE plays an essential role in the regulation of ligand-induced endocytic trafficking and signaling of ErbB receptors. Furthermore, we find that CMT1C-linked SIMPLE mutants are loss-of-function mutants that act in a dominant-negative manner to inhibit SIMPLE function in regulating endosomal trafficking, leading to prolonged ERK1/2 signaling downstream of ErbB activation. Our findings provide novel insights into the mechanism of SIMPLE action in normal physiology and in CMT pathogenesis and have important implications for understanding and treating peripheral neuropathy.

Materials and methods

Plasmids and antibodies

The expression vectors encoding various epitope-tagged human SIMPLE WT, CMT1C-linked mutants, and deletion mutants were described previously (Lee et al., 2011). The rescue expression vectors encoding SIMPLE-targeting shRNA-resistant, epitope-tagged SIMPLE WT, W116G, P135T, and ASAA mutants were generated by site-directed mutagenesis to make two or more silent third-codon substitutions within the shRNA-targeted region of the SIMPLE transcript without altering the amino acid sequence of the SIMPLE protein. HA-tagged STAM1 and NEDD4 expression constructs were provided by Dr. Masa Komada (Tokyo Institute of Technology) and Allan Weissman (National Institutes of Health), respectively, and were used to generate N-terminal His- and GFP-tagged STAM1 and Myc-tagged NEDD4 expression constructs by conventional molecular biological techniques. ShRNA constructs targeting human SIMPLE (NM_004862.1-397s1c1 and NM_004862.1-291s1c1, Sigma) and mouse SIMPLE (NM_019980.1-269s1c1 and NM_019980.1-881s21c1, Sigma) and non-targeting shRNA control construct (SHC001, Sigma) were obtained commercially. Rabbit polyclonal anti-SIMPLE, anti-STAM1, anti-Hrs, and anti-DJ-1 antibodies were generated and affinity purified as described previously (Chin et al., 2001; Lee et al., 2011). Other antibodies used in this study include the following: anti-GFP (B2, Santa Cruz), anti-GST (B14, Santa Cruz), anti-Myc (9E10), anti-HA (12CA5 and 3F10, Roche), anti-EEA1 (BD Transduction), anti-LAMP2 (Iowa Developmental Studies Hybridoma Bank), anti-EGFR (1005, Santa Cruz), anti-ErbB3 (Abgent), anti-ERK1/2 (Cell Signaling), anti-phospho-

ERK1/2 (Cell Signaling), anti-phospho-tyrosine (Cell Signaling), and anti-Actin (C4, Sigma). All secondary antibodies were purchased from Jackson ImmunoResearch Laboratories, Inc.

Yeast two-hybrid screens

The bait plasmid, pPC97-SIMPLE, was generated by subcloning the full-length human SIMPLE into the pPC97 vector (Chin et al., 2001). For the yeast two-hybrid screen, the yeast strain CG-1945 (Clontech) was transformed sequentially with pPC97-SIMPLE and a rat hippocampal/cortical two-hybrid cDNA library (Chin et al., 2001; Li et al., 2002). Positive clones were selected on a 3-aminotrizole-containing medium lacking leucine, tryptophan and histidine, and confirmed by a filter assay for β-galactosidase activity. Prey plasmids from positive clones were rescued and re-transformed into fresh yeast cells with the SIMPLE bait or control baits to confirm the specificity of the identified interactions.

Recombinant protein purification, in vitro binding assays, and GST pull-down assays

His-tagged STAM1 and SIMPLE, GST-tagged SIMPLE full-length WT, deletion, and CMT1C-linked mutants, Hrs, STAM1, and GST proteins were individually expressed in *Escherichia coli* BL21 or ArcticExpress competent cells (Agilent Technologies) and purified as described previously (Li et al., 2001). *In vitro* binding assays were performed as described (Li et al., 2001) by incubation of immobilized GST-tagged proteins or GST with purified proteins for 2 h at 4°C under gentle rocking in 50 mM Tris-HCl (pH 8.0), 150 mM NaCl, and 0.1% Triton-X100. GST pull-down assays were performed as

described (Li et al., 2001) by incubation of immobilized GST-tagged proteins or GST with lysates of transfected HeLa cells as indicated for 2 h at 4°C. Bound proteins were analyzed by SDS-PAGE and immunoblot analyses (Olzmann et al., 2007).

In vitro ubiquitination assays

In vitro ubiquitination assays were performed using a well-established reconstitution system as described previously (Kim et al., 2007; Shimura et al., 2000). Briefly, GST-tagged parkin or SIMPLE protein was incubated at 37°C in 100 µl reaction buffer (50 mM Tris-HCL, pH 7.4, 5 mM $MgCl_2$, 0.6 mM dithiothreitol, and 2 mM ATP) containing 10 µg of ubiquitin, 200 ng of recombinant E1, 400 ng of recombinant E2 as indicated in the presence and absence of His-tagged STAM1 or immunopurified GFP-tagged TSG101. After incubation for 2 h at 37°C, the reaction products were analyzed by SDS-PAGE and immunoblotting.

Cell transfections and immunoprecipitation

HeLa cells or MSC80 mouse Schwann cells (Boutry et al., 1992) were transfected with the indicated plasmids using Lipofectamine 2000 (Invitrogen) in accordance to manufacturer's instructions. Stably transfected cells were selected using 1 mg/ml G418 (Sigma) or 2.5 µg/ml puromycin (Research Products International) as previously described (Lee et al., 2011; Trejo et al., 2000). Immunoprecipitations were carried out with the indicated antibodies as described previously (Olzmann et al., 2007), and immunocomplexes were by recovered by incubation with protein G-sepharose beads

(Upstate). After washing, the immunocomplexes were analyzed by SDS-PAGE and immunoblotting.

Subcellular fractionation

HeLa cells expressing the indicated shRNAs were treated with 100 ng/ml EGF for 15 min or left untreated. Cells were then subjected to subcellular fractionation as previously described (Lee et al., 2011). Briefly, cells were homogenized in 1 ml of homogenization buffer (250 mM sucrose, 10 mM HEPES/KOH, pH 7.4, 10 mM KCl, 10 mM EGTA, 0.1 mM EDTA) containing protease inhibitors and dithiothreitol. After centrifugation at 1,000 × g to remove unbroken cells and nuclei, the post-nuclear supernatants were subjected to a 30 min centrifugation at 100,000 × g to separate into membrane (pellet) and cytosol (supernatant) fractions. Aliquots representing an equal percentage of each fraction were analyzed by SDS-PAGE and immunoblot analyses.

Immunofluorescence confocal microscopy and quantification of colocalization, endosome size and dispersion

Cells were fixed in 4% paraformaldehyde with phosphate buffered saline and were processed for immunofluorescence confocal microscopy as described (Olzmann et al., 2007). Briefly, cells were stained with the indicated primary antibodies followed by secondary antibodies conjugated to FITC, Texas Red, or Cy5 followed by mounting in ProLong Gold antifade reagent (Invitrogen). Cell images were acquired in room temperature with the Nikon Eclipse Ti confocal microscope equipped with 40×/1.3 or 60×/1.4 oil immersion objectives and the Nikon EZ-C1 software, or imaged with the

Zeiss LSM510 confocal microscope equipped with a 63×/1.4 oil immersion objective and the Zeiss LSM510 operating software. For quantification, all images from a given experiment were acquired with the identical settings from the same microscope. Quantification of the colocalization of SIMPLE with various marker proteins was performed on unprocessed images using the ImageJ software with the JACOP plugin as previously described (Bolte and Cordelieres, 2006; Rodal et al., 2011). Single cells were selected by manually tracing the cell outlines. The background was subtracted and the percentage of SIMPLE overlapping with various markers and the percentage of various markers overlapping SIMPLE were determined by Mander's coefficients as described previously (Giles et al., 2009; Lee et al., 2011). The areas of EEA1-positive endosomes were quantified from unprocessed images using Nikon Elements Imaging Software (Nikon Instruments). Areas of endosomes were averaged for each cell from a total of 30-40 randomly selected cells in each group. For the quantification of endosome dispersion, distances between the coordinates of each endosome and the center of mass were quantified using Nikon Elements Imaging Software and averaged for each cell from a total 40-50 randomly selected cells in each group as described (Tuma et al., 1998).

EGF endocytic trafficking assays

TR-EGF endocytosis assays were performed as previously described (Kirk et al., 2006; Webber et al., 2008). Briefly, HeLa cells transfected with the indicated constructs were incubated in serum-free media for 4 h, and then treated with 3 μg/ml TR-EGF (Invitrogen) in the presence of 0.1% bovine serum albumin (BSA) at 37°C for 15 min followed by immunofluorescence microscopic analysis. TR-EGF endosome-to-lysosome

trafficking analysis was performed as previously described (Kirk et al., 2006; Webber et al., 2008). Briefly, cells were first allowed to internalize TR-EGF for 15 min. After washing three times with the media to remove extracellular TR-EGF, cells were incubated for an additional 1 h at 37°C and then processed for immunofluorescence microscopy. Quantification of the amount of intracellular TR-EGF was performed on unprocessed images. ImageJ software (National Institutes of Health) was used to integrate the pixel intensity above background for 50-100 cells in each group from three separate experiments as previously described (Kim et al., 2007).

EGFR and ErbB3 degradation assays

For EGFR degradation assays, HeLa cells transfected with the indicated constructs were serum starved for 18 h and then incubated in the presence or absence of 100 ng/ml EGF (Invitrogen) for 1 h at 37°C. Equal amounts of protein from whole cell lysates were analyzed by immunoblotting and the EGFR levels were quantified as previously described (Kirk et al., 2006; Webber et al., 2008). The degraded EGFR induced by EGF treatment is expressed as a percentage of the EGFR level of corresponding untreated cells. For ErbB3 degradation assays, MSC80 cells transfected with the indicated constructs were serum starved for 18 h and then incubated in the absence or presence of 10 nM NRG1 (R & D Systems) and 100 μg/ml of cycloheximide (Sigma) for 4 h at 37°C. The cells were lysed in 1% SDS, and an equal amount of protein from each lysate was then subjected to immunoblot analyses. The ErbB3 levels were quantified using NIH Image/Scion software as described (Kirk et al., 2006; Webber et al., 2008), and the

degraded ErbB3 induced by NRG1 treatment is expressed as a percentage of the ErbB3 level of corresponding untreated cells.

SIMPLE tyrosine phosphorylation assays

HeLa cells were starved for 18 h and then incubated in the presence or absence of 100 ng/ml EGF (Invitrogen) for 1 h at 37°C. Cells were then lysed in lysis buffer in the presence of 100 μM sodium orthovanadate and subjected to immunoprecipitation with anti-SIMPLE antibody or control rabbit IgG as described previously (Giles et al., 2009; Kwong et al., 2000). After extensive washes, immunoprecipitated proteins were analyzed by SDS-PAGE and immunoblotting.

ERK1/2 phosphorylation assays

HeLa or MSC80 cells transfected with the indicated constructs were starved in serum-free medium for 18 h and then treated with 10 ng/ml EGF or 10 nM NRG-1, respectively, for the indicated times at 37°C as described previously (Xu et al., 2012). After treatment, cells were lysed in 1% SDS. An equal amount of protein from each lysate was subjected to immunoblot analysis using anti-phospho-ERK1/2 and anti-ERK1/2 antibodies.

Statistical analysis

Data were subjected to statistical analyses by Student's t-test or one- or two-way analysis of variance with a Tukey's *post hoc* test using the SigmaPlot software (Systat Software, Inc.) Results are expressed as mean ± s.e.m. A *P*-value of less than 0.05 was considered statistically significant.

Results

SIMPLE interacts and colocalizes with ESCRT-0 and ESCRT-I subunits on early endosomes

To gain insights into the cellular function of SIMPLE, we performed yeast two-hybrid screens for SIMPLE-binding proteins using full-length human SIMPLE as bait. A positive clone isolated from the screens encodes the N-terminal 315 amino acids of STAM1 (Fig. 1A), an ESCRT-0 subunit of the endosomal sorting machinery. We further examined the identified interaction by using an *in vitro* binding assay with purified recombinant proteins and found that immobilized GST-tagged SIMPLE protein, but not GST control, pulled down His-tagged STAM1, indicating that SIMPLE interacts directly with STAM1 (Fig. 1B). Co-immunoprecipitation analysis with lysates from transfected HeLa cells revealed that Myc-tagged SIMPLE co-precipitated with HA-tagged STAM1 (Fig. 1C), confirming the interaction between of SIMPLE with STAM1 in transfected cells. STAM1 forms a tight molecular complex known as ESCRT-0 with the protein Hrs; therefore, we assessed the association of endogenous SIMPLE, STAM1, and Hrs in HeLa cells. We found that the anti-SIMPLE antibody, but not rabbit IgG control, co-immunoprecipitated endogenous SIMPLE, STAM1, and Hrs from HeLa cell lysates (Fig. 1D), indicating that SIMPLE interacts with ESCRT-0 in cells. We performed *in vitro* binding assays to determine the nature of the SIMPLE-Hrs interaction and found that immobilized GST-tagged Hrs protein was only able to pull down His-tagged SIMPLE when His-STAM1 was present (Supplementary Fig. 1A), indicating that SIMPLE does not interact directly with Hrs. In addition, presence of SIMPLE has no effect on the

ability of GST-tagged Hrs to pull down His-tagged STAM1 (Supplementary Fig. 1A), suggesting that SIMPLE and Hrs do not compete for STAM1 binding. Together, these results indicate that SIMPLE interacts with ESCRT-0 via a direct interaction with STAM1.

Next, we analyzed the colocalization of SIMPLE with STAM1 and Hrs by using immunofluorescence confocal microscopy. Double labeling immunocytochemistry analysis revealed overlaps in the distribution of endogenous SIMPLE with STAM1 and Hrs (Fig. 1E-G), indicating that a subpopulation of SIMPLE colocalizes with ESCRT-0 components in HeLa cells. In agreement with our earlier report that SIMPLE resides at the early endosome (Lee et al., 2011), we found that SIMPLE and STAM1 colocalize substantially on EEA1-positive early endosomes but not on LAMP2-positive late endosomes and lysosomes (Supplementary Fig. 2A). In addition, consistent with reported interaction of SIMPLE with TSG101 (Shirk et al., 2005), we observed a colocalization of SIMPLE with TSG101 on EEA1-positive early endosomes but not on LAMP2-positive late endosomes and lysosomes (Supplementary Fig. 2B). These results, together with our biochemical data (Fig. 1B-D), indicate that SIMPLE associates with ESCRT-0 and ESCRT-I subunits on early endosomes.

SIMPLE does not function as an E3 ubiquitin-protein ligase

We were initially intrigued by the hypothesis that SIMPLE might be an E3 ligase because its C-rich domain was thought to be a putative RING finger domain (Moriwaki et al., 2001; Saifi et al., 2005). However, our sequence analysis showed that the C-rich domain of SIMPLE is unlikely to be a RING finger domain because it lacks the conserved His

residue found in the typical RING finger domain (C3H2C3 or C3HC4 type) and it is interrupted by an embedded hydrophobic transmembrane domain (TMD) (Lee et al., 2011). We found that deletion of the TMD from SIMPLE completely disrupted the membrane association of SIMPLE (Supplementary Fig. 3A,B), indicating that the TMD is responsible for anchoring SIMPLE to the membrane. To test whether SIMPLE has an E3 ligase function, we performed *in vitro* ubiquitination assays to assess the E3 ligase activity of SIMPLE. Our results revealed that, unlike GST-tagged parkin which showed robust E3 ligase auto-ubiquitinating activity in the *in vitro* ubiquitination assays (Supplementary Fig. S3C) as previously reported (Zhang et al., 2000), GST-tagged SIMPLE showed no detectable E3 ligase activity for auto-ubiquitinating (Supplementary Fig. S3D) or for ubiquitinating STAM1 or TSG101 (Supplementary Fig. S3E,F) in the presence of E1 ubiquitin-activating enzyme and a variety of E2 ubiquitin-conjugating enzymes. Moreover, co-immunoprecipitation analyses revealed that SIMPLE was unable to interact with the E2 enzymes UbcH5, UbcH7, and UbcH8 in HeLa cells (Supplementary Fig. S2G-I). These results provide evidence that SIMPLE does not function as an E3 ligase.

SIMPLE functions in the regulation of endosome-to-lysosome trafficking and signaling attenuation

To identify SIMPLE function, we depleted endogenous SIMPLE in HeLa cells by stable transfection of SIMPLE-targeting small hairpin RNAs (shRNAs) (Fig. 2A and Supplementary Fig. S5A). We found that, in SIMPLE-depleted cells, EEA1-positive early endosomes were significantly larger than those in the control cells (Fig. 2B,C). In

addition, SIMPLE depletion caused clustering of early endosomes in the perinuclear region (Fig. 2B,D). The endosomal enlargement and clustering induced by SIMPLE depletion are similar to the endosomal morphological phenotypes caused by depletion of ESCRT component STAM, Hrs, or TSG101 (Kanazawa et al., 2003; Razi and Futter, 2006), suggesting that SIMPLE may participate in ESCRT-mediated endosomal trafficking.

Next, we examined the effects of SIMPLE depletion on epidermal growth factor (EGF)-induced endocytic trafficking and degradation of endogenous EGF receptor (EGFR, also known as ErbB1) in HeLa cells, a widely used model for studying endocytic trafficking (Sorkin and Goh, 2009). Binding of EGF to EGFR at the cell surface causes endocytosis of the ligand-receptor complex and subsequent sorting at the early endosome for lysosomal degradation (Kirk et al., 2006; Mellman, 1996a; Mellman, 1996b; Morino et al., 2004). We found that EGF-induced EGFR degradation was significantly decreased in SIMPLE-depleted cells compared with the control cells (Fig. 2E,F), indicating that SIMPLE is required for ligand-induced lysosomal degradation of EGFR. Texas Red conjugated-EGF (TR-EGF) endocytosis assays revealed that SIMPLE-depleted cells internalized a similar amount of TR-EGF compared with the control cells (Fig. 2G,I), indicating that SIMPLE is not involved in EGF-induced endocytosis of ligand-receptor complexes. To determine if SIMPLE depletion affects trafficking of EGF-EGFR complexes after endocytosis, we used a pulse-chase trafficking assay (Kirk et al., 2006; Li et al., 2002) in which cells were allowed to internalize TR-EGF for 15 min and the fate of internalize TR-EGF was monitored after a 1-h chase period. We found that SIMPLE-depleted cells retained significantly more internalized TR-EGF than that of the control

cells after the 1-h chase period (Fig. 2H,J) and the internalized EGF was accumulated in EEA1-positive early endosomes (Fig. 2H). Together, these results indicate that SIMPLE is required for endosome-to-lysosome trafficking of EGF-EGFR complexes but not their endocytosis.

Given the critical role of endosome-to-lysosome trafficking in the attenuation of EGFR signaling (Waterman and Yarden, 2001), we examined whether SIMPLE depletion could affect the mitogen-activated protein (MAP) kinase signaling downstream of EGF-activated EGFR. The kinetics of EGF-dependent activation of MAP kinases (ERK1/2) were monitored over time with phospho-specific antibodies against activated forms of ERK1/2. We found that SIMPLE depletion had no apparent effect on the onset phase of ERK1/2 phosphorylation but significantly altered the inactivation phase of ERK1/2 phosphorylation, leading to prolonged activation of ERK1/2 signaling (Fig. 2K,L). Thus, SIMPLE is required for the attenuation of EGFR-activated MAP kinase signaling. The observed defects in EGFR endosomal sorting and signaling caused by SIMPLE depletion are similar to the phenotypes seen upon depletion of ESCRT-0 or ESCRT-I subunits (Babst et al., 2000; Bache et al., 2004; Doyotte et al., 2005) and provide functional evidence supporting a role of SIMPLE in the regulation of endosomal sorting and trafficking.

SIMPLE promotes recruitment of STAM1, Hrs, and TSG101 to membranes

Our finding that SIMPLE is an early endosomal membrane protein (Lee et al., 2011) that interacts and colocalizes with STAM1, Hrs and TSG101 (Fig. 1) raises the possibility that SIMPLE may participate in the recruitment of these ESCRT subunits to endosome

membranes. To examine this possibility, we performed subcellular fractionation analysis to assess the effects of SIMPLE depletion on membrane association of endogenous STAM1, Hrs, and TSG101 in HeLa cells. We found that, in the control cells, a small pool of these ESCRT subunits were associated with membranes under the normal cell culture condition (Fig. 3B-E), in agreement with previous reports (Bache et al., 2003a; Bache et al., 2003b). In response to EGF stimulation, SIMPLE underwent tyrosine phosphorylation (Fig. 3A), and more STAM1, Hrs, and TSG101 proteins were recruited to membranes in the control cells (Fig. 3B-E). SIMPLE depletion resulted in significant decreases in the levels of membrane-associated ESCRT subunits under both the normal and EGF-stimulated conditions (Fig. 3B-E), indicating that SIMPLE is essential for efficient recruitment of these ESCRT components to membranes. Moreover, we found that SIMPLE depletion has no effect on the protein stability of Hrs and STAM1 (Supplementary Fig. 1B-D), indicating that the inhibition of endosome-to-lysosome trafficking observed in Fig. 2 is not due to reduced levels of ESCRT proteins in cells. Taken together, these results suggest that reduced membrane recruitment of STAM1, Hrs, and TSG101 (Fig. 3B-E) could be a cause of impaired endosome-to-lysosome trafficking in SIMPLE-depleted cells (Fig. 2).

SIMPLE interaction with TSG101 is required for endosome-to-lysosome trafficking

SIMPLE contains a highly conserved PSAP motif (Fig. 4A), a well characterized tetrapeptide motif for binding the UEV domain of TSG101 (Pornillos et al., 2002). Mutation of the PSAP motif of SIMPLE has been shown to abolish the interaction of SIMPLE with TSG101 (Shirk et al., 2005). To determine the functional role of SIMPLE

interaction with TSG101, we performed site-directed mutagenesis to change the PSAP motif of SIMPLE to ASAA and analyzed the effect of this mutation on SIMPLE function. We took advantage of SIMPLE depletion phenotype (Fig. 2E-J) and performed rescue experiments with shRNA-resistant SIMPLE WT and SIMPLE ASAA mutant and assessed their abilities to rescue EGFR trafficking defects in SIMPLE-depleted cells. Western blot analysis confirmed that the expression levels of exogenous SIMPLE proteins were comparable to the level of endogenous SIMPLE protein (Supplementary Fig. S5B). We found that the defective EGFR trafficking phenotype of SIMPLE depletion was rescued by SIMPLE WT (Fig. 4B-E), confirming that the observed trafficking defects in SIMPLE-depleted cells were specifically caused by the loss of SIMPLE protein but not off-target effects of shRNAs. By comparison, SIMPLE ASAA mutant was much less effective than SIMPLE WT in rescuing EGFR trafficking defects in SIMPLE-depleted cells (Fig. 4B-E), indicating that mutation of the PSAP motif of SIMPLE to ASAA causes impairment in SIMPLE function. These results support an essential role for the interaction of SIMPLE with TSG101 in the control of endosome-to-lysosome trafficking.

Both Hrs and SIMPLE contain a PSAP motif that recruits TSG101 to the early endosome membrane. We examined whether over-expression of Hrs could rescue the EGFR trafficking defects in SIMPLE-depleted cells. While Hrs over-expression inhibits EGFR trafficking in control cells as previously reported (Raiborg et al., 2001; Urbe et al., 2003), it had no observable effect on the EGFR trafficking defects in SIMPLE-depleted cells (Supplementary Fig. 4A,B). We also assessed the effects of SIMPLE over-expression in Hrs-depleted cells and found that it did not rescue the EGFR trafficking

defects caused by Hrs depletion (Supplementary Fig. 4C,D). Together, these results indicate that SIMPLE and Hrs have non-redundant roles in regulating endosome-to-lysosome trafficking.

CMT1C-linked SIMPLE mutants impair endosomal trafficking via a loss-of-function and dominant-negative mechanism

Human genetic studies have identified eight CMT1C-linked SIMPLE mutations, which are clustered within or around the TMD of SIMPLE (Fig. 4A). To determine the effects of CMT1C-linked mutations on SIMPLE function, we focused on two representative pathogenic SIMPLE mutations: W116G, which locates in the middle of a cluster of five mutations (A111G, G112S, T115N, W116G, and L122V) near the N-terminus of the TMD, and P135T, which is one of the two mutations (P135S and P135T) at the C-terminus of the TMD (Fig. 4A). We performed rescue experiments by expressing shRNA-resistant CMT1C-linked SIMPLE mutants along with SIMPLE WT in SIMPLE-depleted cells at similar levels to that of endogenous SIMPLE (Supplementary Fig. S5B) and assessed the abilities of the exogenous SIMPLE proteins to rescue EGFR trafficking defects in SIMPLE-depleted cells. Our results revealed that, while SIMPLE WT was able to rescue the defective EGFR trafficking phenotype of SIMPLE depletion, this ability was abrogated by SIMPLE W116G and P135T mutations (Fig. 5). These results support that the CMT1C-linked SIMPLE mutants are loss-of-function mutants which are unable to facilitate endosome-to-lysosome trafficking.

Because CMT1C-linked SIMPLE mutations cause an autosomal dominant form of peripheral neuropathy (Campbell et al., 2004; Gerding et al., 2009; Latour et al., 2006;

Saifi et al., 2005; Street et al., 2003), we investigated whether SIMPLE W116G and P135T mutations have dominant-negative effects on endosome-to-lysosome trafficking. We found that expression of exogenous SIMPLE W116G or P135T mutant, but not SIMPLE WT, significantly impaired EGF-induced EGFR degradation (Fig. 6A,B) and TR-EGF trafficking in cells (Fig. 6C,D). These results support a dominant-negative role for the CMT1C-linked SIMPLE mutants in endosome-to-lysosome trafficking.

We then performed biochemical analyses to explore the potential mechanism underlying the observed dominant-negative effects of SIMPLE mutants. Co-immunoprecipitation analysis (Fig. 7A) and GST pull-down assays (Fig. 7C) revealed that that SIMPLE WT has the ability to self-associate, suggesting that SIMPLE may function as a homodimer in cells. We found that SIMPLE self-association was abolished by deletion of its C-rich domain but not by deletion of its N-terminal proline-rich region (Fig. 7B,C), indicating that the C-rich domain is required for SIMPLE self-association. Our pull-down results showed that SIMPLE W116G and P135T mutants were capable of binding SIMPLE WT (Fig. 7D). CMT1C-linked SIMPLE mutants have been shown to retain the ability to interact with TSG101 (Shirk et al., 2005). Our co-immunoprecipitation analysis revealed that the pathogenic SIMPLE mutants also retained the ability to interact with STAM1 (Fig. 7E). Since the SIMPLE W116G and P135T mutants are partially mislocalized from the early endosome membrane and exist as a cytosolic pool (Lee et al., 2011), we examined whether these SIMPLE mutant proteins associate with STAM1 and TSG101 at the cytosol by performing additional co-immunoprecipitation analyses with cytosolic fractions of HeLa cells. Our results showed that CMT1C-linked SIMPLE mutants interact with STAM1 and TSG101 in the cytosolic fraction (Fig. 7F). In addition, we

found that expression of exogenous SIMPLE W116G or P135T mutant, but not SIMPLE WT (Supplementary Fig. 5C), significantly impaired the recruitment of ESCRT subunits to the endosomal membrane (Fig. 8). These findings, together with the results of functional analyses (Figs. 5 and 6), suggest that CMT1C-linked, loss-of-function SIMPLE mutants act in a dominant-negative manner to impair SIMPLE function by forming a non-functional heterodimer with endogenous SIMPLE WT and/or by sequestering ESCRT subunits to the cytosol away from binding endogenous SIMPLE WT protein.

CMT1C-linked SIMPLE mutants cause dysregulation of NRG1-ErbB signaling in Schwann cells

Neuregulin-1 (NRG1) signaling through ErbB receptor tyrosine kinases has emerged as a major pathway for controlling myelination of peripheral nerves by Schwann cells (Chen et al., 2006; Syed et al., 2010) Our finding of abundant expression of SIMPLE in Schwann cells (Lee et al., 2011) prompted us to determine whether SIMPLE has a role in the regulation of NRG1-ErbB signaling in Schwann cells. Only two members of the ErbB family of receptors, ErbB2 and ErbB3, are expressed in Schwann cells (Nave and Salzer, 2006; Newbern and Birchmeier, 2010). In response to NRG1 binding, ErbB2 and ErbB3 form heterodimers, leading to receptor cross-phosphorylation and activation of downstream signaling pathways (Birchmeier, 2009; Nave and Salzer, 2006; Quintes et al., 2010). Like EGFR/ErbB1, ligand-induced activation causes ErbB3 endocytosis and subsequent degradation by the lysosome although the ErbB3 degradation occurs at a slower rate than that of EGFR (Cao et al., 2007; Sorkin and Goh, 2009). To investigate

the function of SIMPLE in Schwann cells, we depleted endogenous SIMPLE in MSC80 mouse Schwann cells by stable transfection of SIMPLE-targeting shRNAs (Supplementary Fig. S5C). We found that NRG1-induced ErbB3 downregulation was significantly decreased in SIMPLE-depleted Schwann cells compared with the control cells (Fig. 9A,B), indicating that SIMPLE is required for NRG1-induced lysosomal degradation of ErbB3. Analysis of ERK1/2 signaling downstream of NRG1-activated ErbB2/ErbB3 receptors revealed that SIMPLE depletion altered the inactivation phase of ERK1/2 phosphorylation, leading to prolonged activation of ERK1/2 signaling (Fig. 9C,D). These results support a role for SIMPLE in controlling the duration of NRG1-ErbB signaling in Schwann cells.

To determine the effects of CMT1C-linked mutations on NRG1-ErbB signaling in Schwann cells, we expressed Myc-tagged SIMPLE WT, SIMPLE W116G, or SIMPLE P135T in MSC80 Schwann cells by stable transfection (Supplementary Fig. S5D) and analyzed their effects on ERK1/2 signaling downstream of NRG1-activated ErbB2/ErbB3 receptors. We found that expression of exogenous SIMPLE W116G or P135T mutant, but not SIMPLE WT, caused prolonged activation of ERK1/2 signaling (Fig. 9E,F). The altered NRG1-dependent ERK1/2 activation induced by SIMPLE W116G and P135T mutations (Fig. 9E,F) is similar to the phenotype seen upon depletion of SIMPLE (Fig. 9C,D), providing additional evidence supporting the dominant-negative pathogenic mechanism of CMT1C-linked SIMPLE mutations.

Discussion

Despite the identification of SIMPLE mutations as the cause of CMT1C (Campbell et al., 2004; Gerding et al., 2009; Latour et al., 2006; Saifi et al., 2005; Street et al., 2003), very little is known about the biochemical function and cellular role of SIMPLE. Although SIMPLE was hypothesized to be an E3 ligase because its C-rich domain was thought to be a putative RING finger domain (Moriwaki et al., 2001; Saifi et al., 2005), the present study provides evidence that SIMPLE does not function as an E3 ligase, in agreement with our sequence analysis result showing that SIMPLE C-rich domain is not a RING finger domain (Lee et al., 2011). Our findings reveal that SIMPLE is a novel regulator of endosome-to-lysosome trafficking. We find that SIMPLE binds to ESCRT-0 subunits STAM1 and Hrs and ESCRT-I subunit TSG101 and colocalizes with these ESCRT proteins on early endosomes. Furthermore, depleting cells of SIMPLE results in enlargement and clustering of early endosomes and impaired trafficking of internalized EGF–EGFR complexes from early endosomes to the lysosomal pathway for degradation. These results are strikingly similar to the phenotypes seen upon depletion of ESCRT-0 or ESCRT-I subunits (Babst et al., 2000; Bache et al., 2004; Doyotte et al., 2005) and indicate an essential role of SIMPLE in the process of endosomal sorting and trafficking.

Current models of endosomal sorting propose that Hrs, which is localized to early endosomes via an interaction with phosphatidylinositol-3-phosphate, recruits STAM1 from the cytosol to form the ESCRT-0 complex on endosomal membranes. The ESCRT-0 initiates the sorting process by concentrating ubiquitinated cargo underneath clathrin microdomains. Hrs uses its PSAP motif to bind TSG101, leading to recruitment of ESCRT-I, -II and -III complexes to facilitate cargo transport into MVBs for lysosomal degradation (Henne et al., 2011; Roxrud et al., 2010). However, previous studies have

shown that STAM1 can localize to the endosomal membrane in fibroblast cells derived from Hrs knockout mouse embryos (Kanazawa et al., 2003) and that depletion of Hrs only inhibits membrane association of TSG101 by 50% (Bache et al., 2003a), suggesting that additional mechanisms exist to mediate membrane association of ESCRTs. Interestingly, our study reveals that SIMPLE, an early endosomal membrane protein (Lee et al., 2011) which uses its TMD for membrane anchoring, binds to STAM1, Hrs, and TSG101 and that SIMPLE is required for efficient membrane association of these ESCRT subunits. Although Hrs and SIMPLE both interact with STAM1 and TSG101 and are required for their recruitment to the early endosome membrane, our rescue experiments revealed that Hrs and SIMPLE have non-redundant roles in regulating ESCRT function in endosome-to-lysosome trafficking. One key distinction between these proteins is that Hrs tightly associates with STAM to form the ESCRT-0 complex and is required for the structural integrity and stability of STAM (Mizuno et al., 2004), while SIMPLE does not regulate the stability of STAM and Hrs. Moreover, unlike Hrs, SIMPLE does not have known domain or motif implicated in the binding of clathrin and ubiquitinated proteins. The identification of SIMPLE as a crucial protein in recruiting ESCRT subunits, including Hrs, to the endosomal membrane suggests that the endosomal function of Hrs is dependent on SIMPLE. Together, these findings indicate that SIMPLE and Hrs have non-redundant roles and are both necessary components in regulating the membrane localization of ESCRTs and endosome-to-lysosome trafficking.

Endosome-to-lysosome trafficking of cell surface receptors is a major mechanism for controlling the intensity and duration of signal transduction in cells (Katzmann et al., 2002; Waterman and Yarden, 2001). ESCRT-mediated endosomal sorting of signaling

receptors has been shown to play a crucial role in attenuation of signal transduction (Wegner et al., 2011). Consistent with the essential role of SIMPLE in regulation of endosomal sorting and trafficking, our study reveals that SIMPLE is tyrosine phosphorylated by activated EGFR and is required for efficient attenuation of ERK1/2 signaling downstream of EGF-activated EGFR. In addition, SIMPLE is also required for efficient attenuation of ERK1/2 signaling downstream of NRG1-activated ErbB2/ErbB3 receptors. Our findings indicate that SIMPLE acts as a regulator of cell signaling by mediating ligand-induced receptor degradation.

The importance of SIMPLE is underscored by the linkage of SIMPLE mutations to autosomal dominant CMT1C (Campbell et al., 2004; Gerding et al., 2009; Latour et al., 2006; Saifi et al., 2005; Street et al., 2003). Our study is the first to examine the functional consequences of CMT1C-associated SIMPLE mutations. We find that the disease-causing SIMPLE W116G and P135T single mutations specifically impair the function of SIMPLE to regulate endosome-to-lysosome trafficking without affecting the ability of SIMPLE to self-associate or to bind STAM1 and TSG101. These results suggest that CMT1C-linked SIMPLE mutants could act in a dominant-negative manner to inhibit the function of normal *SIMPLE* allele by forming a non-functional heterodimer with endogenous SIMPLE WT and/or competing with endogenous SIMPLE WT for binding TSG101 and STAM1. We have provided several lines of evidence in support of this notion. First, we find that CMT1C-linked SIMPLE W116G and P135T mutants have dominant-negative effects on endosome-to-lysosome trafficking. Second, SIMPLE W116G and P135T mutant proteins are partially mislocalized to the cytosol (Lee et al., 2011), and we show that the cytosolic populations of pathogenic SIMPLE mutant

proteins exert dominant-negative effects by scavenging STAM1 and TSG101 at the cytosol to impair their membrane recruitment by endogenous WT SIMPLE protein. Third, unlike WT SIMPLE which is an integral membrane protein, the pathogenic SIMPLE mutant proteins are partially attached to the membrane via a weak peripheral association (Lee et al., 2011), which could affect the ability of the mutant-WT SIMPLE heterodimer to recruit and to stabilize STAM1 and TSG101 on the early endosome membrane. Taken together, these findings support a loss-of-function and dominant-negative pathogenic mechanism by which heterozygous SIMPLE mutations cause autosomal dominant CMT1C.

Our study reveals a link between dysregulated endosome-to lysosome trafficking and the pathogenesis of demyelinating CMT. We have shown that SIMPLE is a ubiquitously expressed protein which is highly enriched in Schwann cells (Lee et al., 2011). Based on our finding that SIMPLE is a regulator of endosomal trafficking, one would expect that SIMPLE mutations would lead to dysregulation of endosome-to-lysosome in Schwann cells as well as other cell types. The fact that SIMPLE mutations cause demyelinating peripheral neuropathy in human CMT1C patients suggests that, compared to other cell types, Schwann cells are particularly vulnerable to defects in endosomal trafficking. Consistent with this notion, mutations in several ubiquitously expressed regulators of endosome-to-lysosome trafficking, such as MTMR2 (Cao et al., 2008) , MTMR13 (Bolis et al., 2007), and FIG4 (Rutherford et al., 2006), have been identified as the genetic defects for causing demyelinating forms of CMT (Bolino et al., 2000b; Chow et al., 2007; Senderek et al., 2003b). Thus, dysregulation of endosome-to-lysosome trafficking may be a common pathogenic mechanism in a number of

demyelinating CMT diseases. Our analyses reveal that SIMPLE plays an essential role in the regulation of NRG1-induced ErbB degradation and signaling attenuation in Schwann cells. Furthermore, SIMPLE mutations cause dysregulation of NRG1-ErbB signaling, leading to prolonged ERK1/2 activation. These results, together with the reports that persistent ERK1/2 activation leads to demyelination pathways (Nave and Salzer, 2006; Ogata et al., 2004; Quintes et al., 2010; Syed et al., 2010), suggest a pathogenic pathway by which SIMPLE mutations cause dysregulated NRG1-ErbB signaling in Schwann cells and thereby triggers demyelination and subsequent axonal degeneration, leading to peripheral neuropathy. In conclusion, our findings obtained from this work have filled a critical gap in our knowledge about the function of SIMPLE in cells, and they have provided new insights into the pathogenic mechanism of CMT1C-linked SIMPLE mutations in peripheral neuropathy.

Acknowledgments

We thank Yifei Pu for assistance with yeast two-hybrid screens; James Olzmann for the SIMPLE-TSG101 colocalization analysis; Brandi Whatley for generation of Myc-NEDD4 construct; Voruvat Tangpisuthipongsa for generation of His-STAM1 construct; Roman Chrast (University of Lausanne) and Jean-Yves Cesbron (Université Joseph Fourier - Grenoble) for the MSC80 cells; and Masa Komada (Tokyo Institute of Technology) for the HA-STAM1 construct; Allan Weissman (National Institutes of Health) for the HA-NEDD4 construct. This work was supported by NIH grants NS063501 (S.M.L.), NS050650 and AG034126 (L.S.C.), and ES015813 and GM082828

(L.L.). The confocal imaging analysis was performed in Emory Neuroscience Core Facility supported in part by NIH grant NS055077.

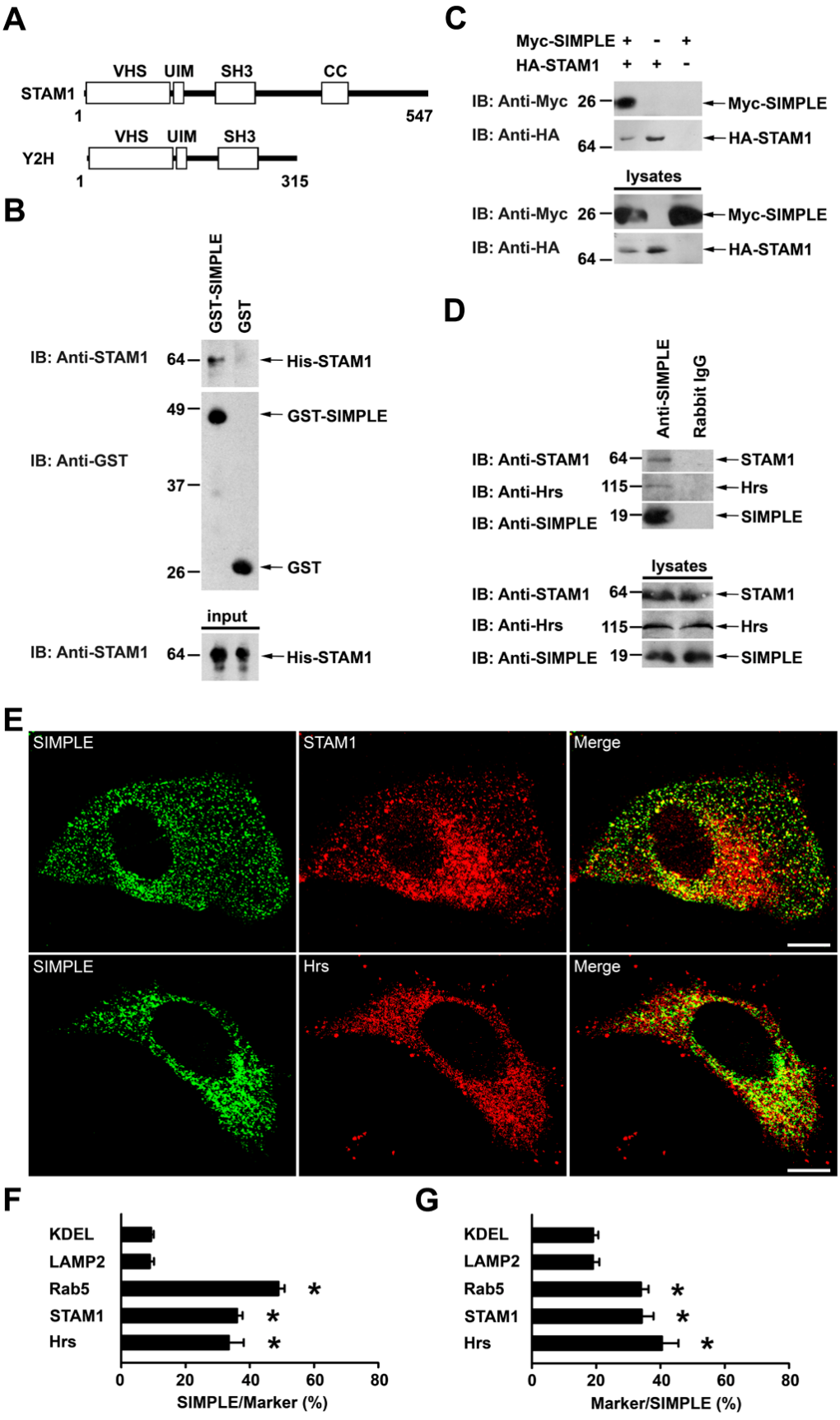
A
STAM1
VHS
UIM
SH3
CC
1
547
Y2H
315
B
GST-SIMPLE
GST
IB: Anti-STAM1
64
His-STAM1
49
GST-SIMPLE
IB: Anti-GST
37
26
GST
input
C
Myc-SIMPLE + - +
HA-STAM1 + + -
IB: Anti-Myc
IB: Anti-HA
Myc-SIMPLE
HA-STAM1
lysates
D
Anti-SIMPLE
Rabbit IgG
IB: Anti-Hrs
IB: Anti-SIMPLE
115
19
STAM1
Hrs
SIMPLE
E
SIMPLE
STAM1
Merge
Hrs
F
KDEL
LAMP2
Rab5
STAM1
Hrs
0
20
40
60
80
SIMPLE/Marker (%)
G
Marker/SIMPLE (%)

Figure 1. SIMPLE associates and colocalizes with STAM1 and Hrs. (A) Domain structure of rat STAM1 (STAM1) and the SIMPLE-interacting clone isolated from yeast two-hybrid screen (Y2H). **(B)** Direct interaction between SIMPLE and STAM1. *In vitro* binding assays were performed by incubation of soluble His-tagged STAM1 protein (input) with immobilized GST or GST-SIMPLE fusion protein. Bound STAM1 protein was detected by immunoblotting. **(C)** Interaction of SIMPLE with STAM1 in transfected cells. Lysates from HeLa cells co-transfected with Myc-tagged SIMPLE or empty Myc vector and HA-tagged STAM1 or empty HA vector were immunoprecipitated with anti-HA antibody followed by immunoblot analyses. **(D)** Association of endogenous SIMPLE with STAM1 and Hrs. HeLa cell lysates were immunoprecipitated with anti-SIMPLE antibody or control rabbit IgG followed by immunoblotting. **(E)** Colocalization of endogenous SIMPLE with STAM1 and Hrs. HeLa cells were double immunostained with antibodies against SIMPLE (green) and STAM1 or Hrs (red). Scale bar = 10 μm. **(F,G)** Quantification of colocalization between SIMPLE and the indicated marker proteins is presented as mean ± s.e.m. * $P < 0.05$ versus the control, one-way analysis of variance with a Tukey's *post hoc* test.

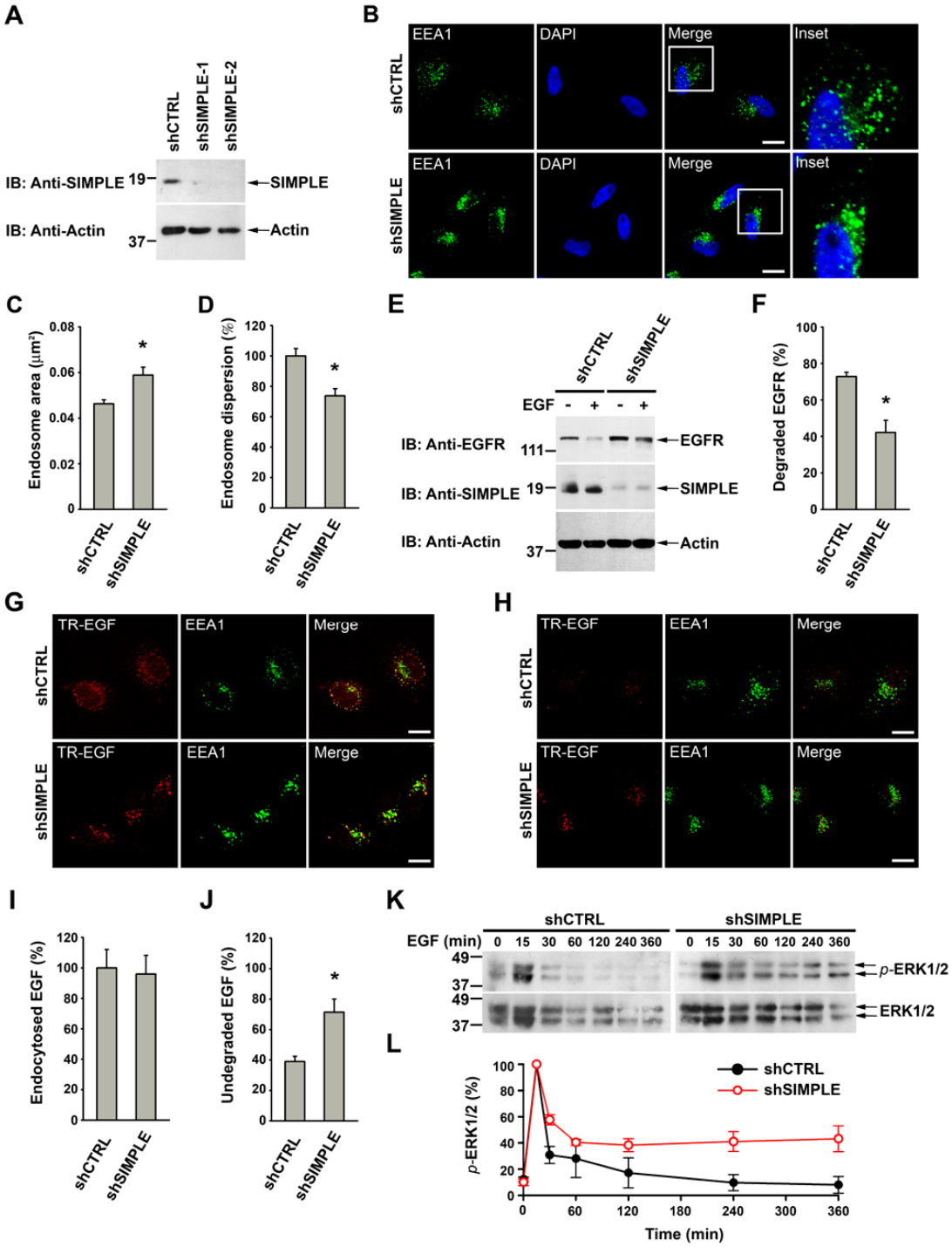

Figure 2. SIMPLE depletion alters endosomal morphology and EGFR endosomal sorting and signaling. **(A)** Immunoblot analysis shows depletion of endogenous SIMPLE in HeLa cells stably transfected with SIMPLE-targeting shRNAs (shSIMPLE-1

and shSIMPLE-2) compared with HeLa cells transfected with non-targeting control shRNAs (shCTRL). **(B-D)** Immunostaining analysis (B) with anti-EEA1 antibody (green) and 4',6-diamidino-2-phenylindole (DAPI, blue) and quantification of endosome area (C) and relative extent of endosome dispersion (D) show altered endosomal morphology and distribution in shSIMPLE-transfected HeLa cells compared with the shCTRL-transfected control. Scale bar = 10 μm. Data represent mean ± s.e.m. (n = 30-50 cells) from three independent experiments. * $P < 0.05$ versus the control, unpaired two-tailed Student's t-test. **(E,F)** EGFR degradation analysis (E) and quantification (F) show reduced levels of degraded EGFR following treatment with 100 ng/ml EGF for 1 h in shSIMPLE-transfected HeLa cells compared with the shCTRL-transfected control. Data represent mean ± s.e.m (n = 3). * $P = 0.012$ versus the control, unpaired two-tailed Student's t-test. **(G,I)** TR-EGF endocytosis analysis (G) and quantification (I) show similar amounts of endocytosed TR-EGF (red) following a 15-min incubation with TR-EGF in shSIMPLE-transfected HeLa cells compared with the shCTRL-transfected control. Scale bar = 10 μm. Data represent mean ± s.e.m. (n = 80-100 cells) from three independent experiments. **(H,J)** TR-EGF endosome-to-lysosome trafficking analysis (H) and quantification (J) show accumulation of undegraded TR-EGF (red) on EEA1-positive early endosomes (green) after 1-h chase of endocytosed TR-EGF in shSIMPLE-transfected HeLa cells compared with the shCTRL-transfected control. Scale bar = 10 μm. Data represent mean ± s.e.m. (n = 80-120 cells) from three independent experiments. * $P = 0.001$ versus the control, unpaired two-tailed Student's t-test. **(K,L)** Immunoblot analysis (K) and quantification (L) show levels of phospho-ERK1/2 (*p*-ERK1/2) and total ERK1/2 at the indicated times following treatment with 10 ng/ml EGF in shSIMPLE- or shCTRL-

transfected HeLa cells. The *p*-ERK1/2 level was normalized to the ERK1/2 level and plotted as a percentage of the peak value of the normalized *p*-ERK1/2 level. Data represent mean ± s.e.m (n = 3).

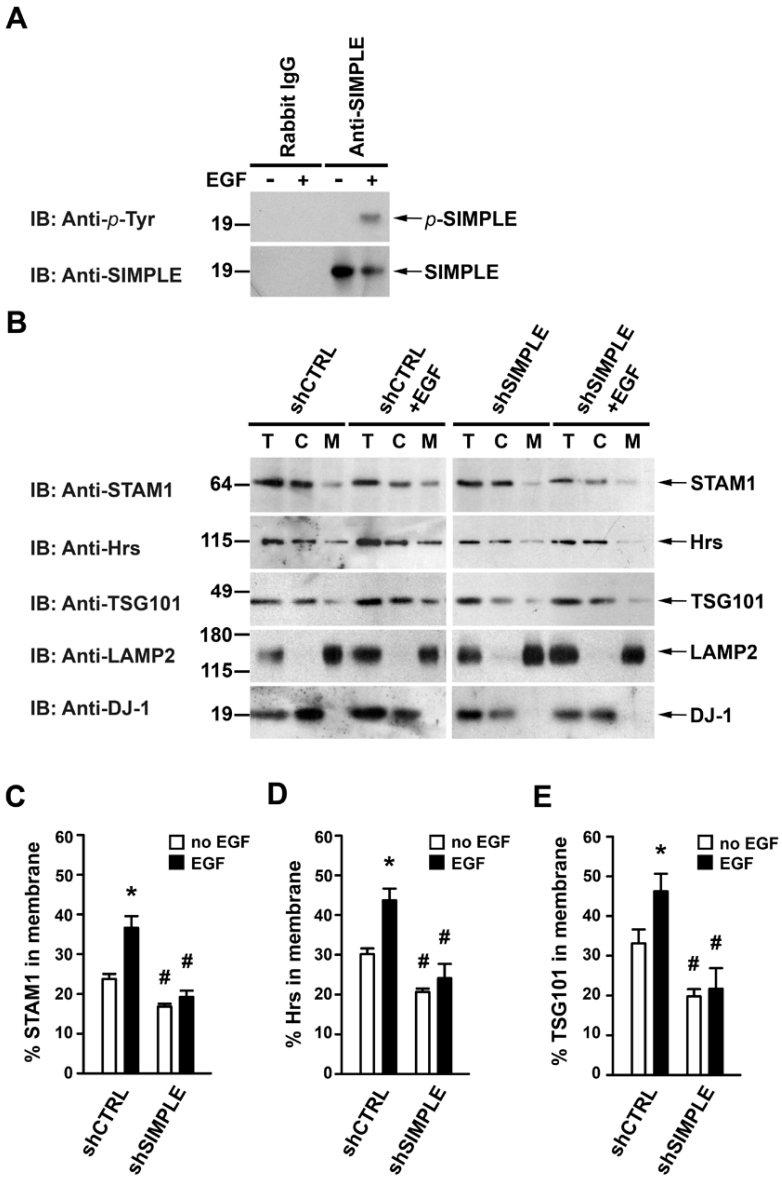

Figure 3. SIMPLE is required for efficient association of STAM1, Hrs and TSG101 with membranes. (A) EGFR activation promotes tyrosoine phosphorylation of SIMPLE. Lysates from untreated or EGF (100 ng/ml for 15 min)-treated HeLa cells were immunoprecipitated with anti-SIMPLE antibody or control rabbit IgG followed by immunoblotting. **(B)** Post-nuclear supernatant (T) from untreated or EGF (100 ng/ml for 15 min)-treated HeLa cells expressing the indicated shRNAs were separated into cytosol (C) and membrane (M) fractions. Aliquots representing an equal percentage of each

fraction were subjected to immunoblot analyses. **(C-E)** The percentages of STAM1 (C), Hrs (D) and TSG101 (E) in the membrane fraction relative to the total amount in the corresponding post-nuclear supernatant (T) were quantified and shown as mean ± s.e.m. from three independent experiments. * $P < 0.05$ versus the untreated control, # $P < 0.05$ compared with the corresponding shCTRL-transfected control, two-way analysis of variance with a Tukey's *post hoc* test.

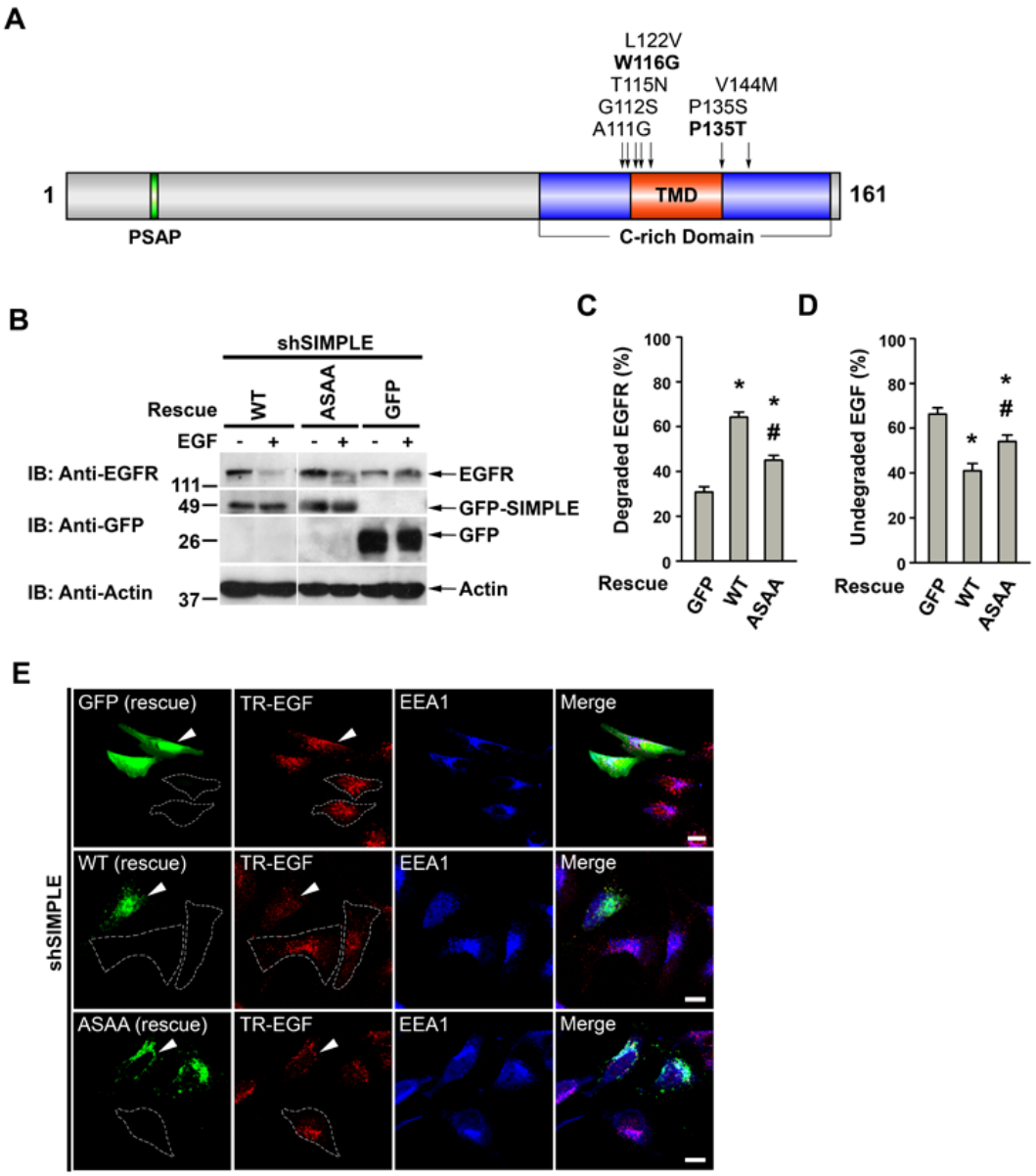

Figure 4. SIMPLE interaction with TSG101 is required for ligand-induced EGFR degradation and EGF endosome-to-lysosome trafficking. **(A)** Domain structure of SIMPLE. The locations of the PSAP motif and CMT1C-linked SIMPLE mutations are indicated on the domain structure. **(B-E)** SIMPLE-depleted HeLa cells with shSIMPLE were "rescued" by transfection with shSIMPLE-resistant SIMPLE WT and SIMPLE

ASAA mutant or GFP control. Analysis of EGF (100 ng/ml for 1 h)-induced EGFR degradation (B) and quantification (C) show that SIMPLE ASAA mutant is much less effective than SIMPLE WT in rescuing the EGFR degradation phenotype of SIMPLE-depleted cells. Data represent mean ± s.e.m (n = 3). * $P < 0.05$ versus the GFP control, # $P < 0.05$ compared with SIMPLE WT, one-way analysis of variance with a Tukey's *post hoc* test. TR-EGF endosome-to-lysosome trafficking analysis (E) and quantification (D) show more accumulation of undegraded TR-EGF (red) on EEA1-positive early endosomes (blue) after 1-h chase of endocytosed TR-EGF in SIMPLE ASAA-rescued cells (green) than that in the SIMPLE WT-rescued cells (green). Scale bar = 10 μm. Data represent mean ± s.e.m. (n = 50-80 cells) from three independent experiments. * $P < 0.05$ versus the GFP control, # $P < 0.05$ compared with SIMPLE WT, one-way analysis of variance with a Tukey's *post hoc* test.

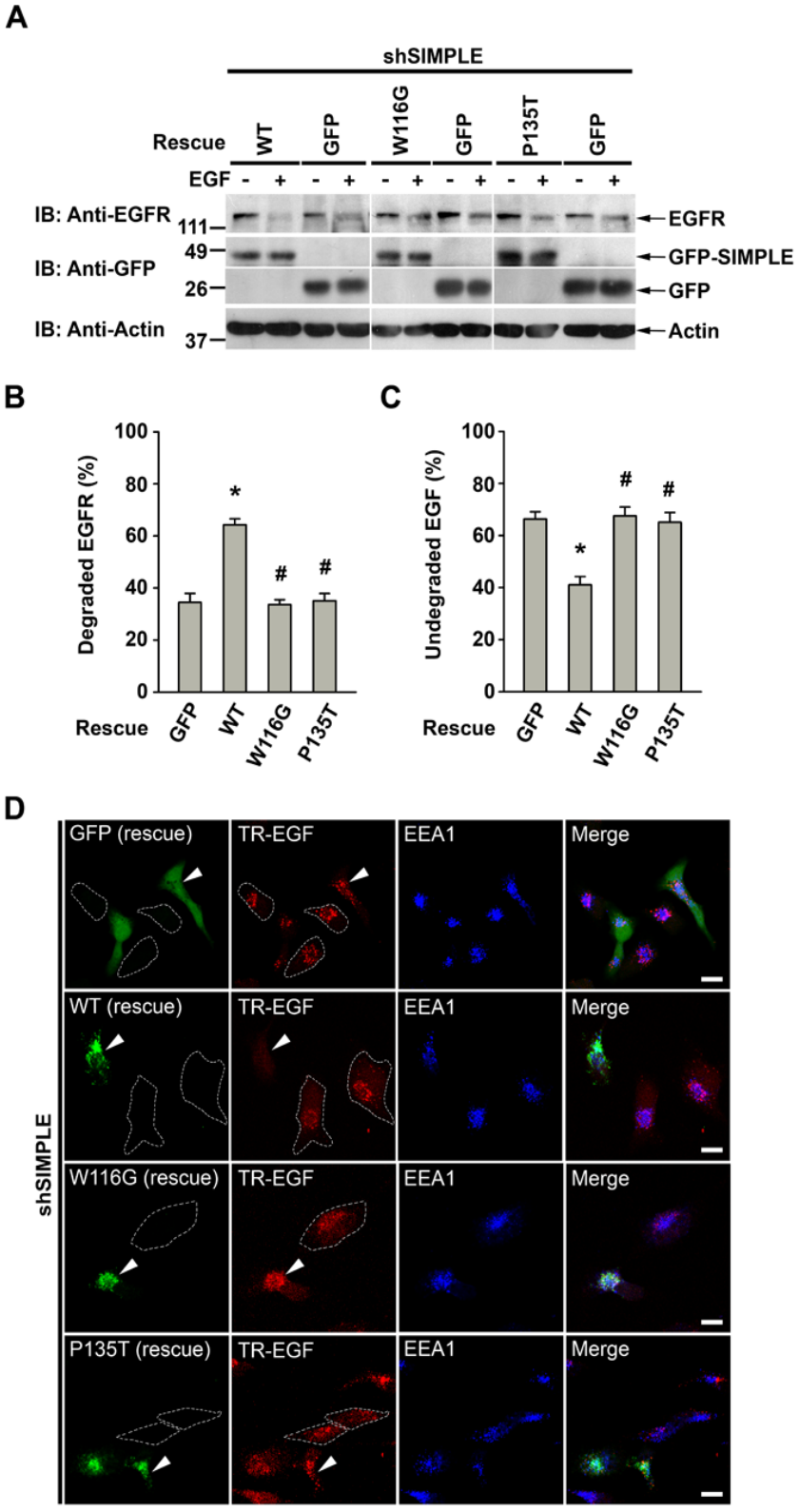
A
shSIMPLE
Rescue
WT
GFP
W116G
GFP
P135T
GFP
EGF - + - + - + - + - + - +
IB: Anti-EGFR
111
EGFR
49
IB: Anti-GFP
GFP-SIMPLE
26
GFP
IB: Anti-Actin
37
Actin
B
Degraded EGFR (%)
100
80
60
40
20
0
*
#
#
Rescue
GFP
WT
W116G
P135T
C
Undegraded EGF (%)
100
80
60
40
20
0
*
#
#
Rescue
GFP
WT
W116G
P135T
D
shSIMPLE
GFP (rescue)
TR-EGF
EEA1
Merge
WT (rescue)
TR-EGF
EEA1
Merge
W116G (rescue)
TR-EGF
EEA1
Merge
P135T (rescue)
TR-EGF
EEA1
Merge

Figure 5. CMT1C-linked mutations cause a loss of SIMPLE function in facilitating EGFR degradation and EGF endosome-to-lysosome trafficking. SIMPLE-depleted HeLa cells with shSIMPLE were "rescued" by transfection with shSIMPLE-resistant SIMPLE WT, SIMPLE W116G, SIMPLE P135T, or GFP control. **(A,B)** Analysis of EGF (100 ng/ml for 1 h)-induced EGFR degradation (A) and quantification (B) show that SIMPLE W116G and SIMPLE P135T are much less effective than SIMPLE WT in rescuing the EGFR degradation phenotype of SIMPLE-depleted cells. Data represent mean ± s.e.m from at least three independent experiments. * $P < 0.001$ versus the GFP control, # $P < 0.001$ compared with SIMPLE WT, one-way analysis of variance with a Tukey's *post hoc* test. **(C,D)** TR-EGF endosome-to-lysosome trafficking analysis (D) and quantification (C) show more accumulation of undegraded TR-EGF (red) on EEA1-positive early endosomes (blue) after 1-h chase of endocytosed TR-EGF in SIMPLE W116G- or SIMPLE P135T-rescued cells (green) than that in the SIMPLE WT-rescued cells (green). Scale bar = 10 μm. Data represent mean ± s.e.m. (n = 50-80 cells) from three independent experiments. * $P < 0.001$ versus the GFP control, # $P < 0.001$ compared with SIMPLE WT, one-way analysis of variance with a Tukey's *post hoc* test.

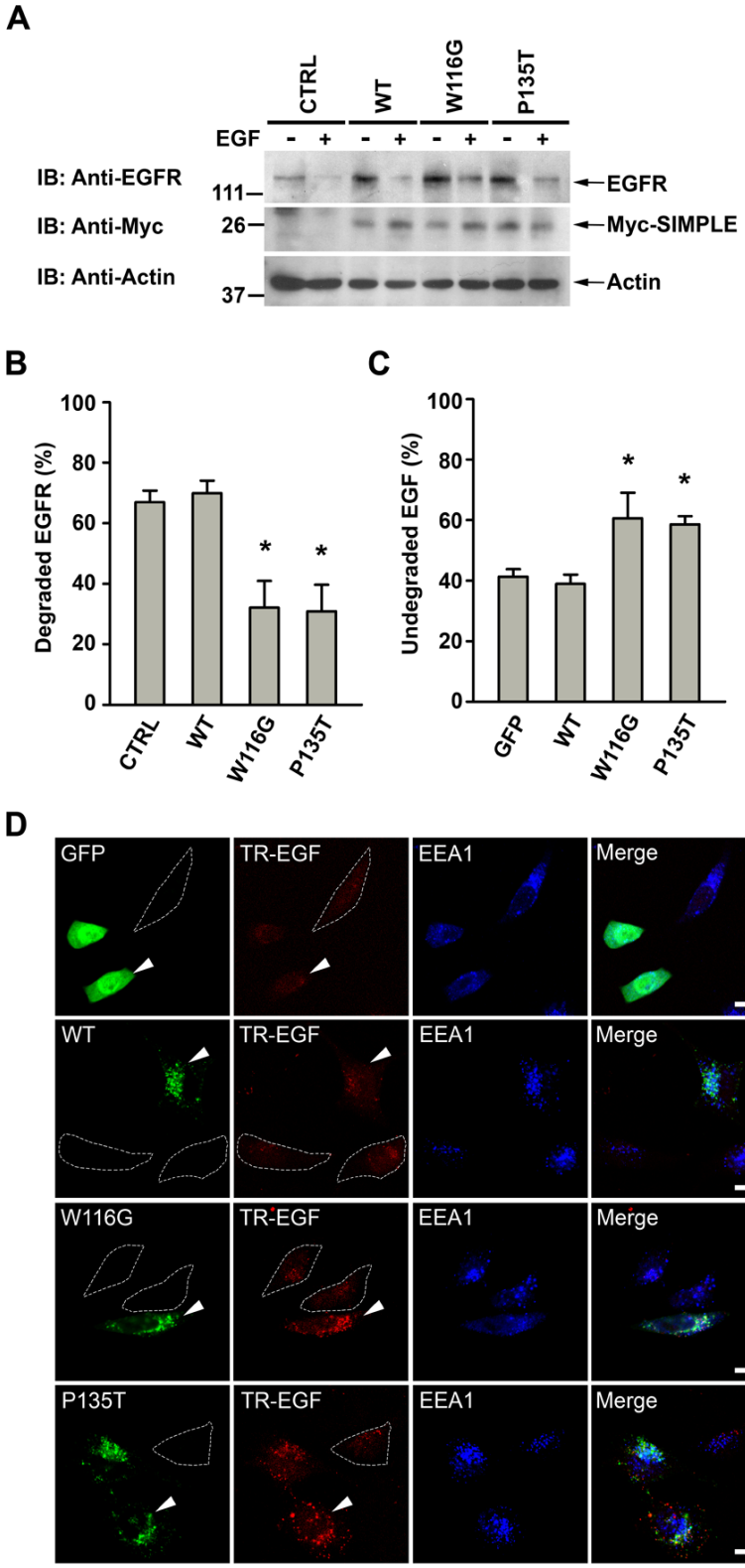
A
CTRL
WT
W116G
P135T
EGF - + - + - + - +
IB: Anti-EGFR
111
EGFR
IB: Anti-Myc
26
Myc-SIMPLE
IB: Anti-Actin
37
Actin
B
Degraded EGFR (%)
100
80
60
40
20
0
CTRL
WT
W116G
P135T
C
Undegraded EGF (%)
GFP
WT
W116G
P135T
D
GFP
TR-EGF
EEA1
Merge
WT
W116G
P135T

Figure 6. CMT1C-linked SIMPLE mutants have dominant-negative effects on EGFR degradation and EGF endosome-to-lysosome trafficking. (A,B) HeLa cells expressing Myc-tagged SIMPLE WT, SIMPLE W116G, SIMPLE P135T, or Myc vector control (CTRL) were incubated with or without 100 ng/ml EGF for 1 h. EGFR degradation analysis (A) and quantification (B) show reduced levels of degraded EGFR in SIMPLE W116G- or SIMPLE P135T-transfected cells compared with SIMPLE WT-transfected cells or the Myc vector control. Data represent mean ± s.e.m from at least three independent experiments. * $P < 0.05$ compared with SIMPLE WT or the vector control, one-way analysis of variance with a Tukey's *post hoc* test. **(C,D)** TR-EGF endosome-to-lysosome trafficking analysis (D) and quantification (C) show more accumulation of undegraded TR-EGF (red) on EEA1-positive early endosomes (blue) after 1-h chase of endocytosed TR-EGF in GFP-tagged SIMPLE W116G- or SIMPLE P135T-transfected cells (green) than that in the GFP-tagged SIMPLE WT- or GFP-transfected cells (green). Scale bar = 10 μm. Data represent mean ± s.e.m. (n = 50-80 cells) from three independent experiments. * $P < 0.05$ compared with SIMPLE WT or the vector control, one-way analysis of variance with a Tukey's *post hoc* test.

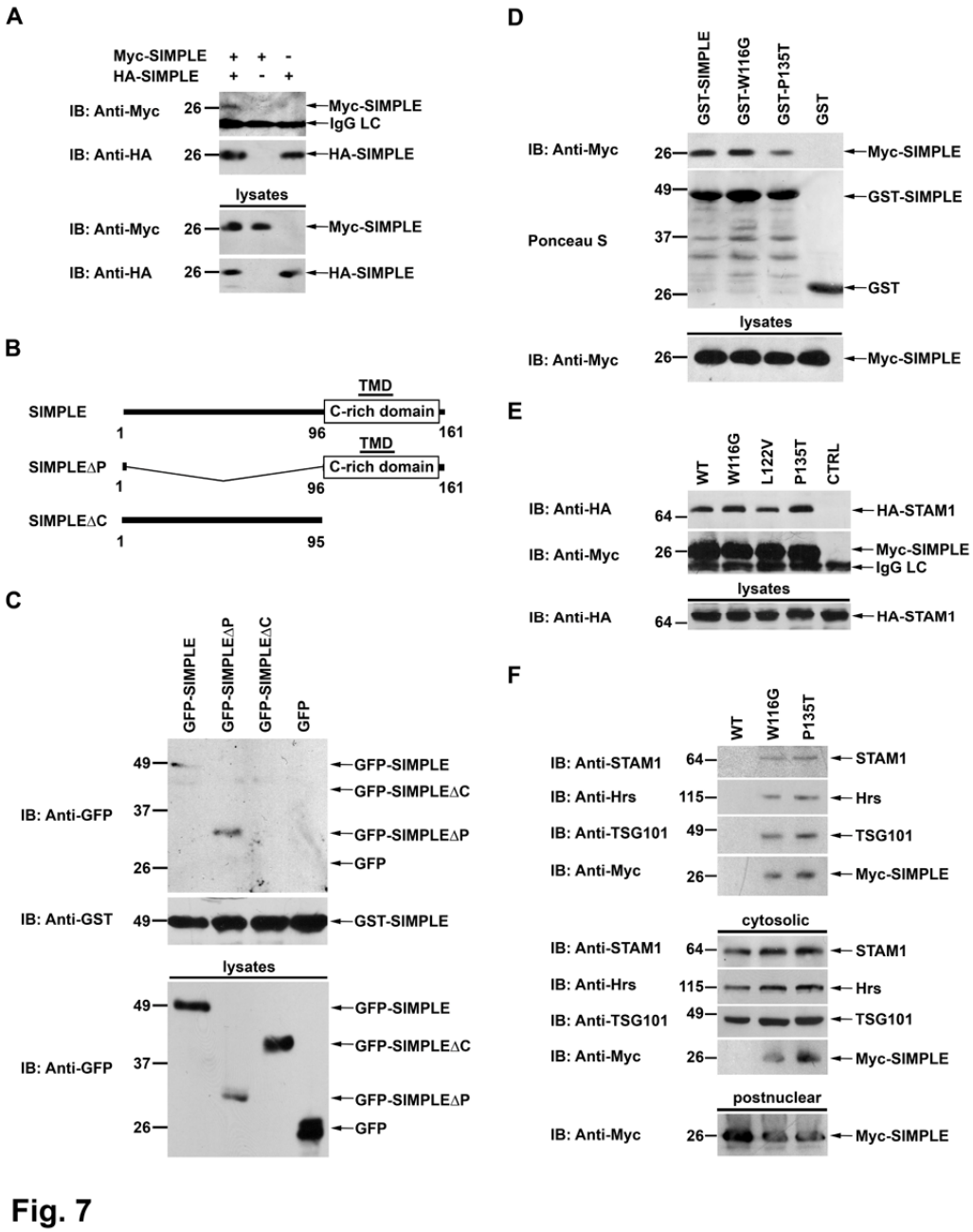

Fig. 7

Figure 7. CMT1C-linked SIMPLE mutants interact with SIMPLE WT, STAM1 and TSG101. (A) SIMPLE self-association in cells. Lysates from HeLa cells expressing Myc-tagged SIMPLE or empty Myc vector and HA-tagged SIMPLE or empty HA vector were immunoprecipitated with anti-HA antibody followed by immunoblot analyses. IgG LC, IgG light chain. **(B)** Schematic illustrating SIMPLE and its deletion mutants encoded

by GFP-tagged cDNA constructs. **(C)** The C-rich domain is required for SIMPLE self-association. GST pull-down assays were performed by incubation of immobilized GST-tagged full-length SIMPLE with lysates of HeLa cells expressing GFP-tagged full-length SIMPLE, SIMPLEΔP, SIMPLEΔC, or GFP control. Bound proteins were detected by immunoblotting. **(D)** Interaction of CMT1C-linked SIMPLE mutants with SIMPLE WT. GST pull-down assays were performed by incubation of immobilized GST-tagged SIMPLE WT, SIMPLE W116G, SIMPLE P135T, or GST control with lysates of HeLa cells expressing Myc-tagged SIMPLE WT. Bound SIMPLE protein was detected by immunoblotting. **(E)** Interaction of CMT1C-linked SIMPLE mutants with STAM1. Lysates from HeLa cells co-transfected with HA-tagged STAM1 and Myc-tagged SIMPLE WT or indicated CMT1C-linked SIMPLE mutant or Myc vector (CTRL) were subjected to immunoprecipitation with anti-Myc antibody followed by immunoblot analyses. **(F)** Interaction of CMT1C-linked SIMPLE mutants with STAM1 and TSG101 in the cytosolic fraction. Post-nuclear supernatants from transfected HeLa cells expressing Myc-tagged SIMPLE WT, SIMPLE W116G, or SIMPLE P135T were separated into cytosolic and membrane fractions, and the cytosolic fractions were immunoprecipitated with anti-Myc antibody followed by immunoblot analysis. IgG LC, IgG light chain.

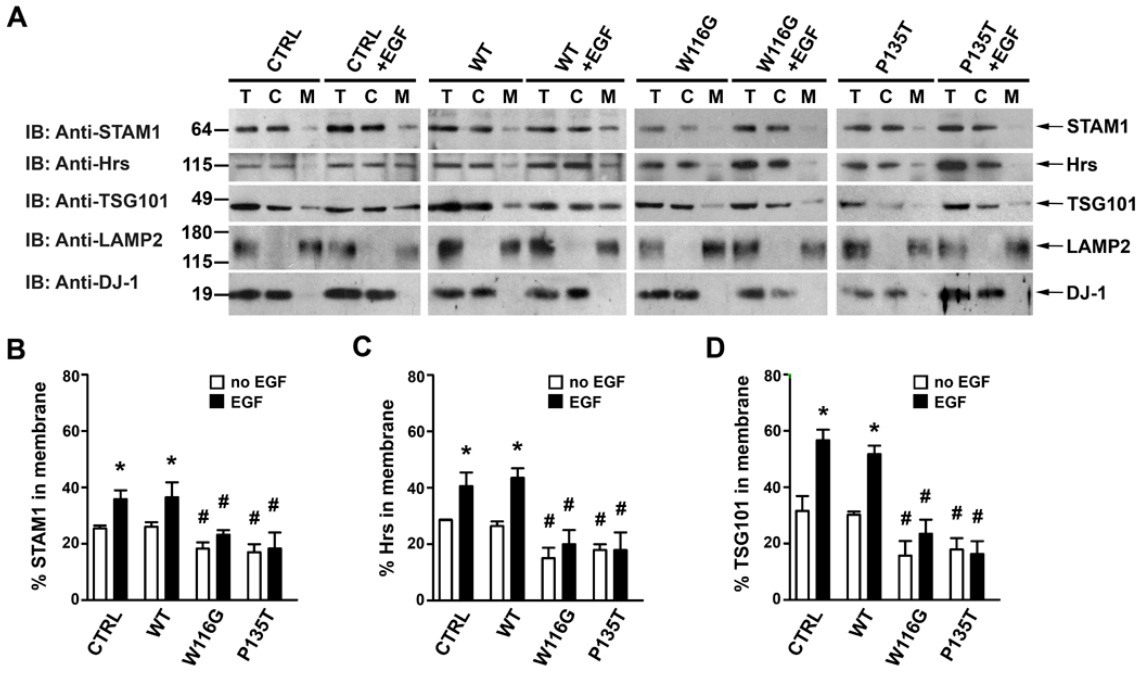

Figure 8. CMT1C-linked SIMPLE mutants inhibit the association of STAM1, Hrs and TSG101 with membranes. (A) Post-nuclear supernatant (T) from untreated or EGF (100 ng/ml for 15 min)-treated HeLa cells expressing Myc-tagged SIMPLE WT, SIMPLE W116G, SIMPLE P135T, or Myc vector control (CTRL) were separated into cytosol (C) and membrane (M) fractions. Aliquots representing an equal percentage of each fraction were subjected to immunoblot analyses. **(B-D)** The percentages of STAM1 (B), Hrs (C) and TSG101 (D) in the membrane fraction relative to the total amount in the corresponding post-nuclear supernatant (T) were quantified and shown as mean ± s.e.m. from three independent experiments. * $P < 0.05$ versus the untreated control and WT-expressing cells, # $P < 0.05$ compared with the corresponding control and WT-expressing cells, two-way analysis of variance with a Tukey's *post hoc* test.

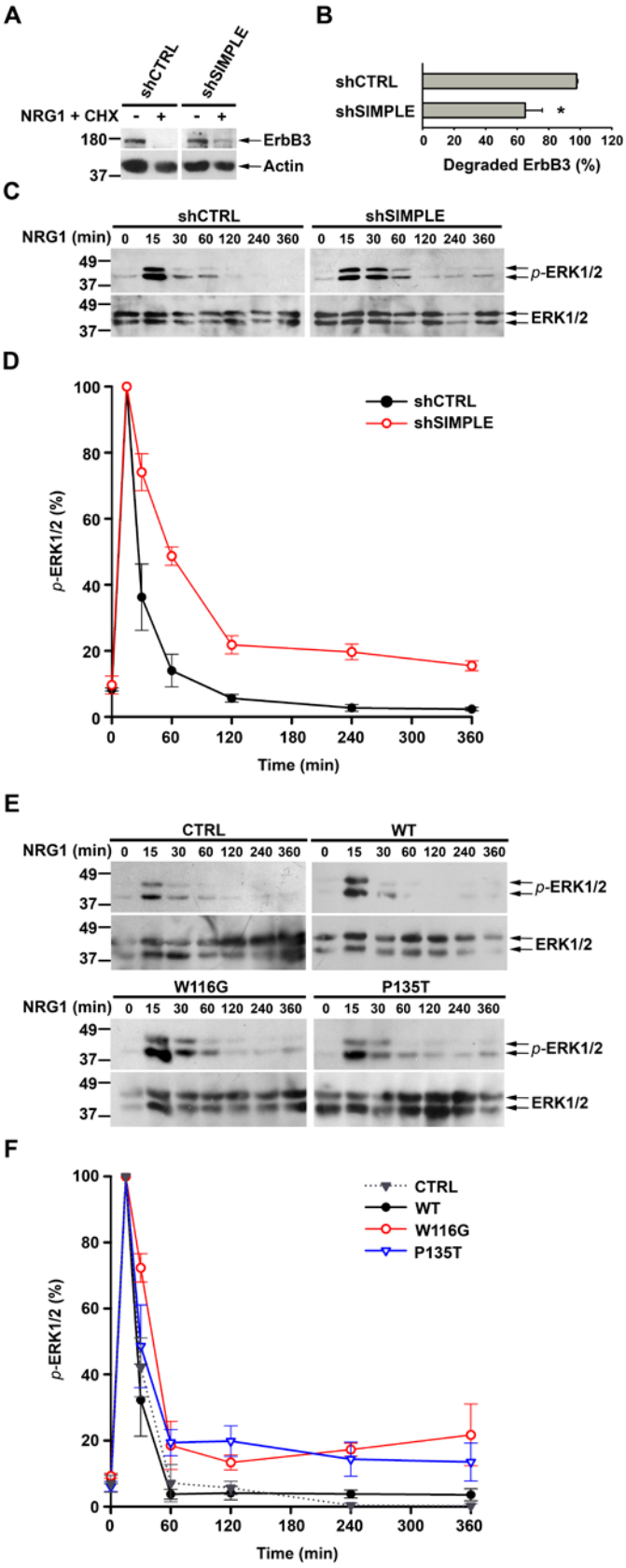
A
shCTRL
shSIMPLE
NRG1 + CHX
-
+
-
+
180
37
ErbB3
Actin
B
shCTRL
shSIMPLE
*
0
20
40
60
80
100
120
Degraded ErbB3 (%)
C
shCTRL
shSIMPLE
NRG1 (min)
0 15 30 60 120 240 360
0 15 30 60 120 240 360
49
37
49
37
p-ERK1/2
ERK1/2
D
shCTRL
shSIMPLE
p-ERK1/2 (%)
100
80
60
40
20
0
0
60
120
180
240
300
360
Time (min)
E
CTRL
WT
NRG1 (min)
0 15 30 60 120 240 360
0 15 30 60 120 240 360
49
37
49
37
p-ERK1/2
ERK1/2
W116G
P135T
NRG1 (min)
0 15 30 60 120 240 360
0 15 30 60 120 240 360
49
37
49
37
p-ERK1/2
ERK1/2
F
CTRL
WT
W116G
P135T
p-ERK1/2 (%)
100
80
60
40
20
0
0
60
120
180
240
300
360
Time (min)

Figure 9. CMT1C-linked SIMPLE mutants have dominant-negative effects on NRG1-ErbB signaling in Schwann cells. (A,B) Mouse MSC80 Schwann cells stably transfected with the indicated shRNAs were incubated in the absence or presence of 10 nM NRG1 and 100 μg/ml cycloheximide (CHX) for 4 h. ErbB3 degradation analysis (A) and quantification (B) show reduced levels of NRG1-induced ErbB3 degradation in shSIMPLE-transfected Schwann cells compared with the shCTRL-transfected control. Data represent mean ± s.e.m (n = 3). * P = 0.039, unpaired two-tailed Student's t-test. **(C,D)** Immunoblot analysis (C) and quantification (D) show levels of *p*-ERK1/2 and total ERK1/2 at the indicated times following treatment with 10 nM NRG1 in shSIMPLE- or shCTRL-transfected Schwann cells. The *p*-ERK1/2 level was normalized to the ERK1/2 level and plotted as a percentage of the peak value of the normalized *p*-ERK1/2 level. Data represent mean ± s.e.m (n = 3). **(E,F)** Immunoblot analysis (E) and quantification (F) show levels of *p*-ERK1/2 and total ERK1/2 at the indicated times following treatment with 10 nM NRG1 in MSC80 cells expressing Myc-tagged SIMPLE WT, SIMPLE W116G, SIMPLE P135T, or the empty Myc vector (CTRL). The *p*-ERK1/2 level was normalized to the ERK1/2 level and plotted as a percentage of the peak value of the normalized *p*-ERK1/2 level. Data represent mean ± s.e.m (n = 3).

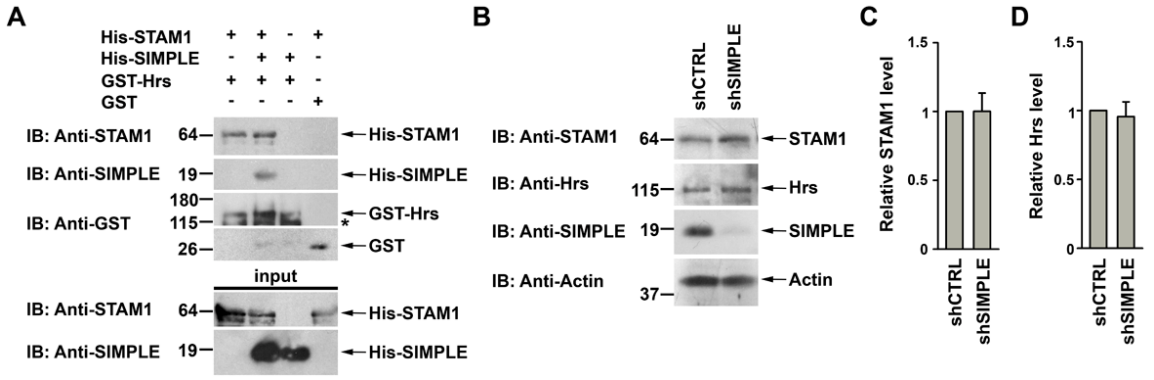

Supplementary figure S1. SIMPLE does not interact directly with Hrs and does not regulate the stability of STAM1 and Hrs. (A) *In vitro* binding assays were performed by incubation of soluble His-tagged STAM1 protein (input) in the presence and absence of soluble His-SIMPLE protein (input) with immobilized GST or GST-Hrs fusion protein. Bound STAM1 and SIMPLE proteins were detected by immunoblotting. **(B-D)** Immunoblot analyses of STAM1 and Hrs protein levels (B) and quantification (C,D) show that depletion of SIMPLE has no affect on STAM1 (C) and Hrs (D) stability. Data represent mean ± s.e.m (n = 3).

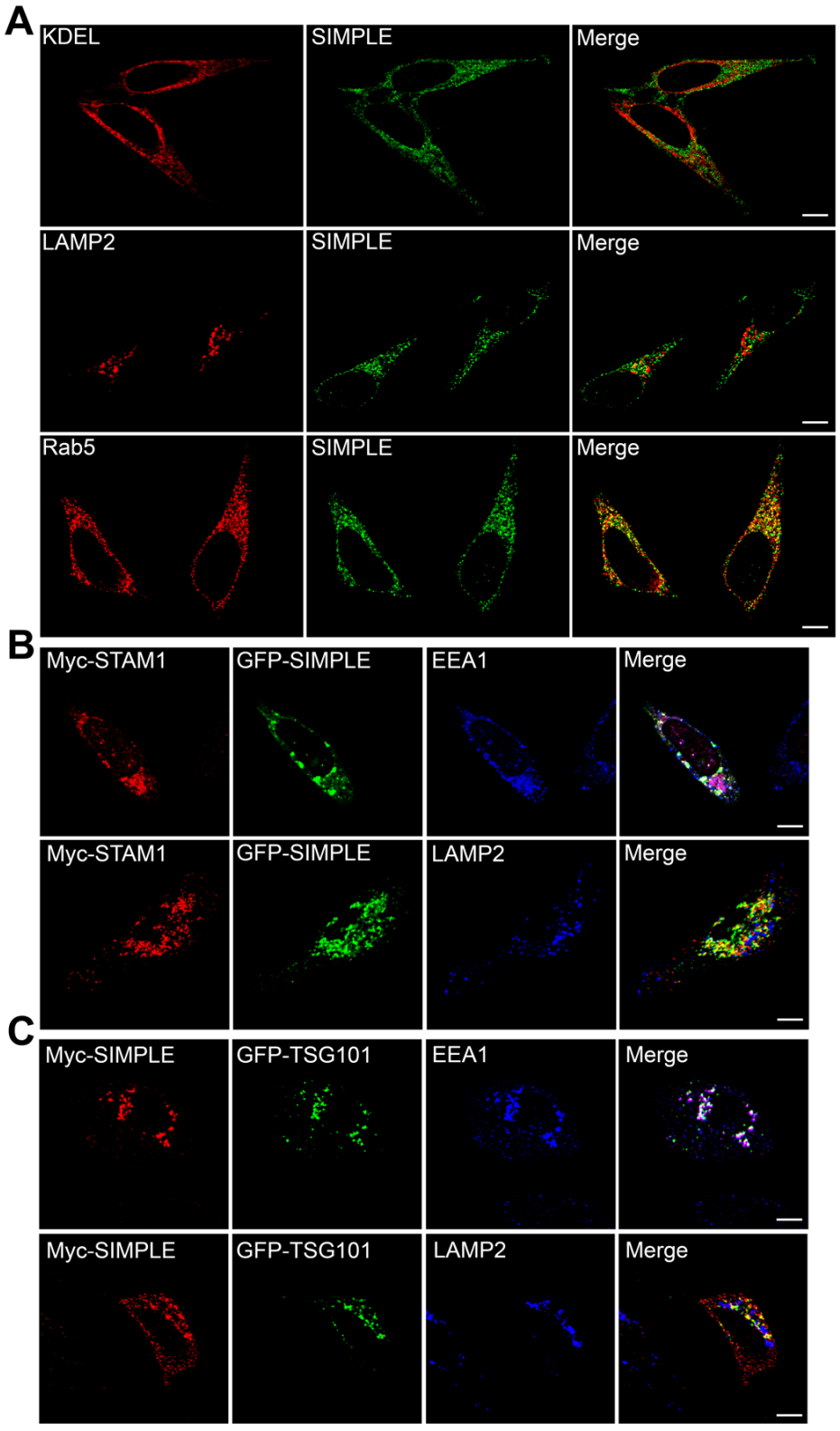
A
KDEL
SIMPLE
Merge
LAMP2
SIMPLE
Merge
Rab5
SIMPLE
Merge
B
Myc-STAM1
GFP-SIMPLE
EEA1
Merge
Myc-STAM1
GFP-SIMPLE
LAMP2
Merge
C
Myc-SIMPLE
GFP-TSG101
EEA1
Merge
Myc-SIMPLE
GFP-TSG101
LAMP2
Merge

Supplementary figure S2. SIMPLE associates with STAM1 and TSG101 on early endosomes. **(A)** HeLa cells were double immunostained with antibodies against SIMPLE (green) and KDEL, LAMP2 or Rab5 (red). **(B)** Colocalization of SIMPLE with STAM1 on early endosomes. HeLa cells expressing Myc-tagged STAM1 and GFP-tagged SIMPLE (green) were immunostained with antibodies against Myc (red) and EEA1 or LAMP2 (blue). **(C)** Colocalization of SIMPLE with TSG101 on early endosomes. HeLa cells expressing Myc-tagged SIMPLE and GFP-tagged TSG101 (green) were immunostained with antibodies against Myc (red) and EEA1 or LAMP2 (blue). Scale bar = 10 μm.

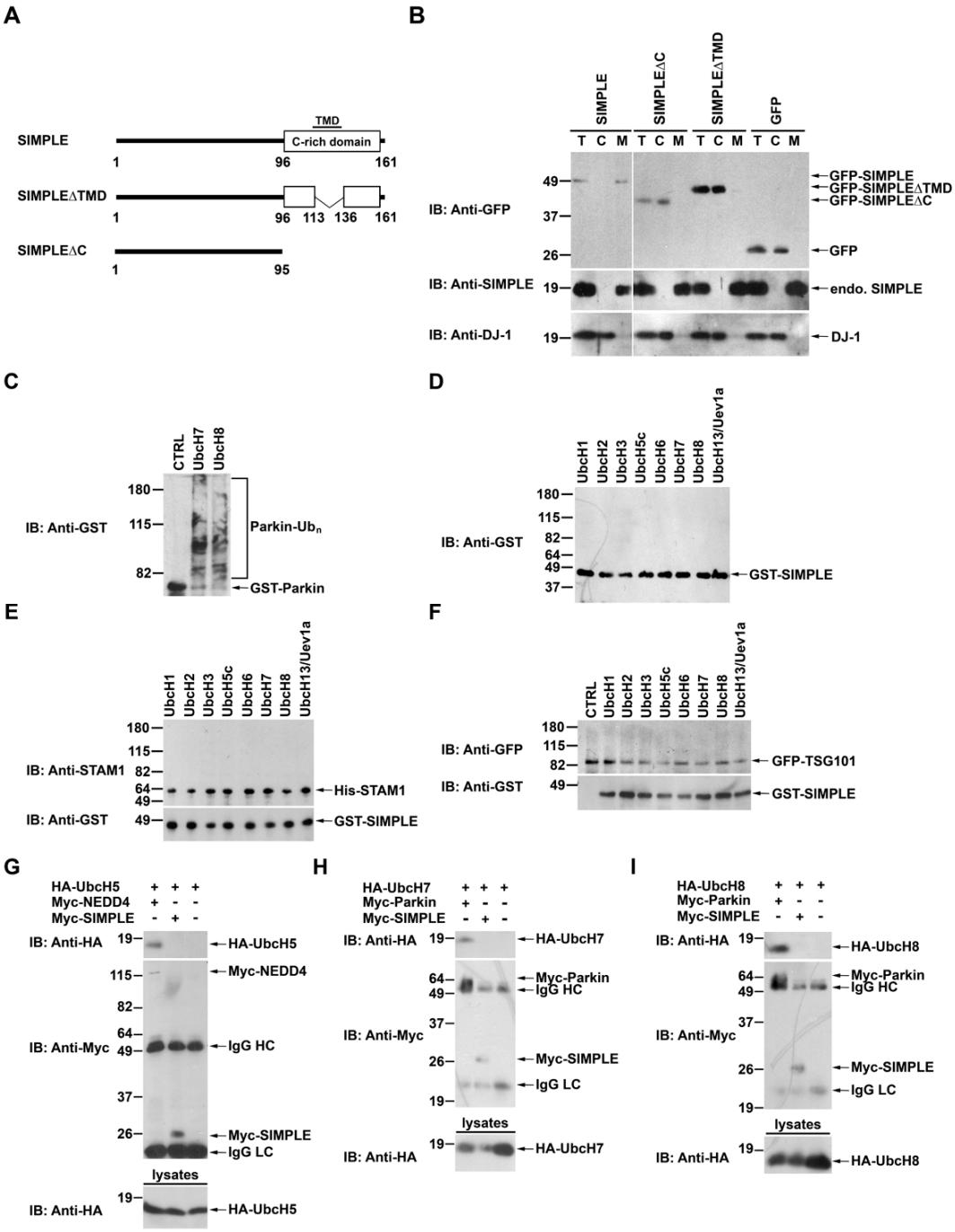

Supplementary figure S3. SIMPLE has no E3 ligase activity and does not interact with E2 enzymes UbcH5, UbcH7, and UbcH8. (A) Schematic illustrating SIMPLE and its deletion mutants encoded by GFP-tagged cDNA constructs. **(B)** Post-nuclear supernatants (T) of HeLa cells expressing GFP-tagged SIMPLE, SIMPLEΔTMD,

SIMPLEΔC, or GFP proteins were separated into cytosol (C) and membrane (M) fractions. Aliquots representing an equal percentage of each fraction were subjected to immunoblot analyses. endo. SIMPLE, endogenous SIMPLE. **(C)** *In vitro* ubiquitination assays with purified GST-tagged parkin protein in the presence of E1 and the indicated E2s demonstrated robust parkin auto-ubiquitinating activity. **(D)** *In vitro* ubiquitination assays with purified GST-tagged SIMPLE protein in the presence of E1 and various E2s show a lack of SIMPLE auto-ubiquitinating activity. **(E)** *In vitro* ubiquitination assays with purified His-tagged STAM1 in the presence of E1, various E2s, and GST-tagged SIMPLE show a lack of E3 ligase activity for SIMPLE to ubiquitinate STAM1. **(F)** *In vitro* ubiquitination assays with immunopurified GFP-tagged TSG101 in the presence of E1, various E2s, and GST-tagged SIMPLE show a lack of E3 ligase activity for SIMPLE to ubiquitinate TSG101. *In vitro* ubiquitination assay with immunopurified GFP-tagged TSG101 in the absence of E2 and GST-tagged SIMPLE was used as the negative control (CTRL). **(G-I)** Lysates from HeLa cells co-transfected with Myc-tagged SIMPLE (G-I), NEDD4 (G), parkin (H,I), or empty Myc vector and HA-tagged UbcH5 (G), UbcH7 (H), or UbcH8 (I) were immunoprecipitated with anti-Myc antibody followed by immunoblot analyses. IgG HC, IgG heavy chain; IgG LC, IgG light chain.

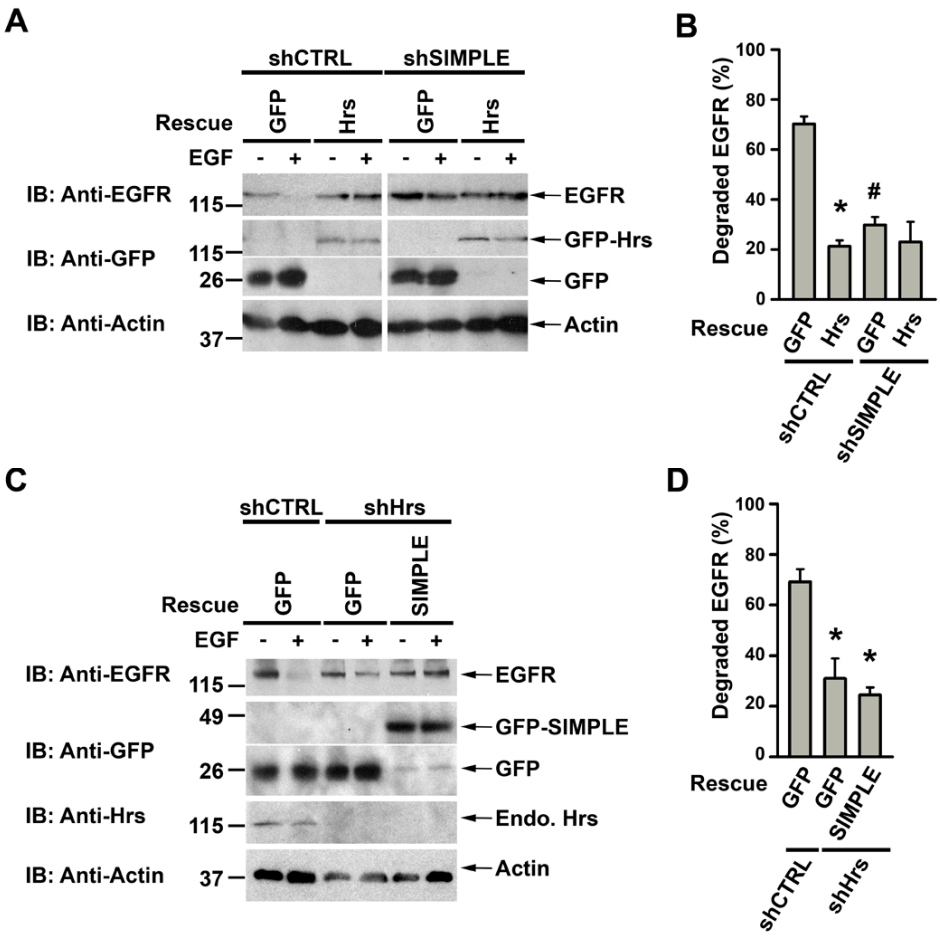

Supplementary figure S4. Hrs and SIMPLE are not functionally redundant in mediating EGFR degradation. (A,B) SIMPLE-depleted HeLa cells with shSIMPLE were subjected to rescue experiments by transfection of GFP-tagged Hrs or GFP control. Analysis of EGF (100 ng/ml for 1 h)-induced EGFR degradation (A) and quantification (B) show that GFP-tagged Hrs expression did not rescue the EGFR degradation phenotype of SIMPLE-depleted cells. Data represent mean ± s.e.m from at least three independent experiments. * $P < 0.001$ versus the GFP control, # $P < 0.001$ compared with the respective shCTRL-transfected control, two-way analysis of variance with a Tukey's *post hoc* test. **(C,D)** Hrs-depleted HeLa cells with shHrs were subjected to rescue experiments by transfection of GFP-tagged SIMPLE, Hrs, or GFP control.

Analysis of EGF (100 ng/ml for 1 h)-induced EGFR degradation (C) and quantification (D) show that GFP-tagged SIMPLE expression, unlike GFP-tagged Hrs, did not rescue the EGFR degradation phenotype of Hrs-depleted cells. Data represent mean ± s.e.m from at least three independent experiments. * $P < 0.001$ versus the GFP control, # $P < 0.001$ compared with the respective shCTRL-transfected control, two-way analysis of variance with a Tukey's *post hoc* test.

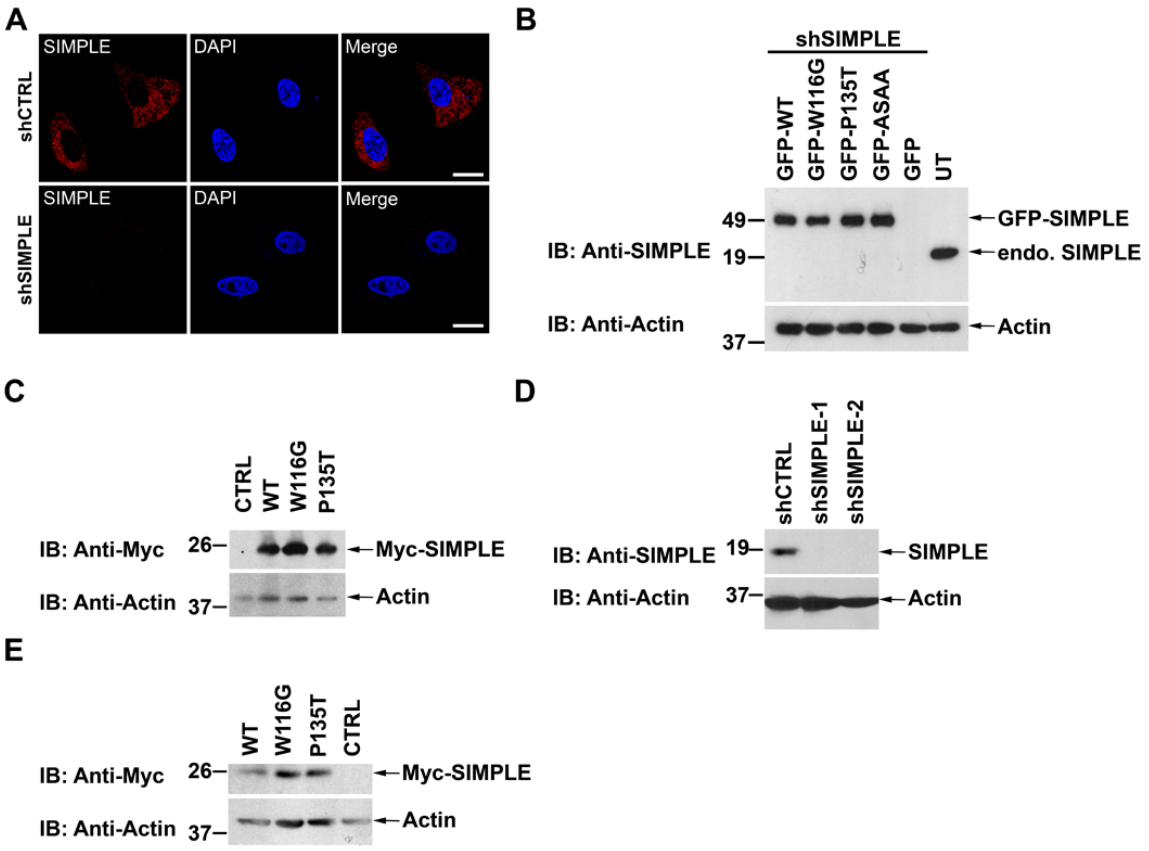

Supplementary figure S5. Analysis of endogenous and exogenous SIMPLE protein expression in stably transfected HeLa and MSC80 cells. **(A)** HeLa cells stably transfected with the SIMPLE-targeting shRNAs (shSIMPLE) or non-targeting control shRNAs (shCTRL) were stained with anti-SIMPLE antibody (red) and DAPI (blue). **(B)** Lysates from untransfected (UT) HeLa cells or SIMPLE-depleted HeLa cells transfected with shSIMPLE-resistant GFP-tagged SIMPLE WT, SIMPLE W116G, SIMPLE P135T, or SIMPLE ASAA or the GFP control were analyzed by immunoblotting. endo. SIMPLE, endogenous SIMPLE. **(C)** Lysates from HeLa cells transiently transfected with Myc-tagged SIMPLE WT, SIMPLE W116G, SIMPLE P135T, or Myc vector control (CTRL) were analyzed by immunoblotting. **(D)** Lysates from MSC80 cells stably

transfected with SIMPLE-targeting shRNAs (shSIMPLE-1 or shSIMPLE-2) or non-targeting control shRNA (shCTRL) were analyzed by immunoblotting. **(E)** Lysates from MSC80 cells stably transfected with Myc-tagged SIMPLE WT, SIMPLE W116G, SIMPLE P135T, or the empty Myc vector (CTRL) were analyzed by immunoblotting.

Chapter 4

Motor and sensory neuropathy due to myelin infolding and paranodal damage in a transgenic mouse model of Charcot-Marie-Tooth disease type 1C

Part of the work described in this Chapter has been submitted to *Human Molecular Genetics*:

Lee, S.M., Mohammed, A.A., Asress, S., Glass, J.D., Chin, L.-S., and Li, L. (2012) Motor and sensory neuropathy due to myelin infolding and paranodal damage in a transgenic mouse model of Charcot-Marie-Tooth disease type 1C. Submitted.

Abstract

Charcot-Marie-Tooth disease type 1C (CMT1C) is a progressive, dominantly inherited motor and sensory neuropathy. Despite human genetic evidence linking missense mutations in SIMPLE to CMT1C, the *in vivo* role of CMT1C-linked SIMPLE mutations remains undetermined. To investigate the molecular mechanism underlying CMT1C pathogenesis, we generated transgenic mice expressing either wild-type or CMT1C-linked W116G human SIMPLE. Mice expressing mutant, but not wild-type, SIMPLE develop a progressive motor and sensory neuropathy that recapitulates key clinical features of CMT1C disease. SIMPLE mutant mice exhibit motor and sensory behavioral impairments accompanied by decreased motor and sensory nerve conduction velocity and reduced compound muscle action potential amplitude. This neuropathy phenotype is associated with focally infolded myelin loops that protrude into the axons at paranodal regions and near Schmidt–Lanterman incisures of peripheral nerves. We find that myelin infolding is often linked to constricted axons with signs of impaired axonal transport and to paranodal defects and abnormal organization of the node of Ranvier. Our findings support that SIMPLE mutation disrupts myelin homeostasis and causes progressive peripheral neuropathy via a combination of toxic gain-of-function and dominant-negative mechanisms. The results from this study suggest that myelin infolding and paranodal damage may represent pathogenic precursors preceding demyelination and axonal degeneration in CMT1C patients.

Introduction

Charcot-Marie-Tooth disease (CMT), also known as hereditary motor and sensory neuropathy, encompasses a genetically heterogeneous group of inherited disorders of the peripheral nervous system (PNS) (Pareyson and Marchesi, 2009; Patzko and Shy, 2011). CMT is categorized into the demyelinating type which accounts for 80% of CMT cases and the axonal degeneration type which accounts for 20% of CMT cases (Nelis et al., 1996). CMT type 1C (CMT1C) is a dominantly inherited, demyelinating type of peripheral neuropathy characterized by slowed motor and sensory nerve conduction velocity with typical CMT clinical symptoms, including progressive motor weakness and sensory loss (Campbell et al., 2004; Gerding et al., 2009; Latour et al., 2006; Saifi et al., 2005; Street et al., 2003). Human genetic studies have revealed that CMT1C is linked to missense mutations in small integral membrane protein of lysosome/late endosome [SIMPLE; also known as lipopolysaccharide-induced TNF-α factor (LITAF)], a ubiquitously expressed protein of unknown function (Campbell et al., 2004; Gerding et al., 2009; Latour et al., 2006; Saifi et al., 2005; Street et al., 2003). Our recent study indicates that endogenous SIMPLE is an early endosomal membrane protein (Lee et al., 2011) rather than a lysosomal/late endosomal protein as previously suggested (Moriwaki et al., 2001). We found that CMT1C-linked mutations map in and around the transmembrane domain of SIMPLE and that these mutations cause mislocalization of SIMPLE protein from the early endosome to the cytosol in cultured cells (Lee et al., 2011). The *in vivo* role of CMT1C-linked SIMPLE mutations remains undetermined.

Molecular analysis of the genotype-phenotype relationship in hereditary peripheral neuropathy is essential for a mechanistic understanding of CMT pathogenesis.

The identified linkage of heterozygous SIMPLE missense mutations to autosomal dominant CMT1C (Campbell et al., 2004; Gerding et al., 2009; Latour et al., 2006; Saifi et al., 2005; Street et al., 2003) raises two possibilities: CMT1C may be due to haplo-insufficiency of SIMPLE or dominant effects of the SIMPLE mutants. To distinguish these possibilities and determine the *in vivo* role of the identified human SIMPLE mutations, we generated transgenic mice expressing CMT1C-linked human SIMPLE W116G mutant or human SIMPLE wild-type (WT) protein. Characterization of these transgenic mice reveals that expression of human SIMPLE W116G mutant, but not human SIMPLE WT, causes a progressive motor and sensory neuropathy in mice that recapitulates key clinical features of CMT1C disease. SIMPLE W116G mutant mice exhibit motor and sensory nerve conduction defects and impaired motor and sensory performance in a dosage-dependent manner. The observed motor and sensory impairments are associated with focally infolded myelin loops that protrude into the axons at paranodal regions and near Schmidt–Lanterman incisures of motor and sensory nerves. By immunohistochemical analysis, we show that the SIMPLE W116G mutant protein, like endogenous SIMPLE protein, is localized in non-compact myelin cytoplasmic regions of myelinating Schwann cells but is absent in axons. Our findings support that SIMPLE mutation causes CMT1C pathogenesis via a combination of toxic gain-of-function and dominant-negative mechanisms.

Materials and methods

Generation and genotyping of SIMPLE WT and SIMPLE W116G transgenic mice

Conventional molecular biological techniques were used to generate the transgenic constructs encoding HA-tagged human SIMPLE WT and SIMPLE W116G mutant under the control of the human CMV promoter in the pCHA vector (Chin et al., 2001). After digestion with Mlu I and Nae I, the linearized SIMPLE transgene DNAs were microinjected into pronuclei of fertilized embryos from the FVB mice and then implanted in pseudo-pregnant female FVB/N mice. Transgenic founder mice were identified by the PCR analyses of genomic DNAs isolated mouse tails using two independent sets of transgene-specific primer pairs and then bred with FVB/N mice to established SIMPLE WT and SIMPLE W116G transgenic lines on a pure FVB/N background. Zygosity of SIMPLE WT and SIMPLE W116G transgenic mice was determined by a well-established protocol using SYBR Green real-time quantitative PCR (Q-PCR) of tail genomic DNAs and comparative C_T ($2^{-\Delta\Delta C}{}_T$) analysis as described (Haurogne et al., 2007; Livak and Schmittgen, 2001; Sakurai et al., 2008). Expression of HA-tagged SIMPLE WT and SIMPLE W116G proteins in transgenic mice was determined by immunoblot and immunostaining analyses using anti-SIMPLE antibody and anti-HA antibody.

Antibodies

The generation and characterization of rabbit polyclonal anti-SIMPLE antibody was described in our previous study (Lee et al., 2011). Other antibodies used in this study include the following: anti-HA (12CA5), anti-Actin (Millipore), anti-Rab5 (BD Transduction), anti-Dlg1 (Enzo), anti-MBP (Millipore), anti-MAG (Millipore), and anti-neurofilament H (Millipore). All secondary antibodies were purchased from Jackson ImmunoResearch Laboratories, Inc.

Teased nerve fibers, Nile red staining, and immunofluorescence confocal microscopy

Mice were perfused with 4% paraformaldehyde in 0.1 M phosphte buffer (pH 7.4). Sciatic nerves were dissected and post-fixed in 4% paraformaldehyde overnight at 4°C and washed in 0.1 M phosphate buffer. Individual fibers were separated in glycerol on glass slides and were immersed in cold acetone for 10 minutes. Teased fibers were then rehydrated in PBS and incubated at room temperature for 30 minutes in a blocking solution containing 10% horse serum, 0.5% Triton X-100, and PBS. For Nile red staining, teased fibers were mounted in Nile red solution (0.5 mg/mL in acetone) diluted 1,000× in 75% glycerol as described (Arnaud et al., 2009). For immunostaining, primary antibodies were diluted in the blocking solution and were incubated with the teased fibers overnight. After washing, teased fibers were incubated with the appropriate secondary antibodies conjugated to FITC, Texas Red, or Cy5, and were mounted with ProLong Gold (Invitrogen). Confocal images were acquired in room temperature with the Nikon Eclipse Ti confocal microscope equipped with 60×/1.4 oil immersion objectives and the Nikon EZ-C1 software.

Schwann cell culture and Western blot analysis

Primary Schwann cells were isolated from postnatal day 2 (P2) to P4 non-transgenic, SIMPLE WT and SIMPLE W116G mutant mice and cultured using established protocols as described (Haastert et al., 2007; Lee et al., 2011; Pannunzio et al., 2005). For western blot analysis, primary Schwann cells were homogenized in 1% SDS and then subjected to SDS-PAGE. The proteins were transferred onto nitrocellulose membranes and probed

with the indicated antibodies. Antibody binding was detected by using the enhanced chemiluminescence (ECL) system (Amersham Biosciences).

Behavioral tests

For the rotarod test, mice were placed on a standard rotarod apparatus (Columbus instruments) and acclimated to a non-accelerating rotarod at an initial speed of 1.25 rpm for 30 min. At the beginning of each trial, rotarod speed was accelerated at the rate of 1 rpm/min, and the latency for a mouse to fall off the accelerating rotarod was recorded. Each animal was tested six times with a 5 min of rest between each trial. For the tail-flick test, mouse tails were immersed in a water bath containing 52 ℃ water as the nociceptive stimulus, and the latency between tail immersion and tail-flick response was measured blindly from recorded videos. The test was repeated three times with a 15 min of rest between each trial, and the mean latency of each mouse over three trials was used for statistical analysis.

Electrophysiology

SIMPLE WT and W116G mutant mice and their non-transgenic littermates were analyzed at 3 months and 1 year of age. Mice were anesthetized with chloral hydrate (400 mg/kg of body weight, i.p.) and placed under a heat lamp to avoid hypothermia. Nerve conduction studies were performed using standard equipment (Nicolet Viking Quest). For sciatic nerve motor conduction assays, stimuli were given at the sciatic notch and at the ankle, and recording electrodes were inserted into interosseous muscles of the left foot while a ground electrode was inserted subcutaneously at the tail. For tail nerve

sensory conduction assays, the recording electrodes were placed at the base of the tail, keeping the anode and the cathode about 5 mm apart, and with a ground electrode placed subcutaneously 2 cm distal. Stimuli were given 4 cm distal, and sensory nerve conduction was averaged over 20 stimuli.

Histological analysis and electron microscopy

Mice were anesthesized followed by perfusion with 4% paraformaldehyde in 0.1 M phosphate buffer (pH 7.4). Dorsal roots, ventral roots, and sciatic nerves were harvested and postfixed by immersion in 4% paraformaldehyde and 2% glutaraldehyde overnight at 4°C. Nerves were then washed in 0.1 M phosphate buffer and embedded in paraffin. Cross and longitudinal semithin (0.5 µm) sections were stained with toluidine blue and were analyzed by light microscopy (Olympus). For ultrastructural studies, nerves were prepared for electron microscopy by post-fixation with OsO_4 followed by *en bloc* staining with uranyl acetate. Cross and longitudinal ultrathin (100 nm) sections were cut and stained with uranyl acetate and lead nitrate. Grids containing the ultrathin nerve sections were examined by a Hitachi H-7500 transmission electron microscope.

Morphometric analyses

Quantitative analyses of focally folded myelin, number of axons, axon roundness, axon diameter, and axon area were performed from 10 randomly selected fields of semithin sciatic nerve cross-sections (150 to 400 nerve fibers per field) per mouse with three mice analyzed per genotype. The number of nerve fibers with focally infolded myelin (internal

myelin loops) and the total number of fibers on each field were counted, and the percentage of nerve fibers with myelin infoldings was calculated. Axon roundness, axon diameter, and axon area were measured by using the ImagePro software (Media Cybermetics), and the axon roundness was calculated by the formula ($perimeter^2/4 \times \pi \times$ area). Myelin thickness and G-ratio were determined as previously described (Kobsar et al., 2003) from electron microscopic images for 50 randomly selected sciatic nerve fibers from three mice per genotype by using the ImagePro software (Media Cybermetics). Quantitative analyses of axonal degeneration and demyelination were performed from 10 randomly selected fields of sciatic nerve electron microscopic images (50 to 100 nerve fibers per field) per mouse with three mice analyzed per genotype. The number of nerve fibers with degenerating axons or demyelinated axons and the total number of fibers on each field were counted, and the percentage of nerve fibers with degenerating axons or demyelinated axons was calculated. Quantitative analysis of the nodal gap length was performed from longitudinal sciatic nerve sections for 12 to 15 nodes of Ranvier from three mice per genotype, and the nodal gap length was measured by using the ImageJ software. All quantitative analyses were performed in a blinded manner.

Statistical analysis

Data were subjected to statistical analyses by Student's t-tests or one-way analysis of variance using the SigmaPlot software (Systat Software, Inc.) Results are expressed as mean ± s.e.m. A *P*-value of less than 0.05 was considered statistically significant.

Results

Generation of transgenic mice expressing human SIMPLE WT or SIMPLE W116G mutant

To investigate the pathogenic role of CMT1C-linked SIMPLE mutation *in vivo*, we generated transgenic mice expressing either N-terminal hemagglutinin (HA)-tagged human SIMPLE W116G mutant or SIMPLE WT protein under the control of the human cytomegalovirus (CMV) promoter (Figure 1A). The CMV promoter was used to drive ubiquitous expression of SIMPLE transgenes because endogenous SIMPLE is a ubiquitously expressed protein (Campbell et al., 2004; Lee et al., 2011). Transgenic founder mice were identified by PCR analysis of tail genomic DNAs (Figure 1B) and bred with FVB/N mice to establish transgenic lines on a pure FVB/N background. The expression of HA-tagged human SIMPLE W116G mutant or SIMPLE WT protein was confirmed by immunoblot analysis of Schwann cell lysates from transgenic mice (Figure 1C) using our anti-SIMPLE antibody which recognizes both mouse and human SIMPLE proteins (Lee et al., 2011). We established three transgenic lines expressing human SIMPLE W116G mutant and selected the line with the highest expression of SIMPLE mutant protein (Figure 1C) for the experiments described below. Quantitative analysis indicated that the expression level of human SIMPLE W116G mutant protein relative to the level of endogenous mouse SIMPLE protein in Schwann cells is 45% for homozygous ($SIMPLE^{W116G/W116G}$) mice and 22% for heterozygous ($SIMPLE^{W116G/+}$) mice. We also established four transgenic lines expressing human SIMPLE WT protein and selected the line with a expression level similar to that in the SIMPLE W116G mutant mice (Figure 1C) for the analyses described below. The expression level of human

SIMPLE WT protein relative to the level of endogenous mouse SIMPLE protein in Schwann cells is 51% for homozygous (*SIMPLE*$^{WT/WT}$) mice and 24% for heterozygous (*SIMPLE*$^{WT/+}$) mice.

SIMPLE is localized to early endosomes in myelinating Schwann cells but is absent in myelin sheath or axons

The cellular and subcellular localization of endogenous SIMPLE protein in myelinated peripheral nerves remains poorly characterized. Therefore, we first performed immunofluorescence confocal microscopic analyses to determine endogenous SIMPLE protein distribution in sciatic nerves from adult non-transgenic mice and rat. We found that endogenous SIMPLE exhibits a punctate staining pattern, and double immunostaining analyses revealed that SIMPLE is localized in myelinating Schwann cells labeled by various Schwann cell markers (Figure 2A and C-F) but not in axons labeled by neurofilament H (Figure 2B). We observed no colocalization of SIMPLE with the compact myelin marker MBP (Figure 2A), indicating that SIMPLE is not a structural component of myelin sheath. We found that SIMPLE is localized in the Dlg1-positive abaxonal cytoplasmic region at the outer side of the compact myelin (Figure 2A,C) as well as in the MAG-positive adaxonal cytoplasmic region at the inner side of the compact myelin facing the axon (Figure 2B,D). In addition, SIMPLE is enriched in the Schmidt-Lanterman incisures (Figure 2E) and paranodal regions (Figure 2F). Consistent with our previous report (Lee et al., 2011), we observed a substantial colocalization of SIMPLE with the early endosome marker Rab5 in myelinating Schwann cells (Figure 2G).

Together, these results indicate that SIMPLE is localized to the early endosomes in non-compact myelin cytoplasmic regions of myelinating Schwann cells but is absent in myelin sheath or axons.

Next, we assessed the localization of human SIMPLE WT and SIMPLE W116G proteins in sciatic nerves from *SIMPLE*$^{WT/WT}$ and *SIMPLE*$^{W116G/W116G}$ transgenic mice. Double labeling immunofluorescence confocal microscopic analyses showed that HA-tagged SIMPLE WT and SIMPLE W116G mutant proteins, like the endogenous SIMPLE protein, are localized in non-compact myelin cytoplasmic regions of myelinating Schwann cells such as Schmidt-Lanterman incisures (Figure 1D) but not in axons (Figure 1E). These results confirm that the SIMPLE WT and SIMPLE W116G proteins are both targeted in a similar manner as the endogenous SIMPLE protein to the cytoplasm of myelinating Schwann cells in our transgenic mice.

SIMPLE W116G mutant mice, but not SIMPLE WT transgenic mice, exhibit motor and sensory impairments

SIMPLE W116G mutant and SIMPLE WT transgenic mice were viable, fertile, and born according to expected Mendelian ratios. They developed normally, and necropsy of these mice showed normally formed organs without any abnormality at 3, 12, and 15 months of age. Histological analysis revealed abnormalities in peripheral nerves (described later) but not in brain or spinal cord of SIMPLE W116G mutant mice (Figure 3 and data not shown). Although no observable behavioral abnormality was observed at the age of 3 and 6 months, *SIMPLE*$^{W116G/W116G}$ mice showed abnormal clenching of toes and clasping

of hind limbs upon tail suspension at 1 year of age, with some of them flexing all four limbs and even their whole body (Figure 4A). This phenotype is also seen in other mouse models of CMT (Arnaud et al., 2009; Dequen et al., 2010; Filali et al., 2011; King et al., 2011; Rosso et al., 2010) and is suggestive of abnormal motor function. In contrast, non-transgenic control mice and *SIMPLE*$^{WT/WT}$ mice extended their hind limbs and paws outwards upon tail suspension (Figure 4A and Figure 5A). To further evaluate the motor function of transgenic mice, we performed the rotarod test and found that *SIMPLE*$^{W116G/W116G}$ mice (Figure 4B and Figure 5B), but not *SIMPLE*$^{WT/WT}$ mice (Figure 5C), showed impaired motor performance compared to their non-transgenic littermates. We also observed that *SIMPLE*$^{W116G/+}$ mice exhibited a small but significant reduction in the rotarod performance at the last trial (Figure 4B), indicating that these mice may also have a mild motor deficit.

In addition to motor abnormalities, we observed that *SIMPLE*$^{W116G/W116G}$ mice occasionally self-mutilated their tails (Figure 4C), which could be a consequence of paresthesia reported in patients with CMT1C (Gerding et al., 2009; Saifi et al., 2005). Analysis of nociceptive sensory function by the tail-flick test revealed that *SIMPLE*$^{W116G/W116G}$ mice (Figure 4D), but not *SIMPLE*$^{WT/WT}$ mice (Figure 5D), performed significantly worse than their non-transgenic littermates, suggesting impaired sensory function. Together, these results indicate that *SIMPLE*$^{W116G/W116G}$ mice have motor and sensory impairments that are consistent with the clinical features of human patients with CMT1C motor and sensory neuropathy (Campbell et al., 2004; Gerding et al., 2009; Latour et al., 2006; Saifi et al., 2005; Street et al., 2003).

SIMPLE W116G mutant mice, but not SIMPLE WT transgenic mice, have motor and sensory nerve conduction defects

The pathophysiological hallmark of demyelinating CMT is slowed motor nerve conduction velocity (MNCV <38 m/s) (Berger et al., 2006; Nave et al., 2007; Patzko and Shy, 2011; Scherer and Wrabetz, 2008). Human CMT1C patients carrying SIMPLE W116G or other mutations show reduced MNCVs with 100% penetrance (Campbell et al., 2004; Gerding et al., 2009; Latour et al., 2006; Saifi et al., 2005; Street et al., 2003). To determine whether SIMPLE W116G mutant mice recapitulate this CMT1C phenotype, we performed electrophysiological analyses of motor nerve conduction in mutant mice and controls at 3 months and 1 year of age. In 3-month-old animals, the MNCVs and compound muscle action potential (CMAP) amplitudes were not significantly different in $SIMPLE^{W116G/W116G}$ and $SIMPLE^{W116G/+}$ mice compared to their non-transgenic littermates (Figure 6B,C). At 1 year of age, however, $SIMPLE^{W116G/W116G}$ mice showed significantly reduced MNCVs (Figure 6A,B) and CMAP amplitudes (Figure 6A,C) compared to their non-transgenic littermates. The 1-year-old $SIMPLE^{W116G/+}$ mice also had significantly lower MNCVs than those of the non-transgenic controls (Figure 6B), although their CMAP amplitudes were not significantly altered (Figure 6C). In contrast, $SIMPLE^{WT/WT}$ and $SIMPLE^{WT/+}$ mice showed no significant difference in the MNCV or the CMAP amplitude compared to the non-transgenic controls at 1 year of age (Figure 8A,B).

In addition to motor nerve conduction defects, electrophysiological analyses of tail sensory nerve conduction also revealed a significant decrease in the sensory nerve conduction velocity (SNCV) in the $SIMPLE^{W116G/W116G}$ and $SIMPLE^{W116G/+}$ mice compared with their non-transgenic littermates at the age of 1 year but not 3 months

(Figure 7A,B). Although the sensory nerve action potential (SNAP) amplitudes of the *SIMPLE*$^{W116G/W116G}$ and *SIMPLE*$^{W116G/+}$ mice did not significantly differ from those of the non-transgenic controls (Figure 7C), we found that sensory nerve action potentials could not be evoked in 2 out of 11 *SIMPLE*$^{W116G/W116G}$ mice tested (Figure 7A,D). The inability to evoke sensory nerve action potentials in a small percentage of CMT1C patients has been previously reported (Campbell et al., 2004) and is correlated with a loss of sensory function. Interestingly, one of the mice with no evoked sensory nerve action potentials exhibited self-injurious behavior shown in Figure 4C, suggesting that the self-mutilation behavior may be resulted from a loss of sensory nerve conduction. In contrast to the SIMPLE W116G mutant mice, *SIMPLE*$^{WT/WT}$ and *SIMPLE*$^{WT/+}$ mice did not show any difference in the SNCV or the SNAP amplitude compared to the non-transgenic controls at 1 year of age (Figure 8C,D). Together, these results indicate that SIMPLE W116G mutant mice, but not SIMPLE WT transgenic mice, display motor and sensory nerve conduction defects that are consistent with the electrophysiological findings from human CMT1C patients (Campbell et al., 2004; Gerding et al., 2009; Latour et al., 2006; Saifi et al., 2005; Street et al., 2003).

SIMPLE W116G mutation causes peripheral nerve dysmyelination with myelin infolding and reduced axon caliber

To investigate the pathological changes underlying the observed motor and sensory neuropathy phenotype in *SIMPLE*$^{W116G/W116G}$ mice, we performed histological analyses of sciatic nerves, ventral roots, and dorsal roots from the mutant mice and the control mice.

At 3 months of age, *SIMPLE*$^{W116G/W116G}$ mice showed no obvious abnormality in the myelin or axonal structure of peripheral nerves (Figure 9A-C). However, analysis of semithin cross sections of peripheral nerves from 1-year-old *SIMPLE*$^{W116G/W116G}$ mice revealed abnormal Schwann cell–axon units with focally infolded myelin sheaths that appeared as single, double, or triple internal myelin rings within a myelinated axon (Figure 10A-C). Myelin infolding was associated with both motor and sensory nerves, and the infolding was more prominent in sciatic nerves which are more distally located with respect to the neuronal cell bodies (Figure 10A) compared to ventral and dorsal roots which are more proximally located (Figure 10B,C). The myelin infolding phenotype appears to be specific to the peripheral nerves, as no myelin infolding was observed in myelinated nerves from the central nervous system of *SIMPLE*$^{W116G/W116G}$ mice even up to 15 months of age (Figure 3). Histological analyses did not reveal obvious signs of demyelination and remyelination, such as thinly myelinated large axons or onion bulb formation in peripheral nerves of 1-year-old *SIMPLE*$^{W116G/W116G}$ mice.

Morphometric analysis indicated that, correlated with significantly increased myelin infoldings (Figure 12A), the axon contours of *SIMPLE*$^{W116G/W116G}$ sciatic nerves were significantly less circular (Figure 12B), and the axon caliber (or axon diameter) and axon area of the mutant nerves were significantly smaller than those of the non-transgenic controls (Figure 12C,D). However, myelin thickness of *SIMPLE*$^{W116G/W116G}$ nerves was unchanged (Figure 12E). In addition, the G-ratio (as calculated by dividing the axon diameter by the fiber diameter) was significantly reduced (Figure 12F) as a direct result of decreased axon caliber (Figure 12C). There was no loss of axons in the *SIMPLE*$^{W116G/W116G}$ mice compared to the non-transgenic controls (Figure 12G).

Myelin infoldings originate from the paranodal regions and near Schmidt-Lanterman incisures

To further characterize the pathological changes in *SIMPLE*$^{W116G/W116G}$ mice, we performed electron microscopic analyses of sciatic nerves from the mutant mice and control mice at 12 to 15 months of age. The results revealed that, unlike non-transgenic controls (Figure 11A), *SIMPLE*$^{W116G/W116G}$ nerves showed abundant myelin abnormalities with focally folded structures (Figure 11B-I). Interestingly, we found only myelin infoldings but no myelin outfoldings. Some myelin infoldings were observed in the orientation perpendicular to the nerve axis with myelin sheath that protrudes into a compressed axon (Figure 11B). More frequently, myelin infoldings were observed in the orientation parallel to the nerve axis, which appeared in cross sections as one or more internal myelin rings inside the myelinated axons of both large and small caliber nerve fibers (Figure 11C-F). The internal myelin rings had the same number of myelin lamellae and periodicity as the myelin sheath surrounding the axon (Figure 11F-H), suggesting that the internal myelin rings are invaginated loops of the myelin sheath.

Light microscopic and electron microscopic analyses of longitudinal sciatic nerve sections revealed that the infolded myelin loops predominantly originated from the myelin sheath at the paranodal regions (Figure 13C,D, H-K) and the internodal regions adjacent to Schmidt-Lanterman incisures (Figure 11I, Figure 13B) in *SIMPLE*$^{W116G/W116G}$ mice. As a complementary approach, we stained the teased sciatic nerves with Nile red, a fluorescent lipophilic dye that strongly labels lipid-rich structures, such as myelin.

Fluorescence confocal microscopic analysis of Nile red-labeled nerves also showed myelin infoldings at paranodal regions and near the Schmidt-Lanterman incisures in teased sciatic nerves from 1-year-old *SIMPLE*$^{W116G/W116G}$ mice (Figure 13F). In contrast, myelin infolding was virtually absent in the longitudinal sciatic nerve sections (Figure 11J, Figure 13A) and teased sciatic nerves (Figure 13E) from the control mice.

SIMPLE W116G mutation disrupts the integrity of Schwann cell–axon units and nodes of Ranvier

Ultrastructural analysis by electron microscopy revealed that *SIMPLE*$^{W116G/W116G}$ axons with myelin infoldings were often displaced, deformed or constricted (Figure 11B-F), consistent with the reduced axon caliber and axon area (Figure 12C,D) from the morphometric analysis of semithin sections. We observed signs of axonal damage and axonal degeneration (Figure 11M-P). Quantitative analysis revealed a small but significant increase in the percentage of sciatic nerves undergoing axonal degeneration in *SIMPLE*$^{W116G/W116G}$ mice compared to the control mice at 12 to 15 months of age (Figure 12H). Furthermore, loss of myelin compaction (Figure 11M) and widened spacing of the Schmidt-Lanterman incisures (Figure 11K,L) were occasionally observed. In addition, a small but significant increase in the percentage of sciatic nerves with demyelinated axons was also observed in the *SIMPLE*$^{W116G/W116G}$ mice compared to the control mice (Figure 11Q,R, Figure 12I).

Given the prominent presence of myelin infoldings at the paranodal regions (Figure 13C,D,F), we analyzed *SIMPLE*$^{W116G/W116G}$ nodes of Ranvier and paranodal

regions in more detail. Analysis of longitudinal sciatic nerve sections revealed that infolded myelin loops protrude into the axon at the paranodal regions, and myelin infolding did not affect the two sides of the node symmetrically in most cases (Figure 13C,D,F,J), although occasionally myelin infolding can be observed in both sides of the node (Figure 13H). Paranodal regions with myelin infolding often exhibited signs of dys/demyelination and axonal damage (Figure 13C,H,I). Non-compacted myelin whorls were found to extend from the compact myelin into the axon (Figure 13C,H,I), suggesting a loss of myelin compaction at the paranodal region that may impair axonal function and integrity. We observed the accumulation of electron-dense organelles, mainly mitochondria, in the axoplasm of the paranodal region next to the infolded myelin, likely as a result of impaired axonal transport (Figure 13H,I). Our data suggest that the focally infolded myelin loops, particularly those protruding deep into the axons perpendicularly (Figure 13C,H,I) may physically block axonal transport, leading to axonal degeneration observed in *SIMPLE*$^{W116G/W116G}$ sciatic nerves (Figure 11M-P, Figure 12H).

Electron microscopic analysis showed that, despite myelin infolding, axoglial junction and Schwann cell microvilli appeared largely intact and the myelin sheath is properly lined by Schwann cell basal lamina (Figure 13H-K), indicating that the overall nodal architecture is intact in the *SIMPLE*$^{W116G/W116G}$ nerves. However, we observed that the nodes of Ranvier with myelin infolding often showed paranodal retraction leading to a substantially larger nodal gap (Figure 13J,K). The enlarged nodal gaps were also observed in the semithin longitudinal sciatic nerve sections (Figure 13D) and Nile red-labeled sciatic nerves (Figure 13G) of 1-year-old *SIMPLE*$^{W116G/W116G}$ mice. Quantitative

analysis indicated that the nodal gap length of *SIMPLE*$^{W116G/W116G}$ nerves is significantly longer than that of the control nerves (Figure 13L).

Discussion

Despite human genetic evidence linking heterozygous SIMPLE missense mutations to dominantly inherited CMT1C (Campbell et al., 2004; Gerding et al., 2009; Latour et al., 2006; Saifi et al., 2005; Street et al., 2003), it is unclear whether these mutations cause peripheral neuropathy via haplo-insufficiency of SIMPLE or dominant effects of the SIMPLE mutants. Our findings from the present study provide strong evidence supporting a dominant role of SIMPLE mutations in CMT1C pathogenesis. We found that expression of CMT1C-linked human SIMPLE W116G mutant protein at 45% of endogenous SIMPLE protein level in *SIMPLE*$^{W116G/W116G}$ transgenic mice is sufficient to cause motor and sensory neuropathy in mice. Furthermore, *SIMPLE*$^{W116G/+}$ mice expressing the W116G mutant protein at 22% of endogenous SIMPLE protein level exhibited a mild motor and sensory phenotype. In contrast, *SIMPLE*$^{WT/WT}$ and *SIMPLE*$^{WT/+}$ mice, which expressed human SIMPLE WT protein at 51% and 24% of endogenous SIMPLE protein level, respectively, developed normally and did not show any motor and sensory deficit. Therefore, the motor and sensory neuropathy phenotypes that we observed in SIMPLE W116G mutant mice are the results of the SIMPLE mutation rather than an overexpression of SIMPLE protein.

Our findings indicate that *SIMPLE*$^{W116G/W116G}$ mice, which expressed human SIMPLE W116G mutant protein at a level similar to that found in CMT1C patients,

developed a motor and sensory neuropathy that recapitulates key clinical features of human CMT1C disease. CMT1C is a progressive motor and sensory neuropathy that often has an age of onset in the third and fourth decade of life (Campbell et al., 2004; Gerding et al., 2009; Latour et al., 2006; Saifi et al., 2005; Street et al., 2003). Consistent with the clinical time course of CMT1C, *SIMPLE*$^{W116G/W116G}$ mice exhibited motor and sensory nerve conduction defects and impaired motor and sensory performance at 1 year but not 3 months of age. Like CMT1C patients (Campbell et al., 2004; Gerding et al., 2009; Latour et al., 2006; Saifi et al., 2005; Street et al., 2003), *SIMPLE*$^{W116G/W116G}$ mice displayed motor impairments accompanied not only by a reduced MNCV (which is characteristic of demyelinating CMT) but also by a reduced CMAP amplitude (which is indicative of axonal degeneration). Furthermore, as reported in CMT1C patients (Campbell et al., 2004; Gerding et al., 2009; Latour et al., 2006; Saifi et al., 2005; Street et al., 2003), *SIMPLE*$^{W116G/W116G}$ mice also exhibited sensory impairments accompanied by a reduced SNCV. In addition, similar to CMT1C where a subgroup of patients with the SIMPLE W116G mutation have no evoked SNAP and show paresthesia (Campbell et al., 2004), we found that a small percentage of *SIMPLE*$^{W116G/W116G}$ mice lost the ability to evoke SNAP and showed self-mutilating behavior which could be caused by the loss of sensory nerve conduction.

CMT1C is a rare form of hereditary motor and sensory neuropathy and biopsy material is scarce. Therefore, our knowledge of the pathology of human CMT1C is very limited. The only published pathological result is a semithin cross-section showing the presence of onion-bulb formations in the sural nerve biopsy material from a CMT1C patient (Street et al., 2003). We did not find obvious evidence for onion-bulb formations

in the peripheral nerves of *SIMPLE*$^{W116G/W116G}$ mice. A similar lack of onion bulb formations has been reported in several other mouse models of human CMT (Bonneick et al., 2005; Tersar et al., 2007; Verhamme et al., 2011), which could be due to the shorter life span of mice, shorter lengths of nerves in mice, and/or some other species difference between mice and humans (Suter and Scherer, 2003).

Despite the lack of onion bulb formations, we found that the motor and sensory functional impairments in *SIMPLE*$^{W116G/W116G}$ mice are associated with focally infolded myelin loops that protrude into the axons at paranodal regions and near Schmidt–Lanterman incisures of motor and sensory nerves. Myelin infolding is often linked to constricted axons with signs of impaired axonal transport, suggesting that focally infolded myelin may physically block axonal transport. Myelin infolding is also linked to paranodal damage, and the node of Ranvier with myelin infolding often has a widened nodal gap. These pathological changes provide a structural basis for the observed motor and sensory nerve conduction defects, including reduced MNCV and SNCV, decreased CMAP amplitude, and a loss of evoked SNAP in *SIMPLE*$^{W116G/W116G}$ mice. The finding of myelin infolding and paranodal damage in 1-year-old but not 3-month-old *SIMPLE*$^{W116G/W116G}$ mice indicates that these pathological changes occur after the myelination has completed and the architecture of Schwann cell–axon units has been established. Therefore, myelin infolding and paranodal damage are likely caused by defects in the maintenance rather than the formation of myelin sheath and Schwann cell–axon units. In addition to myelin infolding and paranodal damage, we have identified a small but significant percentage of peripheral nerves with signs of demyelination and axonal degeneration. Based on our results, we propose that myelin infolding and

paranodal damage may represent pathogenic precursors preceding demyelination and axonal degeneration in CMT1C patients and these pathological changes should be considered as major factors contributing to the motor and sensory neuropathy.

Focally folded myelin, mostly myelin outfolding but also myelin infolding, has been found in several types of inherited demyelinating neuropathies such as CMT1B (Fabrizi et al., 2000; Iida et al., 2012; Kochanski et al., 2003), CMT4A (Chung et al., 2011), and CMT4B (Bird et al., 1997; Quattrone et al., 1996) and chronic inflammatory demyelinating neuropathy (Sander et al., 2000) as well as in various animal models of demyelinating CMT (Bolino et al., 2004; Bolis et al., 2005; Robinson et al., 2008; Tersar et al., 2007) and other peripheral nerve disorders (Cai et al., 2006; Cai et al., 2002). In addition, widened nodal gap has been reported in CMT1A (Yoshikawa et al., 1996) and CMT4C (Arnaud et al., 2009). These shared pathological features in this diverse group of disorders suggest that abnormal myelin folding and nodal disorganization may represent convergent pathogenic mechanisms leading to demyelinating peripheral neuropathy.

Our finding of the CMT1C-like neuropathy phenotype by transgenic expression of human SIMPLE W116G mutant protein on a wild-type SIMPLE background in mice supports that human CMT1C disease is caused by dominant effects of the SIMPLE mutant rather than haplo-insufficiency of wild-type SIMPLE protein. Consistent with this view, a recent study reported that SIMPLE knockout mice developed normally and did not show myelin abnormality or neuropathy phenotype (Somandin et al., 2012). Our immunohistochemical analysis revealed that human SIMPLE W116G transgene, like endogenous SIMPLE, is expressed in myelinating Schwann cells but not in axons. This

result, together with our published data showing that the W116G mutation promotes SIMPLE protein misfolding (Lee et al., 2012; Lee et al., 2011), suggest that SIMPLE mutation causes peripheral neuropathy via a toxic gain-of-function pathogenic mechanism by impairing Schwann cell function and myelin homeostasis.

Our finding that endogenous SIMPLE is localized to the early endosome in myelinating Schwann cells, together with the data showing the interaction of SIMPLE with the endosomal sorting complex required for transport (ESCRT) subunit TSG101 (Shirk et al., 2005), suggest that SIMPLE may act as regulator of endosome-to-lysosome trafficking in Schwann cells. Given our result that CMT1C-linked mutations, including SIMPLE W116G, causes SIMPLE to mislocalize from the early endosome to the cytosol (Lee et al., 2011), it is possible that a dominant negative pathogenic mechanism of SIMPLE mutant may also contribute to CMT1C pathogenesis by disrupting the function of SIMPLE in regulating endosomal trafficking in Schwann cells. The link between endosomal trafficking dysfunction and dysmyelinating neuropathy is supported by the findings that loss-of-function mutations in myotubularin-related 2 and 13 (MTMR2 and MTMR13), two proteins involved in the regulation of endosome-to-lysosome trafficking (Berger et al., 2011; Cao et al., 2008), cause CMT4B with myelin outfolding (Bird et al., 1997; Quattrone et al., 1996). Furthermore, loss-of-function mutations in SH3TC2, an endosomal protein with a role in regulating endosomal recycling, cause CMT4C with a widened nodal gap (Arnaud et al., 2009). These studies raise the possibility that dysregulated endosomal trafficking causes abnormal myelin folding and nodal disorganization, thereby leading to demyelinating peripheral neuropathy. In conclusion, our findings obtained from this study provide new insights into the pathogenic

mechanisms of CMT1C-linked SIMPLE mutations, and the generated transgenic model of CMT1C should facilitate the investigation of CMT pathogenesis and therapeutics.

Acknowledgements

We thank Emory Transgenic Mice Core Facility for the microinjection and implantation service in generation of transgenic mice, Emory Electron Microscopy Core Facility for processing semithin and thin sections of nerve samples, and Emory Neuropathology Core for processing brain samples. This work was supported in part by NIH grants NS063501 (S.M.L.), NS050650 and AG034126 (L.S.C.), and ES015813 and GM082828 (L.L.).

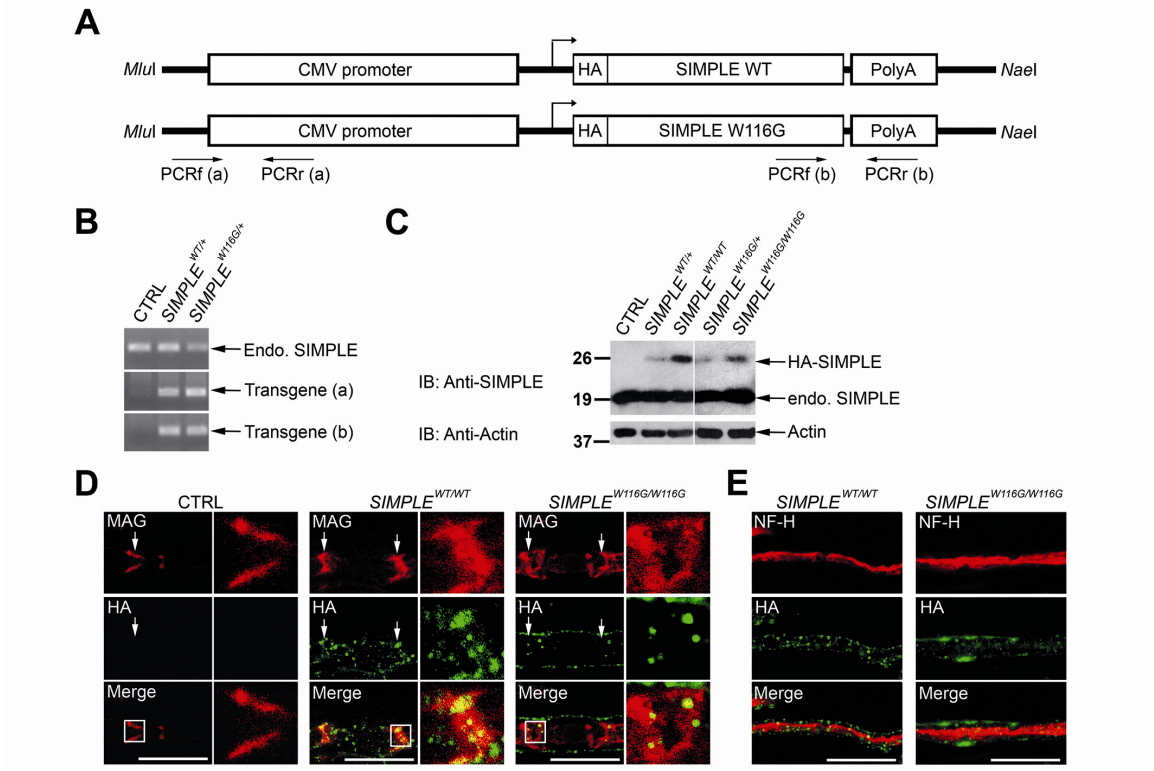

Figure 1. Generation of SIMPLE WT and SIMPLE W116G transgenic mice. (A) Schematic of transgenic constructs encoding HA-tagged human SIMPLE W116G or SIMPLE WT under the control of the CMV promoter. The positions of the PCR primer pairs used to amplify the transgene are indicated. **(B)** Identification of transgenic mice by PCR analysis of tail genomic DNAs using transgene-specific primer pairs indicated in (A). The endogenous (endo.) mouse SIMPLE gene was detected by PCR using a set of primers targeting a mouse SIMPLE-specific genomic region. **(C)** Western blot analysis of SIMPLE expression in Schwann cells from the indicated heterozygous and homozygous transgenic mice or non-transgenic control (CTRL) mice. **(D)** Immunostaining of teased sciatic nerves from the indicated 3-month-old transgenic mice or non-transgenic control (CTRL) mice with anti-HA (green) and anti-MAG (red) antibodies. Arrows indicate the locations of Schmidt-Lanterman incisures. **(E)** Immunostaining of teased sciatic nerves

from the indicated 3-month-old transgenic mice with anti-HA (green) and anti-neurofilament H (NF-H, red) antibodies. Scale bar, 5 μm.

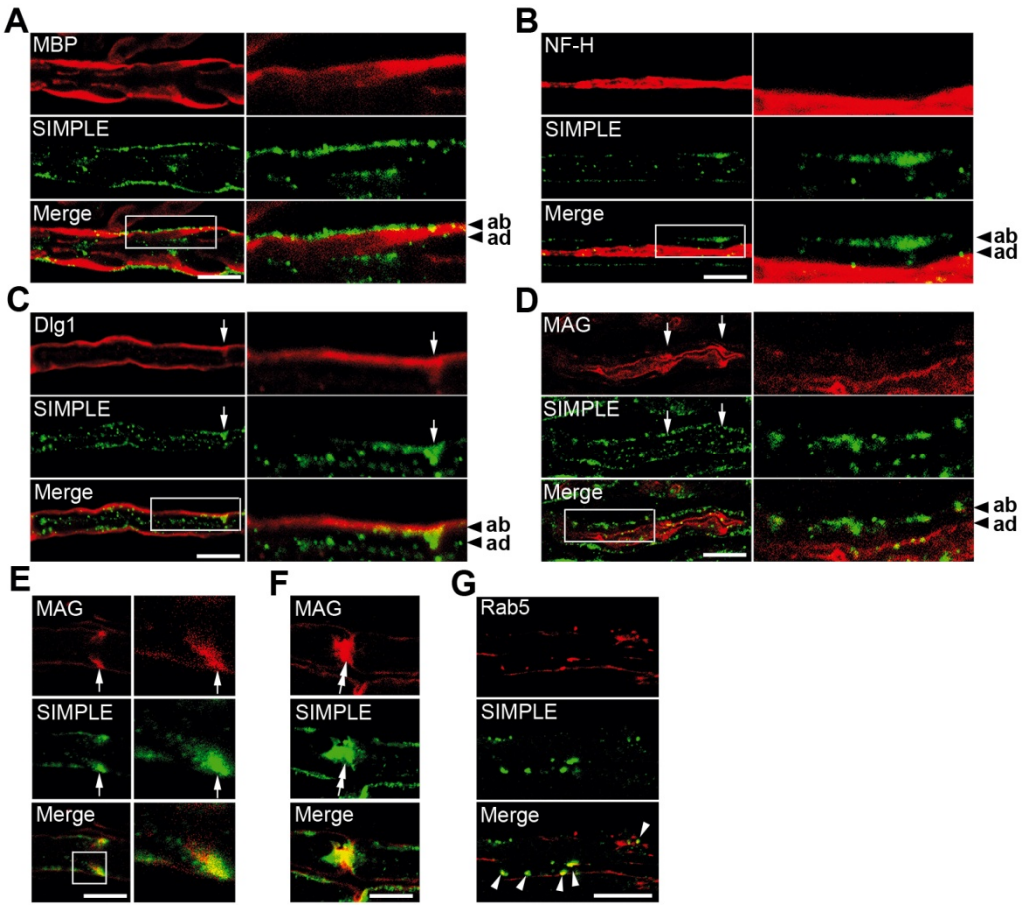

Figure 2. Endogenous SIMPLE is localized to early endosomes in the cytoplasmic regions of myelinating Schwann cells but is absent in the myelin sheath or axons. (A-G) Teased sciatic nerves from 3-month-old non-transgenic mice (A,B,D-F) or rat (C,G) were stained with anti-SIMPLE (green) and anti-MBP (A), NF-H (B), Dlg1 (C), MAG (D-F), or Rab5 (G) (red) antibodies. The locations of Schmidt-Lanterman incisures (arrows), nodes of Ranvier (arrows with double arrowhead), and colocalization of SIMPLE with Rab5 (arrowheads) were indicated. Insets are two-fold magnifications of the original image. Ab, abaxonal domain of Schwann cells; Ad, adaxonal domain of Schwann cells. Scale bar, 5 μm.

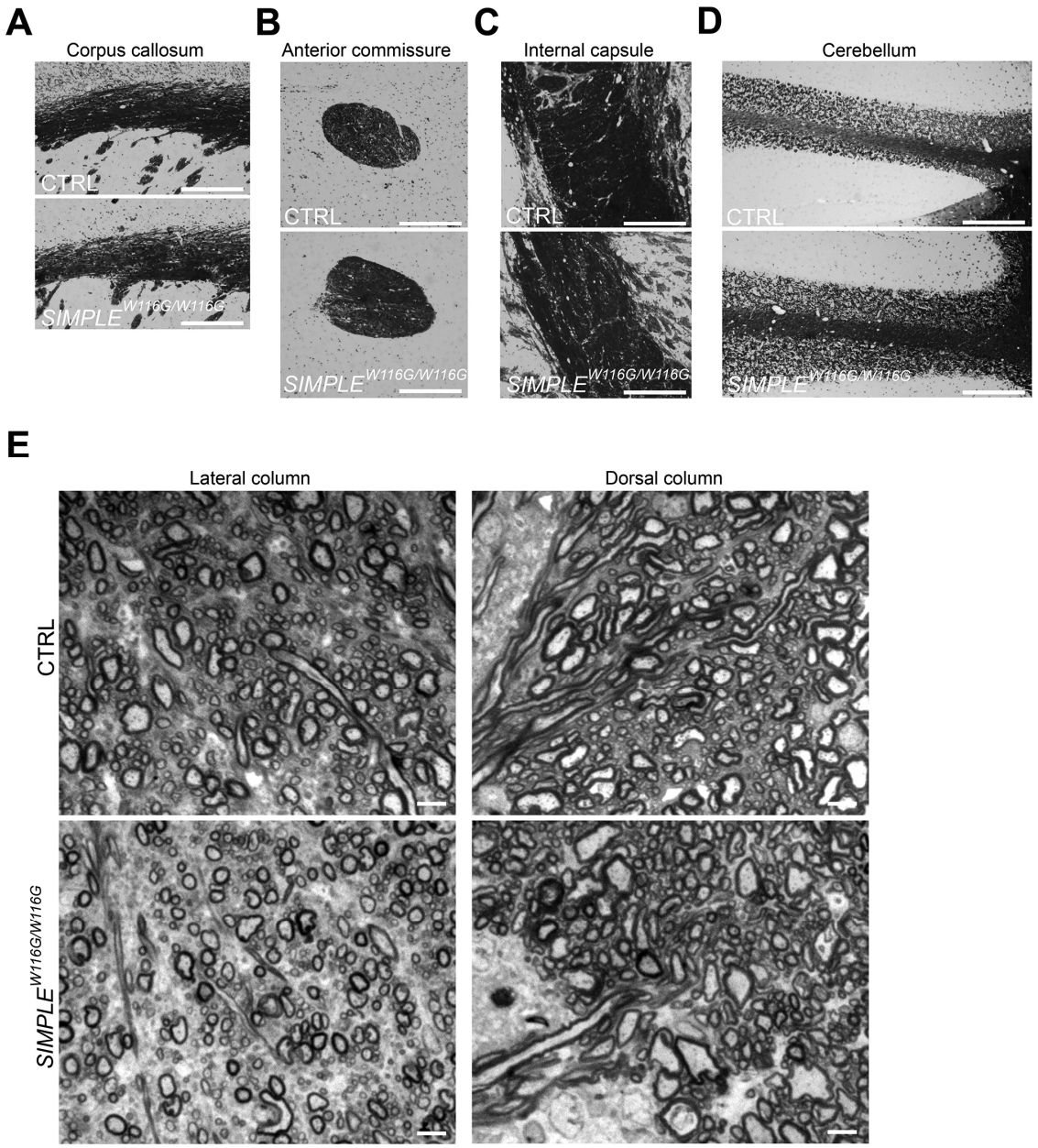

Figure 3. ***SIMPLE*$^{W116G/W116G}$ mice show no abnormality in myelinated structures in the brain and spinal cord.** **(A-D)** Histological analysis of coronal brain sections revealed no obvious abnormality in myelinated structures in the brain, including the corpus callosum (A), anterior commissure (B), internal capsule (C), and folds of the cerebellum (D) in 15-month-old *SIMPLE*$^{W116G/W116G}$ mice compared to the non-transgenic

control (CTRL). Scale bar, 200 μm. **(E)** Histological analysis of cross-sections from the lateral and dorsal columns of the spinal cord showed no obvious morphological abnormality of myelination in 15-month-old *SIMPLE*$^{W116G/W116G}$ mice compared to the control (CTRL). Scale bar, 5 μm.

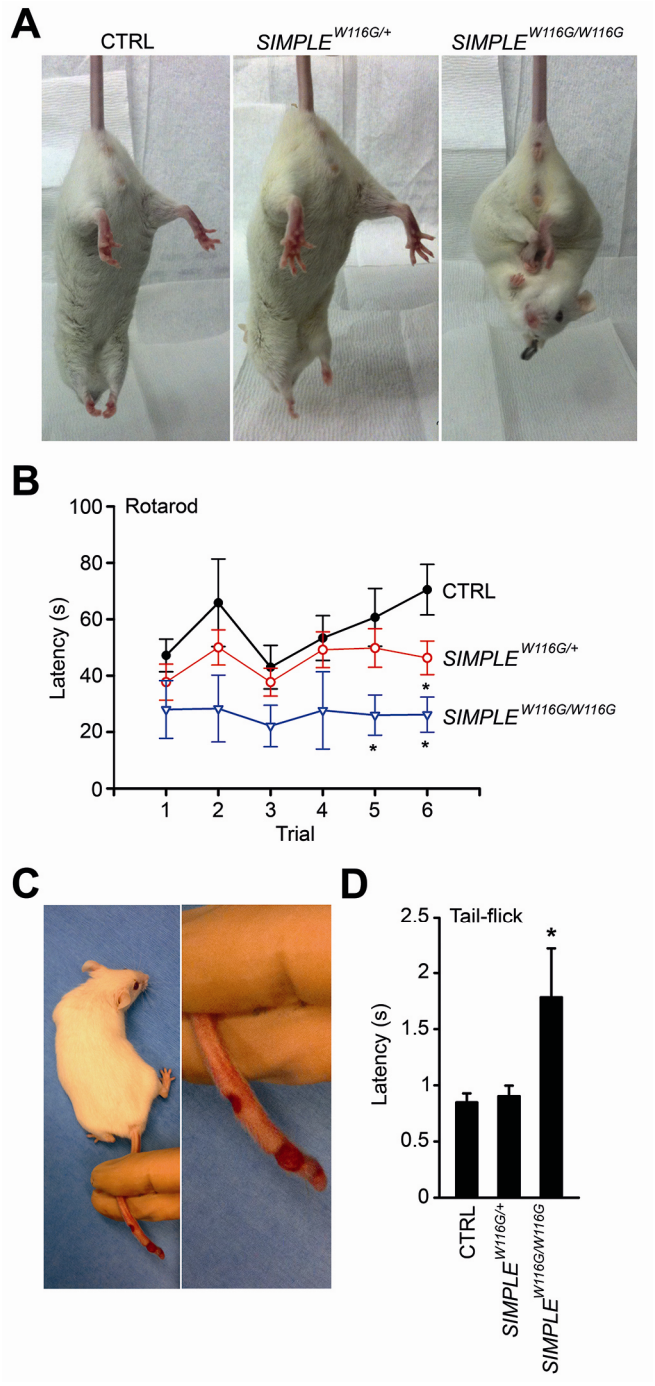

Figure 4. Impaired motor and sensory performance in SIMPLE W116G mutant mice. (A) When suspended by the tail, an abnormal phenotype of hind-limb clasping and occasional limb/body flexing was seen in *SIMPLE*$^{W116G/W116G}$ mice but not in non-transgenic control (CTRL) or *SIMPLE*$^{W116G/+}$ mice at 1 year of age. **(B)** Impaired rotarod

performance in *SIMPLE*$^{W116G/W116G}$ and *SIMPLE*$^{W116G/+}$mice compared to the non-transgenic control (CTRL) mice. The latency was plotted versus the trial number. Data represent mean ± s.e.m. (n = 6-10 mice per genotype). * $P < 0.05$ versus the control. **(C)** Self-mutilation of the tail in a *SIMPLE*$^{W116G/W116G}$ mouse was shown, which was suggestive of paresthesia. **(D)** Impaired tail-flick response in *SIMPLE*$^{W116G/W116G}$ mice compared to the non-transgenic control (CTRL) mice at 1 year of age. Data represent mean ± s.e.m. (n = 6-10 mice per genotype). * $P < 0.05$ versus the control.

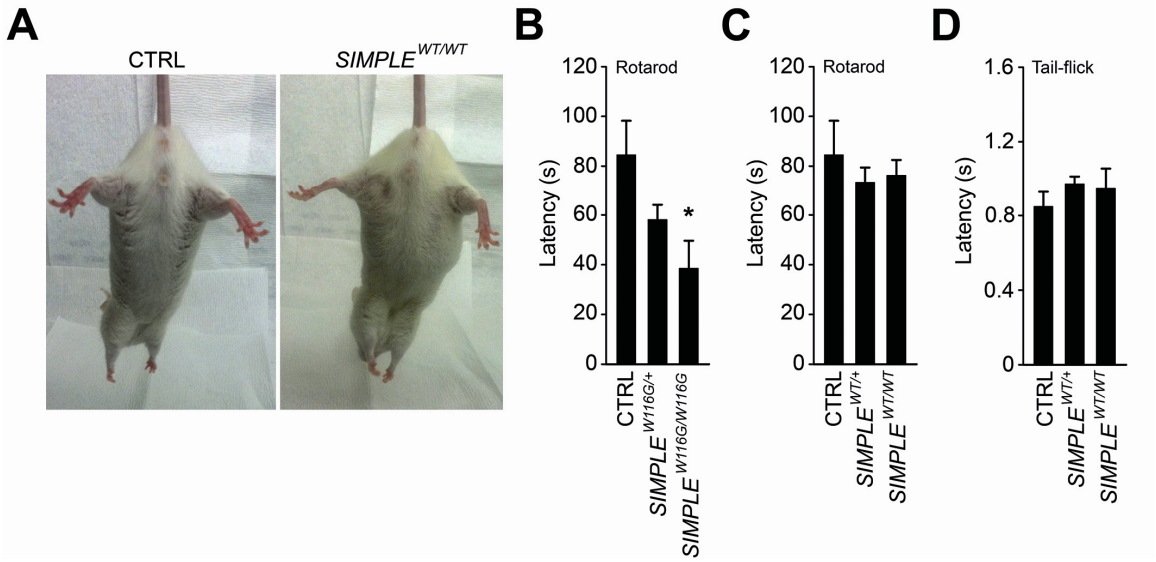

Figure 5. SIMPLE WT mice show normal motor and sensory performance. (A) When suspended by tail, 1-year-old *SIMPLE*$^{WT/WT}$ mice and the non-transgenic control (CTRL) show normal hind-limb spread indicating normal escape reflexes. **(B,C)** Rotarod test was performed on *SIMPLE*$^{W116G/W116G}$, *SIMPLE*$^{W116G/+}$, and their non-transgenic control (CTRL) mice (B) or *SIMPLE*$^{WT/WT}$, *SIMPLE*$^{WT/+}$, and their non-transgenic control (CTRL) mice (C) for 6 trials, and the highest latency out of 6 trials was shown as mean ± s.e.m. (n = 5-10 mice per genotype). * $P < 0.05$ versus the control. **(D)** Analysis of tail-flick response in 1-year-old *SIMPLE*$^{WT/WT}$, *SIMPLE*$^{WT/+}$, and the non-transgenic control (CTRL) mice. Data represent mean ± s.e.m. (n = 5-7 mice per genotype).

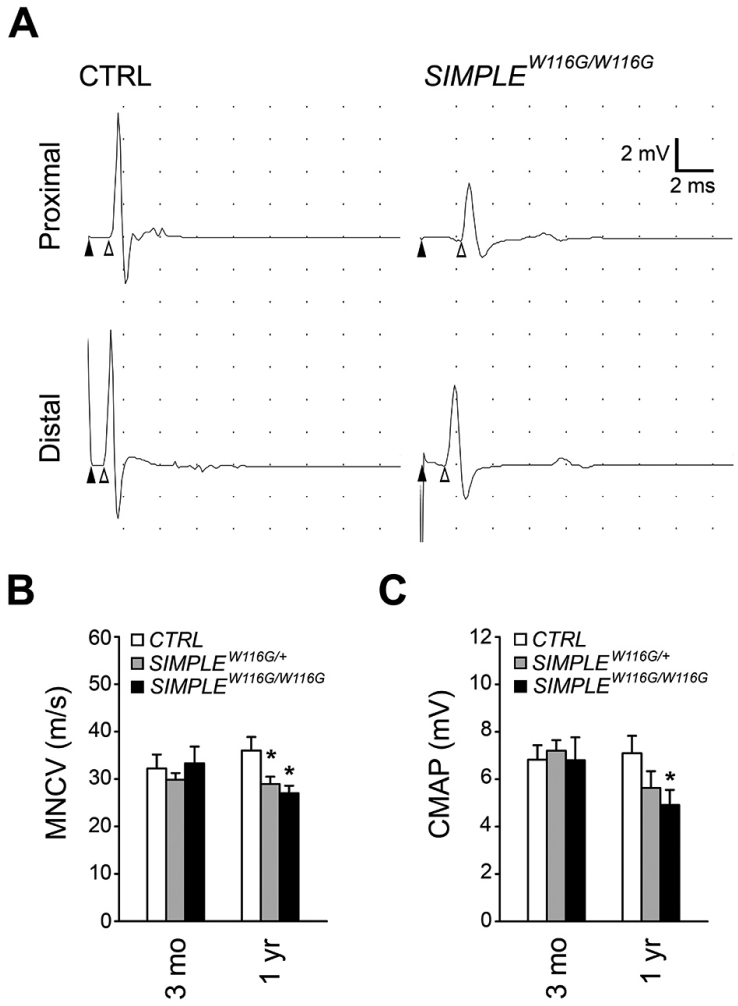

Figure 6. Motor nerve conduction defects in SIMPLE W116G mutant mice. (A) Representative traces of compound muscle action potential (CMAP) recorded from 1-year-old *SIMPLE*$^{W116G/W116G}$ mice and the non-transgenic littermate control (CTRL) mice after stimulation at the sciatic notch (proximal) and at the ankle (distal). The stimulus artifact (closed arrowhead) and the onset of CMAP (open arrowhead) were indicated. **(B,C)** Quantitative analysis of motor nerve conduction velocities (MNCVs) (B) and CMAP amplitudes (C) in *SIMPLE*$^{W116G/W116G}$, *SIMPLE*$^{W116G/+}$, and control (CTRL) mice at the age of 3 months (n = 10-19 mice per genotype) and 1 year (n = 13 mice per genotype). Data represent mean ± s.e.m. * $P < 0.05$ versus the control.

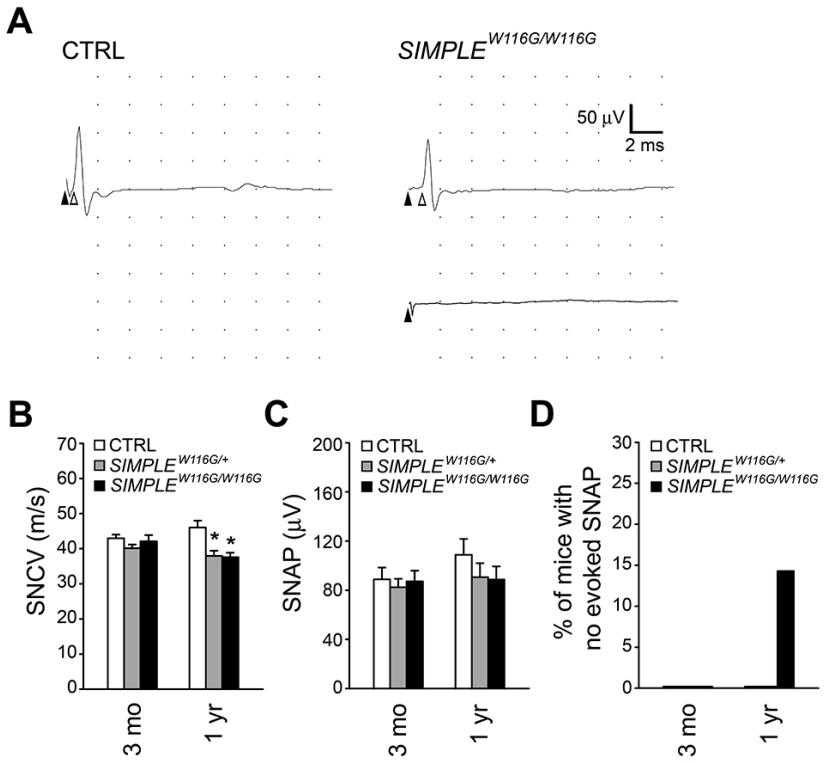

Figure 7. Sensory nerve conduction defects in SIMPLE W116G mutant mice. (A) Representative traces of sensory nerve action potential (SNAP) recorded from 1-year-old SIMPLE$^{W116G/W116G}$ mice and the non-transgenic control (CTRL) mice after stimulation at the tail. The stimulus artifact (closed arrowhead) and the onset of SNAP (open arrowhead) were indicated. **(B-D)** Quantitative analysis of sensory nerve conduction velocities (SNCVs) (B), SNAP amplitudes (C), and percentage of mice with no evoked SNAP (D) in *SIMPLE*$^{W116G/W116G}$, *SIMPLE*$^{W116G/+}$, and control (CTRL) mice at the age of 3 months (n = 10-19 mice per genotype) and 1 year (n = 11-13 mice per genotype). Data represent mean ± s.e.m. * $P < 0.05$ versus the control.

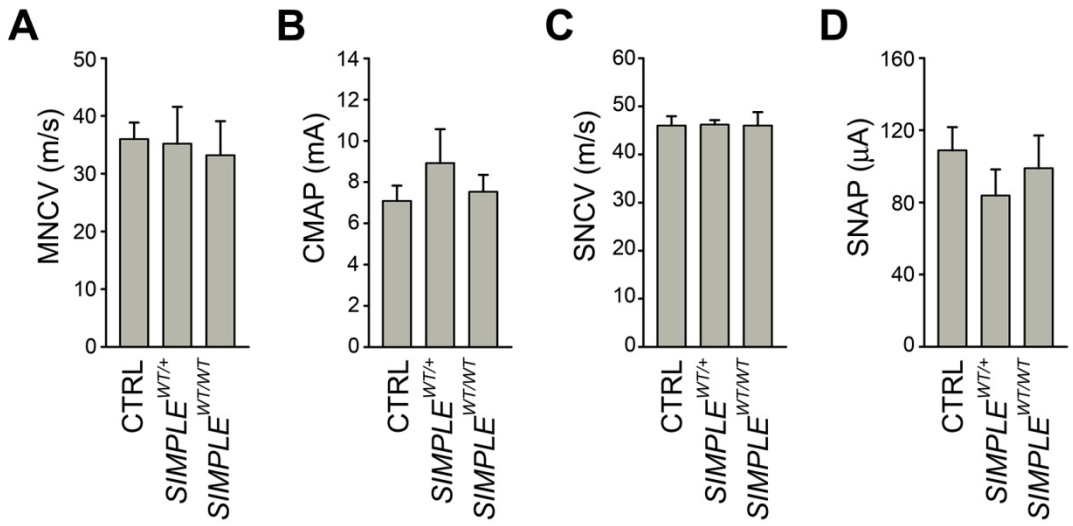

Figure 8. Normal motor and sensory nerve conduction in SIMPLE WT transgenic mice. (A-D) Quantitative analysis of MNCV (A), CMAP amplitude (B), SNCV (C), and SNAP amplitude (D) in 1-year-old *SIMPLE*$^{WT/WT}$, *SIMPLE*$^{WT/+}$, and control (CTRL) mice. Data represent mean ± s.e.m. (n = 5-13 mice per genotype)

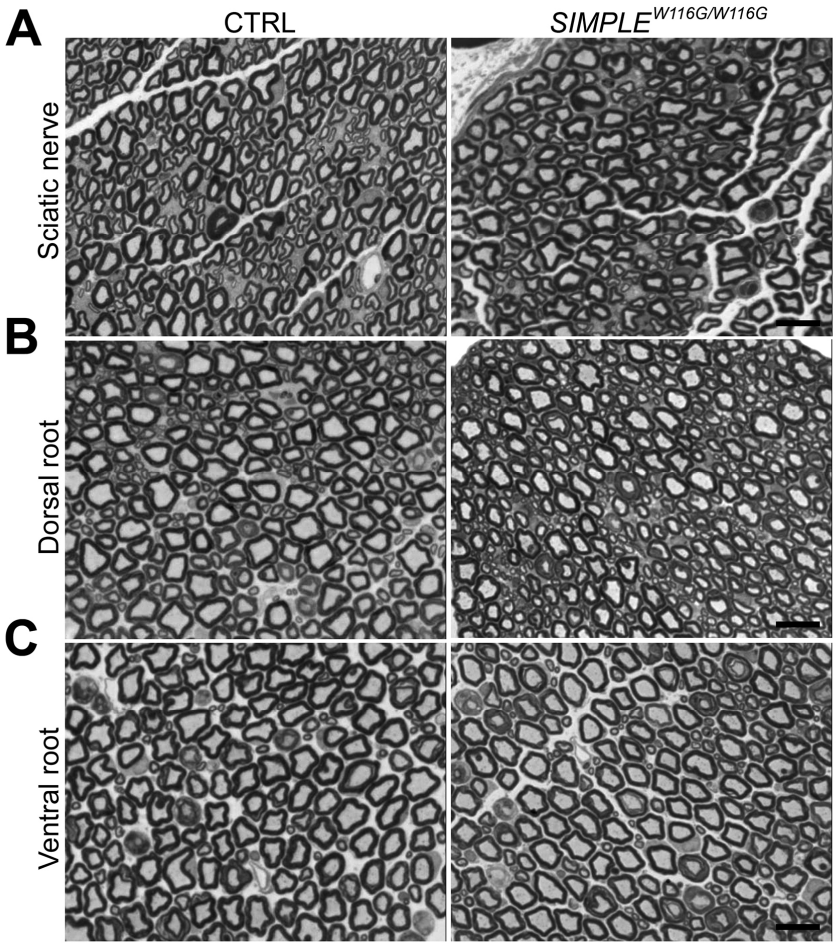

Figure 9. Cross-section analysis of 3-month-old SIMPLE$^{W116G/W116G}$ mice does not show obvious abnormality in the peripheral nerves. (A-C) Semithin cross-section analysis of 3-month-old sciatic nerves (A), dorsal roots (B), and ventral roots (C) did not reveal any difference between control (CTRL) and SIMPLE$^{W116G/W116G}$ mice. Scale bar, 5 μm.

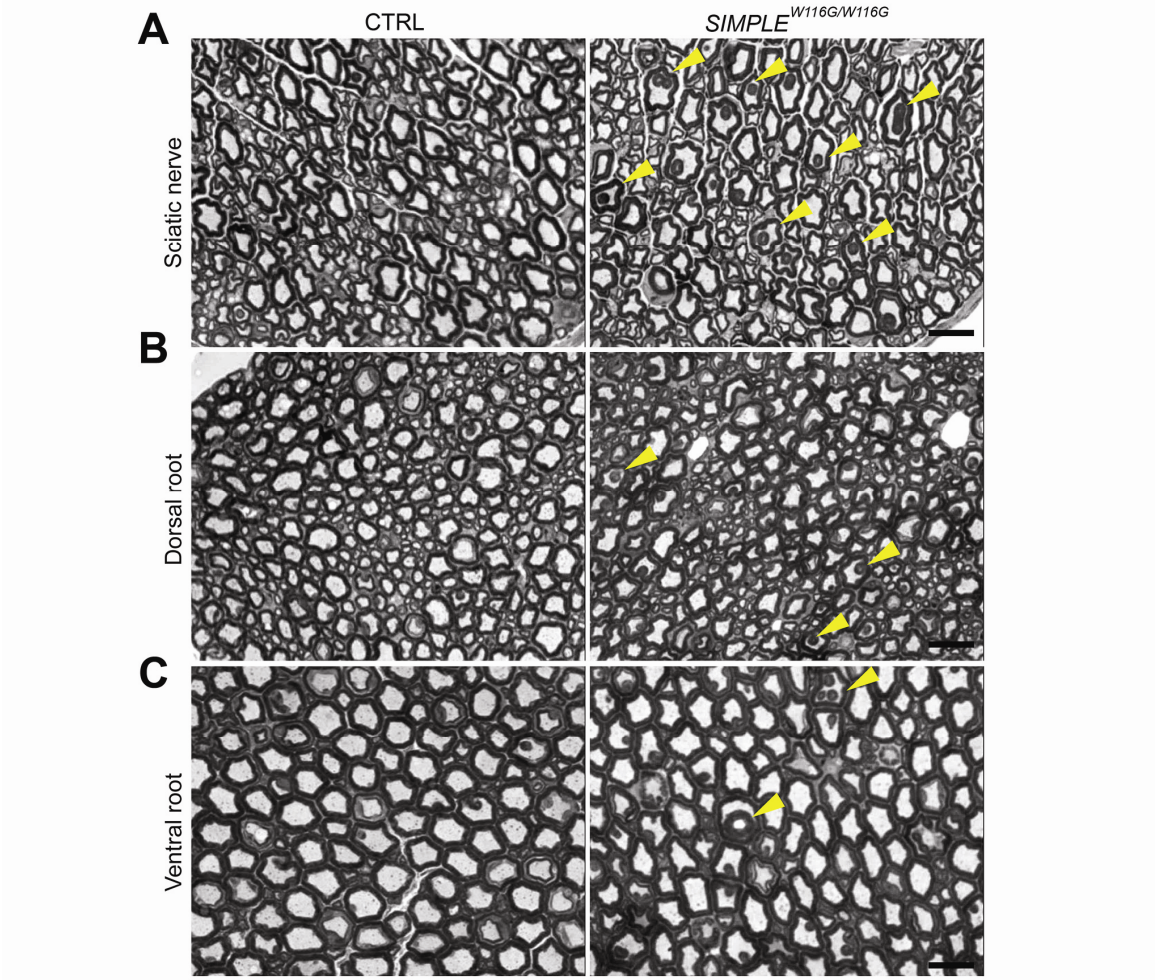

Figure 10. Histological analysis reveals myelin infoldings in 1-year-old SIMPLE W116G mutant mice. Semithin cross-sections of sciatic nerves **(A)**, dorsal roots **(B)**, ventral roots **(C)** from 1-year-old *SIMPLE*$^{W116G/W116G}$ and non-transgenic control (CTRL) mice. Arrowheads indicate myelin infoldings. Scale bar, 10 μm.

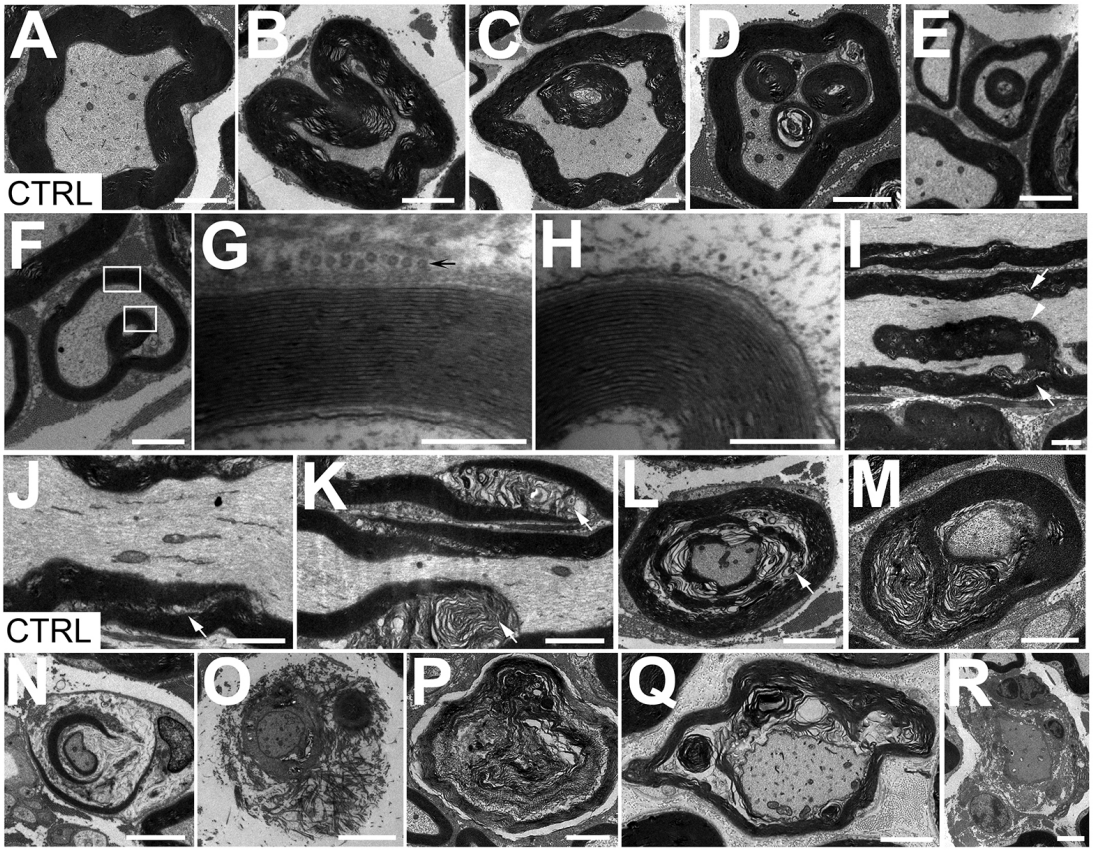

Figure 11. Electron microscopic analysis of myelin abnormalities and axonal degeneration in SIMPLE W116G mutant mice. Ultrastructural analysis of sciatic nerves from 12- to 15-month-old mice showed myelin and axon abnormalities of *SIMPLE*$^{W116G/W116G}$ mice (B-I,K-R) that are virtually absent in the control (CTRL) mice (A,J). The most frequent type of myelin abnormality in the *SIMPLE*$^{W116G/W116G}$ nerves is the focally infolded myelin that protrudes into the axon (B) and the presence of one or more infolded myelin loops within myelinated axons of both large and small calibers (C-F). The infolded myelin loops (H) and the myelin sheath (G) of the axon have the identical periodicity and number of lamellae. Schwann cell cytoplasmic vesicles (G) were indicated by arrows. Longitudinal section showed infolded myelin loop originating from the myelin sheath near the Schmidt-Lanterman incisures (I). Loss of myelin

compaction and widened spacing of the Schmidt-Lanterman incisures were occasionally observed in *SIMPLE*$^{W116G/W116G}$ nerves in longitudinal (K) and cross sections (L) but were absent in the control (J). The Schmidt-Lanterman incisures (I-L) were indicated by arrows, and myelin infolding (I) was indicated by arrowhead. *SIMPLE*$^{W116G/W116G}$ nerve fibers with various stages of axonal degeneration (M-P), intramyelin edema (Q), and demyelinated axons (R) were also occasionally observed. Scale bar, 2 μm (A-F, I-R) or 200 nm (G,H).

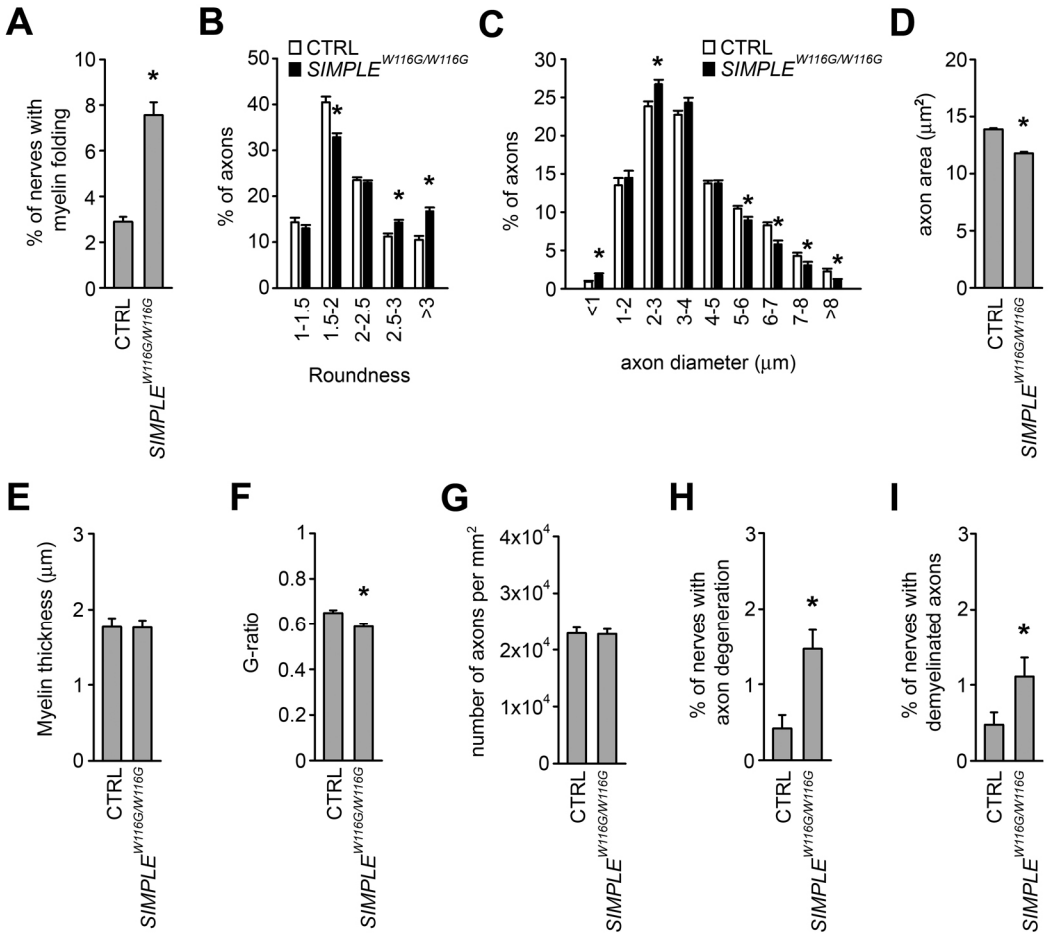

Figure 12. Quantitative analyses of myelin infoldings, axon morphometry, myelin thickness, G-ratio, axon degeneration, and demyelination. **(A)** Quantification of the percentage of myelinated nerves with focally infolded myelin showed increased myelin infolding in *SIMPLE*$^{W116G/W116G}$ nerves compared to the control (CTRL). **(B)** Quantification of the percentage of axons with different ranges of roundness showed that axon fibers in *SIMPLE*$^{W116G/W116G}$ nerves are significantly less circular compared to the control (CTRL). **(C)** Quantification of the percentage of axons with different ranges of axon diameter showed a significantly smaller axon diameter in *SIMPLE*$^{W116G/W116G}$ nerves compared to the control (CTRL) at 12 to 15 months of age. **(D)** Quantification of axon area showed a significant reduction *in SIMPLE*$^{W116G/W116G}$ sciatic nerves compared to the

control (CTRL). **(E,F)** Quantifications of myelin thickness (E) and G-ratio (F) showed a significantly reduced G-ratio with unaltered myelin thickness in *SIMPLE*$^{W116G/W116G}$ nerves compared to the control (CTRL) at 12 to 15 months of age. **(G)** Quantification of axons per mm^2 showed no difference in axon count between *SIMPLE*$^{W116G/W116G}$ and control (CTRL) nerves. **(H,I)** Quantification of the percentage of sciatic nerves undergoing axonal degeneration (H) and demyelination (I) showed a significantly increased axonal degeneration and demyelination in *SIMPLE*$^{W116G/W116G}$ mice compared to the control (CTRL) at 12 to 15 months of age. For all morphometric analyses, three mice per genotype were analyzed. Data represent mean ± s.e.m. * $P < 0.05$ versus the control.

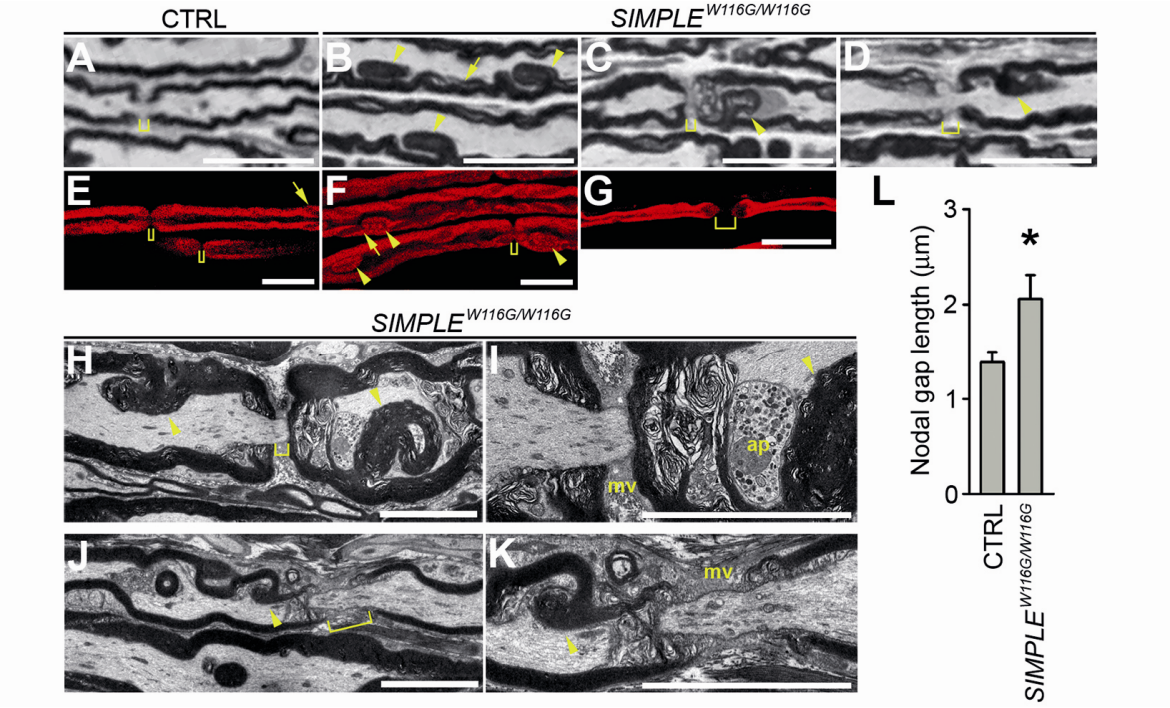

Figure 13. Paranodal myelin infoldings and widened nodes of Ranvier in SIMPLE W116G mutant mice. (A-D) Analysis of longitudinal semithin sections of sciatic nerves from 1-year-old *SIMPLE*$^{W116G/W116G}$ mice showed myelin infolding at the paranodal (C,D) and internodal (B) regions, loss of myelin compaction at the paranodal regions (C,D), and the widening of node of Ranvier (D) that are absent in the control nerves (A). Scale bar, 20 µm. **(E-G)** Nile red-stained teased sciatic nerve fibers from 1-year-old *SIMPLE*$^{W116G/W116G}$ mice showed myelin infolding at the paranodal regions and near Schmidt-Lanterman incisures (F) and occasional widening of the node of Ranvier (G) that are absent in the control (E). Scale bar, 20 µm. **(H-K)** Ultrastructural analysis of longitudinal sciatic nerve sections from *SIMPLE*$^{W116G/W116G}$ mice at 12 to 15 months of age revealed myelin infolding, non-compacted myelin whorls, and accumulations of axoplasm (ap) containing electron-dense organelles at the paranodal regions (H,I). Paranodal retraction of myelin and widening of the node of Ranvier were also observed

(J,K). The compact myelin sheath is lined by basal lamina, and microvilli (mv) and axoglial junctions appeared intact. Scale bar, 10 μm. Myelin infolding (arrowhead), Schmidt-Lanterman incisures (arrows), and nodal gap length (bracket) were indicated (A-K). **(L)** Quantification of the nodal gap length showed a significant widening of the nodes of Ranvier in 1-year-old *SIMPLE*$^{W116G/W116G}$ mice compared the control (CTRL). Three mice per genotype were analyzed. Data represent mean ± s.e.m. * $P < 0.05$ versus the control.

Chapter 5

Summary of findings, discussions, and future directions

Part of the work described in this Chapter has been published:

1. Lee, S.M., Chin, L.-S., and Li, L. (2012) Protein misfolding and clearance in demyelinating peripheral neuropathies: Therapeutic implications. *Commun. Integr. Biol.* **5** (1), 107-10.
2. Lee, S.M., Chin, L.-S., and Li, L. (2012) Therapeutic implications of protein homeostasis in demyelinating peripheral neuropathies. *Exp. Rev. Neurother.* In press.

5. 1. Summary of findings

Genetic studies have identified mutations in SIMPLE to cause demyelinating CMT disease, which has provided us clues to the mechanisms behind peripheral nervous system homeostasis and disease pathogenesis. However, a number of important questions have not been addressed. The cellular and molecular functions of SIMPLE protein in normal physiology are poorly understood, and the detrimental effects of CMT1C-linked mutations remain unknown. Moreover, it is unknown as to why mutations in a ubiquitously expressed protein such as SIMPLE (Moriwaki et al., 2001; Street et al., 2003) can cause a disease phenotype that specifically affects the peripheral nervous system. In Chapters 2 through 4, I have described the experimental results that answered many of these questions.

Localization studies in Chapters 2 and 4 reveal that SIMPLE protein is highly expressed in the peripheral nerves and in Schwann cell cytoplasmic domains. Our finding that SIMPLE protein levels are considerably lower in the brain and muscle helps to explain why mutations in SIMPLE cause a demyelinating peripheral neuropathy rather than a primary central nervous system disease or muscular dystrophy. SIMPLE is also strongly expressed in tissues such as lungs and pancreas; therefore, it may have important functions outside of the neuromuscular system. Results in Chapter 3 have identified a function of SIMPLE in facilitating the endosome-to-lysosome trafficking of ErbB receptors. This endocytic function of SIMPLE is essential for down-regulating activated ErbB receptors and their downstream signaling pathways which may have an important role in controlling a variety of cellular processes.

Mutation analysis in Chapter 2 have examined the effects of CMT1C-linked mutations and found that these mutations disrupt the endosome membrane association of SIMPLE and promote the aggregation of SIMPLE protein in the cytosol and degradation by the proteasome and aggresome-autophagy pathways. The effects of these mutations on the endocytic functions of SIMPLE was assessed in Chapter 3, which found that these mutations cause SIMPLE to act in a dominant-negative manner to inhibit endosomal trafficking and to prolong downstream signaling of ErbB receptor activation by NRG1. Finally, *in vivo* analysis of a CMT1C-linked SIMPLE mutation in transgenic mice as described by Chapter 4 showed that the W116G mutant protein causes a late-onset motor and sensory peripheral neuropathy characterized by pathological infolding of myelin, decrease in axonal caliber, and axonal degeneration in the peripheral nerves. This chapter will discuss the implications of these findings in enhancing our understanding of basic biological processes and the pathogenic mechanisms that contribute to peripheral neuropathy.

5.2. The cell type distribution and subcellular localization of SIMPLE suggests a role in regulating Schwann cell myelination

Given that the SIMPLE transcript is ubiquitously expressed (Moriwaki et al., 2001; Street et al., 2003), it was surprising when genetic studies revealed mutations in SIMPLE to cause demyelinating neuropathy that specifically affect the peripheral nervous system. My protein expression analyses from Chapters 2 and 4 indicated that SIMPLE is an early endosome membrane protein enriched in Schwann cell cytoplasmic subdomains,

particularly at Schmidt-Lanterman incisures and paranodal domains. The active involvement of these subdomains of Schwann cells in vesicular trafficking (Notterpek et al., 1997) and myelin maintenance (Spiegel and Peles, 2002) suggests that SIMPLE may have a functional role in regulating endosomal trafficking necessary for the proper maintenance of myelin sheath.

The role of SIMPLE in regulating myelination *in vivo* was recently explored by Somandin and colleagues (Somandin et al., 2012). Their examination of peripheral nerves from SIMPLE knockout mice up to 18 months of age did not reveal any obvious pathology, which suggests that loss-of-function of SIMPLE may not have a significant effect on Schwann cell functions and that autosomal-dominant CMT1C-linked mutations in SIMPLE are likely to act through dominant mechanisms such as toxic gain-of-function and dominant-negative inhibition to cause peripheral neuropathy. This is in concordance with my *in vivo* and *in vitro* findings which also support a role for dominant mechanisms in causing CMT1C.

Nevertheless, the fact that SIMPLE knockout mice had no observable defect in myelination did not rule out the possibility that SIMPLE loss-of-function can contribute to demyelinating neuropathy in human CMT1C patients. When compared to humans, mice have a shorter relative lifespan and nerve lengths; therefore, the effects of SIMPLE loss-of-function may be undetectable during the life-span of SIMPLE knockout mice. This is supported by the fact that mouse models of peripheral neuropathy often present with considerably milder phenotype compared to humans (Bonneick et al., 2005; Tersar et al., 2007; Verhamme et al., 2011). Moreover, it was reported that SIMPLE knockout mice have a reduced ability in repairing myelin sheath of crushed sciatic nerves

(Somandin et al., 2012). While SIMPLE may not be required for myelin maintenance in a controlled environment, it may be essential for the remyelination after repeated nerve injury throughout a human lifespan. Hence, loss of function in SIMPLE could contribute to the pathogenesis of demyelinating neuropathy as a result of cumulative damage of myelin and a loss of myelin sheath repair.

5.3. SIMPLE recruits ESCRT-0 and ESCRT-I to the endosomal membrane and is required for efficient endosome-to-lysosome trafficking

Ubiquitinated membrane proteins at the early endosome are sorted to intralumenal vesicles of multivesicular bodies (MVBs) for delivery to the lysosome for degradation. The sorting of these ubiquitinated cargoes to the intralumenal vesicles of MVBs require their recognition by the endosomal sorting complex required for transport (ESCRT) machinery composed of ESCRT-0, -I, -II, and –III protein complexes (Raiborg and Stenmark, 2009; Roxrud et al., 2010). Current models suggest that Hrs, which is partially localized to early endosomes via an interaction with phosphatidylinositol-3-phosphate, recruits STAM1 from the cytosol to form the ESCRT-0 complex on endosomal membranes. ESCRT-0 then initiates the sorting process by concentrating ubiquitinated cargo underneath clathrin microdomains. Hrs uses its PSAP motif to interact with TSG101, leading to the recruitment of ESCRT-I, -II and -III complexes to facilitate cargo transport to the intralumenal vesicles of MVBs for lysosomal degradation (Henne et al., 2011; Roxrud et al., 2010). However, previous studies have shown that STAM1 and TSG101 can localize to the endosomal membrane when Hrs is depleted in cells (Bache et

al., 2003a; Kanazawa et al., 2003), suggesting that additional mechanisms exist to recruit ESCRTs to the endosomal membrane.

Results from Chapter 3 identified SIMPLE as a novel regulator of ESCRT recruitment to the early endosome membrane under both basal condition and EGFR activation. SIMPLE depletion has no effect on Hrs and STAM1 stability, suggesting that SIMPLE interacts transiently with ESCRT subunits to facilitate their recruitment to the endosome membrane rather than forming tight molecular complexes with these proteins. While SIMPLE, like Hrs, contains a PSAP motif and recruits both STAM1 and TSG101 to the endosomal membrane, results from Chapter 3 showed that SIMPLE and Hrs are not functionally redundant and that SIMPLE is responsible for recruiting Hrs to the membrane. In addition, SIMPLE function in recruiting ESCRT subunits to the endosomal membrane is up-regulated by EGFR activation, which suggests that SIMPLE is a downstream signaling target of EGFR that promotes ESCRT association with the early endosome membrane.

Endosome-to-lysosome trafficking of receptors serves as a major mechanism for controlling the intensity and duration of signal transduction in cells (Katzmann et al., 2002; Waterman and Yarden, 2001). ESCRT-mediated endosome-to-lysosome sorting of signaling receptors plays a crucial role in attenuation of signal transduction (Wegner et al., 2011). Consistent with these previous findings, results from Chapter 3 indicated that the function of SIMPLE in regulating endosome-to-lysosome trafficking is essential for the degradation of activated receptors and their down-regulation downstream signaling pathways. Therefore, SIMPLE, with its widely distributed protein expression pattern, could act as a regulator of ESCRT-mediated endocytic trafficking in multiple tissues and

cell types. Taken together, these results have provided new insights to the spatial and temporal control of the endosome-to-lysosome trafficking pathway and have important implications in the regulation of receptor signaling that controls a variety of cellular processes.

5.4. Protein misfolding as a mechanism in CMT pathogenesis: therapeutic implications

5.4.1. Protein misfolding is a common feature in demyelinating CMT

Results described in Chapter 2 revealed that mutations causing demyelinating CMT type 1C (CMT1C) are clustered within or around the transmembrane domain of SIMPLE and disrupt SIMPLE insertion into the membrane, leading to the accumulation of misfolded SIMPLE in the cytosol. Similarly, mutations causing the over-expression or single amino acid substitutions of the type III tetra-spanning (Fontanini et al., 2005) membrane protein peripheral myelin protein 22 (PMP22) and type II single-spanning (D'Urso et al., 1990) membrane protein myelin protein zero (MPZ) are linked to the major subtypes of demyelinating CMT, type 1A (CMT1A) and type 1B (CMT1B), respectively, which lead to the misfolding of PMP22 (Fortun et al., 2006; Fortun et al., 2005; Myers et al., 2008) and MPZ (Mandich et al., 2009; Shames et al., 2003). How misfolding of these membrane proteins with different topologies contributes to demyelinating neuropathy remain unknown. As described in Chapter 2, misfolded SIMPLE form abnormal cytosolic aggregates and mediate erroneous interactions with cellular proteins, which are pathogenic mechanisms characteristic of many protein-misfolding diseases (Ovadi et al.,

2004; Selkoe, 2004). These findings suggest that demyelinating CMT may be a protein-misfolding disease of Schwann cells.

5.4.2. The proteasome and aggresome-autophagy pathways protect Schwann cells against toxic build-up of misfolded proteins

Misfolded myelin proteins, such as PMP22 and MPZ (Figure 1, *step 1a*), may be refolded by molecular chaperones at the ER (Pareek et al., 1997) (Figure 1, *step 2*). When refolding is not possible, these misfolded proteins are retrotranslocated to the cytosol (Figure 1, *step 3*) and cleared by the proteasome (Figure 1, *step 3*) in a process known as ER-associated degradation (ERAD) (Ryan et al., 2002). Results described in Chapter 2 showed that misfolded SIMPLE proteins translocated from the early endosome to the cytosol (Figure 1, *step 1b*) are also degraded by the proteasome (Figure 1, *step 4*) but through an ERAD-independent mechanism. Whether this novel ERAD-independent proteasomal degradation is unique to misfolded SIMPLE or also degrades other C-tail anchored membrane proteins will need to be addressed by future studies. In addition, the E3 ligases targeting misfolded proteins for ERAD-dependent and -independent clearance of misfolded proteins in Schwann cells remain to be identified.

The proteasome system only degrades monomeric misfolded proteins but not aggregated proteins. When proteasome is impaired or overwhelmed, misfolded proteins accumulate and form soluble oligomers (Figure 1, *step 5*) that inhibit proteasome function (Figure 1, *step 6*) and may impair Schwann cell functions including myelination (Figure 1, *step 7*). The aggresome-autophagy pathway has emerged as another crucial

protein quality control system in Schwann cells that degrades misfolded and aggregated proteins (Fortun et al., 2003; Olzmann et al., 2008; Ryan et al., 2002). Results described in Chapter 2 and by others (Ryan et al., 2002) indicate that Schwann cells handle misfolded PMP22 and SIMPLE by sequestering them into perinuclear aggresomes through a mechanism requiring microtubule-dependent retrograde transport (Figure 1, *step 8*). Although the signaling events that target misfolded PMP22 and SIMPLE into aggresomes have not been identified, our previous finding (Olzmann et al., 2007) of parkin-mediated K63-linked poly-ubiquitination in targeting misfolded protein to aggresomes via interactions with the dynein adaptor protein HDAC6 suggest that as yet-to-be identified E3 ligases and adaptor proteins could be responsible for targeting misfolded PMP22 and SIMPLE to aggresomes. Moreover, results from Chapter 2 and other groups showed that PMP22- and SIMPLE-positive aggresomes are tightly surrounded by autophagosome markers (Figure 1, *step 9*) and degraded by autophagy (Figure 1, *step 10*).

5.4.3. Impairment in the proteasome and aggresome-autophagy pathways contributes to peripheral neuropathies

The accumulation of misfolded PMP22 and MPZ at the ER (Kamholz et al., 1999; Lee et al., 2010b) suggests that ERAD dysfunction and subsequent ER stress may be involved in causing demyelinating CMT. The fact that misfolded SIMPLE is not cleared by ERAD as described by Chapter 2 indicates that CMT pathogenesis can be mediated by dysfunction in ERAD-independent pathways. Proteasome impairment induced by

misfolded and aggregated proteins was observed in several mouse models of demyelinating CMT1A (Fortun et al., 2005). Moreover, proteasome inhibition by the chemotherapeutic medication bortezomib causes demyelinating neuropathy and worsens the neuropathic symptoms of CMT patients (Filosto et al., 2007; Hamilton et al., 2005). These findings suggest that proteasome dysfunction could contribute to demyelinating CMT pathogenesis.

Impairment of the aggresome-autophagy pathway by microtubule-disrupting drugs such as vincristine, cisplatin, and docetaxel (Figure 1, *step 8*) block aggresome-targeting of misfolded PMP22 (Watanabe et al., 2010) and exacerbates the neuropathy phenotype in CMT patients (Weimer and Podwall, 2006). Inhibition of microtubule polymerization observed in Chediak-Higashi syndrome, a genetic disease caused by *LYST* mutations, leads to severe demyelinating peripheral neuropathy as well (Lockman et al., 1967). Meanwhile, the raise in luminal pH of lysosomes and disruption of autophagosome-lysosome fusion by chloroquine (Spowart and Lum, 2010) also induces peripheral neuropathy (Weimer and Podwall, 2006). These evidence suggests that dysfunction in the aggresome-autophagy pathway is another major contributing factor of demyelinating peripheral neuropathies.

5.4.4. Proteasome and aggresome-autophagy pathways are potential therapeutic targets in CMT

The studies described above suggest that the augmentation of the proteasome and aggresome-autophagy pathways in Schwann cells could help protect against

demyelinating neuropathies. Proteasome activation by oleuroperin (Rigacci et al., 2010) or enhanced targeting to proteasome by an USP14 inhibitor (Lee et al., 2010a) both demonstrated cytoprotective effects. In addition, the chemical compounds B2 and B5 identified from a recent drug screen are inducers of aggresome formation that reduce the cytotoxicity mediated by misfolded proteins (Bodner et al., 2006). These drugs could be evaluated as potential treatments for demyelinating CMT. Findings described in Chapter 2 showing that autophagy activation by rapamycin promotes autophagic degradation of misfolded SIMPLE, together with the reported role of rapamycin in promoting myelination in explant cultures from neuropathic mouse models of CMT1A (Rangaraju et al., 2010), suggest that autophagy activation could be efficacious for treating demyelinating peripheral neuropathy. Future studies to identify Schwann cell-specific E3 ligases and adaptor proteins that target misfolded proteins for clearance will facilitate the development of new therapeutic strategies that are clinically viable in treating demyelinating CMT.

5.5. Dysregulation of axonal NRG1-activated Schwann cell ErbB receptor signaling is involved in CMT pathogenesis: therapeutic implications

5.5.1. Sustained axonal NRG1 activation of Schwann cell ErbB receptors contributes to demyelinating CMT

NRG1, a signaling protein synthesized by the axon which contains an epidermal-growth-factor-like signal domain that activates Schwann cell ErbB receptors, is an essential axonal signal that controls myelination by Schwann cells (Nave and Trapp, 2008; Quintes

et al., 2010). In response to NRG1 binding, ErbB2 and ErbB3 receptors form heterodimers, leading to receptor cross-phosphorylation and activation of downstream signaling pathways including the ERK1/2 and Akt pathways (Birchmeier, 2009; Nave and Salzer, 2006; Quintes et al., 2010). This NRG1-dependent activation of the ERK1/2 and Akt signaling pathways is essential for the proper myelin formation to ensheath peripheral axons in animal models and *in vitro* Schwann cell-neuronal co-cultures (Nave and Salzer, 2006; Ogata et al., 2004; Quintes et al., 2010; Syed et al., 2010), and dysregulation of these pathways has been recently linked dys/demyelination in animal and cell models of peripheral neuropathy (Goebbels et al., 2012; Nave and Salzer, 2006; Ogata et al., 2004; Quintes et al., 2010; Syed et al., 2010).

Results from Chapter 3 indicated that CMT1C-causing mutations impair the function of SIMPLE in regulating endosome-to-lysosome trafficking without affecting its ability to self-associate and to interact with the ESCRT subunits STAM1 and TSG101. These findings suggest that mutant SIMPLE proteins act in a dominant-negative manner to inhibit the function of wild-type SIMPLE protein by forming non-functional heterodimer with wild-type SIMPLE protein and/or competing with the wild-type SIMPLE protein for binding ESCRTs. This notion is supported by the fact that CMT1C-linked SIMPLE W116G and P135T mutants have dominant-negative effects on endosome-to-lysosome trafficking of ErbB receptors and cause persistent activation of downstream ERK1/2 signaling by NRG1 in Schwann cells. These results, together with reports that persistent ERK1/2 activation leads to demyelination (Nave and Salzer, 2006; Ogata et al., 2004; Quintes et al., 2010; Syed et al., 2010), suggest that dysregulation of endosome-to-lysosome trafficking and subsequent persistent NRG1-ErbB signaling in

Schwann cells caused by SIMPLE mutations trigger demyelination and subsequent axonal degeneration seen in CMT1C patients. Moreover, loss-of-function mutations in myotubularin-related 2 and 13 (MTMR2 and MTMR13), two proteins involved in the regulation of endosome-to-lysosome trafficking (Berger et al., 2011; Cao et al., 2008), cause sustained Akt activation and demyelinating CMT4B in human patients (Bird et al., 1997; Quattrone et al., 1996). Furthermore, loss-of-function mutations in SH3TC2, an endosomal protein with a role in regulating endosomal recycling, cause demyelinating CMT4C (Arnaud et al., 2009). Together, these results suggest that the disruption of endocytic trafficking that controls signal transduction in Schwann cells may represent a common etiology of many subtypes of demyelinating neuropathies.

5.5.2. Modulation of NRG1-ErbB receptor trafficking and signaling as possible strategies for treating CMT

The studies described above suggest an intriguing possibility that modulation of receptor trafficking and signaling could be beneficial in treating demyelinating neuropathies. For demyelinating neuropathies with endocytic defects that results in hyperactivation of ERK1/2 or Akt signaling, pharmacological agents that decrease receptor activation of these signaling pathways might be a promising therapeutic approach. Some examples of this approach include the finding that PKI 166, a drug that inhibits ErbB receptor signaling, is efficacious in preventing *mycobacterium leprae*-induced ErbB receptor activation and demyelination in mice (Tapinos et al., 2006). In addition, rapamycin, a drug that has been investigated for its ability to promote proper myelination (Goebbels et

al., 2012; Rangaraju et al., 2010), inhibits mTOR which may have a therapeutic effect from its action in blocking signaling downstream of ErbB receptor activation to prevent the dysregulation of myelination signaling (Goebbels et al., 2012). Although PKI 166 and rapamycin are not likely to be the drugs of choice in treating peripheral neuropathy due to their side effects, the development of pharmacological agents targeting receptors and downstream effectors of the ERK1/2 and/or the Akt/mTOR pathways should help provide novel treatments for these types of demyelinating neuropathies. For demyelinating neuropathies where ERK1/2 and/or Akt signaling are inhibited, drugs that stimulate these signaling pathways may prove beneficial to these patients. A small-molecule screen for agonists of pro-myelination receptors, such as ErbB receptors, may help identify drugs that could promote myelination to treat certain types of demyelinating neuropathies. Moreover, lithium, a drug that has been used as a long-term mood stabilizer in treating bipolar and depressive disorders, was recently found to stimulate peripheral myelin gene expression and myelination of peripheral nerves *in vivo* by inducing the nuclear translocation of β-catenin without affecting the Akt pathway (Makoukji et al., 2012). Compounds similar to lithium could be tested for their ability to reverse subtypes of demyelinating neuropathies where ERK1/2 and/or Akt signaling are dampened. Finally, modulation of endocytic sorting protein machineries to restore receptor trafficking and signaling back to homeostatic levels could be explored as therapeutic options in the future. A better understanding of the molecular pathways regulating receptor trafficking and signaling could lead to novel therapies for treating these debilitating neuropathic disorders.

5.6. Schwann cell dysfunction affects nodal gap width, disrupt axonal transport, and cause axonal degeneration in demyelinating CMT disease

As described in Chapter 4, transgenic mice expressing a CMT1C-linked SIMPLE mutant protein demonstrates motor and sensory neuropathy that recapitulates key behavioral and electrophysiological features of human demyelinating CMT1C disease. The pathology of human CMT1C remained poorly understood, and the only published pathological result is a light microscopy of sural nerve biopsy from a CMT1C patient showing the presence of onion-bulb formation (Street et al., 2003). The nerves of CMT1C transgenic mice did not demonstrate obvious onion-bulb formations. A similar lack of onion bulb formations has been reported in other mouse models of human CMT (Bonneick et al., 2005; Tersar et al., 2007; Verhamme et al., 2011), which may be due to the shorter life span of mice and/or some other species difference between mice and humans (Suter and Scherer, 2003). Nevertheless, histological examination of nerves from CMT1C transgenic mice revealed several pathological findings including a significant number of nerve fibers with myelin infolding originating from the Schmidt-Lanterman incisures and paranodal regions that are largely absent in the control mice. Similar myelin infolding has been found in several types of inherited demyelinating neuropathies such as CMT1B (Fabrizi et al., 2000; Iida et al., 2012; Kochanski et al., 2003), CMT4A (Chung et al., 2011), and CMT4B (Bird et al., 1997; Quattrone et al., 1996) and inflammatory demyelinating neuropathy (Sander et al., 2000) as well as in animal models of demyelinating CMT (Bolino et al., 2004; Bolis et al., 2005; Robinson et al., 2008; Tersar et al., 2007). Our study described in Chapter 4 also showed that myelin infolding is linked to retraction of myelin at the paranode to cause widened demyelinated nodal gaps and slowed nerve conduction velocities. Nodal

retraction are also seen in CMT1A (Yoshikawa et al., 1996), CMT4C (Arnaud et al., 2009), and in mouse models of demyelinating CMT (Arnaud et al., 2009; Bolino et al., 2004), suggesting that myelin infolding and nodal damage may represent convergent pathogenic mechanisms leading to demyelinating peripheral neuropathy.

In addition to primary myelin damage, results described in this dissertation and in other reports (de Waegh and Brady, 1990; de Waegh et al., 1992; Goebbels et al., 2012) also revealed that infolded myelin loops reduce axon caliber, inhibit axonal transport, and cause accumulation of axoplasm containing damaged organelles such as mitochondria. In addition, the infolding and/or outfolding of myelin are associated with secondary axonal degeneration (Bolis et al., 2005; Robinson et al., 2008; Tersar et al., 2007). How myelin abnormalities can cause axonal damage is currently unknown. In the context of CMT1C neuropathy, it is possible that SIMPLE mutations, by disrupting NRG1-ErbB signaling, could affect the synthesis and transport of Schwann cell plasma membrane proteins that are normally involved in axonal contact. This could cause a lack of communication from Schwann cells to axons which may be responsible for the dysfunction in axonal transport and axonal degeneration. Future identification of novel signaling proteins and molecules mediating Schwann cell-axon interaction will help explain the pathogenic mechanisms in the cause and the progression of demyelinating neuropathies.

5.7. Focally folded myelin and increased nodal gap length are pathological findings of age-dependent demyelinating CMT mouse models and patients

The finding of myelin infolding and paranodal damage in older but not younger SIMPLE CMT1C mice indicates that these pathological changes occur after the myelination has completed and the architecture of Schwann cell–axon units has been established. This is consistent with the clinical time course of CMT1C where patients often have a late onset in the third and fourth decades of life (Campbell et al., 2004; Gerding et al., 2009; Latour et al., 2006; Saifi et al., 2005; Street et al., 2003). Therefore, myelin infolding and paranodal damage are likely caused by defects in myelin sheath maintenance rather than the formation of Schwann cell-axon units during development. In addition to myelin infolding, a small but significant percentage of nerve fibers had signs of demyelination and axonal degeneration. These observations suggest the possibility that myelin infolding and nodal disorganization could be pathologic precursors to the late-stage demyelination and axonal degeneration seen in CMT1C patients.

While the pathophysiology of dysmyelination associated with myelin infolding and widened nodal gap is unknown, reports in rodent studies have indicated that mild myelin infolding and paranodal break-down are associated with aging (Ansved and Larsson, 1990; Ceballos et al., 1999; Hinman et al., 2006; Knox et al., 1989; Tersar et al., 2007). This could reflect an age-related failure of the complex systems for handling organelle damage, oxidative stress, and protein misfolding (Basaiawmoit and Rattan, 2010) that affects normal cellular functions and is linked to the pathogenesis of a variety of human diseases. Moreover, a link between endosomal trafficking dysfunction and dysmyelination has been suggested by the findings that loss-of-function mutations in myotubularin-related 2 and 13 (MTMR2 and MTMR13), two proteins involved in the regulation of endosome-to-lysosome trafficking and ErbB receptor signaling (Berger et

al., 2011; Cao et al., 2008), cause CMT4B with myelin infolding and outfolding and a modestly widened nodal gap (Bird et al., 1997; Bolino et al., 2004; Quattrone et al., 1996). Furthermore, loss-of-function mutations in SH3TC2, an endosomal protein with a role in regulating endosomal recycling, cause CMT4C with a widened nodal gap (Arnaud et al., 2009). Based on my study on CMT1C pathogenesis and the above reports on other subtypes of demyelinating CMT, I propose that myelin infolding in human CMT patients and mouse models is caused by a combination of toxic misfolded protein and aggregate accumulation and/or by the cumulative effects of endocytic dysfunction and dysregulated receptor signaling, all of which contributes to the accelerated aging of Schwann cells and cause demyelinating peripheral neuropathy.

5.8. Future directions

5.8.1. Regulation of myelin protein synthesis and trafficking by SIMPLE

The effects of SIMPLE mutations-mediated prolonged NRG1-ErbB receptor signaling on Schwann cell plasma membrane protein composition remain unexamined. It will be critical for future studies to examine whether the expression of proteins implicated in Schwann cell-myelin communications, such as MAG (Martini, 2001), is affected by sustained ErbB receptor signaling to cause demyelinating peripheral neuropathy with secondary axonal defects. In addition to ErbB receptor signaling, the role of SIMPLE in regulating endosome-to-lysosome sorting pathway may be extended to modulating the endosomal trafficking of myelin proteins. The dynamic process of remodeling the myelin sheath (Gould, 1977; Hendelman and Bunge, 1969) in adapting to extracellular

perturbations such as axonal growth, inflammatory responses, and myelin damage requires vigorous endosomal trafficking to recycle and degrade myelin proteins (Spiegel and Peles, 2002). Therefore, the membrane recruitment of ESCRTs by SIMPLE could be essential for the sorting of myelin proteins to the lysosome for degradation, and mutations in SIMPLE may disrupt the trafficking and degradation of these myelin proteins. Future studies examining these processes could have important implications in dysmyelination as well as secondary axonal defects in demyelinating CMT disease.

5.8.2. Identification of the E3 ligase(s) and adapter protein(s) responsible for targeting misfolded SIMPLE to the proteasome and aggresome-autophagy pathways for degradation

The findings discussed in this dissertation indicate that augmentation of the proteasome and aggresome-autophagy pathways may provide therapeutic benefits for treating demyelinating CMT. However, these protein quality control systems are involved in degrading a variety of cellular proteins, and the direct modulation of these pathways may have many unexpected side effects. One potential approach in identifying clinically viable therapeutic targets is to determine which E3 ligases and adaptor proteins are involved in recognizing and targeting specific misfolded proteins implicated in demyelinating CMT. One such candidate is Parkin, an E3 ligase that targets misfolded proteins to the proteasome and aggresome-autophagy pathways for degradation (Olzmann et al., 2008). Parkin is expressed at Schwann cell cytoplasm (Hase et al., 2002), and mutations in parkin that cause early-onset Parkinson disease also result in a

significant demyelinating neuropathy phenotype (Abbruzzese et al., 2004). Therefore, it would be of interest to examine whether parkin is responsible for targeting misfolded protein in Schwann cells such as PMP22 and SIMPLE to these protein quality control pathways for degradation. Future studies identifying Schwann cell-expressed E3 ligases and adaptors involved in protein quality control may provide possible targets for treating demyelinating CMT.

5.8.3. Ubiquitination by NEDD4 may regulate the endocytic function of SIMPLE

Results from Chapter 3 show that SIMPLE recruits ESCRT subunits to the endosome membrane and is a crucial component for the endosome-to-lysosome trafficking of ErbB receptors. SIMPLE contains two PPSY motifs that interact with the WW domains of NEDD4 (Shirk et al., 2005). NEDD4 has emerged as an essential regulator of endocytic sorting and degradation of cell-surface cargos including the epidermal growth factor receptor (EGFR), epithelial sodium channel, β2 adrenergic receptor, and others (Lin et al., 2010; Nabhan et al., 2010; Staub et al., 2000). However, whether the SIMPLE-NEDD4 interaction has a regulatory role in endocytic trafficking remains unclear. Our preliminary data suggests that SIMPLE is ubiquitinated by NEDD4 in cells (data not shown), suggesting that NEDD4 could potentially modulate the endocytic function of SIMPLE. Additional studies investigating the function of NEDD4-mediated ubiquitination of SIMPLE may provide novel insights to the mechanisms regulating endocytic trafficking.

5.8.4. SIMPLE W116G transgenic mice as a CMT1C mouse model for studying pharmacological interventions

The SIMPLE mutant transgenic mice represent the first animal model of CMT1C and provide a valuable tool for investigating potential therapeutics. The autophagy activating drug rapamycin, which has shown therapeutic effects in Schwann-cell-specific knockout *PTEN* mice that demonstrated significant amount of focally infolded/outfolded myelin (Goebbels et al., 2012) as well as in explants cultures of neuropathic PMP22 mutant mice (Rangaraju et al., 2010), could be beneficial for treating demyelinating CMT. In addition, drugs such as oleuroperin that promote proteasome activity could potentially enhance the clearance of misfolded proteins in Schwann cells. Additional studies will be needed to investigate the efficacy of these drugs in treating the peripheral neuropathy in the SIMPLE W116G transgenic mice which may lead to future therapeutics for patients suffering from demyelinating CMT.

5.8.5. Generation of Schwann cell-specific disease-linked mutant SIMPLE transgenic mice

Chapter 4 described the generation and characterization of transgenic mice expressing CMT1C-linked W116G SIMPLE mutant protein in multiple tissues that showed a specific dysmyelinating peripheral neuropathy phenotype. These findings are of significant interest since they indicate that the W116G SIMPLE mutant protein, while present in many cell types, causes a specific impairment in Schwann cell function *in vivo*. Although the expression of W116G SIMPLE mutant protein in multiple tissues is

important in mimicking human CMT1C patients where endogenous SIMPLE protein is ubiquitously expressed, the generation of Schwann cell-specific CMT1C-linked mutant SIMPLE transgenic mice could address whether the primary defect of the peripheral nervous system caused by CMT1C-linked mutations is truly originated from Schwann cell dysfunction rather than by primary axonal dysfunction and/or degeneration.

5.8.6. Examination of peripheral nerve biopsies from CMT1C patients

SIMPLE mutations were first identified in 2003 and the mutations cause a rare form of demyelinating CMT disease. To date, there has been no reported study of the protein levels or subcellular localization of mutant SIMPLE proteins in tissues of human CMT1C patients. I have contacted various sources including authors from publications describing SIMPLE mutations in human CMT1C patients, the neuropathology cores and postmortem tissue banks at Emory and other universities and have not yet been able to obtain CMT1C patient tissues or cells even after several years. Nevertheless, it would be invaluable to examine these human patient tissues for subcellular distribution and protein aggregation of SIMPLE mutant proteins, to assess the ErbB signaling pathway activation, and to evaluate the pathology of early stage vs. late stage CMT1C in order to gain additional insights to the disease.

5.9. Final words

Although Charcot-Marie-Tooth disease (CMT) was first described over a century ago, very few treatment options are currently available for this debilitating disease. Recent efforts have identified causative mutations in over 30 genes which have provided initial clues to the potential pathogenic mechanisms of the disease. A better understanding of the molecular and cellular pathways involved in the pathogenesis of CMT would help identify novel therapeutic targets for treating human patients. The experimental results described in this dissertation have provided new insights to the pathogenesis of a subtype of demyelinating CMT, CMT type 1C (CMT1C), and have implicated protein misfolding and aggregation and the dysfunction of the endocytic trafficking and signaling of ErbB receptors as contributing pathogenic mechanisms of CMT1C. These findings, together with previous reports, indicate that these are converging pathogenic mechanisms shared by multiple forms of demyelinating CMT and suggest that common treatment targets could be explored for treating CMT with similar etiologies. Results from this dissertation also revealed that CMT1C-linked mutant SIMPLE are selectively degraded by both the proteasome and aggresome-autophagy pathways, which implicate these protein quality control pathways as potential therapeutic targets for CMT where misfolded proteins and aggregates are implicated. Furthermore, this dissertation describes the characterization of a CMT1C mouse model demonstrating behavioral, electrophysiological, and pathological features that resembles CMT1C disease which should facilitate the investigation of CMT pathogenesis and therapeutics. Finally, our results have provided mechanistic insights to the degradation of misfolded proteins, intracellular transport and signaling of receptors, and communication between neuronal axons by Schwann cells, which have filled critical

gaps in our knowledge of many important basic biological processes and the pathogenic mechanisms involved in demyelinating diseases.

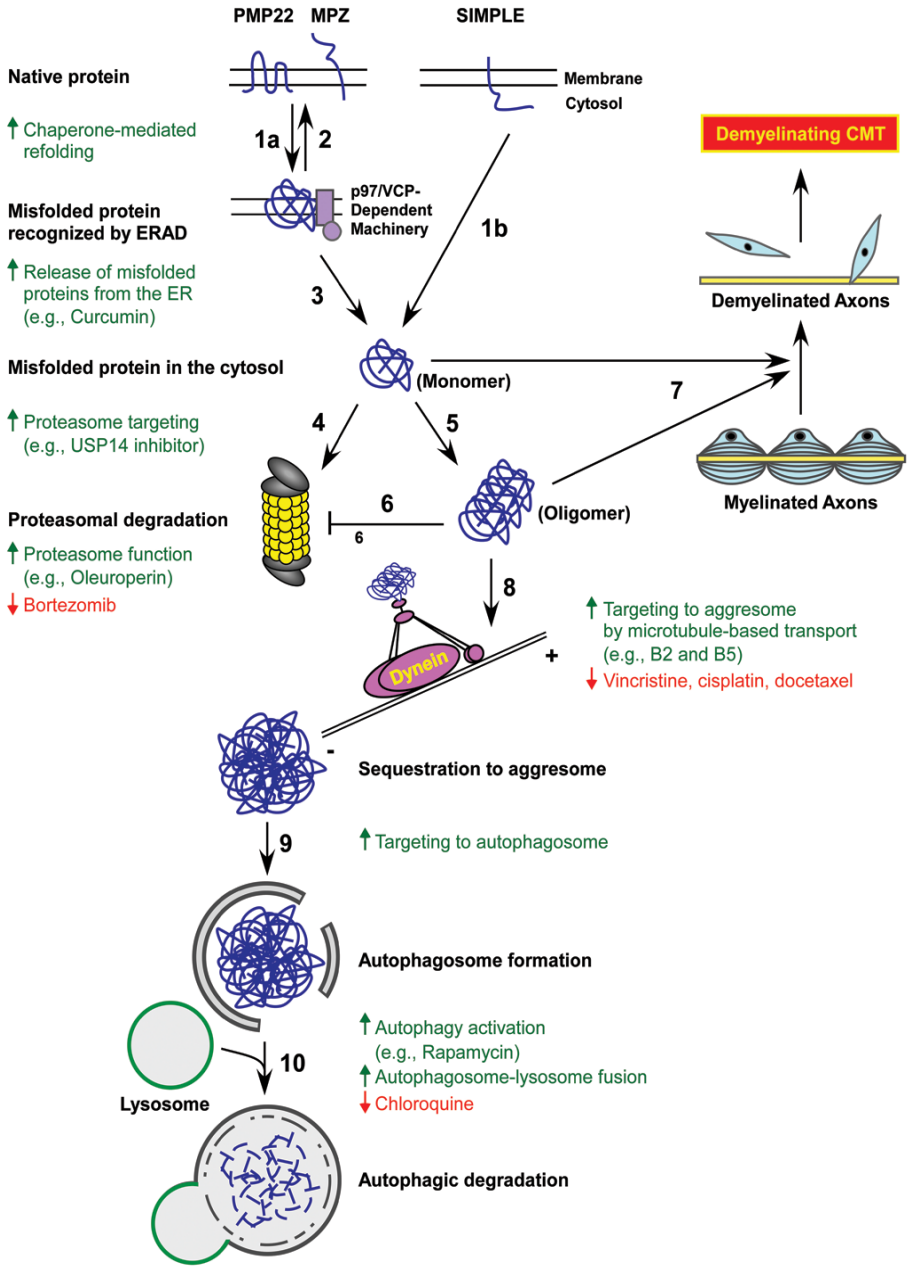

Figure 1. Protein quality control systems are potential targets for mechanism-based treatments of demyelinating CMT. Genetic mutations and increased protein expression levels linked to demyelinating CMT induce misfolding of hydrophobic proteins such as peripheral myelin protein 22 (PMP22), myelin protein zero (MPZ), and SIMPLE in Schwann cells (*step 1a and 1b*). Chaperones at the endoplasmic reticulum (ER) and the

cytosol refold misfolded PMP22 and MPZ proteins (*step 2*), but when refolding is not possible, these proteins are recognized and retrotranslocated to the cytosol by the p97/VCP-dependent ER-associated degradation (ERAD) machinery (*step 3*). In contrast, misfolded SIMPLE is translocated to the cytosol by an ERAD-independent mechanism (*step 1b*). These misfolded proteins are targeted to the 26S proteasome by K48-linked poly-ubiquitination for degradation (*step 4*). When the chaperone and proteasome systems are damaged or overwhelmed, misfolded proteins accumulate and aggregate into toxic oligomers (*step 5*) that could inhibit proteasome function (*step 6*) and impair myelination by Schwann cells, leading to demyelinating CMT (*step 7*). The aggresome-autophagy pathway is another protein quality control system in which misfolded and aggregated proteins are transported by the microtubule-dependent dynein motor complex to the aggresomes (*step 8*). Aggresomes not only sequester toxic misfolded and aggregated proteins but also recruit autophagic membrane for the formation of autophagosomes (*step 9*) and subsequent degradation by lysosomal hydrolases upon autophagosome-lysosome fusion (*step 10*). Therapeutic strategies and currently available agents that enhance the targeting of misfolded and aggregated proteins for turnover are indicated by the color green (upward arrows), and drugs exacerbating the CMT neuropathy phenotype are marked by the color red (downward arrows).

5.10. References

Abbruzzese, G., S. Pigullo, A. Schenone, E. Bellone, R. Marchese, E. Di Maria, L. Benedetti, P. Ciotti, L. Nobbio, V. Bonifati, F. Ajmar, and P. Mandich. 2004. Does parkin play a role in the peripheral nervous system? A family report. *Mov Disord*. 19:978-981.

Abrams, C.K., M.V. Bennett, V.K. Verselis, and T.A. Bargiello. 2002. Voltage opens unopposed gap junction hemichannels formed by a connexin 32 mutant associated with X-linked Charcot-Marie-Tooth disease. *Proc Natl Acad Sci U S A*. 99:3980-3984.

Amit, I., L. Yakir, M. Katz, Y. Zwang, M.D. Marmor, A. Citri, K. Shtiegman, I. Alroy, S. Tuvia, Y. Reiss, E. Roubini, M. Cohen, R. Wides, E. Bacharach, U. Schubert, and Y. Yarden. 2004. Tal, a Tsg101-specific E3 ubiquitin ligase, regulates receptor endocytosis and retrovirus budding. *Genes Dev*. 18:1737-1752.

Ansved, T., and L. Larsson. 1990. Quantitative and qualitative morphological properties of the soleus motor nerve and the L5 ventral root in young and old rats. Relation to the number of soleus muscle fibers. *J Neurol Sci*. 96:269-282.

Antonellis, A., R.E. Ellsworth, N. Sambuughin, I. Puls, A. Abel, S.Q. Lee-Lin, A. Jordanova, I. Kremensky, K. Christodoulou, L.T. Middleton, K. Sivakumar, V. Ionasescu, B. Funalot, J.M. Vance, L.G. Goldfarb, K.H. Fischbeck, and E.D. Green. 2003. Glycyl tRNA synthetase mutations in Charcot-Marie-Tooth disease type 2D and distal spinal muscular atrophy type V. *Am J Hum Genet*. 72:1293-1299.

Arnaud, E., J. Zenker, A.S. de Preux Charles, C. Stendel, A. Roos, J.J. Medard, N. Tricaud, H. Kleine, B. Luscher, J. Weis, U. Suter, J. Senderek, and R. Chrast. 2009. SH3TC2/KIAA1985 protein is required for proper myelination and the integrity of the node of Ranvier in the peripheral nervous system. *Proc Natl Acad Sci U S A*. 106:17528-17533.

Arrasate, M., S. Mitra, E.S. Schweitzer, M.R. Segal, and S. Finkbeiner. 2004. Inclusion body formation reduces levels of mutant huntingtin and the risk of neuronal death. *Nature*. 431:805-810.

Azzedine, H., A. Bolino, T. Taieb, N. Birouk, M. Di Duca, A. Bouhouche, S. Benamou, A. Mrabet, T. Hammadouche, T. Chkili, R. Gouider, R. Ravazzolo, A. Brice, J. Laporte, and E. LeGuern. 2003. Mutations in MTMR13, a new pseudophosphatase homologue of MTMR2 and Sbf1, in two families with an autosomal recessive demyelinating form of Charcot-Marie-Tooth disease associated with early-onset glaucoma. *Am J Hum Genet*. 72:1141-1153.

Babst, M. 2004. GGAing ubiquitin to the endosome. *Nat Cell Biol*. 6:175-177.

Babst, M., G. Odorizzi, E.J. Estepa, and S.D. Emr. 2000. Mammalian tumor susceptibility gene 101 (TSG101) and the yeast homologue, Vps23p, both function in late endosomal trafficking. *Traffic*. 1:248-258.

Bache, K.G., A. Brech, A. Mehlum, and H. Stenmark. 2003a. Hrs regulates multivesicular body formation via ESCRT recruitment to endosomes. *J Cell Biol*. 162:435-442.

Bache, K.G., C. Raiborg, A. Mehlum, and H. Stenmark. 2003b. STAM and Hrs are subunits of a multivalent ubiquitin-binding complex on early endosomes. *J Biol Chem*. 278:12513-12521.

Bache, K.G., T. Slagsvold, A. Cabezas, K.R. Rosendal, C. Raiborg, and H. Stenmark. 2004. The growth-regulatory protein HCRP1/hVps37A is a subunit of mammalian ESCRT-I and mediates receptor down-regulation. *Mol Biol Cell*. 15:4337-4346.

Baethmann, M., G. Gohlich-Ratmann, J.M. Schroder, L. Kalaydjieva, and T. Voit. 1998. HMSNL in a 13-year-old Bulgarian girl. *Neuromuscul Disord*. 8:90-94.

Basaiawmoit, R.V., and S.I. Rattan. 2010. Cellular stress and protein misfolding during aging. *Methods Mol Biol*. 648:107-117.

Baxter, R.V., K. Ben Othmane, J.M. Rochelle, J.E. Stajich, C. Hulette, S. Dew-Knight, F. Hentati, M. Ben Hamida, S. Bel, J.E. Stenger, J.R. Gilbert, M.A. Pericak-Vance, and J.M. Vance. 2002. Ganglioside-induced differentiation-associated protein-1 is mutant in Charcot-Marie-Tooth disease type 4A/8q21. *Nat Genet*. 30:21-22.

Ben Othmane, K., F. Hentati, F. Lennon, C. Ben Hamida, S. Blel, A.D. Roses, M.A. Pericak-Vance, M. Ben Hamida, and J.M. Vance. 1993. Linkage of a locus (CMT4A) for autosomal recessive Charcot-Marie-Tooth disease to chromosome 8q. *Hum Mol Genet*. 2:1625-1628.

Bendtsen, J.D., H. Nielsen, G. von Heijne, and S. Brunak. 2004. Improved prediction of signal peptides: SignalP 3.0. *J Mol Biol*. 340:783-795.

Berger, P., A. Niemann, and U. Suter. 2006. Schwann cells and the pathogenesis of inherited motor and sensory neuropathies (Charcot-Marie-Tooth disease). *Glia*. 54:243-257.

Berger, P., K. Tersar, K. Ballmer-Hofer, and U. Suter. 2011. The CMT4B disease-causing proteins MTMR2 and MTMR13/SBF2 regulate AKT signalling. *J Cell Mol Med*. 15:307-315.

Birchmeier, C. 2009. ErbB receptors and the development of the nervous system. *Exp Cell Res*. 315:611-618.

Bird, T.D. 1993. Charcot-Marie-Tooth Neuropathy Type 1. *In* GeneReviews. R.A. Pagon, T.D. Bird, C.R. Dolan, K. Stephens, and M.P. Adam, editors, Seattle (WA).

Bird, T.D., G.H. Kraft, H.P. Lipe, K.L. Kenney, and S.M. Sumi. 1997. Clinical and pathological phenotype of the original family with Charcot-Marie-Tooth type 1B: a 20-year study. *Ann Neurol*. 41:463-469.

Bodner, R.A., T.F. Outeiro, S. Altmann, M.M. Maxwell, S.H. Cho, B.T. Hyman, P.J. McLean, A.B. Young, D.E. Housman, and A.G. Kazantsev. 2006. Pharmacological promotion of inclusion formation: a therapeutic approach for Huntington's and Parkinson's diseases. *Proc Natl Acad Sci U S A*. 103:4246-4251.

Boerkoel, C.F., H. Takashima, C.A. Bacino, D. Daentl, and J.R. Lupski. 2001. EGR2 mutation R359W causes a spectrum of Dejerine-Sottas neuropathy. *Neurogenetics*. 3:153-157.

Bolcato-Bellemin, A.L., M.G. Mattei, M. Fenton, and S. Amar. 2004. Molecular cloning and characterization of mouse LITAF cDNA: role in the regulation of tumor necrosis factor-alpha (TNF-alpha) gene expression. *J Endotoxin Res*. 10:15-23.

Bolino, A., A. Bolis, S.C. Previtali, G. Dina, S. Bussini, G. Dati, S. Amadio, U. Del Carro, D.D. Mruk, M.L. Feltri, C.Y. Cheng, A. Quattrini, and L. Wrabetz. 2004.

Disruption of Mtmr2 produces CMT4B1-like neuropathy with myelin outfolding and impaired spermatogenesis. *J Cell Biol*. 167:711-721.

Bolino, A., E.R. Levy, M. Muglia, F.L. Conforti, E. LeGuern, M.A. Salih, D.M. Georgiou, R.K. Christodoulou, I. Hausmanowa-Petrusewicz, P. Mandich, A. Gambardella, A. Quattrone, M. Devoto, and A.P. Monaco. 2000a. Genetic refinement and physical mapping of the CMT4B gene on chromosome 11q22. *Genomics*. 63:271-278.

Bolino, A., M. Muglia, F.L. Conforti, E. LeGuern, M.A. Salih, D.M. Georgiou, K. Christodoulou, I. Hausmanowa-Petrusewicz, P. Mandich, A. Schenone, A. Gambardella, F. Bono, A. Quattrone, M. Devoto, and A.P. Monaco. 2000b. Charcot-Marie-Tooth type 4B is caused by mutations in the gene encoding myotubularin-related protein-2. *Nat Genet*. 25:17-19.

Bolis, A., S. Coviello, S. Bussini, G. Dina, C. Pardini, S.C. Previtali, M. Malaguti, P. Morana, U. Del Carro, M.L. Feltri, A. Quattrini, L. Wrabetz, and A. Bolino. 2005. Loss of Mtmr2 phosphatase in Schwann cells but not in motor neurons causes Charcot-Marie-Tooth type 4B1 neuropathy with myelin outfoldings. *J Neurosci*. 25:8567-8577.

Bolis, A., P. Zordan, S. Coviello, and A. Bolino. 2007. Myotubularin-related (MTMR) phospholipid phosphatase proteins in the peripheral nervous system. *Mol Neurobiol*. 35:308-316.

Bolte, S., and F.P. Cordelieres. 2006. A guided tour into subcellular colocalization analysis in light microscopy. *J Microscopy*. 224:213-232.

Bonneick, S., M. Boentert, P. Berger, S. Atanasoski, N. Mantei, C. Wessig, K.V. Toyka, P. Young, and U. Suter. 2005. An animal model for Charcot-Marie-Tooth disease type 4B1. *Hum Mol Genet.* 14:3685-3695.

Borgese, N., S. Brambillasca, and S. Colombo. 2007. How tails guide tail-anchored proteins to their destinations. *Curr Opin Cell Biol*. 19:368-375.

Borgese, N., and E. Fasana. 2011. Targeting pathways of C-tail-anchored proteins. *Biochim Biophys Acta*. 1808:937-946.

Boutry, J.M., J.J. Hauw, A. Gansmuller, N. Di-Bert, M. Pouchelet, and A. Baron-Van Evercooren. 1992. Establishment and characterization of a mouse Schwann cell line which produces myelin in vivo. *J Neurosci Res*. 32:15-26.

Brancolini, C., P. Edomi, S. Marzinotto, and C. Schneider. 2000. Exposure at the cell surface is required for gas3/PMP22 To regulate both cell death and cell spreading: implication for the Charcot-Marie-Tooth type 1A and Dejerine-Sottas diseases. *Mol Biol Cell*. 11:2901-2914.

Bukau, B., J. Weissman, and A. Horwich. 2006. Molecular chaperones and protein quality control. *Cell*. 125:443-451.

Butinar, D., J. Zidar, L. Leonardis, M. Popovic, L. Kalaydjieva, D. Angelicheva, Y. Sininger, B. Keats, and A. Starr. 1999. Hereditary auditory, vestibular, motor, and sensory neuropathy in a Slovenian Roma (Gypsy) kindred. *Ann Neurol*. 46:36-44.

Cagliani, R., N. Bresolin, A. Prelle, A. Gallanti, F. Fortunato, M. Sironi, P. Ciscato, G. Fagiolari, S. Bonato, S. Galbiati, S. Corti, C. Lamperti, M. Moggio, and G.P. Comi. 2003. A CAV3 microdeletion differentially affects skeletal muscle and myocardium. *Neurology*. 61:1513-1519.

Cai, Z., J.W. Finnie, P.C. Blumbergs, J. Manavis, M.N. Ghabriel, and P.D. Thompson. 2006. Early paranodal myelin swellings (tomacula) in an avian riboflavin deficiency model of demyelinating neuropathy. *Exp Neurol*. 198:65-71.

Cai, Z., P. Sutton-Smith, J. Swift, K. Cash, J. Finnie, A. Turnley, P.D. Thompson, and P.C. Blumbergs. 2002. Tomacula in MAG-deficient mice. *J Peripher Nerv Syst*. 7:181-189.

Campbell, R., H. Dorey, M. Naegeli, L.K. Grubstein, K.K. Bennett, F. Bonter, P.K. Smith, J. Grzywacz, P.K. Baker, and W.S. Davidson. 2004. An empowerment evaluation model for sexual assault programs: empirical evidence of effectiveness. *Am J Community Psychol*. 34:251-262.

Cao, C., J.M. Backer, J. Laporte, E.J. Bedrick, and A. Wandinger-Ness. 2008. Sequential actions of myotubularin lipid phosphatases regulate endosomal PI(3)P and growth factor receptor trafficking. *Mol Biol Cell*. 19:3334-3346.

Cao, Z., X. Wu, L. Yen, C. Sweeney, and K.L. Carraway, 3rd. 2007. Neuregulin-induced ErbB3 downregulation is mediated by a protein stability cascade involving the E3 ubiquitin ligase Nrdp1. *Mol Cell Biol*. 27:2180-2188.

Carenini, S., D. Montag, H. Cremer, M. Schachner, and R. Martini. 1997. Absence of the myelin-associated glycoprotein (MAG) and the neural cell adhesion molecule (N-CAM) interferes with the maintenance, but not with the formation of peripheral myelin. *Cell Tissue Res*. 287:3-9.

Cassereau, J., A. Chevrollier, N. Gueguen, V. Desquiret, C. Verny, G. Nicolas, F. Dubas, P. Amati-Bonneau, P. Reynier, D. Bonneau, and V. Procaccio. 2011.

Mitochondrial dysfunction and pathophysiology of Charcot-Marie-Tooth disease involving GDAP1 mutations. *Exp Neurol*. 227:31-41.

Ceballos, D., J. Cuadras, E. Verdu, and X. Navarro. 1999. Morphometric and ultrastructural changes with ageing in mouse peripheral nerve. *J Anat*. 195 (Pt 4):563-576.

Ceresa, B.P., M. Lotscher, and S.L. Schmid. 2001. Receptor and membrane recycling can occur with unaltered efficiency despite dramatic Rab5(q79l)-induced changes in endosome geometry. *J Biol Chem*. 276:9649-9654.

Chamberlain, L.H., R.D. Burgoyne, and G.W. Gould. 2001. SNARE proteins are highly enriched in lipid rafts in PC12 cells: implications for the spatial control of exocytosis. *Proc Natl Acad Sci U S A*. 98:5619-5624.

Chance, P.F., M.K. Alderson, K.A. Leppig, M.W. Lensch, N. Matsunami, B. Smith, P.D. Swanson, S.J. Odelberg, C.M. Disteche, and T.D. Bird. 1993. DNA deletion associated with hereditary neuropathy with liability to pressure palsies. *Cell*. 72:143-151.

Chaudhury, A., X.D. He, and R.K. Goyal. 2009. Role of PSD95 in membrane association and catalytic activity of nNOSalpha in nitrergic varicosities in mice gut. *Am J Physiol Gastrointest Liver Physiol*. 297:G806-813.

Chen, H., and D.C. Chan. 2005. Emerging functions of mammalian mitochondrial fusion and fission. *Hum Mol Genet*. 14 Spec No. 2:R283-289.

Chen, H., A. Chomyn, and D.C. Chan. 2005. Disruption of fusion results in mitochondrial heterogeneity and dysfunction. *J Biol Chem*. 280:26185-26192.

Chen, J., L. Li, and L.S. Chin. 2010. Parkinson disease protein DJ-1 converts from a zymogen to a protease by carboxyl-terminal cleavage. *Hum Mol Genet*. 19:2395-2408.

Chen, S., M.O. Velardez, X. Warot, Z.X. Yu, S.J. Miller, D. Cros, and G. Corfas. 2006. Neuregulin 1-erbB signaling is necessary for normal myelination and sensory function. *J Neurosci*. 26:3079-3086.

Chin, L.S., R.D. Nugent, M.C. Raynor, J.P. Vavalle, and L. Li. 2000. SNIP, a novel SNAP-25-interacting protein implicated in regulated exocytosis. *J Biol Chem*. 275:1191-1200.

Chin, L.S., J.A. Olzmann, and L. Li. 2010. Parkin-mediated ubiquitin signalling in aggresome formation and autophagy. *Biochem Soc Trans*. 38:144-149.

Chin, L.S., M.C. Raynor, X. Wei, H.Q. Chen, and L. Li. 2001. Hrs interacts with sorting nexin 1 and regulates degradation of epidermal growth factor receptor. *J Biol Chem*. 276:7069-7078.

Chow, C.Y., Y. Zhang, J.J. Dowling, N. Jin, M. Adamska, K. Shiga, K. Szigeti, M.E. Shy, J. Li, X. Zhang, J.R. Lupski, L.S. Weisman, and M.H. Meisler. 2007. Mutation of FIG4 causes neurodegeneration in the pale tremor mouse and patients with CMT4J. *Nature*. 448:68-72.

Chung, K.W., Y.S. Hyun, H.J. Lee, H.K. Jung, H. Koo, J.H. Yoo, S.B. Kim, C.I. Park, H.N. Kim, and B.O. Choi. 2011. Two recessive intermediate Charcot-Marie-Tooth patients with GDAP1 mutations. *J Peripher Nerv Syst*. 16:143-146.

Ciechanover, A. 2003. The ubiquitin proteolytic system and pathogenesis of human diseases: a novel platform for mechanism-based drug targeting. *Biochem Soc Trans*. 31:474-481.

Ciechanover, A. 2006. The ubiquitin proteolytic system: from a vague idea, through basic mechanisms, and onto human diseases and drug targeting. *Neurology*. 66:S7-19.

Claeys, K.G., S. Zuchner, M. Kennerson, J. Berciano, A. Garcia, K. Verhoeven, E. Storey, J.R. Merory, H.M. Bienfait, M. Lammens, E. Nelis, J. Baets, E. De Vriendt, Z.N. Berneman, I. De Veuster, J.M. Vance, G. Nicholson, V. Timmerman, and P. De Jonghe. 2009. Phenotypic spectrum of dynamin 2 mutations in Charcot-Marie-Tooth neuropathy. *Brain*. 132:1741-1752.

Cline, K., and H. Mori. 2001. Thylakoid DeltapH-dependent precursor proteins bind to a cpTatC-Hcf106 complex before Tha4-dependent transport. *J Cell Biol*. 154:719-729.

Colby, J., R. Nicholson, K.M. Dickson, W. Orfali, R. Naef, U. Suter, and G.J. Snipes. 2000. PMP22 carrying the trembler or trembler-J mutation is intracellularly retained in myelinating Schwann cells. *Neurobiol Dis*. 7:561-573.

Conforti, F.L., M. Muglia, R. Mazzei, A. Patitucci, P. Valentino, A. Magariello, T. Sprovieri, F. Bono, C. Bergmann, A.L. Gabriele, G. Peluso, R. Nistico, J. Senderek, and A. Quattrone. 2004. A new SBF2 mutation in a family with recessive demyelinating Charcot-Marie-Tooth (CMT4B2). *Neurology*. 63:1327-1328.

Court, F.A., D.L. Sherman, T. Pratt, E.M. Garry, R.R. Ribchester, D.F. Cottrell, S.M. Fleetwood-Walker, and P.J. Brophy. 2004. Restricted growth of Schwann cells lacking Cajal bands slows conduction in myelinated nerves. *Nature*. 431:191-195.

D'Urso, D., P.J. Brophy, S.M. Staugaitis, C.S. Gillespie, A.B. Frey, J.G. Stempak, and D.R. Colman. 1990. Protein zero of peripheral nerve myelin: biosynthesis, membrane insertion, and evidence for homotypic interaction. *Neuron*. 4:449-460.

D'Urso, D., P. Ehrhardt, and H.W. Muller. 1999. Peripheral myelin protein 22 and protein zero: a novel association in peripheral nervous system myelin. *J Neurosci*. 19:3396-3403.

D'Urso, D., R. Prior, R. Greiner-Petter, A.A. Gabreels-Festen, and H.W. Muller. 1998. Overloaded endoplasmic reticulum-Golgi compartments, a possible pathomechanism of peripheral neuropathies caused by mutations of the peripheral myelin protein PMP22. *J Neurosci*. 18:731-740.

De Sandre-Giovannoli, A., V. Delague, T. Hamadouche, M. Chaouch, M. Krahn, I. Boccaccio, T. Maisonobe, E. Chouery, R. Jabbour, S. Atweh, D. Grid, A. Megarbane, and N. Levy. 2005. Homozygosity mapping of autosomal recessive demyelinating Charcot-Marie-Tooth neuropathy (CMT4H) to a novel locus on chromosome 12p11.21-q13.11. *J Med Genet*. 42:260-265.

de Waegh, S., and S.T. Brady. 1990. Altered slow axonal transport and regeneration in a myelin-deficient mutant mouse: the trembler as an in vivo model for Schwann cell-axon interactions. *J Neurosci*. 10:1855-1865.

de Waegh, S.M., V.M. Lee, and S.T. Brady. 1992. Local modulation of neurofilament phosphorylation, axonal caliber, and slow axonal transport by myelinating Schwann cells. *Cell*. 68:451-463.

DeLaBarre, B., J.C. Christianson, R.R. Kopito, and A.T. Brunger. 2006. Central pore residues mediate the p97/VCP activity required for ERAD. *Mol Cell*. 22:451-462.

Delague, V., A. Jacquier, T. Hamadouche, Y. Poitelon, C. Baudot, I. Boccaccio, E. Chouery, M. Chaouch, N. Kassouri, R. Jabbour, D. Grid, A. Megarbane, G. Haase, and N. Levy. 2007. Mutations in FGD4 encoding the Rho GDP/GTP exchange factor FRABIN cause autosomal recessive Charcot-Marie-Tooth type 4H. *Am J Hum Genet*. 81:1-16.

Deng, H.X., C.J. Klein, J. Yan, Y. Shi, Y. Wu, F. Fecto, H.J. Yau, Y. Yang, H. Zhai, N. Siddique, E.T. Hedley-Whyte, R. Delong, M. Martina, P.J. Dyck, and T. Siddique. 2010. Scapuloperoneal spinal muscular atrophy and CMT2C are allelic disorders caused by alterations in TRPV4. *Nat Genet*. 42:165-169.

Dequen, F., M. Filali, R.C. Lariviere, R. Perrot, S. Hisanaga, and J.P. Julien. 2010. Reversal of neuropathy phenotypes in conditional mouse model of Charcot-Marie-Tooth disease type 2E. *Hum Mol Genet*. 19:2616-2629.

Dickson, K.M., J.J. Bergeron, I. Shames, J. Colby, D.T. Nguyen, E. Chevet, D.Y. Thomas, and G.J. Snipes. 2002. Association of calnexin with mutant peripheral myelin protein-22 ex vivo: a basis for "gain-of-function" ER diseases. *Proc Natl Acad Sci U S A*. 99:9852-9857.

Dobson, C.M. 2003. Protein folding and misfolding. *Nature*. 426:884-890.

Dowler, S., R.A. Currie, D.G. Campbell, M. Deak, G. Kular, C.P. Downes, and D.R. Alessi. 2000. Identification of pleckstrin-homology-domain-containing proteins with novel phosphoinositide-binding specificities. *Biochem J.* 351:19-31.

Doyotte, A., M.R. Russell, C.R. Hopkins, and P.G. Woodman. 2005. Depletion of TSG101 forms a mammalian "Class E" compartment: a multicisternal early endosome with multiple sorting defects. *J Cell Sci*. 118:3003-3017.

Eisenhaber, B., P. Bork, and F. Eisenhaber. 1999. Prediction of potential GPI-modification sites in proprotein sequences. *J Mol Biol*. 292:741-758.

Evans, M.J., and J.B. Finean. 1965. The lipid composition of myelin from brain and peripheral nerve. *J Neurochem*. 12:729-734.

Evgrafov, O.V., I. Mersiyanova, J. Irobi, L. Van Den Bosch, I. Dierick, C.L. Leung, O. Schagina, N. Verpoorten, K. Van Impe, V. Fedotov, E. Dadali, M. Auer-Grumbach, C. Windpassinger, K. Wagner, Z. Mitrovic, D. Hilton-Jones, K. Talbot, J.J. Martin, N. Vasserman, S. Tverskaya, A. Polyakov, R.K. Liem, J. Gettemans, W. Robberecht, P. De Jonghe, and V. Timmerman. 2004. Mutant small heat-shock protein 27 causes axonal Charcot-Marie-Tooth disease and distal hereditary motor neuropathy. *Nat Genet*. 36:602-606.

Fabrizi, G.M., F. Taioli, T. Cavallaro, S. Ferrari, L. Bertolasi, M. Casarotto, N. Rizzuto, T. Deconinck, V. Timmerman, and P. De Jonghe. 2009. Further evidence that mutations in FGD4/frabin cause Charcot-Marie-Tooth disease type 4H. *Neurology*. 72:1160-1164.

Fabrizi, G.M., F. Taioli, T. Cavallaro, F. Rigatelli, A. Simonati, G. Mariani, P. Perrone, and N. Rizzuto. 2000. Focally folded myelin in Charcot-Marie-Tooth neuropathy

type 1B with Ser49Leu in the myelin protein zero. *Acta Neuropathol*. 100:299-304.

Filali, M., F. Dequen, R. Lalonde, and J.P. Julien. 2011. Sensorimotor and cognitive function of a NEFL(P22S) mutant model of Charcot-Marie-Tooth disease type 2E. *Behav Brain Res*. 219:175-180.

Filosto, M., G. Rossi, A.M. Pelizzari, S. Buzio, M. Tentorio, L. Broglio, M. Mancuso, M. Rinaldi, M. Scarpelli, and A. Padovani. 2007. A high-dose bortezomib neuropathy with sensory ataxia and myelin involvement. *J Neurol Sci*. 263:40-43.

Fontanini, A., R. Chies, E.L. Snapp, M. Ferrarini, G.M. Fabrizi, and C. Brancolini. 2005. Glycan-independent role of calnexin in the intracellular retention of Charcot-Marie-tooth 1A Gas3/PMP22 mutants. *J Biol Chem*. 280:2378-2387.

Fortun, J., W.A. Dunn, Jr., S. Joy, J. Li, and L. Notterpek. 2003. Emerging role for autophagy in the removal of aggresomes in Schwann cells. *J Neurosci*. 23:10672-10680.

Fortun, J., J.C. Go, J. Li, S.A. Amici, W.A. Dunn, Jr., and L. Notterpek. 2006. Alterations in degradative pathways and protein aggregation in a neuropathy model based on PMP22 overexpression. *Neurobiol Dis*. 22:153-164.

Fortun, J., J. Li, J. Go, A. Fenstermaker, B.S. Fletcher, and L. Notterpek. 2005. Impaired proteasome activity and accumulation of ubiquitinated substrates in a hereditary neuropathy model. *J Neurochem*. 92:1531-1541.

Fruttiger, M., D. Montag, M. Schachner, and R. Martini. 1995. Crucial role for the myelin-associated glycoprotein in the maintenance of axon-myelin integrity. *Eur J Neurosci*. 7:511-515.

Gabreels-Festen, A.A., P.A. Bolhuis, J.E. Hoogendijk, L.J. Valentijn, E.J. Eshuis, and F.J. Gabreels. 1995. Charcot-Marie-Tooth disease type 1A: morphological phenotype of the 17p duplication versus PMP22 point mutations. *Acta Neuropathol*. 90:645-649.

Gabreels-Festen, A.A., F.J. Gabreels, F.G. Jennekens, E.M. Joosten, and T.W. Janssen-van Kempen. 1992. Autosomal recessive form of hereditary motor and sensory neuropathy type I. *Neurology*. 42:1755-1761.

Gabreels-Festen, A.A., J.E. Hoogendijk, P.H. Meijerink, F.J. Gabreels, P.A. Bolhuis, S. van Beersum, T. Kulkens, E. Nelis, F.G. Jennekens, M. de Visser, B.G. van Engelen, C. Van Broeckhoven, and E.C. Mariman. 1996. Two divergent types of nerve pathology in patients with different P0 mutations in Charcot-Marie-Tooth disease. *Neurology*. 47:761-765.

Garcia-Mata, R., Y.S. Gao, and E. Sztul. 2002. Hassles with taking out the garbage: aggravating aggresomes. *Traffic*. 3:388-396.

Gerding, W.M., J. Koetting, J.T. Epplen, and C. Neusch. 2009. Hereditary motor and sensory neuropathy caused by a novel mutation in LITAF. *Neuromuscul Disord*. 19:701-703.

Giles, L.M., J. Chen, L. Li, and L.S. Chin. 2008. Dystonia-associated mutations cause premature degradation of torsinA protein and cell-type-specific mislocalization to the nuclear envelope. *Hum Mol Genet*. 17:2712-2722.

Giles, L.M., L. Li, and L.S. Chin. 2009. Printor, a novel torsinA-interacting protein implicated in dystonia pathogenesis. *J Biol Chem*. 284:21765-21775.

Gillespie, C.S., D.L. Sherman, G.E. Blair, and P.J. Brophy. 1994. Periaxin, a novel protein of myelinating Schwann cells with a possible role in axonal ensheathment. *Neuron*. 12:497-508.

Gillespie, C.S., D.L. Sherman, S.M. Fleetwood-Walker, D.F. Cottrell, S. Tait, E.M. Garry, V.C. Wallace, J. Ure, I.R. Griffiths, A. Smith, and P.J. Brophy. 2000. Peripheral demyelination and neuropathic pain behavior in periaxin-deficient mice. *Neuron*. 26:523-531.

Goebbels, S., J.H. Oltrogge, S. Wolfer, G.L. Wieser, T. Nientiedt, A. Pieper, T. Ruhwedel, M. Groszer, M.W. Sereda, and K.A. Nave. 2012. Genetic disruption of Pten in a novel mouse model of tomaculous neuropathy. *EMBO Mol Med*. 4:486-499.

Goldberg, A.L. 2003. Protein degradation and protection against misfolded or damaged proteins. *Nature*. 426:895-899.

Gould, R.M. 1977. Incorporation of glycoproteins into peripheral nerve myelin. *J Cell Biol*. 75:326-338.

Grandis, M., T. Vigo, M. Passalacqua, M. Jain, S. Scazzola, V. La Padula, M. Brucal, F. Benvenuto, L. Nobbio, A. Cadoni, G.L. Mancardi, J. Kamholz, M.E. Shy, and A. Schenone. 2008. Different cellular and molecular mechanisms for early and late-onset myelin protein zero mutations. *Hum Mol Genet*. 17:1877-1889.

Guilbot, A., N. Ravise, A. Bouhouche, P. Coullin, N. Birouk, T. Maisonobe, T. Kuntzer, C. Vial, D. Grid, A. Brice, and E. LeGuern. 1999. Genetic, cytogenetic and physical refinement of the autosomal recessive CMT linked to 5q31-q33: exclusion of candidate genes including EGR1. *Eur J Hum Genet*. 7:849-859.

Guilbot, A., A. Williams, N. Ravise, C. Verny, A. Brice, D.L. Sherman, P.J. Brophy, E. LeGuern, V. Delague, C. Bareil, A. Megarbane, and M. Claustres. 2001. A mutation in periaxin is responsible for CMT4F, an autosomal recessive form of Charcot-Marie-Tooth disease. *Hum Mol Genet*. 10:415-421.

Gutekunst, C.A., S.H. Li, H. Yi, J.S. Mulroy, S. Kuemmerle, R. Jones, D. Rye, R.J. Ferrante, S.M. Hersch, and X.J. Li. 1999. Nuclear and neuropil aggregates in Huntington's disease: relationship to neuropathology. *J Neurosci*. 19:2522-2534.

Haastert, K., C. Mauritz, S. Chaturvedi, and C. Grothe. 2007. Human and rat adult Schwann cell cultures: fast and efficient enrichment and highly effective non-viral transfection protocol. *Nat Proct.* 2:99-104.

Hamilton, A.L., J.P. Eder, A.C. Pavlick, J.W. Clark, L. Liebes, R. Garcia-Carbonero, A. Chachoua, D.P. Ryan, V. Soma, K. Farrell, N. Kinchla, J. Boyden, H. Yee, A. Zeleniuch-Jacquotte, J. Wright, P. Elliott, J. Adams, and F.M. Muggia. 2005. Proteasome inhibition with bortezomib (PS-341): a phase I study with pharmacodynamic end points using a day 1 and day 4 schedule in a 14-day cycle. *J Clin Oncol*. 23:6107-6116.

Hartl, F.U., and M. Hayer-Hartl. 2009. Converging concepts of protein folding in vitro and in vivo. *Nat Struct Mol Biol*. 16:574-581.

Hase, A., H. Yamada, K. Arai, Y. Sunada, T. Shimizu, and K. Matsumura. 2002. Characterization of parkin in bovine peripheral nerve. *Brain Res*. 930:143-149.

Hasse, B., F. Bosse, H. Hanenberg, and H.W. Muller. 2004. Peripheral myelin protein 22 kDa and protein zero: domain specific trans-interactions. *Mol Cell Neurosci*. 27:370-378.

Haurogne, K., J.M. Bach, and B. Lieubeau. 2007. Easy and rapid method of zygosity determination in transgenic mice by SYBR Green real-time quantitative PCR with a simple data analysis. *Transgenic Res*. 16:127-131.

Hayasaka, K., M. Himoro, W. Sato, G. Takada, K. Uyemura, N. Shimizu, T.D. Bird, P.M. Conneally, and P.F. Chance. 1993. Charcot-Marie-Tooth neuropathy type 1B is associated with mutations of the myelin P0 gene. *Nat Genet*. 5:31-34.

Hendelman, W.J., and R.P. Bunge. 1969. Radioautographic studies of choline incorporation into peripheral nerve myelin. *J Cell Biol*. 40:190-208.

Henne, W.M., N.J. Buchkovich, and S.D. Emr. 2011. The ESCRT pathway. *Dev Cell*. 21:77-91.

Hessa, T., H. Kim, K. Bihlmaier, C. Lundin, J. Boekel, H. Andersson, I. Nilsson, S.H. White, and G. von Heijne. 2005a. Recognition of transmembrane helices by the endoplasmic reticulum translocon. *Nature*. 433:377-381.

Hessa, T., S.H. White, and G. von Heijne. 2005b. Membrane insertion of a potassium-channel voltage sensor. *Science*. 307:1427.

Hinman, J.D., A. Peters, H. Cabral, D.L. Rosene, W. Hollander, M.N. Rasband, and C.R. Abraham. 2006. Age-related molecular reorganization at the node of Ranvier. *The J Comparat Neurol*. 495:351-362.

Hirano, R., H. Takashima, F. Umehara, H. Arimura, K. Michizono, Y. Okamoto, M. Nakagawa, C.F. Boerkoel, J.R. Lupski, M. Osame, and K. Arimura. 2004. SET binding factor 2 (SBF2) mutation causes CMT4B with juvenile onset glaucoma. *Neurology*. 63:577-580.

Hirokawa, T., S. Boon-Chieng, and S. Mitaku. 1998. SOSUI: classification and secondary structure prediction system for membrane proteins. *Bioinformatics*. 14:378-379.

Hoeller, D., C.M. Hecker, S. Wagner, V. Rogov, V. Dotsch, and I. Dikic. 2007. E3-independent monoubiquitination of ubiquitin-binding proteins. *Mol Cell*. 26:891-898.

Houlden, H., S. Hammans, H. Katifi, and M.M. Reilly. 2009a. A novel Frabin (FGD4) nonsense mutation p.R275X associated with phenotypic variability in CMT4H. *Neurology*. 72:617-620.

Houlden, H., M. Laura, L. Ginsberg, H. Jungbluth, S.A. Robb, J. Blake, S. Robinson, R.H. King, and M.M. Reilly. 2009b. The phenotype of Charcot-Marie-Tooth disease type 4C due to SH3TC2 mutations and possible predisposition to an inflammatory neuropathy. *Neuromuscul Disord*. 19:264-269.

Hsieh, S.T., G.J. Kidd, T.O. Crawford, Z. Xu, W.M. Lin, B.D. Trapp, D.W. Cleveland, and J.W. Griffin. 1994. Regional modulation of neurofilament organization by myelination in normal axons. *J Neurosci*. 14:6392-6401.

Huang, Y., and C.L. Bennett. 2007. Litaf/Simple protein is increased in intestinal tissues from patients with CD and UC, but is unlikely to function as a transcription factor. *Inflammat Bowel Dis*. 13:120-121.

Hubbers, C.U., C.S. Clemen, K. Kesper, A. Boddrich, A. Hofmann, O. Kamarainen, K. Tolksdorf, M. Stumpf, J. Reichelt, U. Roth, S. Krause, G. Watts, V. Kimonis, M.P. Wattjes, J. Reimann, D.R. Thal, K. Biermann, B.O. Evert, H. Lochmuller, E.E.

Wanker, B.G. Schoser, A.A. Noegel, and R. Schroder. 2007. Pathological consequences of VCP mutations on human striated muscle. *Brain*. 130:381-393.

Hunter, M., R. Bernard, E. Freitas, A. Boyer, B. Morar, I.J. Martins, I. Tournev, A. Jordanova, V. Guergelcheva, B. Ishpekova, I. Kremensky, G. Nicholson, B. Schlotter, H. Lochmuller, T. Voit, J. Colomer, P.K. Thomas, N. Levy, and L. Kalaydjieva. 2003. Mutation screening of the N-myc downstream-regulated gene 1 (NDRG1) in patients with Charcot-Marie-Tooth Disease. *Hum Mutat*. 22:129-135.

Iida, M., H. Koike, T. Ando, M. Sugiura, M. Yamamoto, F. Tanaka, and G. Sobue. 2012. A novel MPZ mutation in Charcot-Marie-Tooth disease type 1B with focally folded myelin and multiple entrapment neuropathies. *Neuromuscul Disord*. 22:166-169.

Ionasescu, V.V., R. Ionasescu, C. Searby, and D.F. Barker. 1993. Charcot-Marie-Tooth neuropathy type 1A with both duplication and non-duplication. *Hum Mol Genet*. 2:405-410.

Irobi, J., K. Van Impe, P. Seeman, A. Jordanova, I. Dierick, N. Verpoorten, A. Michalik, E. De Vriendt, A. Jacobs, V. Van Gerwen, K. Vennekens, R. Mazanec, I. Tournev, D. Hilton-Jones, K. Talbot, I. Kremensky, L. Van Den Bosch, W. Robberecht, J. Van Vandekerckhove, C. Van Broeckhoven, J. Gettemans, P. De Jonghe, and V. Timmerman. 2004. Hot-spot residue in small heat-shock protein 22 causes distal motor neuropathy. *Nat Genet*. 36:597-601.

Janen, S.B., H. Chaachouay, and C. Richter-Landsberg. 2010. Autophagy is activated by proteasomal inhibition and involved in aggresome clearance in cultured astrocytes. *Glia*. 58:1766-1774.

Jang, S.W., X. Liu, M. Yepes, K.R. Shepherd, G.W. Miller, Y. Liu, W.D. Wilson, G. Xiao, B. Blanchi, Y.E. Sun, and K. Ye. 2010. A selective TrkB agonist with potent neurotrophic activities by 7,8-dihydroxyflavone. *Proc Natl Acad Sci U S A*. 107:2687-2692.

Jani-Acsadi, A., K. Krajewski, and M.E. Shy. 2008. Charcot-Marie-Tooth neuropathies: diagnosis and management. *Sem Neurol*. 28:185-194.

Johansen, T., and T. Lamark. 2011. Selective autophagy mediated by autophagic adapter proteins. *Autophagy*. 7:279-296.

Johnston, J.A., M.E. Illing, and R.R. Kopito. 2002. Cytoplasmic dynein/dynactin mediates the assembly of aggresomes. *Cell Motil Cytoskeleton*. 53:26-38.

Jordanova, A., J. Irobi, F.P. Thomas, P. Van Dijck, K. Meerschaert, M. Dewil, I. Dierick, A. Jacobs, E. De Vriendt, V. Guergueltcheva, C.V. Rao, I. Tournev, F.A. Gondim, M. D'Hooghe, V. Van Gerwen, P. Callaerts, L. Van Den Bosch, J.P. Timmermans, W. Robberecht, J. Gettemans, J.M. Thevelein, P. De Jonghe, I. Kremensky, and V. Timmerman. 2006. Disrupted function and axonal distribution of mutant tyrosyl-tRNA synthetase in dominant intermediate Charcot-Marie-Tooth neuropathy. *Nat Genet*. 38:197-202.

Kabzinska, D., H. Drac, D.L. Sherman, A. Kostera-Pruszczyk, P.J. Brophy, A. Kochanski, and I. Hausmanowa-Petrusewicz. 2006. Charcot-Marie-Tooth type 4F disease caused by S399fsx410 mutation in the PRX gene. *Neurology*. 66:745-747.

Kabzinska, D., A. Niemann, H. Drac, N. Huber, A. Potulska-Chromik, I. Hausmanowa-Petrusewicz, U. Suter, and A. Kochanski. 2011. A new missense GDAP1 mutation disturbing targeting to the mitochondrial membrane causes a severe form of AR-CMT2C disease. *Neurogenetics*. 12:145-153.

Kachhap, S.K., D. Faith, D.Z. Qian, S. Shabbeer, N.L. Galloway, R. Pili, S.R. Denmeade, A.M. DeMarzo, and M.A. Carducci. 2007. The N-Myc down regulated Gene1 (NDRG1) Is a Rab4a effector involved in vesicular recycling of E-cadherin. *PloS one*. 2:e844.

Kalaydjieva, L., D. Gresham, R. Gooding, L. Heather, F. Baas, R. de Jonge, K. Blechschmidt, D. Angelicheva, D. Chandler, P. Worsley, A. Rosenthal, R.H. King, and P.K. Thomas. 2000. N-myc downstream-regulated gene 1 is mutated in hereditary motor and sensory neuropathy-Lom. *Am J Hum Genet*. 67:47-58.

Kalaydjieva, L., A. Nikolova, I. Turnev, J. Petrova, A. Hristova, B. Ishpekova, I. Petkova, A. Shmarov, S. Stancheva, L. Middleton, L. Merlini, A. Trogu, J.R. Muddle, R.H. King, and P.K. Thomas. 1998. Hereditary motor and sensory neuropathy--Lom, a novel demyelinating neuropathy associated with deafness in gypsies. Clinical, electrophysiological and nerve biopsy findings. *Brain*. 121 (Pt 3):399-408.

Kamholz, J., R. Awatramani, D. Menichella, H. Jiang, W. Xu, and M. Shy. 1999. Regulation of myelin-specific gene expression. Relevance to CMT1. *Ann N Y Acad Sci*. 883:91-108.

Kanazawa, C., E. Morita, M. Yamada, N. Ishii, S. Miura, H. Asao, T. Yoshimori, and K. Sugamura. 2003. Effects of deficiencies of STAMs and Hrs, mammalian class E

Vps proteins, on receptor downregulation. *Biochem Biophys Res Commun*. 309:848-856.

Katz, M., K. Shtiegman, P. Tal-Or, L. Yakir, Y. Mosesson, D. Harari, Y. Machluf, H. Asao, T. Jovin, K. Sugamura, and Y. Yarden. 2002. Ligand-independent degradation of epidermal growth factor receptor involves receptor ubiquitylation and Hgs, an adaptor whose ubiquitin-interacting motif targets ubiquitylation by Nedd4. *Traffic*. 3:740-751.

Katzmann, D.J., G. Odorizzi, and S.D. Emr. 2002. Receptor downregulation and multivesicular-body sorting. *Nat Rev Mol Cell Biol*. 3:893-905.

Kessali, M., R. Zemmouri, A. Guilbot, T. Maisonobe, A. Brice, E. LeGuern, and D. Grid. 1997. A clinical, electrophysiologic, neuropathologic, and genetic study of two large Algerian families with an autosomal recessive demyelinating form of Charcot-Marie-Tooth disease. *Neurology*. 48:867-873.

Kim, B.E., K. Smith, C.K. Meagher, and M.J. Petris. 2002. A conditional mutation affecting localization of the Menkes disease copper ATPase. Suppression by copper supplementation. *J Biol Chem*. 277:44079-44084.

Kim, B.Y., J.A. Olzmann, G.S. Barsh, L.S. Chin, and L. Li. 2007. Spongiform neurodegeneration-associated E3 ligase Mahogunin ubiquitylates TSG101 and regulates endosomal trafficking. *Mol Biol Cell*. 18:1129-1142.

King, R.H., D. Chandler, S. Lopaticki, D. Huang, J. Blake, J.R. Muddle, T. Kilpatrick, M. Nourallah, T. Miyata, T. Okuda, K.W. Carter, M. Hunter, D. Angelicheva, G. Morahan, and L. Kalaydjieva. 2011. Ndrg1 in development and maintenance of the myelin sheath. *Neurobiol Dis*. 42:368-380.

King, R.H., I. Tournev, J. Colomer, L. Merlini, L. Kalaydjieva, and P.K. Thomas. 1999. Ultrastructural changes in peripheral nerve in hereditary motor and sensory neuropathy-Lom. *Neuropath Appl Neurbiol*. 25:306-312.

Kirk, E., L.S. Chin, and L. Li. 2006. GRIF1 binds Hrs and is a new regulator of endosomal trafficking. *J Cell Sci*. 119:4689-4701.

Kitamura, K., K. Uyemura, K. Shibuya, Y. Sakamoto, K. Yoshimura, and M. Nomura. 2000. Structure of a major oligosaccharide of PASII/PMP22 glycoprotein in bovine peripheral nerve myelin. *J Neurochem*. 75:853-860.

Kleopa, K.A., E. Zamba-Papanicolaou, X. Alevra, P. Nicolaou, D.M. Georgiou, A. Hadjisavvas, T. Kyriakides, and K. Christodoulou. 2006. Phenotypic and cellular expression of two novel connexin32 mutations causing CMT1X. *Neurology*. 66:396-402.

Knorre, A., M. Wagner, H.E. Schaefer, W.H. Colledge, and H.L. Pahl. 2002. DeltaF508-CFTR causes constitutive NF-kappaB activation through an ER-overload response in cystic fibrosis lungs. *Biol Chem*. 383:271-282.

Knox, C.A., E. Kokmen, and P.J. Dyck. 1989. Morphometric alteration of rat myelinated fibers with aging. *J Neuropath Exp Neurol*. 48:119-139.

Kobsar, I., M. Berghoff, M. Samsam, C. Wessig, M. Maurer, K.V. Toyka, and R. Martini. 2003. Preserved myelin integrity and reduced axonopathy in connexin32-deficient mice lacking the recombination activating gene-1. *Brain*. 126:804-813.

Kochanski, A., H. Drac, H. Jedrzejowska, and I. Hausmanowa-Petrusewicz. 2003. Focally folded myelin in Charcot-Marie-Tooth type 1B disease is associated with

Asn131Lys mutation in myelin protein zero gene: short report. *Eur J Neurol*. 10:547-549.

Kokame, K., H. Kato, and T. Miyata. 1996. Homocysteine-respondent genes in vascular endothelial cells identified by differential display analysis. GRP78/BiP and novel genes. *J Biol Chem*. 271:29659-29665.

Komander, D. 2009. The emerging complexity of protein ubiquitination. *Biochem Soc Trans*. 37:937-953.

Kopito, R.R. 2000. Aggresomes, inclusion bodies and protein aggregation. *Trends Cell Biol*. 10:524-530.

Kubota, H. 2009. Quality control against misfolded proteins in the cytosol: a network for cell survival. *J Biochem*. 146:609-616.

Kutateladze, T.G., K.D. Ogburn, W.T. Watson, T. de Beer, S.D. Emr, C.G. Burd, and M. Overduin. 1999. Phosphatidylinositol 3-phosphate recognition by the FYVE domain. *Mol Cell*. 3:805-811.

Kwong, J., F.L. Roundabush, P. Hutton Moore, M. Montague, W. Oldham, Y. Li, L.S. Chin, and L. Li. 2000. Hrs interacts with SNAP-25 and regulates Ca(2+)-dependent exocytosis. *J Cell Sci*. 113 (Pt 12):2273-2284.

Latour, P., P.M. Gonnaud, E. Ollagnon, V. Chan, S. Perelman, T. Stojkovic, C. Stoll, C. Vial, F. Ziegler, A. Vandenberghe, and I. Maire. 2006. SIMPLE mutation analysis in dominant demyelinating Charcot-Marie-Tooth disease: three novel mutations. *J Peripher Nerv Syst*. 11:148-155.

Lauwers, E., C. Jacob, and B. Andre. 2009. K63-linked ubiquitin chains as a specific signal for protein sorting into the multivesicular body pathway. *J Cell Biol*. 185:493-502.

Le, N., R. Nagarajan, J.Y. Wang, T. Araki, R.E. Schmidt, and J. Milbrandt. 2005. Analysis of congenital hypomyelinating Egr2Lo/Lo nerves identifies Sox2 as an inhibitor of Schwann cell differentiation and myelination. *Proc Natl Acad Sci U S A*. 102:2596-2601.

LeBlanc, S.E., R.M. Ward, and J. Svaren. 2007. Neuropathy-associated Egr2 mutants disrupt cooperative activation of myelin protein zero by Egr2 and Sox10. *Mol Cell Biol*. 27:3521-3529.

Lee, B.H., M.J. Lee, S. Park, D.C. Oh, S. Elsasser, P.C. Chen, C. Gartner, N. Dimova, J. Hanna, S.P. Gygi, S.M. Wilson, R.W. King, and D. Finley. 2010a. Enhancement of proteasome activity by a small-molecule inhibitor of USP14. *Nature*. 467:179-184.

Lee, S.M., L.S. Chin, and L. Li. 2012. Protein misfolding and clearance in demyelinating peripheral neuropathies: Therapeutic implications. *Commun Integr Biol*. 5:107-110.

Lee, S.M., J.A. Olzmann, L.S. Chin, and L. Li. 2011. Mutations associated with Charcot-Marie-Tooth disease cause SIMPLE protein mislocalization and degradation by the proteasome and aggresome-autophagy pathways. *J Cell Sci*. 124:3319-3331.

Lee, Y.C., K.P. Lin, M.H. Chang, Y.C. Liao, C.P. Tsai, K.K. Liao, and B.W. Soong. 2010b. Cellular characterization of MPZ mutations presenting with diverse clinical phenotypes. *J Neurol*. 257:1661-1668.

LeGuern, E., A. Guilbot, M. Kessali, N. Ravise, J. Tassin, T. Maisonobe, D. Grid, and A. Brice. 1996. Homozygosity mapping of an autosomal recessive form of demyelinating Charcot-Marie-Tooth disease to chromosome 5q23-q33. *Hum Mol Genet*. 5:1685-1688.

Li, W., and Y. Ye. 2008. Polyubiquitin chains: functions, structures, and mechanisms. *Cell Mol Life Sci*. 65:2397-2406.

Li, Y., L.S. Chin, A.I. Levey, and L. Li. 2002. Huntingtin-associated protein 1 interacts with hepatocyte growth factor-regulated tyrosine kinase substrate and functions in endosomal trafficking. *J Biol Chem*. 277:28212-28221.

Li, Y., L.S. Chin, C. Weigel, and L. Li. 2001. Spring, a novel RING finger protein that regulates synaptic vesicle exocytosis. *J Biol Chem*. 276:40824-40833.

Liedtke, W. 2005. TRPV4 plays an evolutionary conserved role in the transduction of osmotic and mechanical stimuli in live animals. *J Physiol*. 567:53-58.

Lin, Q., J. Wang, C. Childress, M. Sudol, D.J. Carey, and W. Yang. 2010. HECT E3 ubiquitin ligase Nedd4-1 ubiquitinates ACK and regulates epidermal growth factor (EGF)-induced degradation of EGF receptor and ACK. *Mol Cell Biol*. 30:1541-1554.

Liu, N., J. Yamauchi, and E.M. Shooter. 2004. Recessive, but not dominant, mutations in peripheral myelin protein 22 gene show unique patterns of aggregation and intracellular trafficking. *Neurobiol Dis*. 17:300-309.

Livak, K.J., and T.D. Schmittgen. 2001. Analysis of relative gene expression data using real-time quantitative PCR and the 2(-Delta Delta C(T)) Method. *Methods*. 25:402-408.

Lockman, L.A., W.R. Kennedy, and J.G. White. 1967. The Chediak-Higashi syndrome: electrophysiological and electron microscopic observations on the peripheral neuropathy. *J Pediatr*. 70:942-951.

Lu, C.F., J. Kurjan, and P.N. Lipke. 1994. A pathway for cell wall anchorage of Saccharomyces cerevisiae alpha-agglutinin. *Mol Cell Biol*. 14:4825-4833.

Lukacs, G.L., A. Mohamed, N. Kartner, X.B. Chang, J.R. Riordan, and S. Grinstein. 1994. Conformational maturation of CFTR but not its mutant counterpart (delta F508) occurs in the endoplasmic reticulum and requires ATP. *EMBO J*. 13:6076-6086.

Lupo, V., M.I. Galindo, D. Martinez-Rubio, T. Sevilla, J.J. Vilchez, F. Palau, and C. Espinos. 2009. Missense mutations in the SH3TC2 protein causing Charcot-Marie-Tooth disease type 4C affect its localization in the plasma membrane and endocytic pathway. *Hum Mol Genet*. 18:4603-4614.

Luzio, J.P., M.D. Parkinson, S.R. Gray, and N.A. Bright. 2009. The delivery of endocytosed cargo to lysosomes. *Biochem Soc Trans*. 37:1019-1021.

Maeda, M.H., J. Mitsui, B.W. Soong, Y. Takahashi, H. Ishiura, S. Hayashi, Y. Shirota, Y. Ichikawa, H. Matsumoto, M. Arai, T. Okamoto, S. Miyama, J. Shimizu, J. Inazawa, J. Goto, and S. Tsuji. 2012. Increased gene dosage of myelin protein zero causes Charcot-Marie-Tooth disease. *Ann Neurol*. 71:84-92.

Magyar, J.P., R. Martini, T. Ruelicke, A. Aguzzi, K. Adlkofer, Z. Dembic, J. Zielasek, K.V. Toyka, and U. Suter. 1996. Impaired differentiation of Schwann cells in transgenic mice with increased PMP22 gene dosage. *J Neurosci*. 16:5351-5360.

Makoukji, J., M. Belle, D. Meffre, R. Stassart, J. Grenier, G. Shackleford, R. Fledrich, C. Fonte, J. Branchu, M. Goulard, C. de Waele, F. Charbonnier, M.W. Sereda, E.E. Baulieu, M. Schumacher, S. Bernard, and C. Massaad. 2012. Lithium enhances remyelination of peripheral nerves. *Proc Natl Acad Sci U S A*. 109:3973-3978.

Mandich, P., P. Fossa, S. Capponi, A. Geroldi, M. Acquaviva, R. Gulli, P. Ciotti, F. Manganelli, M. Grandis, and E. Bellone. 2009. Clinical features and molecular modelling of novel MPZ mutations in demyelinating and axonal neuropathies. *Eur J Hum Genet*. 17:1129-1134.

Marchesi, C., M. Milani, M. Morbin, M. Cesani, G. Lauria, V. Scaioli, G. Piccolo, G.M. Fabrizi, T. Cavallaro, F. Taroni, and D. Pareyson. 2010. Four novel cases of periaxin-related neuropathy and review of the literature. *Neurology*. 75:1830-1838.

Martini, R. 2001. The effect of myelinating Schwann cells on axons. *Mus Nerve*. 24:456-466.

Martyn, C.N., and R.A. Hughes. 1997. Epidemiology of peripheral neuropathy. *J Neurol Neurosurg Psychiatry*. 62:310-318.

McDonald, B., and J. Martin-Serrano. 2008. Regulation of Tsg101 expression by the steadiness box: a role of Tsg101-associated ligase. *Mol Biol Cell*. 19:754-763.

McLaughlin, H.M., R. Sakaguchi, W. Giblin, T.E. Wilson, L. Biesecker, J.R. Lupski, K. Talbot, J.M. Vance, S. Zuchner, Y.C. Lee, M. Kennerson, Y.M. Hou, G. Nicholson, and A. Antonellis. 2012. A recurrent loss-of-function alanyl-tRNA synthetase (AARS) mutation in patients with Charcot-Marie-Tooth disease type 2N (CMT2N). *Hum Mutat*. 33:244-253.

McLaughlin, H.M., R. Sakaguchi, C. Liu, T. Igarashi, D. Pehlivan, K. Chu, R. Iyer, P. Cruz, P.F. Cherukuri, N.F. Hansen, J.C. Mullikin, L.G. Biesecker, T.E. Wilson, V. Ionasescu, G. Nicholson, C. Searby, K. Talbot, J.M. Vance, S. Zuchner, K. Szigeti, J.R. Lupski, Y.M. Hou, E.D. Green, and A. Antonellis. 2010. Compound heterozygosity for loss-of-function lysyl-tRNA synthetase mutations in a patient with peripheral neuropathy. *Am J Hum Genet*. 87:560-566.

Mehrpour, M., A. Esclatine, I. Beau, and P. Codogno. 2010. Overview of macroautophagy regulation in mammalian cells. *Cell Res*. 20:748-762.

Mellman, I. 1996a. Endocytosis and molecular sorting. *Annu Rev Cell Dev Biol*. 12:575-625.

Mellman, I. 1996b. Membranes and sorting. *Curr Opin Cell Biol*. 8:497-498.

Mestre-Escorihuela, C., F. Rubio-Moscardo, J.A. Richter, R. Siebert, J. Climent, V. Fresquet, E. Beltran, X. Agirre, I. Marugan, M. Marin, A. Rosenwald, K.J. Sugimoto, L.M. Wheat, E.L. Karran, J.F. Garcia, L. Sanchez, F. Prosper, L.M. Staudt, D. Pinkel, M.J. Dyer, and J.A. Martinez-Climent. 2007. Homozygous deletions localize novel tumor suppressor genes in B-cell lymphomas. *Blood*. 109:271-280.

Miller, S.L., E. Malotky, and J.P. O'Bryan. 2004. Analysis of the role of ubiquitin-interacting motifs in ubiquitin binding and ubiquitylation. *J Biol Chem*. 279:33528-33537.

Miyanomae, Y., Y. Takeuchi, A. Nishimura, S. Kawase, K. Hirai, M. Ochi, and T. Sawada. 1996. Motor nerve conduction studies on children with spinal muscular atrophy. *Acta Paediatr Jpn*. 38:576-579.

Mizuno, E., K. Kawahata, A. Okamoto, N. Kitamura, and M. Komada. 2004. Association with Hrs is required for the early endosomal localization, stability, and function of STAM. *J Biochem*. 135:385-396.

Mizushima, N. 2007. Autophagy: process and function. *Gen Dev*. 21:2861-2873.

Morino, C., M. Kato, A. Yamamoto, E. Mizuno, A. Hayakawa, M. Komada, and N. Kitamura. 2004. A role for Hrs in endosomal sorting of ligand-stimulated and unstimulated epidermal growth factor receptor. *Exp Cell Res*. 297:380-391.

Moriwaki, Y., N.A. Begum, M. Kobayashi, M. Matsumoto, K. Toyoshima, and T. Seya. 2001. Mycobacterium bovis Bacillus Calmette-Guerin and its cell wall complex induce a novel lysosomal membrane protein, SIMPLE, that bridges the missing link between lipopolysaccharide and p53-inducible gene, LITAF(PIG7), and estrogen-inducible gene, EET-1. *J Biol Chem* 276:23065-23076.

Murphy, P., P. Topilko, S. Schneider-Maunoury, T. Seitanidou, A. Baron-Van Evercooren, and P. Charnay. 1996. The regulation of Krox-20 expression reveals important steps in the control of peripheral glial cell development. *Development*. 122:2847-2857.

Murphy, S.M., J. Polke, H. Manji, J. Blake, L. Reiniger, M. Sweeney, H. Houlden, S. Brandner, and M.M. Reilly. 2011. A novel mutation in the nerve-specific 5'UTR of the GJB1 gene causes X-linked Charcot-Marie-Tooth disease. *J Peripher Nerv Syst*. 16:65-70.

Musso, M., P. Balestra, E. Bellone, D. Cassandrini, E. Di Maria, L.L. Doria, M. Grandis, G.L. Mancardi, A. Schenone, G. Levi, F. Ajmar, and P. Mandich. 2001. The

D355V mutation decreases EGR2 binding to an element within the Cx32 promoter. *Neurobiol Dis*. 8:700-706.

Myers, J.K., C.K. Mobley, and C.R. Sanders. 2008. The peripheral neuropathy-linked Trembler and Trembler-J mutant forms of peripheral myelin protein 22 are folding-destabilized. *Biochemistry*. 47:10620-10629.

Nabhan, J.F., H. Pan, and Q. Lu. 2010. Arrestin domain-containing protein 3 recruits the NEDD4 E3 ligase to mediate ubiquitination of the beta2-adrenergic receptor. *EMBO Rep*. 11:605-611.

Naef, R., and U. Suter. 1999. Impaired intracellular trafficking is a common disease mechanism of PMP22 point mutations in peripheral neuropathies. *Neurobiol Dis*. 6:1-14.

Nagarajan, R., J. Svaren, N. Le, T. Araki, M. Watson, and J. Milbrandt. 2001. EGR2 mutations in inherited neuropathies dominant-negatively inhibit myelin gene expression. *Neuron*. 30:355-368.

Nave, K.A., and J.L. Salzer. 2006. Axonal regulation of myelination by neuregulin 1. *Curr Opin Neurobiol*. 16:492-500.

Nave, K.A., M.W. Sereda, and H. Ehrenreich. 2007. Mechanisms of disease: inherited demyelinating neuropathies--from basic to clinical research. *Nat Clin Pract Neurol*. 3:453-464.

Nave, K.A., and B.D. Trapp. 2008. Axon-glial signaling and the glial support of axon function. *Ann Rev Neurosci*. 31:535-561.

Nelis, E., C. Van Broeckhoven, P. De Jonghe, A. Lofgren, A. Vandenberghe, P. Latour, E. Le Guern, A. Brice, M.L. Mostacciuolo, F. Schiavon, F. Palau, S. Bort, M.

Upadhyaya, M. Rocchi, N. Archidiacono, P. Mandich, E. Bellone, K. Silander, M.L. Savontaus, R. Navon, H. Goldberg-Stern, X. Estivill, V. Volpini, W. Friedl, A. Gal, and et al. 1996. Estimation of the mutation frequencies in Charcot-Marie-Tooth disease type 1 and hereditary neuropathy with liability to pressure palsies: a European collaborative study. *Eur J Hum Genet*. 4:25-33.

Nelles, E., C. Butzler, D. Jung, A. Temme, H.D. Gabriel, U. Dahl, O. Traub, F. Stumpel, K. Jungermann, J. Zielasek, K.V. Toyka, R. Dermietzel, and K. Willecke. 1996. Defective propagation of signals generated by sympathetic nerve stimulation in the liver of connexin32-deficient mice. *Proc Natl Acad Sci U S A*. 93:9565-9570.

Newbern, J., and C. Birchmeier. 2010. Nrg1/ErbB signaling networks in Schwann cell development and myelination. *Sem Cell Dev Biol*. 21:922-928.

Nicholson, G., G.M. Lenk, S.W. Reddel, A.E. Grant, C.F. Towne, C.J. Ferguson, E. Simpson, A. Scheuerle, M. Yasick, S. Hoffman, R. Blouin, C. Brandt, G. Coppola, L.G. Biesecker, S.D. Batish, and M.H. Meisler. 2011. Distinctive genetic and clinical features of CMT4J: a severe neuropathy caused by mutations in the PI(3,5)P(2) phosphatase FIG4. *Brain*. 134:1959-1971.

Niemann, A., P. Berger, and U. Suter. 2006. Pathomechanisms of mutant proteins in Charcot-Marie-Tooth disease. *Neuromol Med*. 8:217-242.

Niemann, A., M. Ruegg, V. La Padula, A. Schenone, and U. Suter. 2005. Ganglioside-induced differentiation associated protein 1 is a regulator of the mitochondrial network: new implications for Charcot-Marie-Tooth disease. *J Cell Biol*. 170:1067-1078.

Niemann, S., M.W. Sereda, M. Rossner, H. Stewart, U. Suter, H.M. Meinck, I.R. Griffiths, and K.A. Nave. 1999. The "CMT rat": peripheral neuropathy and dysmyelination caused by transgenic overexpression of PMP22. *Ann N Y Acad Sci*. 883:254-261.

Noack, R., S. Frede, P. Albrecht, N. Henke, A. Pfeiffer, K. Knoll, T. Dehmel, G. Meyer Zu Horste, M. Stettner, B.C. Kieseier, H. Summer, S. Golz, A. Kochanski, M. Wiedau-Pazos, S. Arnold, J. Lewerenz, and A. Methner. 2012. Charcot-Marie-Tooth disease CMT4A: GDAP1 increases cellular glutathione and the mitochondrial membrane potential. *Hum Mol Genet*. 21:150-162.

Notterpek, L., M.C. Ryan, A.R. Tobler, and E.M. Shooter. 1999. PMP22 accumulation in aggresomes: implications for CMT1A pathology. *Neurobiol Dis*. 6:450-460.

Notterpek, L., E.M. Shooter, and G.J. Snipes. 1997. Upregulation of the endosomal-lysosomal pathway in the trembler-J neuropathy. *J Neurosci*. 17:4190-4200.

Ogata, T., S. Iijima, S. Hoshikawa, T. Miura, S. Yamamoto, H. Oda, K. Nakamura, and S. Tanaka. 2004. Opposing extracellular signal-regulated kinase and Akt pathways control Schwann cell myelination. *J Neurosci*. 24:6724-6732.

Okuda, T., Y. Higashi, K. Kokame, C. Tanaka, H. Kondoh, and T. Miyata. 2004. Ndrg1-deficient mice exhibit a progressive demyelinating disorder of peripheral nerves. *Mol Cell Biol*. 24:3949-3956.

Olzmann, J.A., K. Brown, K.D. Wilkinson, H.D. Rees, Q. Huai, H. Ke, A.I. Levey, L. Li, and L.S. Chin. 2004. Familial Parkinson's disease-associated L166P mutation disrupts DJ-1 protein folding and function. *J Biol Chem*. 279:8506-8515.

Olzmann, J.A., and L.S. Chin. 2008. Parkin-mediated K63-linked polyubiquitination: a signal for targeting misfolded proteins to the aggresome-autophagy pathway. *Autophagy*. 4:85-87.

Olzmann, J.A., L. Li, and L.S. Chin. 2008. Aggresome formation and neurodegenerative diseases: therapeutic implications. *Curr Med Chem*. 15:47-60.

Olzmann, J.A., L. Li, M.V. Chudaev, J. Chen, F.A. Perez, R.D. Palmiter, and L.S. Chin. 2007. Parkin-mediated K63-linked polyubiquitination targets misfolded DJ-1 to aggresomes via binding to HDAC6. *J Cell Biol*. 178:1025-1038.

Ovadi, J., F. Orosz, and S. Hollan. 2004. Functional aspects of cellular microcompartmentation in the development of neurodegeneration: mutation induced aberrant protein-protein associations. *Mol Cell Biochem*. 256-257:83-93.

Pannunzio, M.E., I.M. Jou, A. Long, T.C. Wind, G. Beck, and G. Balian. 2005. A new method of selecting Schwann cells from adult mouse sciatic nerve. *J Neurosci Methods*. 149:74-81.

Pareek, S., L. Notterpek, G.J. Snipes, R. Naef, W. Sossin, J. Laliberte, S. Iacampo, U. Suter, E.M. Shooter, and R.A. Murphy. 1997. Neurons promote the translocation of peripheral myelin protein 22 into myelin. *J Neurosci*. 17:7754-7762.

Pareyson, D., and C. Marchesi. 2009. Diagnosis, natural history, and management of Charcot-Marie-Tooth disease. *Lancet Neurol*. 8:654-667.

Pareyson, D., F. Taroni, S. Botti, M. Morbin, S. Baratta, G. Lauria, C. Ciano, and A. Sghirlanzoni. 2000. Cranial nerve involvement in CMT disease type 1 due to early growth response 2 gene mutation. *Neurology*. 54:1696-1698.

Parman, Y. 2007. Hereditary neuropathies. *Curr Opin Neurol.* 20:542-547.

Patzko, A., and M.E. Shy. 2011. Update on Charcot-Marie-Tooth disease. *Curr Neurol Neurosci Rep*. 11:78-88.

Pickart, C.M. 1997. Targeting of substrates to the 26S proteasome. *FASEB J*. 11:1055-1066.

Pickart, C.M., and R.E. Cohen. 2004. Proteasomes and their kin: proteases in the machine age. *Nat Rev Mol Cell Biol*. 5:177-187.

Pizzo, P., and T. Pozzan. 2007. Mitochondria-endoplasmic reticulum choreography: structure and signaling dynamics. *Trends Cell Biol*. 17:511-517.

Pornillos, O., S.L. Alam, R.L. Rich, D.G. Myszka, D.R. Davis, and W.I. Sundquist. 2002. Structure and functional interactions of the Tsg101 UEV domain. *EMBO J*. 21:2397-2406.

Quattrone, A., A. Gambardella, F. Bono, U. Aguglia, A. Bolino, A.C. Bruni, M.P. Montesi, R.L. Oliveri, M. Sabatelli, O. Tamburrini, P. Valentino, C. Van Broeckhoven, and M. Zappia. 1996. Autosomal recessive hereditary motor and sensory neuropathy with focally folded myelin sheaths: clinical, electrophysiologic, and genetic aspects of a large family. *Neurology*. 46:1318-1324.

Quintes, S., S. Goebbels, G. Saher, M.H. Schwab, and K.A. Nave. 2010. Neuron-glia signaling and the protection of axon function by Schwann cells. *J Peripher Nerv Syst*. 15:10-16.

Raiborg, C., K.G. Bache, A. Mehlum, E. Stang, and H. Stenmark. 2001. Hrs recruits clathrin to early endosomes. *EMBO J*. 20:5008-5021.

Raiborg, C., and H. Stenmark. 2009. The ESCRT machinery in endosomal sorting of ubiquitylated membrane proteins. *Nature*. 458:445-452.

Rangaraju, S., J.D. Verrier, I. Madorsky, J. Nicks, W.A. Dunn, Jr., and L. Notterpek. 2010. Rapamycin activates autophagy and improves myelination in explant cultures from neuropathic mice. *J Neurosci*. 30:11388-11397.

Razi, M., and C.E. Futter. 2006. Distinct roles for Tsg101 and Hrs in multivesicular body formation and inward vesiculation. *Mol Biol Cell*. 17:3469-3483.

Reilly, M.M., and M.E. Shy. 2009. Diagnosis and new treatments in genetic neuropathies. *J Neurol Neurosurg Psychiatry*. 80:1304-1314.

Ren, X., and J.H. Hurley. 2010. VHS domains of ESCRT-0 cooperate in high-avidity binding to polyubiquitinated cargo. *EMBO J*. 29:1045-1054.

Reyes-Turcu, F.E., K.H. Ventii, and K.D. Wilkinson. 2009. Regulation and cellular roles of ubiquitin-specific deubiquitinating enzymes. *Ann Rev Biochem.* 78:363-397.

Rigacci, S., V. Guidotti, M. Bucciantini, M. Parri, C. Nediani, E. Cerbai, M. Stefani, and A. Berti. 2010. Oleuropein aglycon prevents cytotoxic amyloid aggregation of human amylin. *J Nutr Biochem*. 21:726-735.

Robaglia-Schlupp, A., J. Pizant, J.C. Norreel, E. Passage, D. Saberan-Djoneidi, J.L. Ansaldi, L. Vinay, D. Figarella-Branger, N. Levy, F. Clarac, P. Cau, J.F. Pellissier, and M. Fontes. 2002. PMP22 overexpression causes dysmyelination in mice. *Brain*. 125:2213-2221.

Roberts, R.C., A.A. Peden, F. Buss, N.A. Bright, M. Latouche, M.M. Reilly, J. Kendrick-Jones, and J.P. Luzio. 2010. Mistargeting of SH3TC2 away from the recycling

endosome causes Charcot-Marie-Tooth disease type 4C. *Hum Mol Genet*. 19:1009-1018.

Robertson, A.M., J. Perea, A. McGuigan, R.H. King, J.R. Muddle, A.A. Gabreels-Festen, P.K. Thomas, and C. Huxley. 2002. Comparison of a new pmp22 transgenic mouse line with other mouse models and human patients with CMT1A. *J Anat*. 200:377-390.

Robinson, F.L., and J.E. Dixon. 2005. The phosphoinositide-3-phosphatase MTMR2 associates with MTMR13, a membrane-associated pseudophosphatase also mutated in type 4B Charcot-Marie-Tooth disease. *J Biol Chem*. 280:31699-31707.

Robinson, F.L., and J.E. Dixon. 2006. Myotubularin phosphatases: policing 3-phosphoinositides. *Trends Cell Biol*. 16:403-412.

Robinson, F.L., I.R. Niesman, K.K. Beiswenger, and J.E. Dixon. 2008. Loss of the inactive myotubularin-related phosphatase Mtmr13 leads to a Charcot-Marie-Tooth 4B2-like peripheral neuropathy in mice. *Proc Natl Acad Sci U S A*. 105:4916-4921.

Rodal, A.A., A.D. Blunk, Y. Akbergenova, R.A. Jorquera, L.K. Buhl, and J.T. Littleton. 2011. A presynaptic endosomal trafficking pathway controls synaptic growth signaling. *J Cell Biol*. 193:201-217.

Ross, C.A., and M.A. Poirier. 2004. Protein aggregation and neurodegenerative disease. *Nat Med*. 10 Suppl:S10-17.

Ross, C.A., and M.A. Poirier. 2005. Opinion: What is the role of protein aggregation in neurodegeneration? *Nat Rev Mol Cell Biol*. 6:891-898.

Rosso, G., K. Cal, L. Canclini, J.P. Damian, P. Ruiz, H. Rodriguez, J.R. Sotelo, C. Vazquez, and A. Kun. 2010. Early phenotypical diagnoses in Trembler-J mice model. *J Neurosci Methods*. 190:14-19.

Rost, B., G. Yachdav, and J. Liu. 2004. The PredictProtein server. *Nucleic Acids Res*. 32:W321-326.

Roxrud, I., H. Stenmark, and L. Malerod. 2010. ESCRT & Co. *Bio Cell*. 102:293-318.

Runker, A.E., I. Kobsar, T. Fink, G. Loers, T. Tilling, P. Putthoff, C. Wessig, R. Martini, and M. Schachner. 2004. Pathology of a mouse mutation in peripheral myelin protein P0 is characteristic of a severe and early onset form of human Charcot-Marie-Tooth type 1B disorder. *J Cell Biol*. 165:565-573.

Rutherford, A.C., C. Traer, T. Wassmer, K. Pattni, M.V. Bujny, J.G. Carlton, H. Stenmark, and P.J. Cullen. 2006. The mammalian phosphatidylinositol 3-phosphate 5-kinase (PIKfyve) regulates endosome-to-TGN retrograde transport. *J Cell Sci*. 119:3944-3957.

Ryan, M.C., E.M. Shooter, and L. Notterpek. 2002. Aggresome formation in neuropathy models based on peripheral myelin protein 22 mutations. *Neurobiol Dis*. 10:109-118.

Saifi, G.M., K. Szigeti, W. Wiszniewski, M.E. Shy, K. Krajewski, I. Hausmanowa-Petrusewicz, A. Kochanski, S. Reeser, P. Mancias, I. Butler, and J.R. Lupski. 2005. SIMPLE mutations in Charcot-Marie-Tooth disease and the potential role of its protein product in protein degradation. *Hum Mutat*. 25:372-383.

Sakakura, M., A. Hadziselimovic, Z. Wang, K.L. Schey, and C.R. Sanders. 2011. Structural basis for the Trembler-J phenotype of Charcot-Marie-Tooth disease. *Structure*. 19:1160-1169.

Sakurai, T., A. Kamiyoshi, S. Watanabe, M. Sato, and T. Shindo. 2008. Rapid zygosity determination in mice by SYBR Green real-time genomic PCR of a crude DNA solution. *Transgenic Res*. 17:149-155.

Sander, S., G.A. Nicholson, R.A. Ouvrier, J.G. McLeod, and J.D. Pollard. 1998. Charcot-Marie-Tooth disease: histopathological features of the peripheral myelin protein (PMP22) duplication (CMT1A) and connexin32 mutations (CMTX1). *Mus Nerve*. 21:217-225.

Sander, S., R.A. Ouvrier, J.G. McLeod, G.A. Nicholson, and J.D. Pollard. 2000. Clinical syndromes associated with tomacula or myelin swellings in sural nerve biopsies. *J Neurol Neurosurg Psychiatry*. 68:483-488.

Santonico, E., F. Belleudi, S. Panni, M.R. Torrisi, G. Cesareni, and L. Castagnoli. 2010. Multiple modification and protein interaction signals drive the Ring finger protein 11 (RNF11) E3 ligase to the endosomal compartment. *Oncogene*. 29:5604-5618.

Sargiannidou, I., N. Vavlitou, S. Aristodemou, A. Hadjisavvas, K. Kyriacou, S.S. Scherer, and K.A. Kleopa. 2009. Connexin32 mutations cause loss of function in Schwann cells and oligodendrocytes leading to PNS and CNS myelination defects. J Neurosci. 29:4736-4749.

Scarpini, E., G. Meola, P. Baron, S. Beretta, M. Velicogna, and G. Scarlato. 1986. S-100 protein and laminin: immunocytochemical markers for human Schwann cells in vitro. *Exp Neurol*. 93:77-83.

Scherer, S.S., and L. Wrabetz. 2008. Molecular mechanisms of inherited demyelinating neuropathies. *Glia*. 56:1578-1589.

Scherer, S.S., Y.T. Xu, P.G. Bannerman, D.L. Sherman, and P.J. Brophy. 1995. Periaxin expression in myelinating Schwann cells: modulation by axon-glial interactions and polarized localization during development. *Development*. 121:4265-4273.

Scherer, S.S., Y.T. Xu, A. Messing, K. Willecke, K.H. Fischbeck, and L.J. Jeng. 2005. Transgenic expression of human connexin32 in myelinating Schwann cells prevents demyelination in connexin32-null mice. *J Neurosci*. 25:1550-1559.

Scherer, S.S., Y.T. Xu, E. Nelles, K. Fischbeck, K. Willecke, and L.J. Bone. 1998. Connexin32-null mice develop demyelinating peripheral neuropathy. *Glia*. 24:8-20.

Seaton, G.J., L. Hall, and R. Jones. 2000. Rat sperm 2B1 glycoprotein (PH20) contains a C-terminal sequence motif for attachment of a glycosyl phosphatidylinositol anchor. Effects of endoproteolytic cleavage on hyaluronidase activity. *Biol Reprod*. 62:1667-1676.

Selkoe, D.J. 2004. Cell biology of protein misfolding: the examples of Alzheimer's and Parkinson's diseases. *Nat Cell Biol*. 6:1054-1061.

Senderek, J., C. Bergmann, C. Stendel, J. Kirfel, N. Verpoorten, P. De Jonghe, V. Timmerman, R. Chrast, M.H. Verheijen, G. Lemke, E. Battaloglu, Y. Parman, S. Erdem, E. Tan, H. Topaloglu, A. Hahn, W. Muller-Felber, N. Rizzuto, G.M. Fabrizi, M. Stuhrmann, S. Rudnik-Schoneborn, S. Zuchner, J. Michael Schroder, E. Buchheim, V. Straub, J. Klepper, K. Huehne, B. Rautenstrauss, R. Buttner, E. Nelis, and K. Zerres. 2003a. Mutations in a gene encoding a novel SH3/TPR

domain protein cause autosomal recessive Charcot-Marie-Tooth type 4C neuropathy. *Am J Hum Genet*. 73:1106-1119.

Senderek, J., C. Bergmann, S. Weber, U.P. Ketelsen, H. Schorle, S. Rudnik-Schoneborn, R. Buttner, E. Buchheim, and K. Zerres. 2003b. Mutation of the SBF2 gene, encoding a novel member of the myotubularin family, in Charcot-Marie-Tooth neuropathy type 4B2/11p15. *Hum Mol Genet*. 12:349-356.

Shames, I., A. Fraser, J. Colby, W. Orfali, and G.J. Snipes. 2003. Phenotypic differences between peripheral myelin protein-22 (PMP22) and myelin protein zero (P0) mutations associated with Charcot-Marie-Tooth-related diseases. *J Neuropathol Exp Neurol*. 62:751-764.

Shimura, H., N. Hattori, S. Kubo, Y. Mizuno, S. Asakawa, S. Minoshima, N. Shimizu, K. Iwai, T. Chiba, K. Tanaka, and T. Suzuki. 2000. Familial Parkinson disease gene product, parkin, is a ubiquitin-protein ligase. *Nat Genet*. 25:302-305.

Shirk, A.J., S.K. Anderson, S.H. Hashemi, P.F. Chance, and C.L. Bennett. 2005. SIMPLE interacts with NEDD4 and TSG101: evidence for a role in lysosomal sorting and implications for Charcot-Marie-Tooth disease. *J Neurosci Res*. 82:43-50.

Shy, M.E., A. Jani, K. Krajewski, M. Grandis, R.A. Lewis, J. Li, R.R. Shy, J. Balsamo, J. Lilien, J.Y. Garbern, and J. Kamholz. 2004. Phenotypic clustering in MPZ mutations. *Brain*. 127:371-384.

Shy, M.E., and A. Patzko. 2011. Axonal Charcot-Marie-Tooth disease. *Curr Opin Neurol*. 24:475-483.

Sigismund, S., S. Polo, and P.P. Di Fiore. 2004. Signaling through monoubiquitination. *Curr Top Microbiol Immuno*. 286:149-185.

Siskind, C.E., S.M. Murphy, R. Ovens, J. Polke, M.M. Reilly, and M.E. Shy. 2011. Phenotype expression in women with CMT1X. *J Peripher Nerv Syst*. 16:102-107.

Sivera, R., C. Espinos, J.J. Vilchez, F. Mas, D. Martinez-Rubio, M.J. Chumillas, F. Mayordomo, N. Muelas, L. Bataller, F. Palau, and T. Sevilla. 2010. Phenotypical features of the p.R120W mutation in the GDAP1 gene causing autosomal dominant Charcot-Marie-Tooth disease. *J Peripher Nerv Syst*. 15:334-344.

Somandin, C., D. Gerber, J.A. Pereira, M. Horn, and U. Suter. 2012. LITAF (SIMPLE) regulates Wallerian degeneration after injury but is not essential for peripheral nerve development and maintenance: Implications for Charcot-Marie-Tooth disease. *Glia*.

Sorek, N., D. Bloch, and S. Yalovsky. 2009. Protein lipid modifications in signaling and subcellular targeting. *Curr Opin Plant Biol*. 12:714-720.

Sorkin, A., and L.K. Goh. 2009. Endocytosis and intracellular trafficking of ErbBs. *Exp Cell Res*. 315:683-696.

Spence, J., S. Sadis, A.L. Haas, and D. Finley. 1995. A ubiquitin mutant with specific defects in DNA repair and multiubiquitination. *Mol Cell Biol*. 15:1265-1273.

Spiegel, I., and E. Peles. 2002. Cellular junctions of myelinated nerves (Review). *Mol Membr Biol* 19:95-101.

Spowart, J., and J.J. Lum. 2010. Opening a new DOR to autophagy. *EMBO Rep*. 11:4-5.

Staub, O., H. Abriel, P. Plant, T. Ishikawa, V. Kanelis, R. Saleki, J.D. Horisberger, L. Schild, and D. Rotin. 2000. Regulation of the epithelial Na+ channel by Nedd4 and ubiquitination. *Kidney Internatl*. 57:809-815.

Stendel, C., A. Roos, H. Kleine, E. Arnaud, M. Ozcelik, P.N. Sidiropoulos, J. Zenker, F. Schupfer, U. Lehmann, R.M. Sobota, D.W. Litchfield, B. Luscher, R. Chrast, U. Suter, and J. Senderek. 2010. SH3TC2, a protein mutant in Charcot-Marie-Tooth neuropathy, links peripheral nerve myelination to endosomal recycling. *Brain*. 133:2462-2474.

Street, V.A., C.L. Bennett, J.D. Goldy, A.J. Shirk, K.A. Kleopa, B.L. Tempel, H.P. Lipe, S.S. Scherer, T.D. Bird, and P.F. Chance. 2003. Mutation of a putative protein degradation gene LITAF/SIMPLE in Charcot-Marie-Tooth disease 1C. *Neurology*. 60:22-26.

Street, V.A., J.D. Goldy, A.S. Golden, B.L. Tempel, T.D. Bird, and P.F. Chance. 2002. Mapping of Charcot-Marie-Tooth disease type 1C to chromosome 16p identifies a novel locus for demyelinating neuropathies. *Am J Hum Genet*. 70:244-250.

Stuffers, S., A. Brech, and H. Stenmark. 2009. ESCRT proteins in physiology and disease. *Exp Cell Res*. 315:1619-1626.

Suter, U., and S.S. Scherer. 2003. Disease mechanisms in inherited neuropathies. *Nat Rev Neurosci*. 4:714-726.

Syed, N., K. Reddy, D.P. Yang, C. Taveggia, J.L. Salzer, P. Maurel, and H.A. Kim. 2010. Soluble neuregulin-1 has bifunctional, concentration-dependent effects on Schwann cell myelination. *J Neurosci.* 30:6122-6131.

Tan, J.M., E.S. Wong, D.S. Kirkpatrick, O. Pletnikova, H.S. Ko, S.P. Tay, M.W. Ho, J. Troncoso, S.P. Gygi, M.K. Lee, V.L. Dawson, T.M. Dawson, and K.L. Lim. 2008. Lysine 63-linked ubiquitination promotes the formation and autophagic clearance of protein inclusions associated with neurodegenerative diseases. *Hum Mol Genet*. 17:431-439.

Tapinos, N., M. Ohnishi, and A. Rambukkana. 2006. ErbB2 receptor tyrosine kinase signaling mediates early demyelination induced by leprosy bacilli. *Nat Med*. 12:961-966.

Taylor, J.P., F. Tanaka, J. Robitschek, C.M. Sandoval, A. Taye, S. Markovic-Plese, and K.H. Fischbeck. 2003. Aggresomes protect cells by enhancing the degradation of toxic polyglutamine-containing protein. *Hum Mol Genet*. 12:749-757.

Tersar, K., M. Boentert, P. Berger, S. Bonneick, C. Wessig, K.V. Toyka, P. Young, and U. Suter. 2007. Mtmr13/Sbf2-deficient mice: an animal model for CMT4B2. *Hum Mol Genet*. 16:2991-3001.

Timmerman, V., P. De Jonghe, C. Ceuterick, E. De Vriendt, A. Lofgren, E. Nelis, L.E. Warner, J.R. Lupski, J.J. Martin, and C. Van Broeckhoven. 1999. Novel missense mutation in the early growth response 2 gene associated with Dejerine-Sottas syndrome phenotype. *Neurology*. 52:1827-1832.

Tobler, A.R., L. Notterpek, R. Naef, V. Taylor, U. Suter, and E.M. Shooter. 1999. Transport of Trembler-J mutant peripheral myelin protein 22 is blocked in the intermediate compartment and affects the transport of the wild-type protein by direct interaction. *J Neurosci*. 19:2027-2036.

Tompkins, M.M., and W.D. Hill. 1997. Contribution of somal Lewy bodies to neuronal death. *Brain Res*. 775:24-29.

Topilko, P., G. Levi, G. Merlo, S. Mantero, C. Desmarquet, G. Mancardi, and P. Charnay. 1997. Differential regulation of the zinc finger genes Krox-20 and Krox-24 (Egr-1) suggests antagonistic roles in Schwann cells. *J Neurosci Res*. 50:702-712.

Topilko, P., S. Schneider-Maunoury, G. Levi, A. Baron-Van Evercooren, A.B. Chennoufi, T. Seitanidou, C. Babinet, and P. Charnay. 1994. Krox-20 controls myelination in the peripheral nervous system. *Nature*. 371:796-799.

Trejo, J., Y. Altschuler, H.W. Fu, K.E. Mostov, and S.R. Coughlin. 2000. Protease-activated receptor-1 down-regulation: a mutant HeLa cell line suggests novel requirements for PAR1 phosphorylation and recruitment to clathrin-coated pits. *J Biol Chem*. 275:31255-31265.

Tsunematsu, T., E. Yamauchi, H. Shibata, M. Maki, T. Ohta, and H. Konishi. 2010. Distinct functions of human MVB12A and MVB12B in the ESCRT-I dependent on their posttranslational modifications. *Biochem Biophys Res Commun*. 399:232-237.

Tuma, M.C., A. Zill, N. Le Bot, I. Vernos, and V. Gelfand. 1998. Heterotrimeric kinesin II is the microtubule motor protein responsible for pigment dispersion in Xenopus melanophores. *J Cell Biol*. 143:1547-1558.

Turner, C.E., and D.M. Shotton. 1989. Effects of capping on the non-ionic detergent solubility of rat thymocyte glycoproteins. *Eur J Cell Biol*. 50:324-332.

Tusnady, G.E., and I. Simon. 2001. The HMMTOP transmembrane topology prediction server. *Bioinformatics*. 17:849-850.

Urbe, S., M. Sachse, P.E. Row, C. Preisinger, F.A. Barr, G. Strous, J. Klumperman, and M.J. Clague. 2003. The UIM domain of Hrs couples receptor sorting to vesicle formation. *J Cell Sci*. 116:4169-4179.

Uyemura, K., H. Asou, and Y. Takeda. 1995. Structure and function of peripheral nerve myelin proteins. *Prog Brain Res*. 105:311-318.

Vance, J.M., D. Barker, L.H. Yamaoka, J.M. Stajich, L. Loprest, W.Y. Hung, K. Fischbeck, A.D. Roses, and M.A. Pericak-Vance. 1991. Localization of Charcot-Marie-Tooth disease type 1a (CMT1A) to chromosome 17p11.2. *Genomics*. 9:623-628.

Vanlandingham, P.A., and B.P. Ceresa. 2009. Rab7 regulates late endocytic trafficking downstream of multivesicular body biogenesis and cargo sequestration. *The J Biol Chem*. 284:12110-12124.

Vembar, S.S., and J.L. Brodsky. 2008. One step at a time: endoplasmic reticulum-associated degradation. *Nat Rev Mol Cell Biol*. 9:944-957.

Verhamme, C., R.H. King, A.L. ten Asbroek, J.R. Muddle, M. Nourallah, R. Wolterman, F. Baas, and I.N. van Schaik. 2011. Myelin and axon pathology in a long-term study of PMP22-overexpressing mice. *J Neuropathol Exp Neurol*. 70:386-398.

Verhoeven, K., P. De Jonghe, K. Coen, N. Verpoorten, M. Auer-Grumbach, J.M. Kwon, D. FitzPatrick, E. Schmedding, E. De Vriendt, A. Jacobs, V. Van Gerwen, K. Wagner, H.P. Hartung, and V. Timmerman. 2003. Mutations in the small GTP-ase late endosomal protein RAB7 cause Charcot-Marie-Tooth type 2B neuropathy. *Am J Hum Genet*. 72:722-727.

Vogel, K., and P.A. Roche. 1999. SNAP-23 and SNAP-25 are palmitoylated in vivo. *Biochem Biophys Res Commun*. 258:407-410.

Wang, D., J. Liu, K. Tang, Z. Xu, X. Xiong, Q. Rao, M. Wang, and J. Wang. 2009. Expression of pig7 gene in acute leukemia and its potential to modulate the chemosensitivity of leukemic cells. *Leuk Res*. 33:28-38.

Warner, L.E., P. Mancias, I.J. Butler, C.M. McDonald, L. Keppen, K.G. Koob, and J.R. Lupski. 1998. Mutations in the early growth response 2 (EGR2) gene are associated with hereditary myelinopathies. *Nat Genet*. 18:382-384.

Warner, L.E., J. Svaren, J. Milbrandt, and J.R. Lupski. 1999. Functional consequences of mutations in the early growth response 2 gene (EGR2) correlate with severity of human myelinopathies. *Hum Mol Genet*. 8:1245-1251.

Watanabe, T., K. Nagase, M. Chosa, and K. Tobinai. 2010. Schwann cell autophagy induced by SAHA, 17-AAG, or clonazepam can reduce bortezomib-induced peripheral neuropathy. *Brit J Cancer*. 103:1580-1587.

Waterman, H., and Y. Yarden. 2001. Molecular mechanisms underlying endocytosis and sorting of ErbB receptor tyrosine kinases. *FEBS Lett*. 490:142-152.

Webber, E., L. Li, and L.S. Chin. 2008. Hypertonia-associated protein Trak1 is a novel regulator of endosome-to-lysosome trafficking. *J Mol Biol*. 382:638-651.

Wegner, C.S., L.M. Rodahl, and H. Stenmark. 2011. ESCRT proteins and cell signalling. *Traffic*. 12:1291-1297.

Weimer, L.H., and D. Podwall. 2006. Medication-induced exacerbation of neuropathy in Charcot Marie Tooth disease. *J Neurol Sci*. 242:47-54.

Weimer, L.H., and N. Sachdev. 2009. Update on medication-induced peripheral neuropathy. *Curr Neurol Neurosci Rep*. 9:69-75.

Weissman, A.M. 2001. Themes and variations on ubiquitylation. *Nat Rev. Molecular cell biology*. 2:169-178.

White, I.J., A. Souabni, and N.M. Hooper. 2000. Comparison of the glycosyl-phosphatidylinositol cleavage/attachment site between mammalian cells and parasitic protozoa. *J Cell Sci*. 113 (Pt 4):721-727.

Wise, C.A., C.A. Garcia, S.N. Davis, Z. Heju, L. Pentao, P.I. Patel, and J.R. Lupski. 1993. Molecular analyses of unrelated Charcot-Marie-Tooth (CMT) disease patients suggest a high frequency of the CMTIA duplication. *Am J Hum Genet*. 53:853-863.

Witt, A., and S.T. Brady. 2000. Unwrapping new layers of complexity in axon/glial relationships. *Glia*. 29:112-117.

Wrabetz, L., M. D'Antonio, M. Pennuto, G. Dati, E. Tinelli, P. Fratta, S. Previtali, D. Imperiale, J. Zielasek, K. Toyka, R.L. Avila, D.A. Kirschner, A. Messing, M.L. Feltri, and A. Quattrini. 2006. Different intracellular pathomechanisms produce diverse Myelin Protein Zero neuropathies in transgenic mice. *J Neurosci*. 26:2358-2368.

Xu, P., D.M. Duong, N.T. Seyfried, D. Cheng, Y. Xie, J. Robert, J. Rush, M. Hochstrasser, D. Finley, and J. Peng. 2009. Quantitative proteomics reveals the function of unconventional ubiquitin chains in proteasomal degradation. *Cell*. 137:133-145.

Xu, T.R., R.F. Lu, D. Romano, A. Pitt, M.D. Houslay, G. Milligan, and W. Kolch. 2012. Eukaryotic translation initiation factor 3, subunit a, regulates the extracellular signal-regulated kinase pathway. *Mol Cell Biol*. 32:88-95.

Xu, W., M. Shy, J. Kamholz, L. Elferink, G. Xu, J. Lilien, and J. Balsamo. 2001. Mutations in the cytoplasmic domain of P0 reveal a role for PKC-mediated phosphorylation in adhesion and myelination. *J Cell Biol*. 155:439-446.

Yamashita, A., K. Tanaka, R. Kamata, T. Kumazawa, N. Suzuki, H. Koga, K. Waku, and T. Sugiura. 2009. Subcellular localization and lysophospholipase/transacylation activities of human group IVC phospholipase A2 (cPLA2gamma). *Biochim Biophys Acta*. 1791:1011-1022.

Yin, X., T.O. Crawford, J.W. Griffin, P. Tu, V.M. Lee, C. Li, J. Roder, and B.D. Trapp. 1998. Myelin-associated glycoprotein is a myelin signal that modulates the caliber of myelinated axons. *J Neurosci*. 18:1953-1962.

Yoshihara, T., F. Kanda, M. Yamamoto, H. Ishihara, K. Misu, N. Hattori, K. Chihara, and G. Sobue. 2001. A novel missense mutation in the early growth response 2 gene associated with late-onset Charcot--Marie--Tooth disease type 1. *J Neurol Sci*. 184:149-153.

Yoshikawa, H., T. Nishimura, M. Kaido, K. Toyooka, H. Fujimura, S. Sakoda, and T. Yanagihara. 1996. Cation binding at the node of Ranvier in biopsied peripheral nerves of patients with Charcot-Marie-Tooth disease type 1A and hereditary neuropathy with liability to pressure palsies. *Acta Neuropathol*. 91:587-594.

Yum, S.W., K.A. Kleopa, S. Shumas, and S.S. Scherer. 2002. Diverse trafficking abnormalities of connexin32 mutants causing CMTX. *Neurobiol Dis.* 11:43-52.

Zhang, Y., J. Gao, K.K. Chung, H. Huang, V.L. Dawson, and T.M. Dawson. 2000. Parkin functions as an E2-dependent ubiquitin- protein ligase and promotes the degradation of the synaptic vesicle-associated protein, CDCrel-1. *Proc Natl Acad Sci U S A*. 97:13354-13359.

Zhou, J., Z. Yang, T. Tsuji, J. Gong, J. Xie, C. Chen, W. Li, S. Amar, and Z. Luo. 2011. LITAF and TNFSF15, two downstream targets of AMPK, exert inhibitory effects on tumor growth. *Oncogene*. 30:1892-1900.

Zuchner, S., I.V. Mersiyanova, M. Muglia, N. Bissar-Tadmouri, J. Rochelle, E.L. Dadali, M. Zappia, E. Nelis, A. Patitucci, J. Senderek, Y. Parman, O. Evgrafov, P.D. Jonghe, Y. Takahashi, S. Tsuji, M.A. Pericak-Vance, A. Quattrone, E. Battaloglu, A.V. Polyakov, V. Timmerman, J.M. Schroder, and J.M. Vance. 2004. Mutations in the mitochondrial GTPase mitofusin 2 cause Charcot-Marie-Tooth neuropathy type 2A. *Nat Genet*. 36:449-451.